T-4818

A MATHEMATICAL MODEL FOR MECHANICAL BUCKLING OF DRILLSTRINGS WITHIN CURVED BOREHOLES

by

Jorge Hygino Braga Sampaio Junior

T-4818

A thesis submitted to the Faculty and the Board of Trustees of the Colorado School of Mines in partial fulfillment of the requirements for the degree of Doctor of Philosophy (Petroleum Engineering).

Golden, Colorado

Date: Oct 23, 1996_____

Signed: _____
Jorge Hygino Braga Sampaio Junior

Approved: _____
Dr. Billy J. Mitchell
Thesis Advisor

Golden, Colorado

Date: Nov 8,1996_____

_____
Dr. Craig W. Van Kirk
Professor and Head,
Department of Petroleum Engineering

Abstract

An innovative mathematical model to describe the mechanical buckling of drillstrings within curved bore-holes was developed. The *hypergeometric model* congregates the *curved bore-hole theory* and the *generalized beam-column theory,* both developed and presented in this work. The curved bore-hole theory dictates the conditions a drillstring must satisfy to buckle within a curved bore-hole. The generalized beam-column theory describes the singular behavior of an inclined beam-column subjected to a distributed weight and axial forces applied on its ends. The differential equation of the inclined beam-column was derived using the energy method and the general solution was written in a closed form using generalized hypergeometric functions. The conditions required by the curved bore-hole theory are then imposed to the general solution of the differential equation. This results in a numerical procedure with which the buckling force can be calculated for any point along a curved bore-hole, called *local buckling force*. From this force derives the *causational buckling force* which accounts for the effects of the distributed weight and friction. Curves plotted using these two forces, called *buckling graphs*, permit a complete analysis of the buckling behavior of the drillstring for constant cross-sectional drillstrings, tapered drillstrings, tapered bore-holes, and multi-curved bore-holes. All this is possible using the *P-curve shifting method* developed and presented in this work. The buckling graph and the *P*-curve shifting method constitute a unique tool for designing optimal drillstrings to drill horizontal oil, gas, and geothermal wells. The model was experimentally validated using a medium-scale apparatus designed and constructed in the Colorado School of Mines. Predictions using the *hypergeometric model* and results of the experiments are presented.

Table Of Contents

Abstract.....**iii**
List Of Figures.....**ix**
List Of Tables.....**xiii**
Nomenclature.....**xv**
Numerical Constants.....**xviii**
Acknowledgments.....**xix**
Dedication.....**xx**
Chapter 1 Introduction.....**1**
1.1 What is Mechanical Buckling?.....2
1.2 An Overview of the Problem Associated with Drilling.....3
1.3 Novelties of this Investigation.....7
1.4 General Assumptions.....9
1.5 The Unloading Buckling Force.....10
1.6 Limitations of this Investigation.....12
Chapter 2 Literature Review And Comments.....**13**
2.1 The Work of Lubinski and Collaborators.....13
2.2 The Work of Cheatham and Pattillo.....19
2.3 The Work of Paslay and Bogy.....20
2.4 The Work of Dawson and Paslay.....23
2.5 The Work of Kwon.....26
2.6 The Work of Chen, Lin and Cheatham.....27
2.7 The Work of Schuh.....31
2.8 The Work of Adrichem and Newman.....33
2.9 The Work of He and Kyllingstad.....34

2.10 The Work of Wu and Juvkam-Wold.....37
2.11 The Work of Heisig.....39
2.12 The Work of Salies, Azar and Sorem.....40
2.13 The Work of Suryanarayana and McCann.....45
Chapter 3 The Trigonometric Model And The Curved Bore Hole Theory.....47
3.1 Buckling of Weightless Columns under Static Compressive Axial Force.....47
3.2 Columns Subjected to a Compressive Force and Moment at the Ends.....52
3.3 The Curved Bore-Hole Theory.....56
3.3.1 Constraints Imposed on Buckled Columns.....56
3.3.2 Starting a Buckling Process.....57
3.3.3 Buckling of a Column Subjected to Two Concentric Circular Constraints.....62
3.4 End Effects.....67
3.5 Conclusions of the Chapter.....68
Chapter 4 The Generalized Beam-Column Theory.....70
4.1 Theories Including Distributed Weight.....70
4.1.1 The Flagpole Theory.....71
4.1.2 The Lubinski Model for Vertical Buckling.....72
4.1.3 The Beam-Column Theory.....74
4.2 The Generalized Beam-Column Theory.....75
4.2.1 The Principle of Virtual Work and The Energy Method.....76
4.2.2 Work Done by the External and Body Forces.....80
4.2.3 Strain Energy.....85
4.2.4 Total Potential Energy.....85
4.2.5 Differential Equation of the Generalized Beam-Column.....86
4.2.6 Rearranging the Differential Equation.....88
4.2.7 General Solution of the Differential Equation.....93
4.2.8 Imposing the Boundary Conditions to the General Solution.....95

4.3 The Solution Using Superposition.....97
4.4 Conclusions of the Chapter.....99
Chapter 5 Analysis Of The Behavior Of A Generalized Beam Column.....100
5.1 Evaluation of the Generalized Hypergeometric Functions.....100
5.2 Determining the Singularities of the Boundary Matrix.....101
5.3 Behavior in the Neighborhood of Critical Points.....104
5.3.1 Generalized Beam-Column Example.....104
5.3.2 Singular Behavior of a Generalized Beam-Column.....106
5.4 Conclusions of the Chapter.....115
Chapter 6 The Hypergeometric Model.....117
6.1 Differences Between Building and Dropping Bore-Holes.....118
6.2 Analysis of the Build Section of a Curved Bore-hole.....118
6.2.1 Frictional Effects.....120
6.2.2 Local Buckling Force at a Given Angle θ.....122
6.2.3 Functional Measurement of the Fit.....122
6.2.3.1 Numerical Evaluation of the Vector Fit Function $f(X_1,X_2)$.....126
6.2.4 Searching for the Fit.....130
6.2.4.1 Reducing the Order of the System.....131
6.2.4.2 Full Rank Least Square Method.....131
6.2.4.3 Advancing One Step and Stop Criteria.....133
6.2.4.4 Initial Guess and Process Guidance During Search.....134
6.2.5 Spotting the Buckling Point Region.....137
6.3 Graphical Representation of the Results.....137
6.3.1 Buckling Graphs Structure.....138
6.3.2 Tapered Drillstrings and The *P*-curve shifting method.....140
6.4 Conclusions of the Chapter.....143
Chapter 7 Experimental And Numerical Results.....144

7.1 Predictions for the Experiments....144
7.2 Field Simulations....156
7.2.1 Case No.1: $17^1/_2$ *in* Bore-Hole - API 5 *in* Drill Pipe....157
7.2.2 Case No.2: $12^1/_4$ *in* Bore-Hole - API 5 *in* Drill Pipe....160
7.2.3 Case No.3: $12^1/_4$ *in* Bore-Hole - API $4^1/_2$ *in* Drill Pipe....161
7.2.4 Case No.4: 6 *in* Bore-Hole - API $3^1/_2$ *in* Drill Pipe....161
7.3 Conclusions of the Chapter....162
Chapter 8 Conclusions....167
8.1 Conclusions....168
8.2 Future Work....170
Cited References....172
Appendix A Tables Of Numeric Results (Abridged)....176
Appendix B Locus Of The Center Of Curvature....224
Appendix C Euler-Lagrange Differential Equation And Boundary Conditions For F(x,y,y´,y´´)....226
Appendix D Series Solution Of The Differential Equation....231
Appendix E Numerical Evaluation Of The Hypergeometric Functions....246
E.1 Series Expansion of the Functions....247
E.2 Path Integration of Differential Equations....254
E.2.1 Integration for Functions Type ${}_0F_1[\beta;(x^3/9)]$....255
E.2.2 Integration for Functions Type ${}_1F_2[\alpha;\beta_1,\beta_2;(x^3/9)]$....256
E.2.3 Integration for Functions Type ${}_2F_3[\alpha_1,\alpha_2;\beta_1,\beta_2,\beta_3;(x^3/9)]$....258
E.2.4 Properties at x=0....260
E.2.5 Integration of the Systems of Differential Equations....262
E.3 Asymptotic Expansions....268
E.3.1 Expansion for Functions Type ${}_0F_1$ [Functions $N_2(x)$, $R_1(x)$, $R_2(x)$, $N_1(x)$]....273
E.3.1.1 Function $N_2(x) = {}_0F_1(^1/_3;x^3/9)$....274

E.3.1.2 Function $R_1(x) = {}_0F_1(^2/_3;x^3/9)$.....277
E.3.1.3 Function $R_2(x) = x\ {}_0F_1(^4/_3;x^3/9)$.....279
E.3.1.4 Function Function $N_1(x) = x^2/2\ {}_0F_1(^5/_3;x^3/9)$.....282
E.3.2 Expansion for Functions Type ${}_1F_2$ [Functions $M_1(x)$, $M_2(x)$, $N_3(x)$, $R_3(x)$].....285
E.3.2.1 Function $M_1(x)= x\ {}_1F_2(^1/_3;^2/_3,^4/_3;x^3/9)$.....286
E.3.2.2 Function $M_2(x)= x^2/2\ {}_1F_2(^2/_3;^4/_3,^5/_3;x^3/9)$.....290
E.3.2.3 Function $N_3(x)= 2x\ {}_1F_2(1;^2/_3,^4/_3;x^3/9)$.....294
E.3.2.4 Function $R_3(x)= x^2\ {}_1F_2(1;^4/_3,^5/_3;x^3/9)$.....299
E.3.3 Expansion for Functions Type ${}_2F_3$ [Function $M_3(x)$].....303
E.3.3.1 Function $M_3(x)= x^3/3\ {}_2F_3(1,1;^4/_3,^5/_3,2;x^3/9)$.....304
E.3.4 Numerical Implementation.....311
Appendix F The Newton-Raphson Method For A Non-Square System Of Non-Linear Equations.....312
Appendix G Buckling Force Calculation For The Trigonometric Model.....316
G.1 Iterative Process to Determine the Parameters of the Center Line.....318
G.2 Approximate Solution.....321
G.3 Drill Bit End Condition.....325
G.4 Near-Bit End Condition.....329

List Of Figures

Figure 1.1: A schematic of a horizontal bore-hole drilling.....6
Figure 1.2: A cyclic process of loading and unloading a drillstring.....11
Figure 2.1: A fully developed helix.....15
Figure 2.2: Buckling force of a beam on an elastic foundation.....29
Figure 3.1: Bending of a beam element.....48
Figure 3.2: A slender column buckling under axial compressive force.....50
Figure 3.3: Displacement of the center of the column.....52
Figure 3.4: Solutions of a buckling problem for n=1, 2, and 3.....53
Figure 3.5: Column subjected to axial force and moment at the ends.....54
Figure 3.6: Column subjected to an eccentric axial force.....55
Figure 3.7: Two different concepts of buckling.....58
Figure 3.8: A straight column inside the curved constraints.....59
Figure 3.9: Buckling a column inside the curved constraints.....61
Figure 3.10: A buckled column touching the outer constraint.....61
Figure 3.11: Fitting a half-period of a sine curve inside the constraints.....63
Figure 3.12: Locus of the center of curvature of a sinusoidal curve.....64
Figure 3.13: Fitting $1^1/_2$-periods of a sine curve inside the constraints.....66
Figure 3.14: Two buckled waves inside the curved constraints.....67
Figure 3.15: A schematic of the drill bit end condition.....69
Figure 3.16 A schematic of the near-bit end condition.....69
Figure 4.1: A Weighted inclined beam-column under axial force.....77
Figure 4.2: Decomposition of the loading acting upon a beam-column.....80
Figure 4.3: Axial displacement on an infinitesimal element of the column.....82
Figure 4.4: Lateral displacement of an infinitesimal element of the beam.....84

Figure 5.1: Roots of the boundary determinant for L_D=2.0.....103
Figure 5.2: Roots of the boundary determinant for L_D=2.8.....103
Figure 5.3: Configuration for $P \rightarrow P_1^-$.....107
Figure 5.4: Maximum lateral displacement for $P \rightarrow P_1^-$.....108
Figure 5.5: Configuration for $P \rightarrow P_1^+$.....109
Figure 5.6: Maximum lateral displacement for $P \rightarrow P_1^+$.....110
Figure 5.7: Configuration for $P \rightarrow P_2^-$.....111
Figure 5.8: Maximum lateral displacement for $P \rightarrow P_2^-$ and X-X_2=-1.2.....112
Figure 5.9: Configuration for $P \rightarrow P_2^+$.....112
Figure 5.10: Configuration for $P \rightarrow P_3^-$.....113
Figure 5.11: Configuration for $P \rightarrow P_3^+$.....115
Figure 6.1: A generic buckled portion of a drillstring.....123
Figure 6.2: Six quarter of wave with six points that satisfy Equation (6.2).....128
Figure 6.3: Strip for the subcritical buckling of 3rd mode.....135
Figure 6.4: Structure of the buckling graph with a shift of the P-curve at 10 deg.....139
Figure 6.5: Buckling analysis for a tapered drillstring.....141
Figure 7.1: Predictions and experimental results for in steel rod - 2 in well.....149
Figure 7.2: Predictions and experimental results for in steel rod - 1 in well.....150
Figure 7.3: Predictions and experimental results for in steel rod - 2 in well.....151
Figure 7.4: Predictions and experimental results for in steel rod - 1 in well.....152
Figure 7.5: Predictions and experimental results for in steel rod - 2 in well.....153
Figure 7.6: Predictions and experimental results for in steel rod - 1 in well.....154
Figure 7.7: Predictions and experimental results for in aluminium rod - 2 in well.....155
Figure 7.8: Contact between a tool joint and the bore-hole wall.....157
Figure 7.9: Position of the buckled portion of the drillstring.....160
Figure 7.10: Case No.1 with multiple build gradients.....163
Figure 7.11: Case No.2 with multiple build gradients.....164

Figure 7.12: Case No.3 with multiple build gradients.....165
Figure 7.13: Case No.4 with multiple build gradients.....166
Figure B.1: Center of curvature of a function.....225
Figure E.1: Plot of $R_1(x)$ using series expansion with 15 digits f.p.a.....248
Figure E.2: Plot of $R_2(x)$ using series expansion with 15 digits f.p.a.....250
Figure E.3: Plot of $R_3(x)$ using series expansion with 15 digits f.p.a.....250
Figure E.4: Plot of $M_1(x)$ using series expansion with 15 digits f.p.a.....251
Figure E.5: Plot of $M_2(x)$ using series expansion with 15 digits f.p.a.....251
Figure E.6: Plot of $M_3(x)$ using series expansion with 15 digits f.p.a.....252
Figure E.7: Plot of $N_1(x)$ using series expansion with 15 digits f.p.a.....252
Figure E.8: Plot of $N_2(x)$ using series expansion with 15 digits f.p.a.....253
Figure E.9: Plot of $N_3(x)$ using series expansion with 15 digits f.p.a.....253
Figure E.10: Plot of R1(x) using path integration of the differential equation.....263
Figure E.11: Plot of R2(x) using path integration of the differential equation.....264
Figure E.12: Plot of R3(x) using path integration of the differential equation.....264
Figure E.13: Plot of M1(x) using path integration of the differential equation.....265
Figure E.14: Plot of M2(x) using path integration of the differential equation.....265
Figure E.15: Plot of M3(x) using path integration of the differential equation.....266
Figure E.16: Plot of N1(x) using path integration of the differential equation.....266
Figure E.17: Plot of N2(x) using path integration of the differential equation.....267
Figure E.18: Plot of N3(x) using path integration of the differential equation.....267
Figure E.19: Plot of the asymptotic expansion of $N_2(x)$.....276
Figure E.20: Plot of the asymptotic expansion of $R_1(x)$.....279
Figure E.21: Plot of the asymptotic expansion of $R_2(x)$.....282
Figure E.22: Plot of the asymptotic expansion of $N_1(x)$.....285
Figure E.23: Plot of the asymptotic expansion of $M_1(x)$.....290
Figure E.24: Plot of the asymptotic expansion of $M_2(x)$.....294

Figure E.25: Plot of the asymptotic expansion of $N_3(x)$.....299
Figure E.26: Plot of the asymptotic expansion of $R_3(x)$.....303
Figure E.27: Plot of the asymptotic expansion of $M_3(x)$.....310
Figure F.1: Newton-Raphson made easy.....313
Figure G.1: Geometric relations in the buckled portion of a column.....319
Figure G.2: Bit condition imposed at one end.....326
Figure G.3: Near-bit condition imposed at one end.....330

List Of Tables

Table 5.1: Roots of det[S(X_2)].....105
Table 7.1: Angular positions for axial forces and buckled portions.....146
Table A.1: $^1/_8$ *in* steel rod - 2 *in* bore-hole - 113 *ft* radius of curvature.....177
Table A.2: $^1/_8$ *in* steel rod - 2 *in* bore-hole - 58 *ft* radius of curvature.....178
Table A.3: $^1/_8$ in steel rod - 2 *in* bore-hole - 40 *ft* radius of curvature.....179
Table A.4: 1/8 in steel rod - 1 in bore-hole - 113 ft radius of curvature.....180
Table A.5: 1/8 in steel rod - 1 in bore-hole - 58 ft radius of curvature.....181
Table A.6 1/8 in steel rod - 1 in bore-hole - 40 ft radius of curvature.....182
Table A.7: 3/16 in steel rod - 2 in bore-hole - 113 ft radius of curvature.....183
Table A.8: 3/16 in steel rod - 2 in bore-hole - 58 ft radius of curvature.....184
Table A.9: 3/16 in steel rod - 2 in bore-hole - 40 ft radius of curvature.....185
Table A.10: 3/16 in steel rod - 1 in bore-hole - 113 ft radius of curvature.....186
Table A.11: 3/16 in steel rod - 1 in bore-hole - 58 ft radius of curvature.....187
Table A.12: 3/16 in steel rod - 1 in bore-hole - 40 ft radius of curvature.....188
Table A.13: 1/4 in steel rod - 2 in bore-hole - 113 ft radius of curvature.....189
Table A.14: 1/4 in steel rod - 2 in bore-hole - 58 ft radius of curvature.....190
Table A.15: 1/4 in steel rod - 2 in bore-hole - 40 ft radius of curvature.....191
Table A.16: 1/4 in steel rod - 1 in bore-hole - 113 ft radius of curvature.....192
Table A.17: 1/4 in steel rod - 1 in bore-hole - 58 ft radius of curvature.....193
Table A.18: 1/4 in steel rod - 1 in bore-hole - 40 ft radius of curvature.....194
Table A.19: 1/4 in aluminium rod - 2 in bore-hole - 113 ft radius of curvature.....195
Table A.20: 1/4 in aluminium rod - 2 in bore-hole - 58 ft radius of curvature.....196
Table A.21: 1/4 in aluminium rod - 2 in bore-hole - 40 ft radius of curvature.....197
Table A.22: 5 in 19.5 lb/ft drill-pipe - 171/2 in bore-hole - 2°/100ft BG.....198

Table A.23: 5 in 19.5 lb/ft drill-pipe - 171/2 in bore-hole - 3°/100ft BG.....199
Table A.24: 5 in 19.5 lb/ft drill-pipe - 171/2 in bore-hole - 4°/100ft BG.....200
Table A.25: 5 in 19.5 lb/ft drill-pipe - 171/2 in bore-hole - 5°/100ft BG.....201
Table A.26: 5 in 19.5 lb/ft drill-pipe - 171/2 in bore-hole - 6°/100ft BG.....202
Table A.27: 5 in 19.5 lb/ft drill-pipe - 171/2 in bore-hole - 7°/100ft BG.....203
Table A.28: 5 in 19.5 lb/ft drill-pipe - 171/2 in bore-hole - 2°/100ft BG.....204
Table A.29: 5 in 19.5 lb/ft drill-pipe - 121/4 in bore-hole - 3°/100ft BG.....205
Table A.30: 5 in 19.5 lb/ft drill-pipe - 121/4 in bore-hole - 4°/100ft BG.....206
Table A.31: 5 in 19.5 lb/ft drill-pipe - 121/4 in bore-hole - 5°/100ft BG.....207
Table A.32: 5 in 19.5 lb/ft drill-pipe - 121/4 in bore-hole - 6°/100ft BG.....208
Table A.33: 5 in 19.5 lb/ft drill-pipe - 121/4 in bore-hole - 7°/100ft BG.....209
Table A.34: 41/2 in 16.6 lb/ft drill-pipe - 121/4 in bore-hole - 2°/100ft BG.....210
Table A.35: 41/2 in 16.6 lb/ft drill-pipe - 121/4 in bore-hole - 3°/100ft BG.....211
Table A.36: 41/2 in 16.6 lb/ft drill-pipe - 121/4 in bore-hole - 4°/100ft BG.....212
Table A.37: 41/2 in 16.6 lb/ft drill-pipe - 121/4 in bore-hole - 5°/100ft BG.....213
Table A.38: 41/2 in 16.6 lb/ft drill-pipe - 121/4 in bore-hole - 6°/100ft BG.....214
Table A.39: 41/2 in 16.6 lb/ft drill-pipe - 121/4 in bore-hole - 7°/100ft BG.....215
Table A.40: 31/2 in 13.3 lb/ft drill-pipe - 6 in bore-hole - 2°/100ft BG.....216
Table A.41: 31/2 in 13.3 lb/ft drill-pipe - 6 in bore-hole - 3°/100ft BG.....217
Table A.42: 31/2 in 13.3 lb/ft drill-pipe - 6 in bore-hole - 4°/100ft BG.....218
Table A.43: 31/2 in 13.3 lb/ft drill-pipe - 6 in bore-hole - 5°/100ft BG.....219
Table A.44: 31/2 in 13.3 lb/ft drill-pipe - 6 in bore-hole - 6°/100ft BG.....220
Table A.45: 31/2 in 13.3 lb/ft drill-pipe - 6 in bore-hole - 7°/100ft BG.....221
Table A.46: 31/2 in 13.3 lb/ft drill-pipe - 6 in bore-hole - 10°/100ft BG.....222
Table A.47: $3^{1}/_{2}$ in 13.3 lb/ft drill-pipe - 6 in bore-hole - 12°/100ft BG.....223

Nomenclature

Symbol	Definition	Dimension[1]	Unit
α	Cross-sectional beam-column constant	L	in
β	Angle at the bit	1	rad
δ	Axial displacements	L	ft
ε_{ij}'	Strain tensor	1	
φ	Angle	1	rad
κ	Curvature	L^{-1}	rad/ft
θ	Angle of inclination	1	rad
ρ	Radius of curvature	L	ft
	Density	mL^{-3}	lbm/ft^3
σ_{ij}'	Stress tensor	FL^{-2}	lb/in^3
$\Gamma(x)$	Gamma function	1	
$\Psi(x)$	Digamma function	1	
b	Coefficients vector (b_1, b_2, b_3, b_4)	1	
c	Diametrical clearance	L	ft
c_i	Constants		
d	Diameter	L	ft
e	Eccentricity	L	ft
n	Buckling mode	1	
s	Arc length	L	ft
w	Distributed weight	FL^{-1}	lb/ft
w_c	Axial distributed weight	FL^{-1}	lb/ft

1 F=force, m=mass, L=length, t=time

Symbol	Definition	Dimension	Unit
w_s	Lateral distributed weight	FL^{-1}	lb/ft
x	Axial coordinate	L	ft
y	Lateral displacement coordinate	L	ft
y_{max}	Maximum displacement	L	ft
A	Area	L^2	in^2
BG	Build gradient	L^{-1}	°/100ft
B'_i	Acceleration field	Lt^{-2}	ft/s^2
E	Modulus of elasticity	FL^{-2}	lb/in^2
F_r	Radial force	F	lb
F_t	Tangential force	F	lb
${}_pF_q$	Generalized hypergeometric functions	1	
I	Moment of inertia	L^4	in^4
ID	Inside diameter of pipes	L	in
L, l	Length of a beam-column	L	ft
L_1,L′	Complementary buckling length	L	ft
L_D	Dimensionless length of a beam-column	1	
M	Moment	FL	lb · ft
OD	Outside diameter of pipes	L	in
P	Axial force	F	lb
P'_θ	Local buckling force	F	lb
${}_{\theta 1}P'_{\theta 2}$	Causational buckling force	F	lb
P_{crit}	Critical force	F	lb
P_n	n^{th} critical force		lb
R, r	Radius of curvature	L	ft
S	Shear force	F	lb

Symbol	Definition	Dimension	Unit
S(P)	Boundary matrix		
T'_i	Surface traction	FL^{-2}	lb/in^2
U	Total potential energy	FL	$lb \cdot ft$
U_w	Potential energy of external and body forces	FL	$lb \cdot ft$
V	Volume	L^3	in^3
	Strain energy	FL	$lb \cdot f$
V_b	Strain energy of bending	FL	$lb \cdot ft$
WOB	Weight on bit	F	lb
W_p	Work done by a force P	FL	$lb \cdot ft$
W_{Wc}	Work done by the distributed weight W_c	FL	$lb \cdot ft$
W_{Ws}	Work done by the distributed weight W_s	FL	$lb \cdot ft$
X	Dimensionless axial coordinate	1	
X_1	Dimensionless coordinate of the lower end of an inclined beam-column	1	
X_2	Dimensionless coordinate of the upper end of an inclined beam-column	1	

Numerical Constants

First positive non-zero root of the transcendental equation $\psi = \tan(\psi)$:

$\psi=$ 4.4934 09457 90906 41753 07880 92728...

Gamma function:

$\Gamma(1/3)=$ 2.6789 38534 70774 76336 55692 94099...

$\Gamma(2/3)=$ 1.3541 17939 42640 04169 45288 02815...

$\Gamma(4/3)=$ .89297 95115 69249 21121 85643 13664...

$\Gamma(5/3)=$ .90274 52929 50933 61129 68586 85434...

Digamma function

$\Psi(1/3)=$ -3.1320 33780 02080 63229 96419 07429...

$\Psi(2/3)=$ -1.3182 34415 78658 84724 02340 81664…

Acknowledgments

I would like to express my deepest gratitude to my advisor, Emeritus Professor Billy J. Mitchell, for his experience, support, and encouragement which were invaluable to the development of this dissertation.

I wish also to express my gratitude to the members of my doctoral committee, Professor Richard Christiansen and Professor Robert S. Thompson from the Petroleum Engineering Department, Professor Joan R. Hundhausen and Professor Erik S. Van Vleck from the Mathematical and Computer Sciences Department, and Professor Graham G. W. Mustoe from the Engineering Department for the assistance and motivation they provided during this research.

I gratefully acknowledge the help from Gokham Gurakin during the time we spent together constructing and running the experimental apparatus, and Robin N. Heim in reading and reviewing the text.

I would like to thank the Brazilian State Oil Company, PETROBRAS, for the support and opportunity, in special to Eng. Eduardo C. S. Santos.

Dedication

To my Parents

Jorge and Marilena

and

To my Family

Christina, Natália, and Júlio César

Chapter 1

Introduction

The theories invented and developed in this work are sufficiently general to apply to the buckling of long cylindrical columns which are totally contained within curved tubes or structures of circular cross sections. Further, these new theories may be viewed as another step toward the completeness in the field of theoretical buckling mechanics. One of the more immediate applications of these theories is the design and understanding of drillstrings which form the basis of the rotary bore-hole drilling system.

The work in this thesis led to the invention and development of the new and original *hypergeometric model* whose fundamentals are based on the new *curved bore-hole theory* and the new *generalized beam-column theory.* The *hypergeometric model* is a new tool available for bore-hole drilling. For the first time the buckling behavior of drillstrings within curved bore-holes can be determined using a *fully analytical* model. Every detail of the *hypergeometric model* formulation was developed with the specific goal of solving the problem of buckling of drillstrings within curved bore-holes. The model is entirely self-contained and does not resort to any result or formulation from buckling in straight bore-holes or to any kind of adjustable factors to fit field results. The mathematical and physical fundamentals of this model, along with its experimental validation, make this model unique in its area.

Mechanics of materials, embodied in the *generalized beam-column theory,* and mathematics, embodied in a long list of topics, are chained by an innovative idea: the *curved bore-hole theory.*

The modeling has everything the industry needs: a strong mathematical basis, and an efficient implementation. A model that cannot be efficiently implemented has a high probability of ending up resting on a library shelf.

This work concentrates on the phenomenon of mechanical buckling of drillstrings within and while drilling bore-holes. The problems arising from this phenomenon have been a major topic in the petroleum industry for more than 40 years. The most critical of these problems associated with this phenomenon is the limitation of the reach of near-horizontal bore-holes.

1.1 What is Mechanical Buckling?

Several definitions have been given to the phenomenon of mechanical buckling. Field engineers consider mechanical buckling as the imminent or instantaneous collapse of a structure due to external and/or internal loads which would not be sufficiently intense to cause mechanical yield of the material in the structure. It is considered a total instability of the structure. Theoretical engineers contemplate mechanical buckling as a confluence of stable and unstable equilibrium states of a system, which includes the structure and its loads, and under which conditions the total potential energy of the system becomes or stays stationary. Mathematicians, on the other hand, ponder buckling as possible states that a system may assume which will show abrupt changes in its behavior. These states may be mathematically characterized by bifurcations, eigenvalues or singularities.

Mechanical buckling can occur in columns, beams, plates, shells, arches, rings, and more complex engineering elements and structures. Axial and lateral force, moment, torque, and pressure are the most common driving loads.

The phenomenon of mechanical buckling has been studied for centuries and constitutes a well developed but still incomplete branch of the mechanics of materials. One area of incompleteness is the mechanical buckling of drillstrings within curved bore-holes. For simplicity, the term *buckling* will be used in this work, instead of the more correct *mechanical buckling*.

1.2 An Overview of the Problem Associated with Drilling

To drive a drill bit through geological formations and open a bore-hole, axial force on the drill bit and drill bit rotation are required at the bottom of a drillstring where the drill bit is located. The drill bit is rotated by turning the drillstring at the surface, or by special motors located at the bottom of the drillstring. Usually these motors are positive displacement motors (PDM), powered by the hydraulic energy of the flowing drilling fluid.

The axial force comes from the weight of thick walled tubes called drill collars, which are normally positioned in the lower portion of the drillstring. The axial force is applied on the drill bit by slacking off part of the weight of the drillstring. A lower portion of the drillstring will be in compression while an upper portion will be subjected to axial tension. Increases in weight on the drill bit will eventually buckle the lower portion of the drillstring. Drill collars are normally placed in the compressed section to prevent the fatigue of drill pipes. The drill collars will not fatigue because of their wall thickness and resulting stiffness.

When a drillstring buckles inside the bore-hole, its geometrical configuration changes. The drillstring interacts with the wall of the bore-hole in such a way that both the contact length and the contact force increase during buckling. This interaction results in a friction force, known as drag, which can absorb part or all the weight reserved for the

drill bit. If the available force at the bit falls below a threshold value, the drill bit cannot advance and drilling must be terminated. Moreover, to rotate the bit operating under drillstring buckling conditions requires higher torque. This fatigues the drillstring reducing its life. To keep the drill bit advancing economically, excessive drillstring buckling must be prevented.

To prevent excessive drillstring buckling it is necessary to identify and control the mechanical parameters which affect the phenomenon. A number of competent researchers have dedicated their careers to the investigation, modeling, understanding, and explanation of drillstring buckling. Their works were pertinent to three types of straight bore-hole configurations: vertical, inclined, and horizontal. Their models for vertical, inclined, and horizontal straight bore-holes have been presented, discussed, and employed in congresses, technical magazines, and companies. Also, large amounts of money have been invested in research centers and centers for advanced studies to accurately describe and model this phenomenon.

With the number of horizontal oil and gas wells at its crescent, and the range of well configurations at a new zenith, new and perplexing well designs challenge the drilling industry. For example, horizontal drilling in shallow formations requires higher build gradients (BG) than those usually found in conventional directional wells. Also, in order to apply weight on the drill bit while drilling the horizontal section of a horizontal well, it may become necessary to transfer the drill collars from just above the bit to the vertical section of the bore-hole. Drill pipes are positioned below the drill collars to mechanically transmit the weight of the drill collars to the drill bit. This common practice has its technical problems in that the drill pipes below the new position of the drill collars will be under compressive force and, therefore, have increased risk of buckling. Drill collars should not be placed in the curved section of the bore-hole as the stiffness and large diameters create excessive drag. Figure (1.1) shows a schematic of a horizontal

bore-hole with the drill collars in the vertical section. Under this circumstance, the drill pipe section below the drill collars will be at risk of buckling.

The analysis of drillstring buckling in this thesis is concerned with buckling in the curved section of a bore-hole. Buckling in vertical and horizontal sections have been thoroughly investigated. Several models which analyze drillstring buckling in straight vertical, horizontal, and inclined bore-holes have been developed and validated experimentally. They will be discussed in Chapter 2. These models are essential for the design of drillstrings.

After a detailed literature review, I concluded that no complete analytical study exists dealing with the buckling of drillstrings constrained within curved bore-holes. However, there are models developed for curved bore-holes whose fundamentals were taken from straight bore-hole theory. Some of these models require the assignment of unrealistic values to critical parameters to match field data. Other models adjust some parameters to account for the effects of the curvature of the bore-hole. These models cannot account for all the parameters and the real effects of the curved constraints in the buckling behavior of drillstrings.

The *hypergeometric model* bridges this gap. In addition, the *generalized beam-column theory* is a new contributions to the field of mechanics of material.

In practical applications it is fundamental, in the design of a drillstring, that the buckling in the curved section be balanced with the designs in the other two sections. In other words, the risk of buckling should be about the same in all sections. Also, balance within a section is critical. The hypergeometric model provides the tools to accomplish such a balanced design. Further, the balance must be maintained as an element of the drillstring exits one section of the bore-hole and enters another. The knowledge of bit performance would greatly assist in this area of drillstring design for buckling.

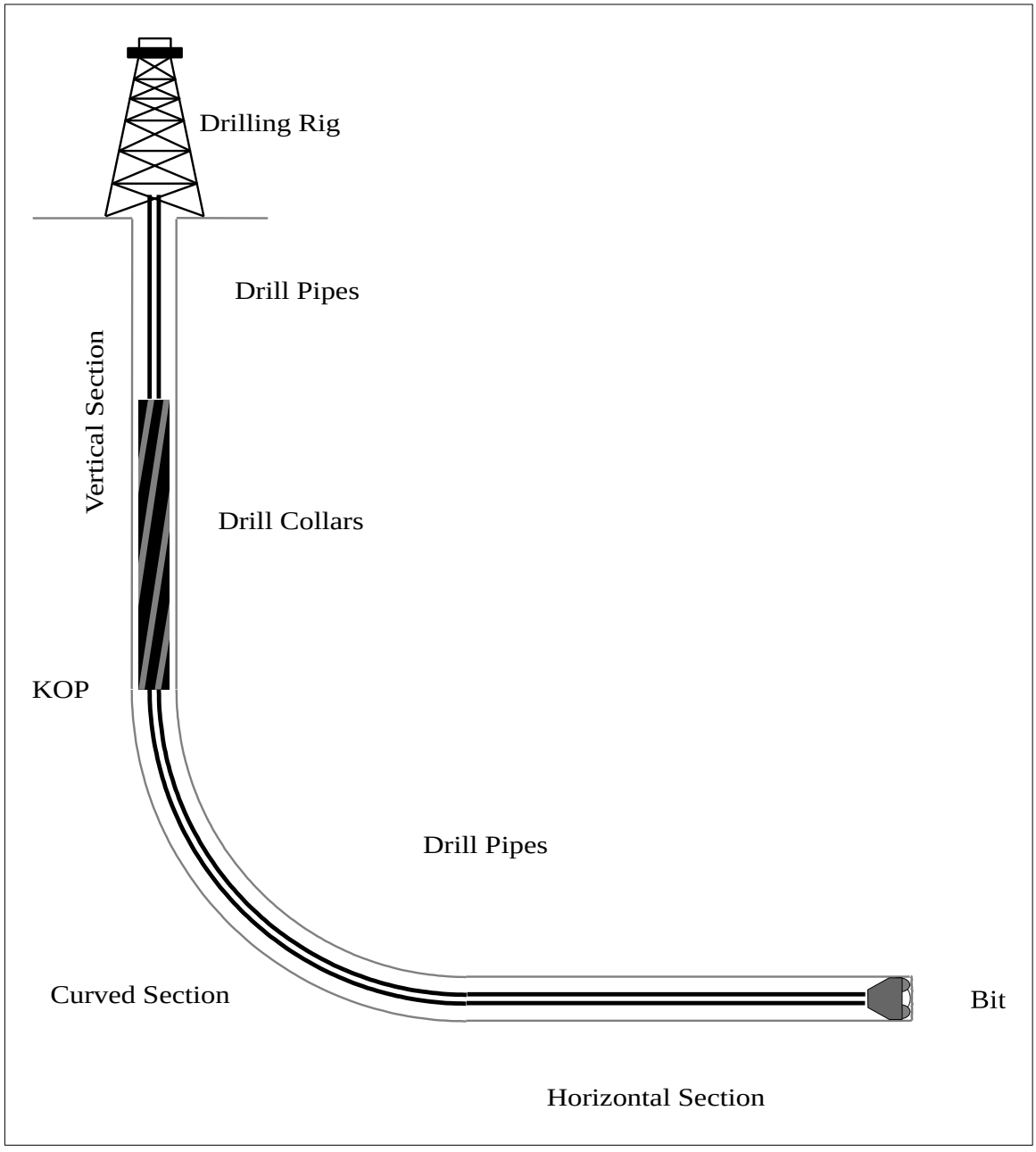

Figure 1.1: A schematic of a horizontal bore-hole drilling[1]

1 The schematic shows the drillstring centered in the bore-hole when it should be shown lying on the lower side of the bore-hole.)

There is little concern about drill collars buckling in the vertical section of the bore-hole because buckling here creates little risk to the drilling operation. The use of stabilizers in this section may further reduce any risk.

The product of this work should be applied in conjunction with other advanced drilling techniques. It is one more tool the drilling engineer has to design optimal horizontal and extended reach wells. Its application is not limited to the curved section of the bore-hole but also to all curves within the horizontal and vertical sections. A clever application of this model will result in a substantial increase of the range of horizontal wells.

1.3 Novelties of this Investigation

This investigation models the phenomenon of buckling of a weighted drillstring forced to remain inside *two circular concentric constraints*. This is not a limitation because the same ideas developed here may be made more general to include a wider range of curved configurations.

The drillstring is allowed to displace only in one plane and therefore it is a two dimensional (2D) model. The plane of displacements, however, does not need to be a vertical plane. It may be any plane in a three dimensional (3D) space, as long as the distributed weight of the drill pipe is projected in this plane.

To account for the influence of the constraints in the buckling behavior of the drillstring, concepts of plane differential geometry were used. To present these concepts and understand how they influence the buckling behavior of the drillstring, a reduced model is initially developed. This model does not consider the distributed weight of the drillstring and is based on the *Euler column theory.* Even under this limiting assumption, the reduced model, named *trigonometric model*, is able to reasonably predict the buckling

force and, more important, allows the drilling engineer to have an insight into the buckling phenomenon owing to its simplicity and flexibility.

The model also furnishes the wave-length of the buckled portion of the drillstring, and the position of the tangency point. The tangency point is the first point at which the drillstring touches the bore-hole above the bit. Two cases are considered: (1) drill bit pinned end, and (2) near-bit built-in end. The mathematical solution includes the following parameters: the tilt at the bit, the resulting axial and lateral forces, and the moment acting at the bit. These parameters are important in evaluating the future trajectory of the bit.

The enhanced model, named *hypergeometric model*, was developed to account for the distributed weight of the drillstring. The hypergeometric model uses the same concepts adopted by the trigonometric model. However, instead of using Euler column theory, a new and original *generalized beam-column theory* is used.

The generalized beam-column theory was developed as part of this work and is for the first time presented. The new theory includes the derivation of differential equation with the associated appropriate boundary conditions and the complete solution of the differential equation in a closed form. I also included a thorough analysis of the behavior of a generalized beam-column up to the third critical force.

The implementation of the model requires numerical procedures to deal with nonlinear systems. Several advanced numerical techniques are employed to guarantee the convergence and stability of these systems. The solution using the hypergeometric model requires an iterative process. To start this iterative process, a pre-processing is made using the trigonometric model to generate the initial values for the buckling force and for the wave-length. The functions used in the closed form solution of the generalized beam-column differential equation are numerically generated using asymptotic expansions.

A medium-scale apparatus for experimental validation was designed and built at the Colorado School of Mines. This apparatus uses new techniques to apply axial forces to rods, and new methods to measure displacements and points of tangency.

A graphical technique is presented to analyze and optimize tapered drillstrings. This technique is based on graphs for constant stiffness drillstrings generated by the hypergeometric model.

1.4 General Assumptions

Several assumptions are made during the development of this work. Assumptions of physical and mathematical character are stated in the text. Assumptions inherent to this model are presented in the following list and should be considered for future improvements of the model. The sequence presented is that toward the less restrictive.

1- Displacements are planar.
2- Torque along the drillstring is not considered.
3- The contact between the drillstring and the wall of the bore-hole is free of friction.
4- The constraints are considered infinitely rigid.
5- The top end of the drillstring in the curved section must always remain aligned with the axis of the bore-hole, although it is free to move in the radial direction (this reflects the fact that the loads at the top end come from a heavy and infinitely stiff assembly of drill collars).
6- The only loads that can be externally applied to the rod are axial forces and moments (called active loads). No radial force can be applied unless it results from reaction against the constraints (passive loads). Loads at bits, near-bits, and stabilizers are consider passive loads.

1.5 The Unloading Buckling Force

In this investigation the buckling force predicted and measured is that for an *unloading process*, and the force determined is called the *unloading buckling force*. This force is defined as the minimum force required to sustain a state of buckling in the drillstring in which the shape of the drillstring is a *curved helicoid*.

The *loading buckling force* is the force that will cause buckling to a drillstring and is larger than the unloading buckling force. The determination of this force will not be addressed in this work. The cyclic process of loading and unloading a drillstring is shown schematically in Figure (1.2).

When a drillstring in a curved bore-hole is loaded with an increasing axial force, the axial end displacement to axial force relationship is linear (line 1-2). At a certain magnitude of the axial force (loading buckling force, point 2), a large axial end displacement occurs (line 2-3) and the drillstring buckles. Beyond this value, the drillstring is in a post-buckling state with linear relationship (line3-4). If the axial force is decreased, the process follows a linear relationship (line 5-6) in which the drillstring unbuckles when the axial force decreases to a certain magnitude (unloading buckling force, point 6) less than the loading buckling force. The drillstring unbuckles with a large axial end displacement (line 6-7).

Below the unloading buckling force the drillstring follows a linear relationship in the unbuckled state (line 7-8). This characterizes a hysteresis in the behavior of the drillstring. Between the two buckling forces, two stable states exist.

The determination of the unloading buckling force is essential in preventing the drillstring from buckling. In a drilling operation, if the axial force is above the unloading buckling force but below the loading buckling force, perturbations due to the rotation of the drillstring, vibrations, impacts and other external factors can induce buckling in the drillstring.

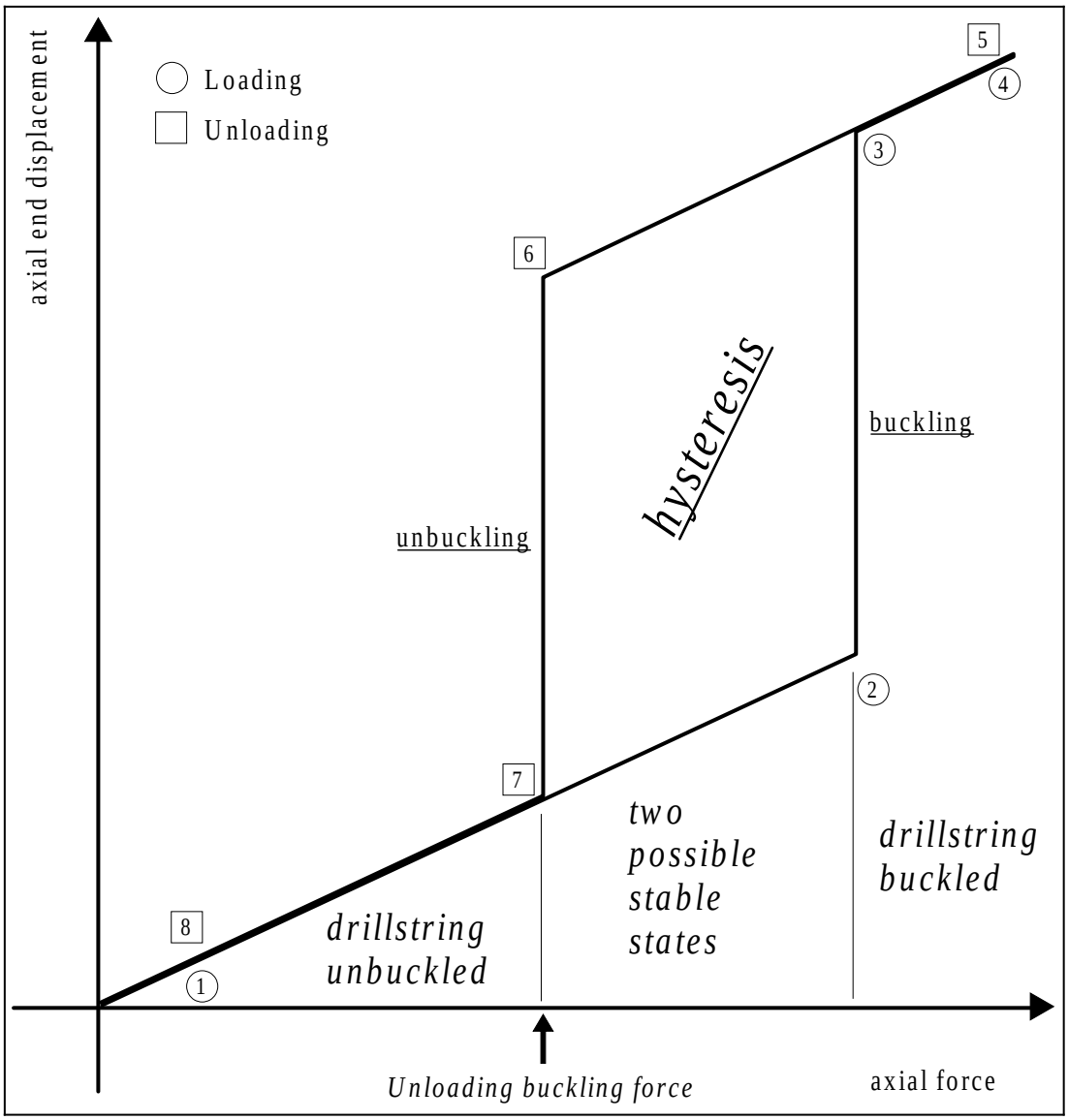

Figure 1.2: A cyclic process of loading and unloading a drillstring.

1.6 Limitations of this Investigation

This investigation is a first analytical approach to the problem of drillstring buckling constrained within curved bore-holes. The model developed is limited in some aspects. One limitation is the 2D restriction. The degree of freedom lost when the displacements are restricted to a plane results in a larger value for the buckling force than is expected for a 3D configuration. Nevertheless, the comparisons between the 2D predictions with the hypergeometric model and the results from the experiments show very good agreement. This agreement occurs because of the type of buckling force the model predicts and the experiments measure.

The assumption of frictionless contact is not a limitation but a convenience. Experimental validations in which friction is eliminated or minimized are easier to control and repeat. It will be shown that friction does not influence the *local buckling force* of a drillstring. Friction, however, affects the force that must be applied at any point of the drillstring to cause or sustain buckling at a deeper point. The distribution of this force determines the position along the curved bore-hole with the minimum resistance to buckling, and consequently the maximum force that can be applied on the drill bit. Despite the difficulty in accurately assessing the magnitude of friction coefficients, frictional effects can easily be modeled as shown in Chapter 6.

Chapter 2

Literature Review
And Comments

2.1 The Work of Lubinski and Collaborators

The literature concerned with mechanical buckling of drillstrings begins with a classical paper published by Arthur Lubinski (1950). This paper represents the first engineering and mathematical approach to the problem of buckling as applied to the drilling of oil and gas wells.

Lubinski obtained the expression and solution for the differential equation governing the buckling of long drillstrings laterally constrained within a cylindrical vertical bore-hole. The solution determines several parameters: the critical weight on the drill bit (WOB_{crit}), the location of the contact points between the drillstring and the bore-hole wall, the location and values of maximum stresses along the drillstring, the tilt of the drill bit, the resultant force acting on the drill bit, and the final shape of the buckled drillstring. A more detailed analysis of the mathematics of this model, which is restricted to 2D displacements, will be presented in Chapter 4. Following works (Lubinski 1951, Lubinski and Blenkarn 1957) gave some insight into mechanical buckling of drillstrings with 3D displacements.

A helical buckling analysis was presented by Lubinski, Althouse and Logan (1962). The model is restricted to vertical bore-holes and was developed assuming that the drillstring buckles into a helix. The weight on the drill bit results from the slacking off

of the drillstring and, since the drillstring is weighted, the axial force decreases from the bottom toward the top. Consequently the pitch of the helix changes along the bore-hole.

To develop the model the authors initially assumed that the drillstring is weightless and that it takes the shape of a helix with pitch[1] *p* and radius *r*. The coordinates of the helix is given by

$$\begin{cases} z = \dfrac{p}{2\pi} t \\ x = r\cos t \\ y = r\sin t \end{cases}$$

The pitch *p* is unknown and is obtained, for a given compressive force *F* acting on the top of the helix, by the minimization of the total potential energy of the system (the sum of the strain energy of the drillstring and the potential energy of the external forces). The assumption that the drillstring buckles into a helix makes the solution simpler. The minimization process turns into a differential problem instead of a variational problem which normally arises when no assumption about the final configuration is made.

A drillstring of length *L* is compressed by the force *F* acting at the top of the helix. The compressed length of the drillstring is L_c as shown in Figure (2.1).

The strain energy is composed of two parts, one due to the compression of the drillstring and one due to the bending of the drillstring. The compressive axial force F_a was calculated by Lubinski and is given by

$$F_a = \frac{F}{\sin\theta},$$

1 In this chapter I keep the original notations used by different authors. These notation are not included in the nomenclature of this work.

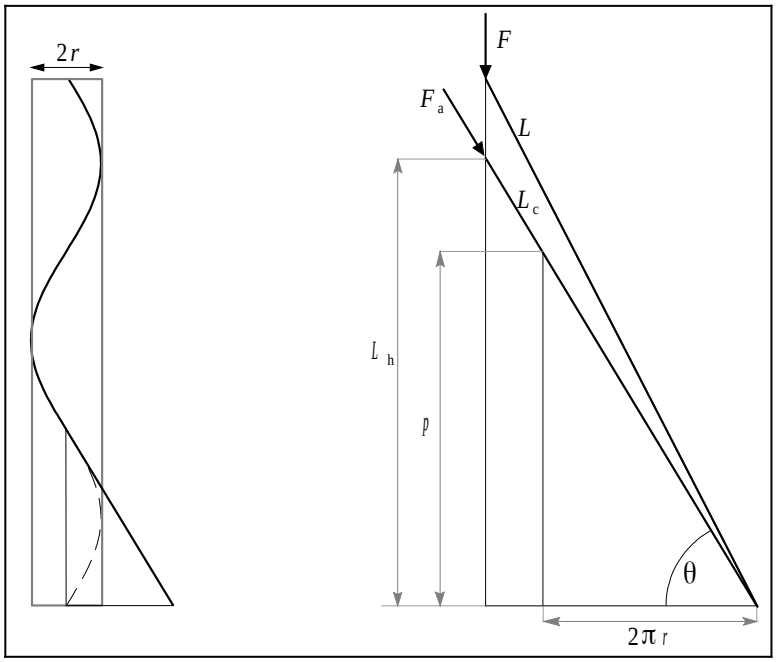

Figure 2.1: A fully developed helix

where θ is the helix angle.

The strain energy of compression is given by (Hartog 1949, eq. [30a])

$$U = \frac{s^2}{2E} \cdot volume,$$

which results in

$$U_{\mathrm{c}} = \frac{F_{\mathrm{a}}^2 L}{2A_{\mathrm{c}}E} = \frac{F^2 L}{2A_{\mathrm{c}}E}\frac{p^2 + 4\pi^2 r^2}{p^2}.$$

The strain energy of bending is obtained from (Hartog 1949, eq. [30d])

$$U = \int_L \frac{M^2}{2EI} dl.$$

Since the moment is a function of the curvature κ of a helix, and the curvature is constant, the expression for the bending energy becomes

$$U_\mathrm{b} = \int_L \left(\frac{(EI\kappa)^2}{2EI} \right) dl = \frac{\kappa^2 EIL}{2}.$$

The curvature κ can be calculated from the expression (Struik 1961, eq. [4-6])

$$\kappa^2 = \mathbf{x}'' \cdot \mathbf{x}''.$$

where **x** is the vector given by the parametric representation of the curve and the double prime $''$ represents the second derivative with respect to the arc-length. Performing these operations yields to

$$\kappa = \frac{4\pi^2 r}{p^2 + 4\pi^2 r^2}.$$

Therefore the bending energy is given by

$$U_\mathrm{b} = \frac{8\pi^4 r^2 EIL}{\left(p^2 + 4\pi^2 r^2\right)^2}.$$

The authors do not consider the term corresponding to torsion because the drillstring is initially straight and the contact between the drillstring and the bore-hole

wall is considered frictionless.

The potential energy of the sole external force *F* is

$$U_{\mathrm{f}} = FL_{\mathrm{h}} + c,$$

where *c* is an arbitrary constant. The height of the force *F* in Figure (2.1) after compression is given by

$$L_{\mathrm{h}} = L_{\mathrm{c}} \sin\theta.$$

Since L_{c} is the length of the drillstring compressed by the force F_{a}, L_{h} is given by

$$L_{\mathrm{h}} = L\left(1 - \frac{F_{\mathrm{a}}}{AE}\right)\sin\theta = L\left(\frac{p}{\sqrt{p^2 + 4\pi^2 r^2}} - \frac{F}{AE}\right).$$

Therefore, the potential energy of the external force is

$$U_{\mathrm{f}} = \frac{FLp}{\sqrt{p^2 + 4\pi^2 r^2}},$$

where the constant *c was* arbitrary set to $c = \frac{F^2 L}{AE}$ for convenience. Whence the total potential energy is

$$U_{\mathrm{T}} = U_{\mathrm{c}} + U_{\mathrm{b}} + U_{\mathrm{f}} = \frac{F^2 L}{2A_{\mathrm{c}}E}\frac{p^2 + 4\pi^2 r^2}{p^2} + \frac{8\pi^4 r^2 EIL}{\left(p^2 + 4\pi^2 r^2\right)^2} + \frac{FLp}{\sqrt{p^2 + 4\pi^2 r^2}}.$$

Stationary values for U_{T} are obtained by making $\frac{\partial U_{\mathrm{T}}}{\partial p}$. Performing this operation yields to

$$\frac{\left(p^2+4\pi^2r^2\right)^3}{AEp^3}F^2-\left(p^2+4\pi^2r^2\right)^{3/2}F+8\pi^2EIp=0.$$

Solving this quadratic equation for *F* and taking the smallest root results in

$$F=\frac{AEp^3}{2\left(p^2+4\pi^2r^2\right)^{3/2}}\left(1-\sqrt{1-\frac{32\pi^2I}{Ap^2}}\right).$$

To solve this expression for *p*, Lubinski used the fact that $p^2\gg 4\pi^2r^2$ and that $\frac{32\pi^2I}{Ap^2}\ll 1$ to write[2]

$$\sqrt{1-\frac{32\pi^2I}{Ap^2}}\simeq 1-\frac{16\pi^2I}{Ap^2},$$

and hence

$$F=\frac{8\pi^2EI}{p^2}. \tag{2.1}$$

It is important to stress that the expression in Equation (2.1) does not calculate the force to buckle the drillstring into a helix. The equation represents the relationship

2 A Taylor's series expansion of $\sqrt{1-x}$ justifies this approximation for small *x*.

between the axial force *F* and the resulting helical pitch *p*. It is assumed that for a given drillstring of length *L*, and for any axial force *F*, the drillstring will buckle into a helix with pitch *p* given by Equation (2.1). From the first work by Lubinski (1950) it is known that a minimum WOB given by

$$WOB_{\text{crit}} = 1.94\sqrt[3]{EIw^2}$$

is required to buckle the drillstring. Below this value, the drillstring is straight and no helix can form. For values above this minimum, the drillstring may or may not buckle into a helix. From the pitch *p*, the force the column exerts along the contact line between the drillstring and the bore-hole wall can be determined.

2.2 The Work of Cheatham and Pattillo

Cheatham and Pattillo (1984) discussed the same ideas for helical buckling under a different point of view. From the same expression for the total potential energy obtained by Lubinski, the derivative with respect to the radius *r* was taken instead of with respect to the pitch *p*. Using the same approximations the relationship obtained is

$$F = \frac{4\pi^2 EI}{p^2}.$$

This expression differs from the Lubinski's result by a factor of two. The reason for this difference rests in the degree of freedom of the system. To minimize the total potential energy using the derivative with respect to *r*, the system may be free to vary in the radial direction. This is not possible during a loading process in which the drillstring must be touching the bore-hole wall along its length. In this case the only freedom is in

the pitch *p*. However, during an unloading process, the radius of the helix may shrink allowing the calculation of the derivative in this direction. Therefore, the two expressions describe theoretical boundaries for the relationship between the force and pitch in a cyclic process of loading and unloading the drillstring, that is

$$F = \begin{cases} \dfrac{8\pi^2 EI}{p^2} \text{ during loading (Lubinski),} \\ \dfrac{4\pi^2 EI}{p^2} \text{ during unloading (Cheatham).} \end{cases}$$

This represents a hysteresis caused by the difference in the degree of freedom of the system during the process, and not by non-conservative forces like friction. However, friction contributes to the hysteresis phenomenon and causes the deviation of the experimental results from the theoretical predictions.

2.3 The Work of Paslay and Bogy

The effects due to the moment applied at the ends and the inclination of the bore-hole was first studied by Paslay and Bogy (1964). In their model it was assumed that the cylindrical rod (drillstring) remains in contact with the bore-hole wall. Until a critical force is reached, the rod rests straight along the lower generatrix of the inclined circular cylinder (the constraint). The energy method was used to obtain the stability limits. Since no final configuration is assumed for the string, the variational method is required in the quest for equilibrium.

To determine the strain energy of the rod for a given restricted field of displacement, the strain tensor ε_{ij} is obtained using a suitable system of cylindrical coordinates which expresses the strain in any point of the rod in terms of the initial

parameters $\overline{R}$, Φ, and Z, and the final position after deformation in terms of ξ, ϕ, and z. The measure of the local deformation is the difference of the scalar product given by (Segel 1977, ch. 4)

$$ds \cdot ds – dS \cdot dS.$$

The strain energy is then calculated from

$$U = \int_{\text{vol}} \left(G\varepsilon_{ij}\varepsilon_{ij} + \frac{G\nu}{1-2\nu}\varepsilon_{ii}\varepsilon_{jj}\, dV. \right. \tag{2.2}$$

The potential energy of the external and body forces is found to be

$$\begin{aligned} \Omega =& P\left(1+\varepsilon_1+\frac{\varepsilon_2}{2}\right)L - M\xi(L) - M\phi(L) + \\ & \int_0^L \rho A g \left\{ \cos\alpha \left(1+\varepsilon_1+\varepsilon_2\frac{Z}{2L}\right) Z + \sin\alpha\overline{R}[(1-\cos\xi)\right\} dZ. \end{aligned} \tag{2.3}$$

The first three terms of Equation (2.3) account for the energy of the external0 force *P*, the energy of moment *M* under circular translation, and the energy of moment *M* under twist. The integral term accounts for the body force due to translation (term with $\cos\alpha$) and due to the effect of *lifting* around the bore-hole wall (term with $\sin\alpha$).

e initially at *Z*, due to loading, is given by

$$z = \left[1 - \frac{P+\rho L}{EA} + \frac{\rho L\cos\alpha}{EA}\frac{Z}{2L}\right]Z = \left(1+\varepsilon_1+\varepsilon_2\frac{Z}{2L}\right)Z.$$

The total potential energy is then given by

$$V = U + \Omega.$$

The conditions for stability are obtained from the analysis of the first and second variations of *V*, namely,

$$\delta V = 0, \quad \delta^2 V > 0.$$

As long as these conditions are satisfied the equilibrium configuration is stable. Therefore a loading state is investigated which makes the system unstable. Since the second variation was found positive definite, the only chance of instability occurs when the cross sections of the rod translate relative to the cylinder. After considering the second variation of *V*, Paslay and Bogy came up with a differential equation in the variation $\delta\xi$ which governs the limit of stability for the system expressed as

$$(1-\nu)EI\overline{R}^2\delta^4\xi + \overline{R}^2\left[P + \rho Ag\cos(\alpha)(L-Z)\right]\delta^2\xi \\ - \rho Ag\overline{R}^2\cos(\alpha)\delta\xi + (1-\nu)\rho Ag\overline{R}\sin(\alpha)\xi = 0,$$

with boundary conditions given by

$$\delta\xi(0) = \delta\xi(L) = \delta^2\xi(0) = \delta^2\xi(L) = 0.$$

An approximate solution of this differential equation was written using a finite sine series which satisfies the boundary conditions:

$$\delta\xi = \sum_{n=1}^{k} \xi_{0_n} \sin\left(\frac{n\pi Z}{L}\right).$$

Using this solution an expression for the second variation was obtained.

Three cases were analyzed by the authors. The most important case is the horizontal configuration. The critical force was found to be

$$P_{\text{crit}}(n) = (1 - \nu)EI\frac{\pi^2}{L^2}\left[n^2 + \frac{1}{n^2}\frac{L^4 \rho A g}{\pi^4 EI\overline{R}}\right], \tag{2.4}$$

where

$$E = \frac{2G(1-\nu)}{1-2\nu}.$$

It is important to stress that Paslay and Bogy's model is a *sinusoidal model*. At no moment it is assumed that the final configuration is a helix. The geometric assumption is that the rod remains in contact with the bore-hole wall during the buckling process. The critical force obtained is that in which the equilibrium of the straight rod is no longer stable.

2.4 The Work of Dawson and Paslay

Dawson and Paslay (1984) used the results from Paslay and Bogy for horizontal configurations to generalize for inclined holes. Some restrictions however apply to their process of generalization.

Starting with the expression for the critical force in Equation (2.4), the influence of the inclination was introduced on the magnitude of the distributed mass ρ and obtained

$$P_{\text{crit}}(n) = (1-\nu)EI\frac{\pi^2}{L^2}\left[n^2 + \frac{1}{n^2}\frac{L^4\rho Ag\sin\alpha}{\pi^4 EI\overline{R}}\right]. \tag{2.5}$$

However, Equation (2.4) was obtained by setting the angle α to 90° in a more general expression which eliminated the terms in $\cos\alpha$. (See Equation (2.3).) These terms account for the axial effect of the distributed weight on the behavior of the drillstring. When the angle was reintroduced, these terms were not recovered and the final expression has no means to account for the axial effect of the distributed weight. This restriction does not apply to horizontal bore-holes and has been used by several investigators. However, it does apply for inclined bore-holes and, in particular, for the two models for curved bore-holes occurring in the literature.

The buckling mode number n in Equation (2.5) is an integer number by nature. However, since n^2 enters in the equation in a direct and an reciprocal fashion, the value of *n* which minimizes the expression depends on the value of the fraction inside brackets, in particular the value of L. For long drillstrings the term in $\frac{1}{n^2}$ may be significant compared with n^2 and the minimum critical force may be different from that for $n=1$. To handle this, Dawson and Paslay assumed that *n* could be treated as a continuous variable (not restricted to integer values). Taking the derivative of the critical force with respect to n and setting the result to zero they obtained the expression for the value of n^2 which minimizes the critical force:

$$n^2 = \left(\frac{L^4\rho Ag\sin\alpha}{\pi^4 EIr}\right)^{1/2}.$$

The value of n so calculated will seldom be an integer. However, substituting back into the expression for the critical force a formula independent of n and L follows:

$$P_{\text{crit}} = 2(1-\nu)\left[\frac{EI\rho Ag\sin\alpha}{r}\right]^{1/2}, \tag{2.6}$$

where $r = \overline{R}$ is the radial clearance.

Equation (2.6) is not the final expression derived by Dawson and Paslay. In most models for bending and buckling some assumptions are made to reduce the mathematical complexity of the problem. Some of the assumptions are those associated with *thin geometry* in the Euler-Bernoulli beam theory (Segel 1977, ch. 5).

In the Euler-Bernoulli beam theory, lateral deformations due to Poisson's ratio are small compared to the deformations due to bending and are, therefore, neglected. This represents the implicit assumption that $\nu = 0$. As a result all lateral displacements are perpendicular to, and the same as that of the center line, and the expression for the strain energy (Equation (2.2)) reduces to

$$U = \frac{E}{2}\int_{\text{vol}} \varepsilon_{ij}\varepsilon_{ij} dV.$$

Assuming $\nu = 0$, Dawson and Paslay arrived at the following expression:

$$F_{\text{crit}} = 2\left[\frac{EI\rho Ag\sin\alpha}{r}\right]^{1/2}. \tag{2.7}$$

In a paper to be discussed later, Wu and Juvkam-Wold (1993) derived Equation (2.7) for $\alpha = 90^\circ$ considering only the strain energy associated to bending. By using the strain energy associated with bending, and consequently Euler-Bernoulli beam theory, the derivation assumes intrinsically that $\nu = 0$ Nevertheless, it is important to stress that the critical force as given by Equation (2.7) does not completely account for

the effect of the inclination and should be used with restrictions when inclination is present.

2.5 The Work of Kwon

Kwon (1988) presented an analysis which extended the work of Lubinski (1962) for helical buckling. In that work, Lubinski developed a model for weightless drillstrings. The results for weighted drillstrings were developed only to the extent of calculating the shortening ΔL_2 of the drillstrings due to the helical buckling.

Kwon determined the varying helix pitch and other parameters, in particular the tool clearance[3] using the generalized beam-column equation[4] expressed by

$$EI\frac{d^4\vec{u}}{dz^4} - F_e\frac{d^2\vec{u}}{dz^2} - W\frac{d\vec{u}}{dz} - \vec{Q} = 0. \tag{2.8}$$

This equation was obtained by introducing a term to account for the distributed weight into the differential equation for weightless pipes originally attributed to Mitchell (1982). Equation (2.8) does not consider the distributed weight in an appropriate way. The displacement vector $\vec{u}$ has components $(u_{\mathrm{x}}, u_{\mathrm{y}})$ and it also does not consider the axial displacement u_{z} and consequently the effect on the potential energy due to this displacement. As a result, the differential equation does not include a term of the form

$$W(L-z)\frac{d^2\vec{u}}{dz^2},$$

3 The clearance between the internal diameter of a curved hole and the diameter of a cylindrical tool of given length required for free movement inside the hole.

4 This equation is not the equation of same name to be derived in Chapter 4.

as it would if the displacement u_z had been considered.

Kwon expressed the displacement vector in a constrained polar coordinate system and obtained a nonlinear differential equation which describes the polar angle θ of a point in the helix as function of the depth *z*:

$$\frac{d^4\theta}{dz^4} + \left[\frac{F_e}{EI} - 6\left(\frac{d\theta}{dz}\right)^2\right]\frac{d^2\theta}{dz^2} - \frac{W}{EI}\frac{d\theta}{dz} = 0.$$

An approximate solution to this equation was obtained as a finite power series of the form

$$\theta(z) = b_0 + b_1 z + b_2 z^2 + b_3 z^3 + b_4 z^4.$$

The pitch relates locally to θ(*z*) by

$$\frac{2p}{p} = \frac{d\theta}{dz} = b_1 + 2b_2 z + 3b_3 z^2 + 4b_4 z^3 = a_0 + a_1 z + a_2 z^2 + a_3 z^3.$$

Applying the expression for $\frac{d\theta}{dz}$ into the nonlinear differential equation and using appropriate boundary conditions, Kwon obtained the expressions for the coefficients $\{a_i, i=0..3\}$ in terms of F_e, *E*, *I*, *L*, and *W* and consequently a formula for the helix pitch *p*(*z*).

2.6 The Work of Chen, Lin and Cheatham

A study for sinusoidal and helical buckling for horizontal bore-holes (again incorrectly extended for inclined bore-holes) was performed by Chen, Lin and Cheatham

(1990). Using an intermediary expression[5] for the critical force by Dawson and Paslay (1984) with $\alpha = 90°$, an expression analogous to the expression for buckling of beams on elastic foundations was found:

$$\frac{P_{\text{crit}}}{\sqrt{kEI}} = \left(n\frac{\pi}{\sqrt{2}\xi L}\right)^2 + \left(\frac{1}{n}\frac{\sqrt{2}\xi L}{\pi}\right)^2, \tag{2.9}$$

where $\xi = \sqrt[4]{\frac{k}{4EI}}$ and $k = \frac{w}{r}$.

While investigating this expression, an analysis by Hartog (1952) was used to obtain the buckling mode. This analysis was proved to be wrong and corrected in the discussion of the paper by Wu and Juvkam-Wold (1990). Hartog's analysis concluded that it is immaterial if a beam buckles with one half-wave of length A_2 or two half-waves of length $A_1 = A_2/2$ when the dimensionless length of the beam corresponds to A_2 (Figure [2.2]). Using the same reasoning, when the dimensionless length of the beam corresponds to B_2, the same critical force buckles the beam with one half-wave of length B_2 or three half-waves of length $B_1 = B_2/3$. Working inductively Hartog came out with an inequality to determine the buckling mode given by

$$\sqrt{n} \leq \frac{\sqrt{2}}{\pi} \leq \sqrt{n+1}.$$

This is the same inequality used by Chen, Lin and Cheatham.

However, as shown in Figure (2.2), the force required to buckle the beam with two half-waves of length $B_2/2$ is considerably smaller than the force required to buckle it with one or three half-waves. For a beam with length corresponding to D_2, for example,

5 The expression obtained before the determination of n which minimizes the critical force, however using $\nu = 0$.

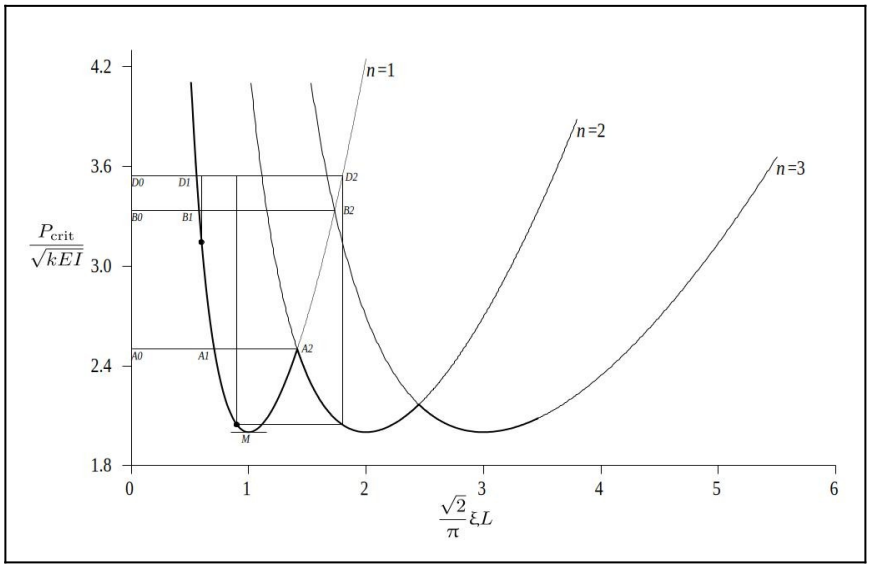

Figure 2.2: Buckling force of a beam on an elastic foundation

although the force required to buckle the beam with three half-waves is smaller then the force required to buckle it with one half-wave, as predicted by Hartog's inequality, the force required to buckle it with two half-waves is still smaller and the correct one.

The correct inequality to determine the buckling mode was obtained by Wu and Juvkam-Wold by algebraic manipulation of Equation (2.9), and is given by

$$\sqrt{n-1}\sqrt{n} \leq \frac{\sqrt{2}}{\pi}\xi l \leq \sqrt{n}\sqrt{n+1}.$$

When the buckling mode *n* is determined, the sinusoidal critical force is calculated using Equation (2.9). The length of the half-wave *l* is given by

$$l = \frac{L}{n}.$$

Nevertheless, for long beams, the sinusoidal critical force calculation presented by Chen, Lin and Cheatham, and given also by Hartog, namely

$$F_{\mathrm{s}} = 2\sqrt{EIw/r},$$

represents a minimum which will be obtained only for beams with integer dimensionless lengths or very long beams.

The expression for the critical force obtained by Chen, Lin and Cheatham is the same expression derived by Dawson and Paslay, Equation (2.7), except for the factor $\sin\alpha$. The two results could not be different because they originate from the same initial expression. For lengths other than the dimensionless length, Equation (2.9), should be used. This equation reduces to the equation for integer dimensionless lengths, since

$$\frac{1}{n}\frac{\sqrt{2}\xi L}{p} = 1.$$

The expression for helical buckling was obtained using energy balance. Assuming that the drillstring initially rests straight in the lower generatrix of the horizontal bore-hole and that under axial force it buckles into a helix, the increase in the potential energy plus the strain energy equals the work done by the compressive force. This statement is expressed as

$$wLr + \frac{8\pi^4 EILr^2}{(L/n)^4} = \frac{2\pi^2 Lr^2}{(L/n)^2}F_{\mathrm{h}},$$

where *n* is the number of periods of the helix. The potential energy is obtained by considering that, for a horizontal helix, the drillstring is raised, on average, by an amount equal to the radius r of the cylinder. Solving for F_h and treating n as a continuous

variable the minimum value for F_h is determined and given by

$$F_{\mathrm{h}} = 2\sqrt{2}\sqrt{EIw/r} = \sqrt{2}F_{\mathrm{s.}}$$

Therefore, according to the analysis from Chen, Lin and Cheatham, the critical forces for sinusoidal and for helical buckling are related by the constant $\sqrt{2}$.

2.7 The Work of Schuh

The first published work to study buckling in curved bore-holes was presented by Schuh (1991). He proposed a method for determining the critical buckling force in curved bore-holes, the bending stresses along the drillstrings, and the effect of the tool-joints. The idea is to take an expression for buckling in a straight bore-hole and apply a geometric correction to account for the curvature.

According to Schuh, the first issue concerns the choice of the formula for the critical force between two conflicting formulas. He decided to use the Dawson and Paslay formula over the Chen, Lin and Cheatham formula for reasons to be discussed later. I point out however that no conflict exists. Cheatham has two models, as discussed before, one for sinusoidal buckling and one for helical buckling. The model of Dawson and Paslay is a sinusoidal model considering that it is derived from the model of Paslay and Bogy. As mentioned before both the sinusoidal model of Chen, Lin, and Cheatham and the model of Dawson and Paslay furnishes the very same critical force.

The sinusoidal model is a better choice because the calculations using this model show that “the pipe to wall contact force that exists at the top of the helix” is exactly zero and any slight decrease in the axial force will make the drillstring return to its unbuckled configuration. Therefore it calculates the unloading buckling force.

Schuh suggests modifying the value for the clearance *r* between the drillstring and the bore-hole wall to account for the curvature of the bore-hole. A subtractive factor Δ*r* is introduced such that the expression for the critical force becomes:

$$F_{\mathrm{c}} = 2\sqrt{\frac{EIw\sin\theta}{r-\Delta r}}.$$

According to Schuh, Δr is positive for building bore-holes and negative for dropping bore-holes.

In my opinion, however, the difference in the critical force between building and dropping bore-holes is not due to a geometric effect but to the distributed weight w. Moreover, the geometric effect does not depend if the bore-hole angle is building (increasing) or dropping (decreasing), and only positive values for Δr should be used. The curved geometry always increases the critical force compared with the straight case. Figure 6 in Schuh's paper should, therefore, be a horizontally symmetric image of Figure 2 of the same paper.

Based on Figure 8 of the paper, I concluded that the term Δr is the sag of a circle with radius of curvature ρ=1/*b* and chord *p*/2 (half of the pitch). The following relation exists for the length of the arrow:

$$\Delta r = \rho - \sqrt{\rho^2 - \frac{p^2}{16}} = \rho\left(1 - \sqrt{1 - \frac{p^2}{16\rho^2}}\right).$$

For small clearance r compared to ρ, the ratio inside the square root is small and the following approximation applies:

$$\Delta r = \rho\left(1 - \sqrt{1 - \frac{p^2}{16\rho^2}}\right) = \frac{p^2}{32\rho} = \frac{bp^2}{32}.$$

This expression, along with the expression for the pitch derived by Lubinski (Equation[2.1]), and the modified formula for sinusoidal critical force yields to

$$F_c^2 = \frac{4EIw\sin\theta}{r - \Delta r} = \frac{4EIw\sin\theta}{r - \frac{bp^2}{32}} = \frac{4EIw\sin\theta}{r - \frac{b}{4}\frac{\pi^2 EI}{F}} = \frac{16F_c EIw\sin\theta}{4rF_c - b\pi^2 EI}.$$

Solving for the curvature *b* results in

$$b = \frac{4rF_c}{p^2 EI} - \frac{16w\sin\theta}{p^2 F_c}.$$

This is the expression obtained by Schuh (omitting some unit conversions) which relates the curvature of the bore-hole b to the critical force F_c.

There is an inaccuracy in the model. The half-pitch $p/2$ is not the correct length of the chord for use in calculating the arrow Δr. The boundary conditions at the tangency points require that the chord be longer than $p/2$. This results in a larger value for Δr and, consequently, a larger value for the critical force. This increased chord length enters in the formulation as a square which further intensifies the inaccuracy of the calculations.

2.8 The Work of Adrichem and Newman

In a paper dedicated to coiled-tubing penetration predictions, Adrichem and Newman (1992) mentioned an effect that influences the critical force for coiled-tubing

running into curved bore-holes. A pipe in a curved bore-hole tends to remain *seated* against the outer generatrix of the bore-hole. To unseat the pipe a much larger compressive force is required. They did not present the model formulation for this case although they mentioned that a full theory for handling the effect of bore-hole curvature was being developed. It is not clear in the article who is developing the theory, but to my knowledge such a theory has not been presented to date.

In my opinion, the effect of the curvature is analogous to that occurring in an arch, namely, that the higher the loading the more stable the structure becomes. The structure fails either by compression or because it is allowed to deflect perpendicularly to the plane of the loading.

2.9 The Work of He and Kyllingstad

A paper related to coiled-tubing by He and Kyllingstad (1993) introduces a so-called improved formula for the critical buckling force of a drillstring in curved bore-holes. The first assertion presented is that the use of the straight formulation from Dawson and Paslay for sinusoidal buckling, and from Chen, Lin and Cheatham for helical buckling, will result in values too conservative, that is, much lower than the field data indicates.

The effect of increasing the critical buckling force because of the curvature had already been considered to some extent. He and Kyllingstad realized that the distributed lateral force term $w \sin\theta$ in the formula for sinusoidal and helical buckling does not represent the actual distributed force occurring along the contact line for a curved bore-hole.

When a weightless and perfectly flexible rope is wound around a frictionless circular surface and tensioned by a force F, the distributed inwards radial force f_r is given

by (capstan effect)

$$f_{\mathrm{r}} = \frac{F}{\rho} = F\theta'.$$

where ρ is the radius of curvature of the circular surface. The same expression is valid when a drillstring is tangentially compressed against the internal circle of a cylindrical surface, although the radial distributed force now points outwards.

The outwards distributed force *w* adds to the distributed force due to the curvature, which results in the following distributed force acting radially at a point of inclination θ along the curved bore-hole:[6]

$$f_{\mathrm{rt}} = w\sin\theta + F\theta'.$$

In addition, the change in azimuth will generate a distributed force f_s, perpendicular to f_{rt} given by

$$f_{\mathrm{s}} = F\varphi'\sin\theta.$$

Therefore, a total distributed force f_{n} results from the composition of these two orthogonal terms, and is given by

$$f_{\mathrm{n}} = \sqrt{f_{\mathrm{rt}}^2 + f_{\mathrm{s}}^2}.$$

6 The derivative here is with respect to the arc length.

Now, when f_{n} replaces $w\sin\theta$ in the expression for the critical buckling force the expression becomes

$$\left(\frac{F}{F_{\mathrm{s\vee h}}}\right)^4 = \left(1+\frac{F_{\mathrm{s\vee h}}\theta'}{w\sin\theta}\frac{F}{F_{\mathrm{s\vee h}}}\right)^2 + \left(\frac{F_{\mathrm{s\vee h}}\phi'}{w}\frac{F}{F_{\mathrm{s\vee h}}}\right)^2.$$

$F_{\mathrm{s\vee h}}$ means that either the sinusoidal (unloading) or the helical (loading) critical force may be used. Making $F_{\mathrm{n}} = \frac{F}{F_{\mathrm{s\vee h}}}$, $a_1 = \frac{F_{\mathrm{s\vee h}}\theta'}{w\sin\theta}$, and $a_2 = \frac{F_{\mathrm{s\vee h}}\varphi'}{w}$, yields to

$$F_{\mathrm{n}}^4 = (1+a_1F_{\mathrm{n}})^2 + (a_2F_{\mathrm{n}})^2.$$

The new parameters F_{n}, a_1, and a_2 are called respectively normalized critical buckling force, normalized inclination change gradient, and normalized azimuth change gradient. For known a_1 and a_2, the smallest positive root of this quartic equation gives the critical force of a drillstring within a curved bore-hole.

Experimental results show agreement with the model and support the idea that the curvature will increase the buckling resistance of the drillstring. Nevertheless, some restrictions apply to this model. The first is the use of the Dawson and Paslay model for inclined straight bore-hole and its inherent limitations. The second is an apparently contradictory relationship between the distributed force due to the curvature and the resistance to buckling.

In a building bore-hole, the distributed weight *w* contributes to an increase in the resistance to buckling because an amount of work is spent to raise the column in average a height equal to the clearance *r*. The distributed force due to the curvature f_{n} will require additional work to raise or displace it the same amount *r*. This means that the higher the distributed force due to the curvature, the more stable the column becomes. Therefore, for a given curvature, if the axial force is increased to a value close to the critical force, an

additional increase will make the column more stable. From all this, I conclude that the relationship between curvature and buckling force requires a more careful analysis.

2.10 The Work of Wu and Juvkam-Wold

Wu and Juvkam-Wold (1993) obtained an expression for a sinusoidal critical force identical to that derived by Dawson and Paslay, and by Chen, Lin and Cheatham for horizontal bore-holes but, apparently, independent of the results of Paslay and Bogy. Dawson and Paslay restricted the Paslay and Bogy expression for the critical force by assuming that Poison's ratio equals zero. Wu and Juvkam-Wold used the theory of bending, or the Euler-Bernoulli beam theory, which implicitly assumes that Poisson's ratio is equal to zero (Segel 1977, ch. 5), to obtain an expression for the sinusoidal critical force. The Dawson and Paslay expression, and the Wu and Juvkam-Wold expression are the same because in both cases Poisson's ratio is assumed equal to zero.

The importance of the Wu and Juvkam-Wold paper is in the analysis of the formula for helical buckling obtained by Chen, Lin and Cheatham, namely

$$F_{\mathrm{h}} = 2\sqrt{2}\sqrt{EIw/r} = \sqrt{2}F_{\mathrm{s}}.$$

In the energy equation used to derive this equation the term expressing the work done by the axial force assumes that this force remains constant during the loading process.

The loading process starts with the column resting on the lower generatrix of the horizontal bore-hole. When the axial force reaches the critical helical force it buckles into a helix. Based on experimental results, Wu and Juvkam-Wold claim that before the column buckles into a helix it buckles into a sinusoidal shape and then, with *increasing axial force,* it turns into a helix. Therefore the force inside the integral of the work is not constant and cannot be moved outside the integral.

Keeping the expression for the work in the integral form and proceeding exactly in the same way as Chen, Lin and, Cheatham, they obtained

$$\frac{1}{\delta}\int_0^{\delta} F(u)du = \overline{F_{\mathrm{h}}} = \sqrt{2}F_{\mathrm{s}}.$$

Consequently, the force obtained by Chen, Lin, and Cheatham represents the average force during the buckling process. The integral cannot be evaluated because the expression for the force $F(u)$ is unknown during the process. The only information known is that $F(0) = F_{\mathrm{s}}$ and $F(\delta) = F_{\mathrm{h}}$.

From experimental results, Wu and Juvkam-Wold suggest that the force $F(u)$ increases linearly during the process. Therefore one can write:

$$F(u) = F_{\mathrm{s}} + (F_{\mathrm{h}} - F_{\mathrm{s}})\frac{u}{\delta}.$$

Using this expression in the integral and solving for F_{h} yields to

$$F_{\mathrm{h}} = (2\sqrt{2} - 1)F_{\mathrm{s}}.$$

This study can be improved further. Since the axial force does not remain constant during the entire buckling process (sinusoidal and helical), a term accounting for the compressive energy must be included in the energy equation. Part of the work produced by the axial force is transformed into elastic energy of compression and the final force to keep the column helically buckled will be larger than that obtained by Wu and Juvkam-Wold. Support for this idea comes from the results obtained by Heisig (1995) using the finite element method.

2.11 The Work of Heisig

Heisig's buckling model uses a 3D "flexural-torsional-extensional" beam element which should account for the varying axial force during the process of buckling. Results obtained using the model agree very well with theory for vertical bore-hole. For horizontal bore-holes, however, the transition from sinusoidal into helical buckling occurred for axial forces given by

$$F_{\mathrm{h}} = 2.3F_{\mathrm{s}},$$

a value about 26% larger than that obtained by Wu and Juvkam-Wold. For an unbuckling process, the transition from helical into sinusoidal buckling occurred for axial forces given by

$$F_{\mathrm{h}} = 1.3F_{\mathrm{s}}.$$

These two results characterize a phenomenon of hysteresis in a loading-unloading process similar to that presented earlier by Cheatham and Pattillo for a vertical case. Non-conservative forces such as friction are neglected in the numerical model. Hysteresis, in this case, occurs due to difference in the degree of freedom that exist during loading and unloading, and not from non-conservative forces.

Heisig's paper shows different patterns for different axial forces during loading and unloading processes. Sinusoidal and helical configurations are shown, as expected from analytical models. Heisig called configurations with pitch reversals "chaotic". These pitch reversals had been noticed by other investigators in experimental analysis (He and Kyllingstad 1993, Salies, Azar and Sorem 1995, Suryanarayana and McCann 1995).

This “chaotic” configuration is not an unexpected result. It is a possible solution for a sinusoidally buckled drillstring which, under large axial force, behaves and buckles as a plate inside the bore-hole. To facilitate the understanding one can draw a sine curve on a clear plastic sheet and roll it along its axis to obtain pitch reversals similar to the “chaotic” configuration mentioned by Heisig.

When a sinusoidal configuration starts to form in the lower generatrix of the horizontal bore-hole, the waves must “climb” the wall of the cylinder. If this climbing continues without the drillstring snapping into a helix the “chaotic” configuration is reached. The helical buckling force obtained by Heisig during an unloading process is almost half of that obtained during loading, which is even smaller than the expected helical critical force as given by Chen, Lin and Cheatham.

The finite element method simulation does not produce an analytical expression and depends on some criteria to determine when the drillstring buckles. These criteria, not explained by Heisig, should use numerical results from simulations. The interpretations of the numerical results may vary between investigators.

2.12 The Work of Salies, Azar and Sorem

The unloading buckling force from Heisig should be compared with the results obtained by Salies, Azar and Sorem (1995). The work presents results from several experiments along with numerical simulation using finite element method, and an analytical solution for helical buckling in horizontal bore-holes. The expression derived by Salies, Azar and Sorem for the helical critical force is the same obtained previously for the sinusoidal critical force, namely,

$$F_{\mathrm{h}} = 2\sqrt{\frac{EIw}{r}} = F_{\mathrm{s}}.$$

Based on experimental analysis it is stated that when the sinusoidal critical force is reached, the drillstring will buckle into a sinusoidal shape, and if the force is sustained, the drillstring will continually deform into a helix with virtually no change in the axial force. When a complete helix is formed, that is, when the drillstring touches the bore-hole wall along its whole length, any additional displacement will require an increase in the axial force with a corresponding increase in the contact force between the drillstring and the bore-hole wall. This statement goes against the experimental results from other investigators which support that the transition between sinusoidal and helical buckling is not continuous but occurs with snap-through jumps and with an increase in the axial force.

To determine the critical buckling force, Salies, Azar and Sorem established a reasonable criterion to characterize the helical buckling. The criterion states that, since the transition occurs continuously, the instant a complete helix is formed is defined by the moment the drillstring just touches the upper generatrix of the bore-hole without exerting any pressure at that point. Therefore, if the expression for the radial contact force (as a function of the axial force) is known, the helical critical force is obtained by solving the expression when the contact force equals zero on the upper generatrix. The same criterion had already been used by Schuh. It is expected that the critical force obtained is the same as the sinusoidal critical force because the model is based on the behavior exhibited in the transition between sinusoidal and helical.

The expression for the radial contact force is determined using the theorem of virtual work. The total potential energy is obtained for a virtual displacement of one end, expressed in terms of the pitch of the helix. The total potential energy is given by

$$E_{\mathrm{t}} = \frac{8\pi^4 r^2 EIL}{p^4} - \frac{2\pi^2 r^2 L}{p} F + wrL,$$

which uses the same terms already calculated by other investigators. The pitch p is the only real degree of freedom in this expression, but to calculate the radial contact force one needs a virtual displacement in the radial direction.

I stress here that the expression for the total potential energy, as given, assumes a fully developed helix. The force F is any axial force larger than the critical axial force (not yet determined), and the pitch *p* is any pitch related to a virtual displacement of the force F. These facts were not mentioned by the authors.

The relationship between the axial force F, and the pitch p, found previously, is obtained when the total potential energy is stationary and given by

$$\frac{\partial E_{\mathrm{t}}}{\partial p} = 0.$$

Performing that operation, it is found that

$$F = \frac{8\pi^2 EI}{p^2}.$$

Now the total potential energy can be written in terms of p and r only:

$$E_{\mathrm{t}} = wrL - \frac{8\pi^4 r^2 EIL}{p^4}.$$

The radial contact force was calculated by Salies, Azar, and Sorem, using the theorem of virtual work which is not appropriate in this case. The expression used to obtain the radial force was:

$$\frac{\partial E_{\mathrm{t}}}{\partial p} = F_{\mathrm{lat}}.$$

The variable r can only be used as a direction to absorb work if the problem is symmetric, which is not the case because of the distributed weight w. Although the final relation is correct, the procedure used was not canonical.

The distributed weight in the radial contact force only has an additive vertical component. The correct way to obtain the final expression for radial contact force is by assuming that the drillstring is initially weightless (in this case the problem becomes symmetric), and afterward include the effects of the distributed weight. For a weightless drillstring the total potential energy is

$$E'_{\mathrm{t}} = -\frac{8\pi^4 r^2 EIL}{p^4}.$$

In the mathematical expression for the theorem of virtual work, the direction of both the virtual displacement and the external force must be compatible. Since the radial external force (the action of the bore-hole wall on the drillstring) acts inward and the radial direction is an outward variable, the correct expression for the theorem of the virtual work is

$$\frac{\partial E'_{\mathrm{t}}}{\partial r} = -F'_{\mathrm{lat}}.$$

Using this expression yields to

$$F'_{\mathrm{lat}} = \frac{16\pi^4 rEIL}{p^4}.$$

If p^2 is expressed in terms of the axial force F and substituted into the last equation the result is

$$\frac{F'_{\mathrm{lat}}}{L} = \frac{F^2 r}{4EI},$$

which is the expression for the radial distributed contact force obtained previously by Mitchell (1988). Now the effect of the distributed weight is added. Since the distributed weight acts vertically, only the radial component adds to the radial distributed weight. The final expression is, therefore, given by

$$\frac{F_{\mathrm{lat}}}{L} = \frac{16\pi^4 rEI}{p^4} + w\cos\beta,$$

where β is the polar angle of r measured from the lower generatrix of the horizontal bore-hole.

Using this expression along with the helical buckling criterion (zero contact force at the upper generatrix of the bore-hole) results in

$$\left(\frac{F_{\mathrm{lat}}}{L}\right)_{\beta=180^\circ} = 0 = \frac{16\pi^4 rEI}{p^4} - w.$$

Solving for p^2 and substituting into the expression for the axial force gives

$$F_{\mathrm{h}} = 2\sqrt{\frac{EIw}{r}} = F_{\mathrm{s}}.$$

My interpretation for this result is similar to the interpretation for the results obtained by Cheatham and Pattillo. The helical critical force so obtained represents the

minimum axial force required to keep the drillstring helically buckled during an unloading process. Again, the freedom required to calculate the derivative of the total potential energy with respect to the radial clearance can only be obtained in an unloading process. Using this interpretation the helical critical force is, to some extent, compatible with the results obtained by Heisig.

2.13 The Work of Suryanarayana and McCann

The final work discussed is the experimental study presented by Suryanarayana and McCann (1995). Through experimentation they tried to qualify and describe the effects of important factors on drillstring buckling, in particular friction (and its connection with hysteresis, snap-through and pitch reversals), radial clearance, inclination, and curvature.

Experimental data suggest that the hysteresis is mainly a consequence of non-conservative forces like friction. To evaluate models that do not include friction it is required that the experiments minimize the friction between the moving elements.

To minimize friction it is common to make use of smooth surfaces, lubricants, and high frequency vibrations. It is difficult to experimentally validate models which incorporate friction because of the formidable task of controlling all variables affecting friction, but it is possible to predict its effects and in which direction the experimental results will deviate from the theoretical predictions. Apart from the quantification of these deviations and their effects on real behavior, the analysis made by Suryanarayana and McCann presents a very lucid discussion of the subject, in particular, the strong influence of hysteresis during a cyclic process of loading and unloading.

Is my opinion that hysteresis is comprised of at least three components. One component is friction. The others are the difference in the degree of freedom during

loading and unloading, and geometric effects. Finite element simulations where friction is neglected still show hysteresis, supporting the conclusion that hysteresis is caused not only by friction. The effect of the number of degrees of freedom has already been discussed and is fundamental in obtaining expressions for critical force. Models in which the potential energy is minimized by taking derivatives with respect to the radial clearance require freedom in the radial direction. This freedom exists only during unloading processes.

The geometric effect is nonexistent for straight bore-holes but is extremely evident in curved bore-holes. During the loading process of buckling a drillstring within a curved bore-hole, the natural tendency is for the drillstring to displace outwards. This is prevented by the bore-hole wall. This tendency must be overcome in order for buckling to occur. Therefore, the drillstring must buckle *inwards*. To buckle inwards an extra amount of energy is required to force the drillstring to cross an unstable region between the two stable equilibria. This extra amount of energy is noticed as snap-through behavior. This snap-through does not exist during unloading because when the drillstring unbuckles, the natural tendency is also to unbuckle with outward displacements. In this moment, no restrictions are imposed by the bore-hole wall. Intuitively, when the drillstring buckles, it reaches a stable equilibrium in which the lateral force acting in the inner constraint is greater than zero. This non-zero lateral force is associated with an axial force in the same fashion as for straight holes. The drillstring, however will not unbuckle until this inner lateral force becomes zero, which is associated with a smaller axial force. This characterizes hysteresis in the loading-unloading cycle. The total hysteresis is composed of these three components added together. The relative weight of each component varies for different configurations. Frictional hysteresis is dominant for straight and slightly curved bore-holes. Geometrical hysteresis is dominant for medium and highly curved bore-holes. Hysteresis due to number of degrees of freedom is always present but probably overshadowed by the two other components.

Chapter 3

The Trigonometric Model
And The
Curved Bore Hole Theory

The simplest case of buckling of a drillstring within curved bore-holes is that for a weightless drillstring. The model developed in this chapter is not complete as it does not consider either friction or distributed weight. Consequently, the effect of the inclination upon the critical force and upon the final shape of the buckled drillstring cannot be assessed. Still, the model furnishes good approximations for the buckling forces.

The most important facts in the development of this model are: (1) the understanding of the geometric effects of the constraints, (2) the establishment of a procedure for solving the problem, and (3) to serve as an initial guess to start the iterative process which will be used in the hypergeometric model. The solution is based on trigonometric functions resulting from the application of Euler column theory for buckling. The use of trigonometric functions allows a fast approximation for the solution of the problem.

3.1 Buckling of Weightless Columns under Static Compressive Axial Force

The Euler-Bernoulli beam theory, on which most of the mathematical models for beam and columns are based, assumes that plane cross sections perpendicular to the axis of the beam before the displacement, remain plane and perpendicular to the axis after deformation (Reddy 1993). Under this assumption, and also assuming that the curvature

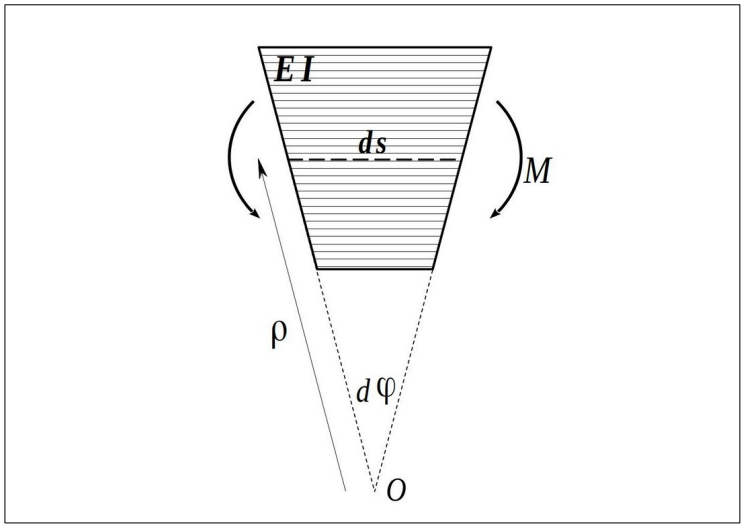

Figure 3.1: Bending of a beam element

at any point of the center line depends only on the magnitude of the bending moment at that point (Timoshenko 1958, part II), the angle $d\varphi$ between two faces of an infinitesimal element of length *ds* and stiffness EI, subjected to a bending moment M, is given by (Figure [3.1])

$$\frac{d\varphi}{ds} = \frac{M}{EI} = \frac{1}{\rho}. \tag{3.1}$$

where ρ is the radius of curvature of the center line of the element. The angle φ relates to $y(x)$ by

$$\varphi = \arctan\left(\frac{dy}{dx}\right). \tag{3.2}$$

If s is the arc length measured along the column, one obtains

$$\frac{dx}{ds} = \frac{1}{\sqrt{1+\left(\frac{dy}{dx}\right)^2}}. \tag{3.3}$$

Substituting Equations (3.2) and (3.3) into Equation (3.1) results immediately in the following nonlinear differential equation:

$$\frac{\frac{d^2y}{dx^2}}{\left[1+\left(\frac{dy}{dx}\right)^2\right]^{3/2}} = \frac{M}{EI}. \tag{3.4}$$

For small displacements and consequently small slopes, this nonlinear differential equation may be approximated by the linear differential equation

$$\frac{d^2y}{dx^2} = \frac{M}{EI}. \tag{3.5}$$

Equation (3.5) is the basic differential equation for bending.

The *trigonometric model* is developed using Euler column theory which consists of the analysis of the possible solutions of a slender, homogeneous, straight, constant cross-sectional column, with pinned-ends, subjected to a compressive axial force applied at the center of gravity at the ends. Figure (3.2) shows a slender column under axial force. The axial force is conservative because the direction of the line of action does not change during the process. By conservative, it is understood that the work done by the external forces is independent of the path between any two possible configurations (Langhaar 1989).

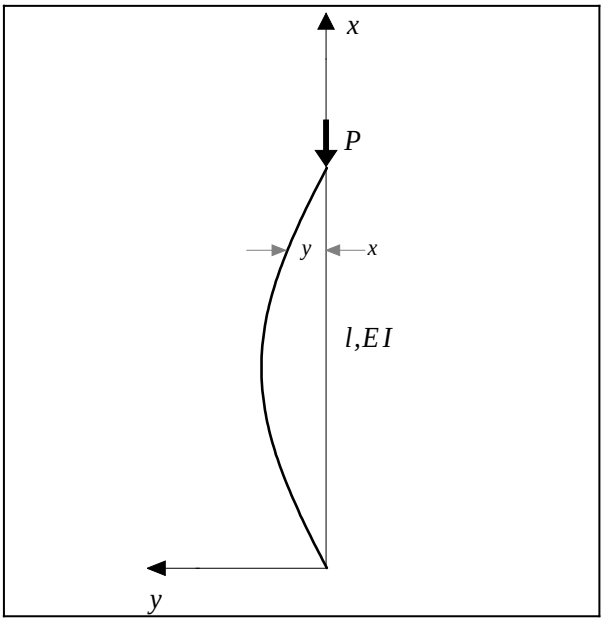

Figure 3.2: A slender column buckling under axial compressive force.

The analysis of the phenomenon of buckling of such a column was first studied by Leonard Euler (1744). The moment M at any point x along the column in Figure (3.2) is given by $M = -Py(x)$. Substituting into Equation (3.5) the following *eigenvalue boundary problem* is obtained:

$$\begin{cases} \dfrac{d^2y}{dx^2} + \dfrac{P}{EI}y = 0, \\ y(0) = y(i) = 0. \end{cases}$$

The eigenvalues are the critical forces P_n given by

$$P_n = \left(\frac{n\pi}{l}\right)^2 EI. \tag{3.6}$$

Non-trivial solutions exist only for the critical forces and are expressed by

$$y(x) = c_1 \sin\left(\frac{n\pi}{l} x\right) . \tag{3.7}$$

These solutions represent displacements of the column center line for which it is possible to have equilibrium. The constant c_1 in Equation (3.7) is undetermined. It can assume any real value, including zero. The value of c_1 is limited by the assumptions made to derive the differential equation describing the phenomenon, and by the mechanical properties of the material which composes the column. The approximation leading to Equation (3.5) implies that the undetermined constant c_1 has to be relatively small. Euler column theory indicates that for axial forces which differ from any critical force P_{n} the only possible solution is the trivial $y(x) \equiv 0$.

For an axial force P equal to one of the critical forces, infinite solutions of the form of Equation (3.7) exist, including the trivial. This behavior may be represented by the graph in Figure (3.3) which shows the displacements of the central point of the column. The intersection between the vertical path (column straight) and horizontal path (column under buckling) represents a point of bifurcation of the behavior on the column. Black paths represent stable solutions and gray paths represent unstable solutions.

The graph shows cut-off points to reinforce the limitation of the model to small displacements. Imperfections in the geometry of the column, in the centralization of the axial force, and in the approximation of Equation (3.5) make experimental results to differ substantially from the prediction of the model.

If the boundaries of the problem are set instead to $x = -l/2$ and $x = l/2$, the expression for the center line becomes

$$y(x) = c_1 \sin\left[\frac{n\pi}{l}\left(\frac{l}{2} + x\right)\right] . \tag{3.8}$$

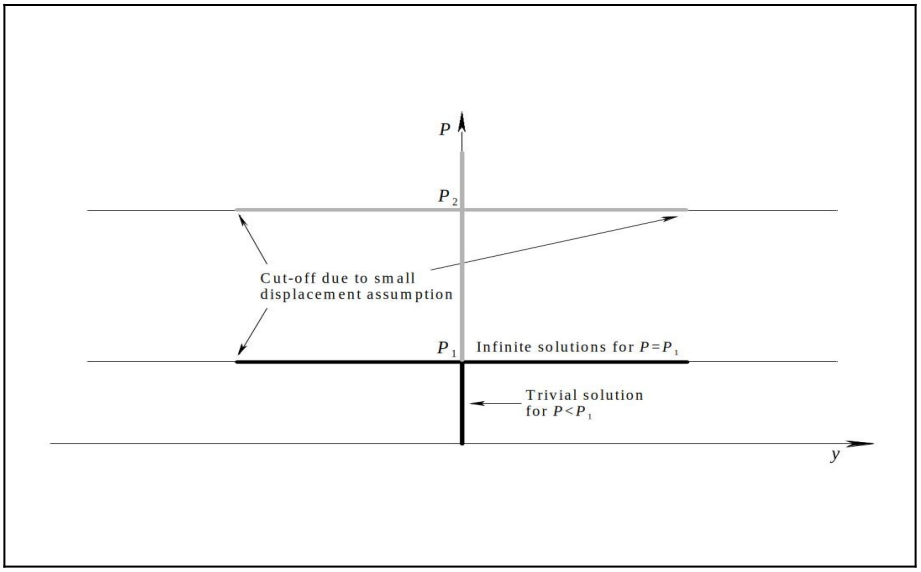

Figure 3.3: Displacement of the center of the column

Figure (3.4) shows Equation (3.8) for $c_1 = 1$, $l = 10$ and $n = 1$=1, 2 and 3. These three modes will be considered in the following sections.

3.2 Columns Subjected to a Compressive Force and Moment at the Ends

Euler column theory can be extended to account for moments applied at the ends. Considering a column with constant stiffness EI and length L_1, its third critical force[1] $P_{\text{crit}} = P_3$, is given by

$$P_{\text{crit}} = P_3 = \left(\frac{3\pi}{L_1}\right)^2 EI. \tag{3.9}$$

1 Any other mode can be used.

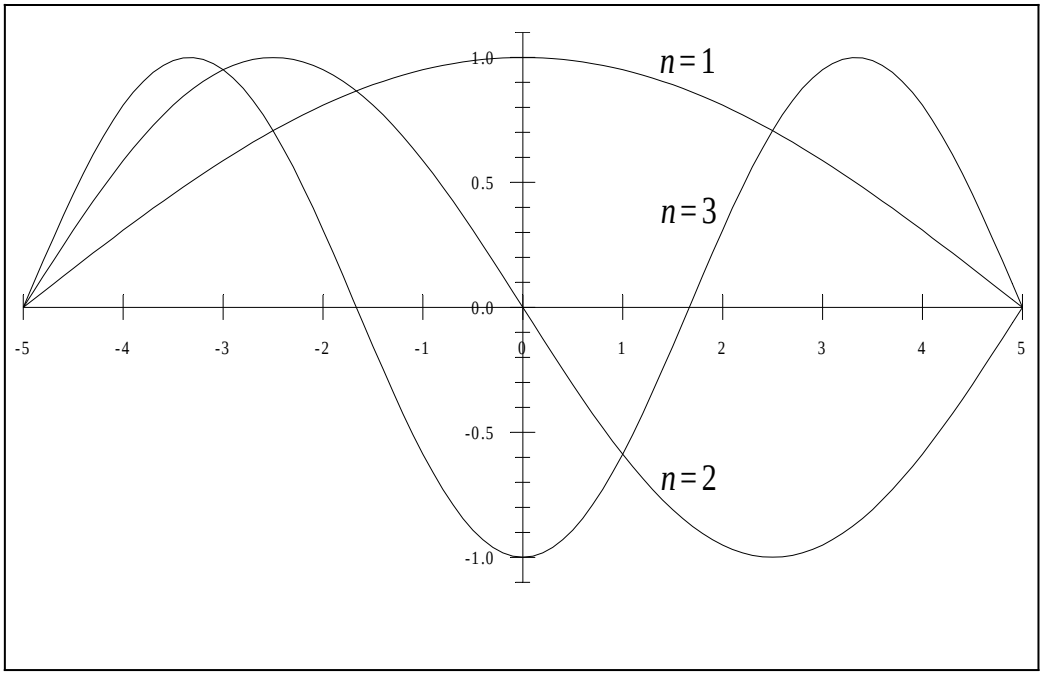

Figure 3.4: Solutions of a buckling problem for *n*=1, 2, and 3

Choosing $c_1 = y_{\max}$ and using Equation (3.8) for symmetry, the expression for the center line of the buckled column becomes (see Figure [3.5-a]):

$$y(x) = y_{\max} \sin\left[\frac{3\pi}{L_1}\left(\frac{L_1}{2} + x\right)\right] = -y_{\max} \cos\left(\frac{3\pi x}{L_1}\right). \tag{3.10}$$

Taking any point $x_0 = \frac{L}{2}$ along the axis between $L_1/6$ and $L_1/2$ and its symmetrical -x_0, the displacements of the column at these points are given by

$$y_0 = y(x_0) = y(-x_0) = -y_{\max} \cos\left(\frac{3\pi x_0}{L_1}\right).$$

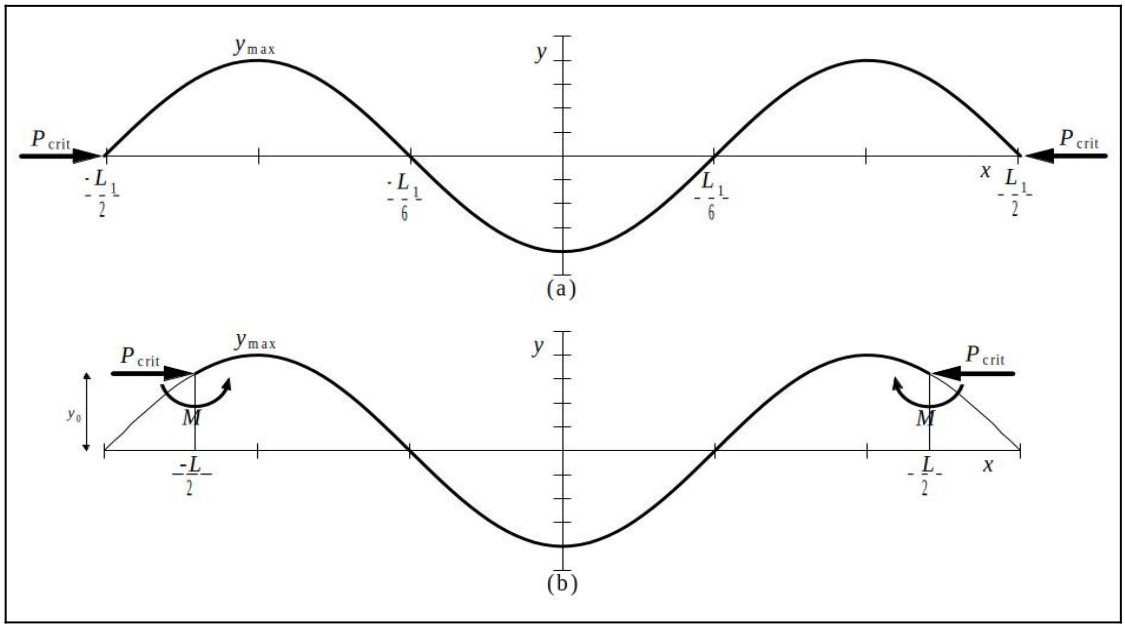

Figure 3.5: Column subjected to axial force and moment at the ends

The column is in equilibrium and the loads acting on the cross section of the column at $x = -x_0$ are the force P_{crit} and the moment $M = -y_0 P_{\text{crit}}$. The same occurs at $x = x_0$. Therefore, if the column is cut at these two points and the loads P_{crit} and M are applied at these two points, the column, now with length L, will remain in equilibrium and in a state of buckling (see Figure [3.5-b]).

Working backwards, starting with a column of length L subjected to an axial force P and moment of magnitude M at its ends, the equilibrium configuration can be determined. Contrary to buckling under axial force only, in which infinite solutions exist at the critical force, the moment applied to the ends will define *one unique equilibrium configuration*, that is, no indeterminacy will exist. The loads P and M acting on the ends can be resolved as one unique force P acting with an eccentricity e on the ends of the column. The eccentricity e is calculated from

$$e = \frac{M}{P}.$$

Considering the members of the family of center lines given by Equation (3.10) in which $y(\frac{L}{2}) = y(-\frac{L}{2}) = e$, the two parameters $y_{\max}$ and L_1 are no longer independent. Using Equation (3.9), the length L_1 is chosen such that its third buckling force is equal to P.

Only one length is possible for L_1. If the selected length is shorter than L_1, the force *P* is less than the critical force, resulting in the trivial solution. In this case the condition $y(L/2) = y(-L/2) = e$ could not be satisfied. If the selected length is longer than L_1, the force is greater than the critical force and the only solution is the trivial. Again the condition $y(L/2) = y(-L/2) = e$ could not be satisfied. (See Figure [3.6].) This is the idea used by Westergaard and Osgood (1928) to model buckling of columns under eccentric axial force. It is also used in the Secant Formula (Hartog 1949, Bleich 1952) to determine the maximum compressive stress acting on the column submitted to eccentric compressive axial forces.

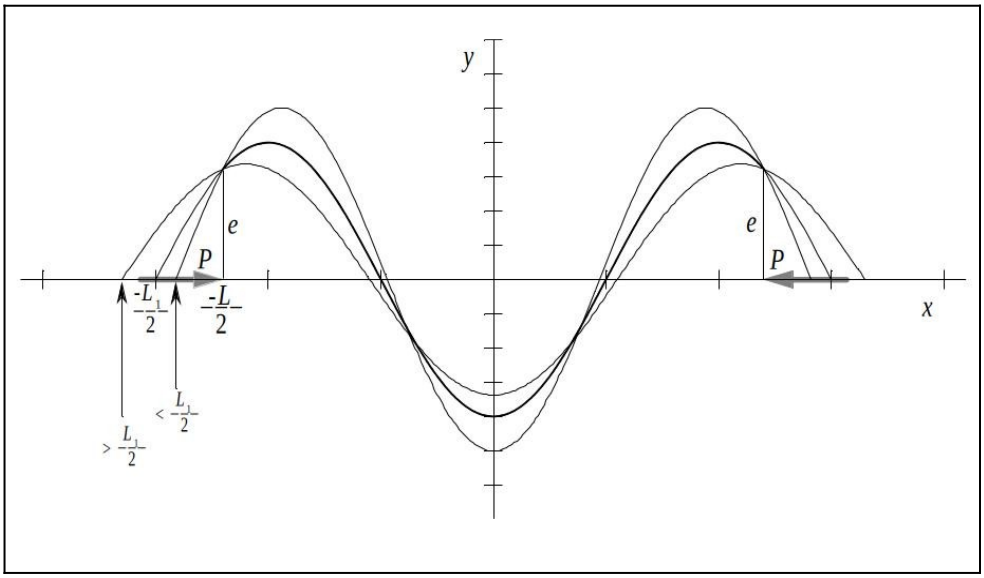

Figure 3.6: Column subjected to an eccentric axial force

3.3 The Curved Bore-Hole Theory

The new and original *curved bore-hole theory* describes how and under which conditions a drillstring can buckle within a curved bore-hole. The *trigonometric model* for buckling of drillstrings within curved bore-holes results from the association of the curved bore-hole theory with the concepts developed in the previous section.

3.3.1 Constraints Imposed on Buckled Columns

The amplitude of a buckled column is not determined by the solution of the eigenvalue boundary problem. However, if the displacement is constrained at any position in the space of solutions, a maximum value for the constant c_1 in Equation (3.8) can be calculated.

If a column is confined within a circular cylinder and subjected to a buckling force, it will buckle until it touches the wall of the cylinder. At the contact points on the wall of the cylinder, reaction forces are generated. These reaction forces change the loading applied to the column. When this happens, the Euler column differential equation and its solutions are no longer valid and the problem has to be modified to account for the new loading.

Here the assumption that the constraints are rigid and impenetrable is used. This assumption represents the fact that the column must remain within the limits imposed by the constraints, no matter how intense the contact forces are. It is also assumed that the cross section along the column do not change in shape due to the external forces and due to the displacement of the column.

If the constraints are two concentric circles, at every contact point between the column and the constraints (except for the two ends for now) the following conditions must be satisfied:

1- the column must be tangent to the circle,
2- if the contact occurs with the outer circle, the curvature of the column at the contact point must be equal to or greater than the curvature of the circle,
3- if the contact occurs with the inner circle, the curvature of the column must be equal to or less than the curvature of the circle (including reverse curvature).

These conditions are simple, but they are fundamental to understand the effects of the constraints upon the buckling process.

3.3.2 Starting a Buckling Process

The discussion of how a column buckles inside circular constraints requires the description of the process of inserting and loading a column inside these constraints. Initially, the process of forcing a held-ends[2] column of length L and stiffness EI to fit between two parallel rigid flat surfaces apart by a distance $d<L$ is considered, as shown in Figure (3.7-a). A compressive reaction axial force F will act at both ends because of the elastic resistance of the column.

Next, the same column is considered but with pinned-ends, loaded by the same force F applied by a suspended body of weight F as shown in Figure (3.7-b). The magnitude of the loading for both columns are the same and the pinned-ends column is buckled. Hence $F = P_{\text{crit}}$. However, the *nature* of the two forces differs substantially. In case (a), the final shape is the only possible stable configuration the column may assume

2 A held support is a support which prevents longitudinal and traverse displacement but permits rotation.

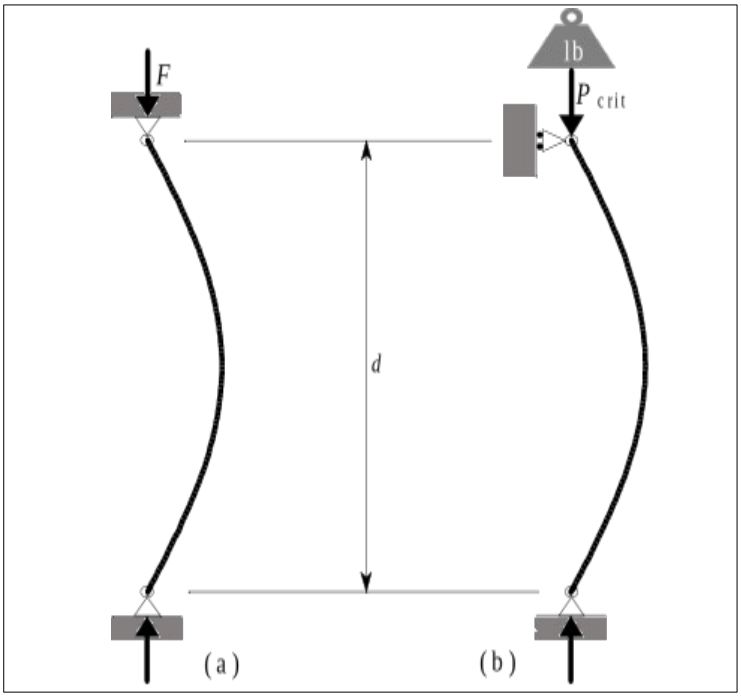

Figure 3.7: Two different concepts of buckling

whereas in case (b), the final shape is one among infinite possibilities. Another fundamental difference is that the column in case (b) may exchange mechanical energy with the surroundings, that is, the suspended body of weight $F = P_{\text{crit}}$ may produce or absorb work. The force F in case (a) cannot displace and, therefore, cannot produce or absorb work.

The reason for the two different natures in the loading is that in case (a), a given fixed shortening (or displacement) is imposed between the ends of the column with a resulting force *F*. In case (b) the force $F = P_{\text{crit}}$ is applied and the displacement is a consequence. It is clear that the column in case (b) has a freedom that the column in case (a) does not have. Under the point of view of the physical and mathematical definition of buckling, case (b) embodies an example of buckling in all its essence, whereas case (a) does not.

Considering the two concentric circles as in Figure (3.8), the maximum length a column of diameter *d* may have in order to fit with no bend inside the constraints is well determined and given by

$$L_{\max} = 2\sqrt{R^2 - (r+d)^2}.$$

Columns longer than $L_{\max}$, must be in a bent configuration as shown in Figure (3.8). It is commonly thought that under these circumstances the column is already buckled, but, in fact, it is bent and not buckled.

The displacement is due to the lateral forces required to force the column to fit inside the constraint. Moreover, the component of the radial force F_{r}, in the line connecting the ends, is less than the critical force required to buckle the column.

There are at least three points of contact between the column and the constraints: the two ends and the mid point of the column. With no friction, the reactions at the ends are radial and to reach equilibrium the column must touch the inner circle. In addition, the curvature of the column in the middle point cannot be larger than the curvature of the

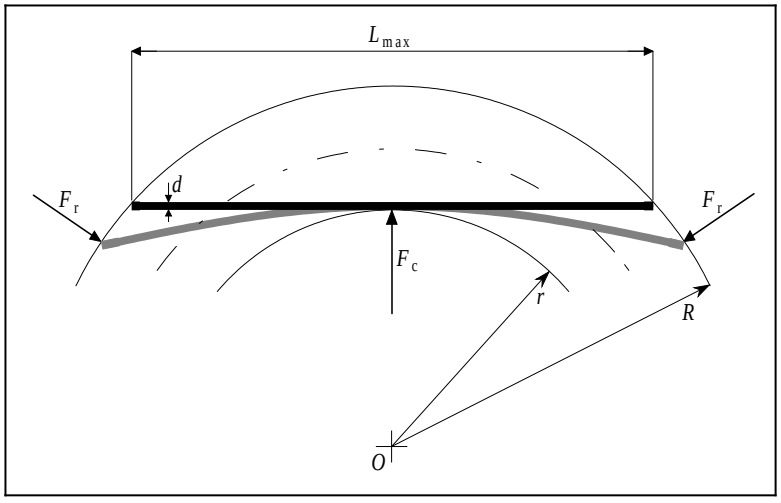

Figure 3.8: A straight column inside the curved constraints

inner circle.

Increasing the length of the column increases the curvature at the central point. Therefore, there will be a length interval in which the curvature at the center of the column equals the curvature of the central circle. A minimum radius of curvature for the inner circle exists if one wants to avoid plastic deformation of the column. This minimum value is given by[3]

$$r_{\min} = \frac{E}{Y}\frac{d}{2},$$

where Y is the yield point of the material. Now, if tangential forces are applied at both ends of the column to preclude slippage and the length of the column is increased, a length exists in which the column will no longer touch the inner circle as shown in Figure (3.9). In this case, the radial force F_{r} and the tangential force F_{t} should resolve to P_{crit}. The column buckles in the sense of case (a) in Figure (3.7). A similar configuration is reached if one increases the tangential force F_{t} and permits one or both ends to slide along the outer circle. In this case the column buckles in the sense of case (b).The column can be further buckled until it touches the outer circle. This point corresponds to the point of maximum curvature of the column which has to be larger than the curvature of the outer circle. At the contact point a reaction force F_{c} is generated as shown in Figure (3.10). Even without calculating this reaction force, some results can be anticipated. The force F_{c} must be balanced by changing the forces F_{t} and/or F_{r}. These changes, whatever they are, will increase the ratio $F_{\mathrm{t}}/F_{\mathrm{r}}$ This means that at the contact point the moment will decrease and consequently the column will flatten locally. It will flatten until the curvature equals the curvature of the outer circle. From this point, any

3 This relation is easily obtained from Equation (3.1) and $s(y) = My/EI$ for the stress at any position y on the cross section of the column. This is a lower limit for the radius of the inner circle. A more detailed calculation should involve the composition of stresses due to axial load, shear and torque.

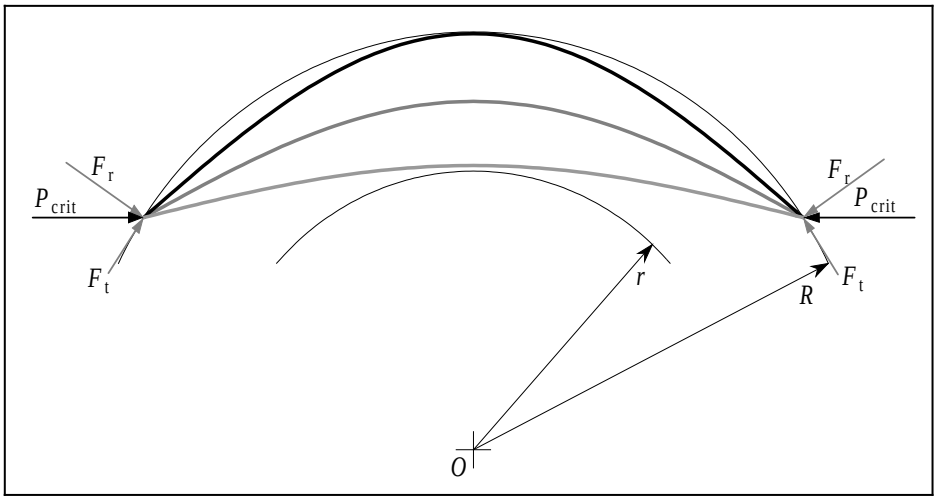

Figure 3.9: Buckling a column inside the curved constraints.

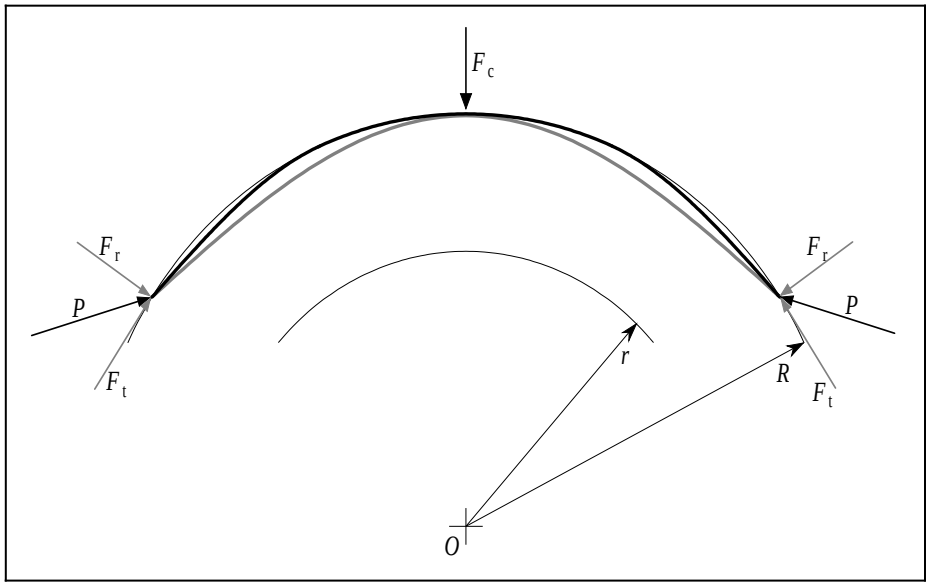

Figure 3.10: A buckled column touching the outer constraint.

increase of the tangential force will make the column conform to the curvature of the constraint. Eventually, as the circular portion of the column approaches the ends of the column, the decrease of the lever arm will require an increase of the tangential force to unbounded values. Therefore, the only way to make the whole column become circular is by applying enough moment at the ends to make the curvature at the ends equal to the curvature of the outer circle. In this case, the ends of the column will be tangent to the constraint, and the column will conform to the curvature of the outer constraint.

It is important to stress that in this process the only active external loads applied to the column are tangential (axial) forces and moments. The radial forces are passive forces resulting from the contact between the column and the constraints.

3.3.3 Buckling of a Column Subjected to Two Concentric Circular Constraints

Applying an axial force to a column inside a circular constraint will eventually force the column to conform to the curvature of the constraint. To balance the tangential force, a distributed force is generated along the contact line. If the outer constraint is removed the column will collapse outwards. The constraints contribute to the increase of the resistance to buckling of the column. Consequently, if the column buckles it will do so in an inward fashion. To prove this conjecture, it will be shown that there exists at least one inward equilibrium buckling configuration.

To show the existence of inward equilibrium buckling configuration a reverse construction will be used. Initially, buckling a column of length L^* with its first buckling mode is attempted. The column critical force is P_1 (known) and the maximum displacement is $y_{\max}$ (arbitrary). The shape of the buckled column is a half-period sine curve. From its ends are drawn perpendiculars which cross at a point O as shown in Figure (3.11). From center O, a circle of radius r is drawn tangent to the sine curve at its

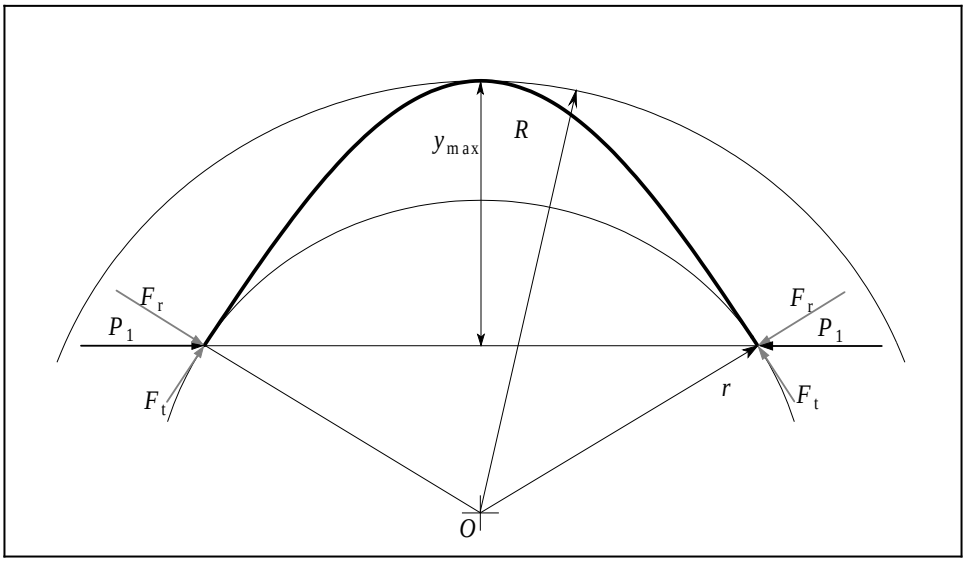

Figure 3.11: Fitting a half-period of a sine curve inside the constraints.

ends. A second circle of radius R, with center at O, is drawn tangent to the sine curve at its maximum. With this configuration, the buckled column satisfies the requirement of being tangent to the constraints at its contact points. The force P_1 can be decomposed into its radial and tangential components. However, the radial component has to be an active force, which contradicts one of the assumptions of the model. Therefore, this configuration is not admissible.

The next possibility is to subject the same column to its second critical force P_2. This possibility is immediately discarded because it is impossible to draw a circle tangent to both ends of a full-period sine curve.

The successful case is when the column is subjected to its third critical force P_3 with maximum displacement $y_{\max}$ as shown in Figure (3.12). However, the construction here is not as simple as the case of the first critical force. Perpendiculars cannot be drawn from its ends to determine the center of the circles because the curvature at the ends is zero and part of the column would be outside the constraints.

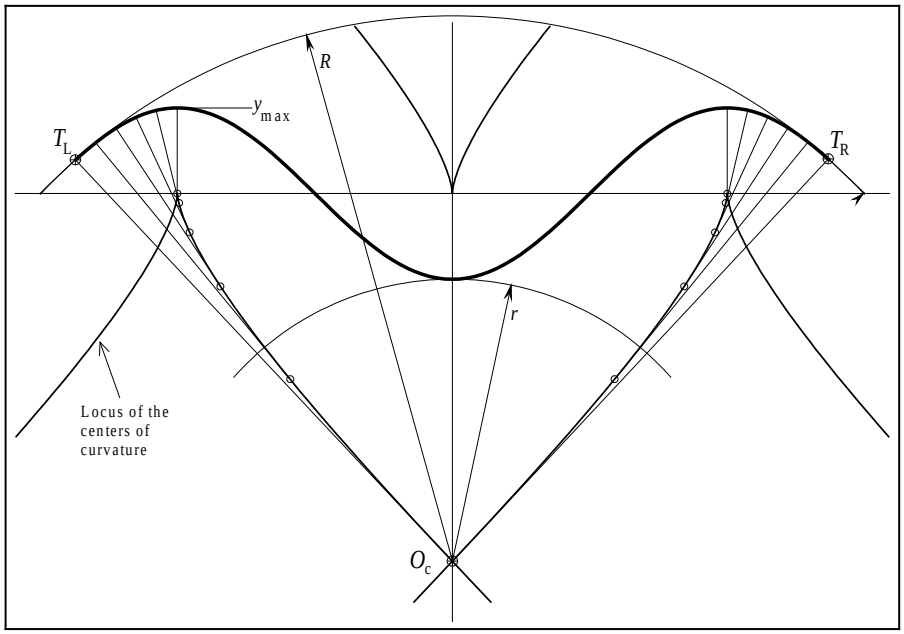

Figure 3.12: Locus of the center of curvature of a sinusoidal curve

The points of tangency are the two symmetrical points T_{L} and T_{R} along the sine curve where their radii of curvature are equal to the radius of curvature of the outer circle. From these two points, perpendiculars are drawn which cross at O. From O, a circle is drawn passing through the points T_{L} and T_{R}. The inner circle is drawn from O tangent to the central wave of the curve at its minimum. The best way to understand this is by plotting the locus of the centers of curvature as shown in Figure (3.12).

The locus is made of several asymptotic branches. In the $1^1/_2$-periods portion shown, two branches cross at point O, which represents the center of the two constraining circles. In this case, a portion of the two extremities of the column of length L^* are "outside the constraints". The length L of the column between the points T_{L} and T_{R} is the maximum length the column may have to fit inside the circular constraints as a portion of $1^1/_2$-periods of a sine curve. This establishes the relationship between a column of length L under buckling of amplitude $y_{\max}$, and the radii R and r of the constraints.

The above procedure suggests the case of the buckling of a column subjected to a compressive force and a moment applied at the ends presented in Section 3.2. At the ends of the column of length L, the loads are the force P_3, which is decomposed into the tangential force F_{t} and the radial force F_{r}, and the moment $M = eP_3$ as shown in Figure (3.13).

The radial force F_{r} point inward and result from the reactions of the column against the outer constraint. There is no reaction against the inner circle. The inner circle is solely used to determine the maximum displacement of the column. The forces that must be directly applied to the column are the tangential force F_{t} and the moment M at both sides of the column. These are active loads allowed by the assumptions of the model which make this configuration admissible. Following this procedure it is possible to present a buckling configuration under suitable loading which proves the conjecture that at least one buckling force exists and that the column buckles inwards.

It is expected that another buckling force should exist, not as a higher mode of buckling but of different nature. The process presented will provide the *minimum tangential force* able to keep the column buckled. If the tangential force is less than this minimum the column returns to its circular configuration similar to the column in Figure (3.10). This characterizes the buckling force in an *unloading process*, that is, in a process starting with the column in a postbuckling configuration in which the tangential force decreases until it unbuckles.

The minimum tangential force is not enough to buckle the column in a loading process. To do that, it is required a higher tangential force to overcome the tendency of the column to buckle outward.

Another detail needs to be discussed. Rarely will a column have exactly the maximum length to fit inside the constraints. In most cases it will be longer than the maximum length, even several times longer like in drillstrings. There are two cases to be

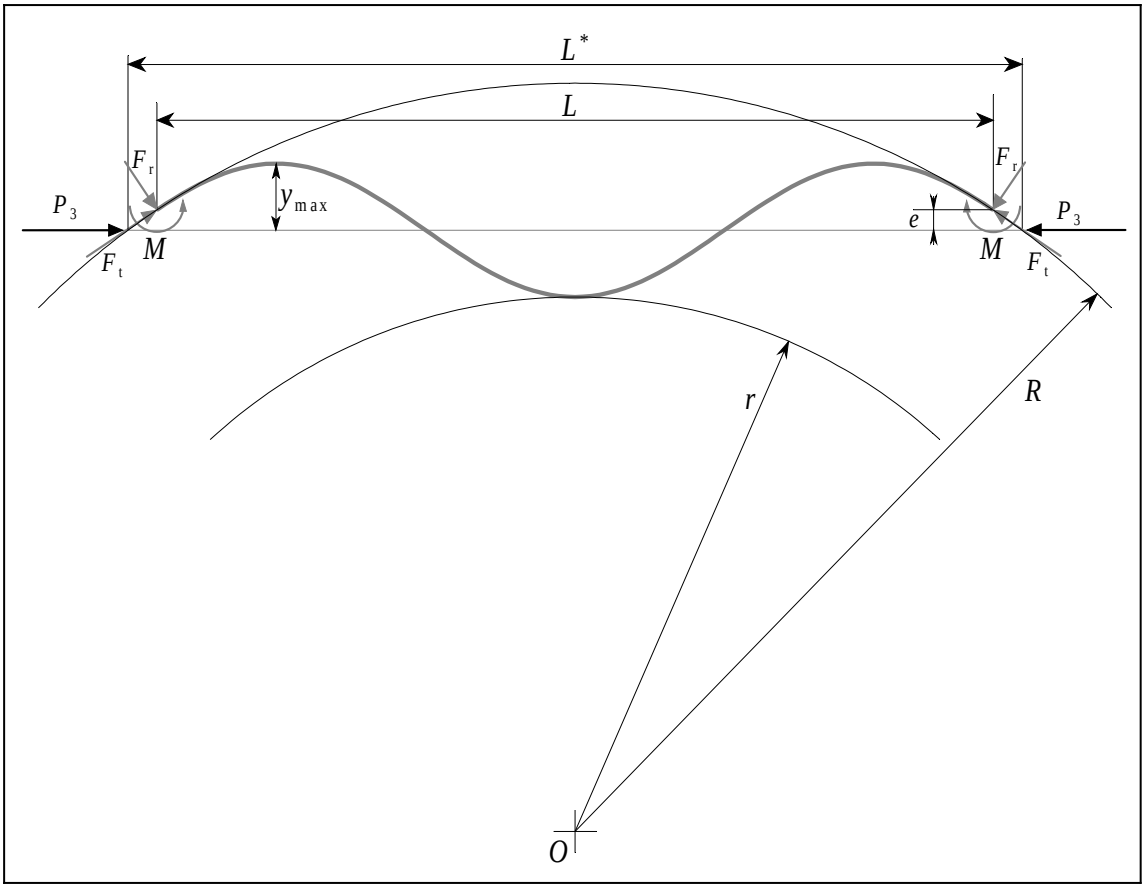

Figure 3.13: Fitting $1^{1}/_{2}$-periods of a sine curve inside the constraints.

investigated. The first is when the column is longer than L but shorter than $2L$, and the second when the column is equal to or longer than $2L$. When a column longer than L but shorter than $2L$ is forced by buckling to fit inside the constraint, the portion ΔL that exceeds L must conform to the constraints and will be circular in shape. When the column is equal to or longer than $2L$, two or more buckled waves of length L may form as shown in Figure (3.14). The buckling force calculations and associated method for the trigonometric model are presented in Appendix G. An approximate solution is also given.

3.4 End Effects

The modeling above is concern only with central portions of the column. At the upper end of the column where the axial force is applied it is assumed that the column is tangent to the outer circle. At the lower end of the column, two boundary conditions can

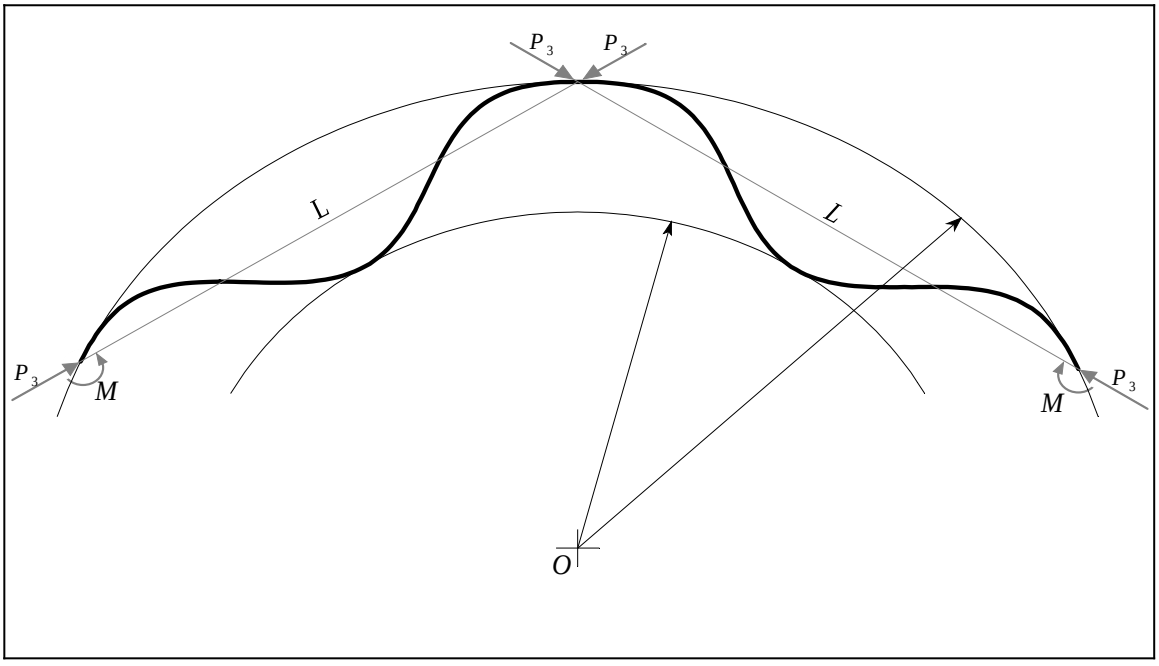

Figure 3.14: Two buckled waves inside the curved constraints

be applied: (1) the drill bit end condition, and (2) the near-bit end condition.

The drill bit and the near-bit end conditions affect the shape of the column up to the first contact point with the constraint. Beyond that point the behavior is independent of the end condition.

A drill bit end condition is that in which the column is centered and held between the constraining circles. Figure (3.15) shows this configuration. A near-bit is a stabilizer positioned at the top of the drill bit in order to decrease the tilt and consequently to force the drill bit to drill straight. Therefore, a near-bit end condition is that in which the column is centered, built-in, and aligned with the axial direction of the constraints. Figure (3.16) shows this configuration. The formulations for the drill bit condition and near-bit condition are presented in Appendix G.

3.5 Conclusions of the Chapter

The curved bore-hole theory explains how and under which conditions a drillstring buckles inside a curved bore-hole. The theory is independent of the nature of the model used to describe the behavior of the column. The trigonometric model results from the association of the curved bore-hole theory with Euler column theory. Trigonometric functions are used to describe the displacements of the center line of the buckled column. This makes the implementation of the model computationally affordable. Predictions using this model are shown in Chapter 7.

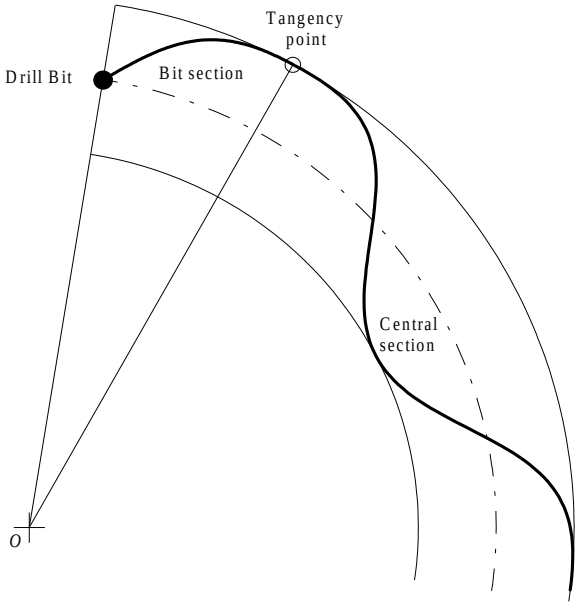

Figure 3.15: A schematic of the drill bit end condition

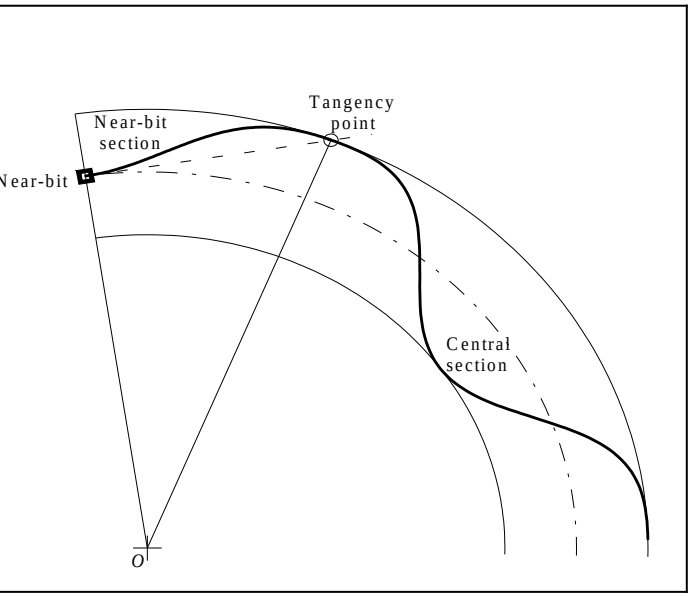

Figure 3.16 A schematic of the near-bit end condition

Chapter 4

The Generalized Beam-Column Theory

In the previous chapter, a reduced model for buckling of columns within circular constraints was developed. The idea was to use Euler column theory and search for a fit inside the constraints using the curved bore-hole theory. A strong limitation of that model rests in its inability to account for the distributed weight of the column. The model describes the case of buckling in the absence of gravity. In a real case, however, the distributed weight inserts a new ingredient into the buckling behavior of a column.

Theories already exist for vertical weighted columns and horizontal beam-columns and will be briefly discussed in this chapter. For the case of a curved bore-hole, however a theory for a generalized beam-column needs to be developed which includes the inclination that an element of the drillstring has along the curved bore-hole. The purpose of this chapter is to develop this theory. Solutions using this theory will then be associated with the curved bore-hole theory to determine the buckling force and other features that characterize the buckling behavior of weighted drillstrings within circular constraints.

4.1 Theories Including Distributed Weight

Euler column theory does not consider the effect of the distributed weight of the column. Theories for buckling which consider the distributed weight will be briefly presented, including the differential equation, boundary conditions and solutions. These models are extensively described in the literature.

4.1.1 The Flagpole Theory

The flagpole problem is a classical problem in elasticity and advanced mechanics and has been discussed broadly by several authors (Love 1944, Timoshenko 1988, Hartog 1952). The problem consists of finding the equilibrium configuration of a column vertically built-in at the lower end, with the upper end free, loaded by the distributed weight along its length. The differential equation and boundary conditions for this problem may be obtained by using either differentials or the energy method, and is given by

$$\begin{cases} EI\dfrac{d^3y}{dx^3} + w(l-x)\dfrac{dx}{dx} = 0, \\ \\ y(0) = y'(0) = y''(l) = 0. \end{cases}$$

Note that the trivial function $y(x) \equiv 0$ satisfies the differential equation and the boundary conditions. Non-trivial solutions exist for particular discrete values of the distributed weight w, thereby defining this as an eigenvalue problem. Exact non-trivial solutions may be obtained using power series which can be expressed in terms of Bessel functions, integrals involving Airy functions, and hypergeometric functions. An example is the solution obtained by Love:

$$\begin{aligned} p(x) &= \frac{dy}{dx} = \left[aJ_{1/3}(\xi) + bJ_{-1/3}(\xi)\right](l-x)^{1/2}, \\ \xi(x) &= \frac{2}{3}\sqrt{\frac{w}{EI}}(l-x)^{3/2}. \end{aligned} \tag{4.1}$$

where *a* and *b* are constants to be determined, and J_ν's are Bessel functions of fractional order. This expression has to be integrated once to obtain $y(x)$. The first critical weight

that causes instability of the column, here expressed as $(wl)_{\text{crit}}$[1], is given by

$$(wl)_{\text{crit}} = 7.837\frac{EI}{l^2}.$$

Approximate solutions can also be obtained using Rayleigh's method and suitably picked simple functions, like trigonometric functions, which satisfy the boundary conditions (Timoshenko 1988, Hartog 1952). Flagpoles submitted to lateral and/or axial force applied to the upper end have also been studied.

Another related problem is the case of a vertical column with pinned-ends. Although this does not represent a flagpole, the nomenclature is kept because it involves essentially the same differential equation with different boundary conditions. The problem is described by the following equations:

$$\begin{cases} EI\dfrac{d^4y}{dx^4} + \dfrac{d}{dx}w(l-x)\dfrac{dx}{dx} = 0, \\ y(0) = y(l) = y''(0) = y''(l) = 0. \end{cases} \tag{4.2}$$

The derivation of this differential equation will be shown later in this chapter.

4.1.2 The Lubinski Model for Vertical Buckling

In his classical paper, Lubinski (1950) derived the differential equation for a vertical weighted column using force and moment balance. The main goal was to establish a model for buckling of a drillstring within a vertical cylindrical bore-hole. His

1 This represents the maximum weight of a column of stiffness *EI*.

approach was unique in which new techniques were used in modeling the problem and in specifying boundary conditions due to a specific column load configuration.

The column considered is very long and hung at its upper end. It is lowered inside a vertical well usually filled with drilling fluid. Before the column touches the bottom of the bore-hole, the entire column is under tension and the neutral point of buckling[2] is located at the lower end. As the lower end of the column comes in contact with the bore-hole, weight is applied on the drill bit and the neutral point of buckling moves upward putting the lower portion under compression. The column becomes unstable when the critical weight on bit is reached.

The origin of the coordinate axes is at the neutral point of buckling and the *x*-axis is oriented downward. As the neutral point moves, the origin moves with it. The differential equation obtained by Lubinski is

$$EIy''' + wxy' + F_2 = 0, \tag{4.3}$$

where w is the distributed weight incorporating the buoyancy effect of the drilling fluid, and F_2 is the lateral force occurring at the lower end as a result of the buckled configuration (a value to be determined). The boundary conditions are the same as the flagpole with pinned-ends, namely,

$$\mathrm{y}(\mathrm{x}_1) = y(x_2) = y''(x_1) = y''(x_2) = 0,$$

where x_1 and x_2 are the coordinates of the upper and lower ends respectively. The solution for Equation (4.3) was obtained using power series.

---

2 Neutral point of buckling is the position along the drillstring where the suspended weight equals the weight of the column above this point.

Lubinski investigated the effects of different lengths for x_1 and the resulting neutral point required to buckle the column. Written in terms of dimensionless lengths X_1 and X_2, when X_1 is less than -6, the value of X_2 does not vary much from 1.94. Assuming this value as a limit for the critical length, the critical force for buckling in terms of the tension applied at the upper end is[3]

$$W_1 = w\left[L - 1.94\left(\frac{EI}{w}\right)^{\frac{1}{3}}\right].$$

In addition, the model furnishes the lateral force at the bit, the tilt of the bit, the position where the drillstring touches the bore-hole wall, and the force at the contact point. Higher buckling modes are also considered and the results discussed.

For $X_1 = 0$ the critical dimensionless length X_2 is 2.65 for any vertical column. This can be used to calculate the critical length of stands of drill pipes and drill collars vertically stacked.

4.1.3 The Beam-Column Theory

Beam-column is the name given to a beam subjected to an axial compressive force in addition to a lateral distributed weight. The analysis and solution of this problem are also in the literature (Timoshenko 1988). The differential equation is given by

$$\frac{d^4y}{dx^4} + P\frac{d^2y}{dx^2} = q(x) \not\equiv 0. \tag{4.4}$$

---

3 This is not the expression obtained by Lubinski but it essentially conveys his idea that $1.94(EI/w)^{1/3}$ is the length of the column below the neutral point. Lubinski also refined the expression to account for tapered columns.

where P is the axial force and $q(x)$ the distributed weight.

In contrast to the flagpole, the trivial function $y(x) \equiv 0$ is not a solution of the differential equation. For $q(x) = q_0$, a solution for the differential equation is

$$\begin{aligned} y(x) &= \frac{q_0 l^4}{16EIu^4}\left[\frac{\cos(u - 2ux/l)}{\cos u} - 1\right] - \frac{q_0 l^2}{8EIu^2}x(l-x), \\ u &= \frac{l}{2}\sqrt{\frac{P}{EI}}. \end{aligned} \tag{4.5}$$

The term $\cos u$ in the denominator of the first term indicates that no solution exists for $u = \pi/2$.[4] Therefore, the value $u = \pi/2$ represent a critical value of the problem. The definition of u results in

$$\frac{\pi}{2} = \frac{l}{2}\sqrt{\frac{P_{\text{crit}}}{EI}} \longrightarrow P_{\text{crit}} = \frac{\pi^2 EI}{l^2}$$

The value for the critical force is the same for the Euler column. However the nature of the critical forces for the Euler column and for the beam-column differ significantly. For the Euler column it represents an eigenvalue of the problem and for the beam-column it represents a *singularity.*

4.2 The Generalized Beam-Column Theory

The *generalized beam-column* theory is the kernel of the hypergeometric model. Its principal characteristic is to account for the inclination of the column during buckling processes. The inclination is meaningful only in models that consider the distributed

4 Consider $\cos(u\text{-}2ux/l)/\cos(u) = \cos(2ux/l) + \tan(u)\sin(2ux/l) \to \infty$ as $u \to \pi/2$ for $0 < x < l$.

weight of the column. This model is important because the inclination of an element of the drillstring changes along a curved bore-hole.

A column with the same characteristics of the column in Section 3.1 is considered. In addition, the column has a constant distributed weight *w* and is supported at both ends in an *inclined position*, making angle θ with the vertical as shown in Figure (4.1-a).[5] The column is loaded by a compressive axial force *P* acting on the line connecting the centers of both ends. Due to the finite stiffness of the column, for all inclinations except vertical, the column will *always* show some lateral displacement, even for $P=0$. This means that no trivial solution exists and, in addition, any compressive axial force will generate moment along the column. This contrasts with a weightless column in which no lateral displacement may exist for non-critical forces. For any axial force P (even $P=0$), a configuration like the one in Figure (4.1-b) exists. This is a characteristic of beam-columns.

For vertical columns, the buckling phenomenon is an *eigenvalue* problem, that is, a problem in which non-trivial solutions exist only for discrete values, maybe infinitely many, of a particular parameter of the problem. For beam-columns the buckling phenomenon is a *singular* problem, for which non-trivial solutions exist for any value of a parameter except for discrete values, maybe infinitely many, for which no regular solution exists.

4.2.1 The Principle of Virtual Work and The Energy Method

To derive the differential equation which describes a generalized beam-column, the *energy method* will be applied. This is the most suitable method for dealing with

5 The directions of the coordinate axes should be noted for future references.

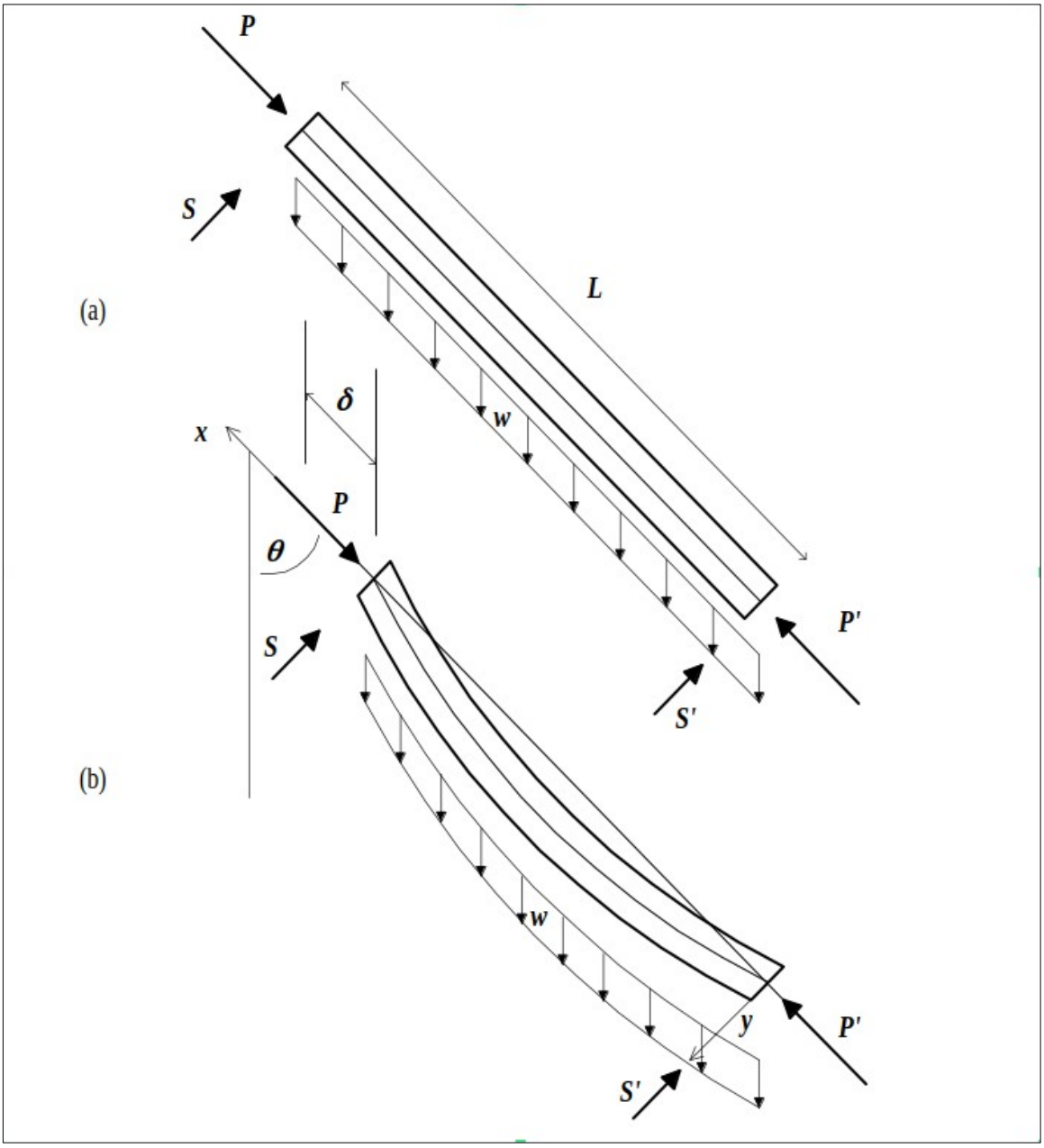

Figure 4.1: A Weighted inclined beam-column under axial force

stability problems of structures (Bleich - 1952). Since this method requires the existence of a total potential surface, it is applicable only to conservative systems.

The energy method is based on the principle of virtual work which states that if an elastic body or system in equilibrium is given a small displacement or deformation, then the work done by all external and body forces acting on the system equals the increase of strain energy stored in the system. In integral form the theorem is expressed as

$$\int_A T_i u_i dA + \int_V \rho B_i u_i dV = -\int_V \sigma_{ij} \varepsilon_{ij} dV. \tag{4.6}$$

Here T_i are surface tractions, u_i are displacements, ρB_{i} are body forces, σ_{ij} are stresses, and ε_{ij} are strains. The displacements u_i and strains ε_{ij} should satisfy the compatibility conditions for infinitesimal strain components (Lai, Rubin, Krempl - 1993). The first and second integrals in Equation (4.6) express the work done by the external and internal forces respectively, and the third integral expresses the strain energy.

Using the concept of potential energy, the left side of Equation (4.6) represents the decrease (or increase) of the potential energy of the forces acting upon the system and the right side represents the increase (or decrease) internal energy of the system. In differential form and using the same concepts this can be written as

$$dU_{\mathrm{w}} + dV = d(U_{\mathrm{w}} + V) = dU = 0 \tag{4.7}$$

This means that if a system in equilibrium is given a small displacement or deformation the *total potential energy* does not change. In variational terms it is said that, in the equilibrium state, the total potential energy is *stationary.* This is expressed as

$$U = U_{\mathrm{w}} + V = \text{“}stationary\text{”} \tag{4.8}$$

If the total potential energy is both stationary and at a local minimum, the equilibrium is stable. If the total potential energy is both stationary and at a local maximum, the equilibrium is unstable. In both cases, the system is in equilibrium.

To apply the energy method to the structure of Figure (4.1) the work done by the external forces, the work done by the body forces, and the strain energy of the column need to be calculated. Three assumptions must be made: (1) the lateral displacements and strains are small, (2) the total effect of the distributed weight can be decomposed into two separate additive effects, one effect due to an axial distributed weight and one effect due to a lateral distributed weight, and (3) the compressive part of the strain energy occurs in the early part of the loading process such that when the loading approximates the first critical force, the increase of the strain energy occurs due to the increase in bending.

Assumption (3) is admissible considering that in a buckling process the bending increases much faster than the compression for an increase of the axial force. In addition, assumption (3) implies that the energy due to shear stresses does not change significantly during the buckling process.

The decomposition of the loading is shown in Figure (4.2). The forces at the supports are easily calculated from statics. These forces cannot produce or absorb work because they cannot displace along their lines of action. The distributed weights are given by

$$\begin{cases} w_{\mathrm{s}} = w \sin\theta, \\ w_{\mathrm{c}} = w \cos\theta. \end{cases} \tag{4.9}$$

Since the body forces are conservative, the work done by the distributed weight is equal to the sum of the work done by its components.

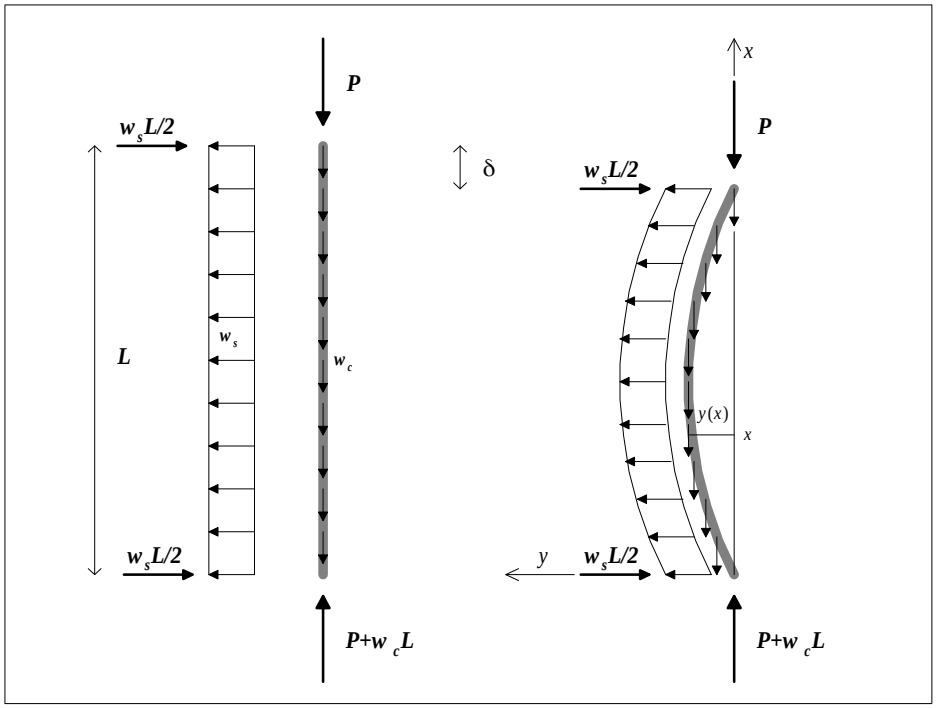

Figure 4.2: Decomposition of the loading acting upon a beam-column.

4.2.2 Work Done by the External and Body Forces

The work done by the axial force P is $W_{\mathrm{P}} = P\delta$ in which the force P remains essentially constant during the buckling process. The displacement δ can be calculated as follows: the length L of the column after buckling is given by (See Hartog - 1952)

$$L = \int_0^{L-\delta} \sqrt{1+y'^2}\,dx = \int_0^{L} \sqrt{1+y'^2}\,dx - \int_{L-\delta}^{L} \sqrt{1+y'^2}\,dx$$

Since δ is presumably small, the second integral at the right can be approximated to δ. This results in

$$L = \int_0^L \sqrt{1+y'^2}\,dx - \delta. \tag{4.10}$$

Expanding the square root in Taylor's series yields to

$$\sqrt{1+y'^2} = 1 + \frac{1}{2}y'^2 - \frac{1}{8}y'^4 + \frac{1}{16}y'^6 - \frac{5}{128}y'^8 + \dots .$$

For small deflections this expansion may be truncated after the second term resulting in

$$\sqrt{1+y'^2} \simeq 1 + \frac{1}{2}y'^2.$$

Substituting the last result in Equation (4.10) the following expression is obtained:

$$L = \int_0^L \left(1 + \frac{1}{2}y'^2\right) dx - \delta.$$

Therefore, the axial displacement δ is given by

$$\delta = \int_0^L \frac{1}{2}y'^2\,dx,$$

and the work done by the force P can be calculated as

$$W_{\mathrm{P}} = P\delta = \int_0^L \frac{P}{2}y'^2\,dx. \tag{4.11}$$

The work done by the distributed weight w is the sum of the work done by the axially distributed weight w_{c} and by the work done by the laterally distributed weight w_{s}. To calculate the work done by w_{c}, we consider an infinitesimal element of length dx displaced axially by the amount $\delta(x)$ as shown in Figure (4.3). The work done by the axial body forces on this element is given by

$$dW_{w_{\mathrm{c}}} = (w_{\mathrm{c}} dx)\delta(x),$$

and the total work done by w_{c} is

$$W_{w_{\mathrm{c}}} = \int_0^L w_{\mathrm{c}}\delta(x)dx.$$

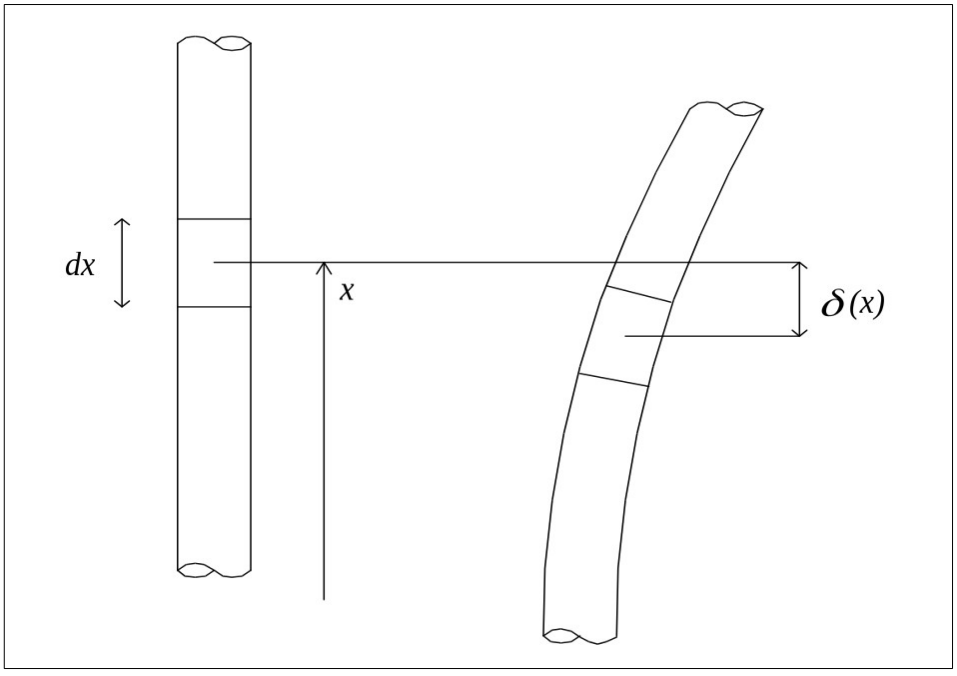

Figure 4.3: Axial displacement on an infinitesimal element of the column

The axial displacement $\delta(x)$ can be calculated in the same manner as before but integrating from zero to x, that is,

$$\delta(x) = \int_0^x \frac{1}{2} y'^2 d\xi.$$

Substituting this expression into the expression for the work results in

$$W_{w_c} = w_c \int_0^L \left(\frac{1}{2} \int_0^x y'^2 d\xi \right) dx.$$

Integrating the last expression by parts and using the fundamental theorem of calculus yields to

$$W_{w_c} = \frac{w_c}{2} \left(x \int_0^x y'^2 d\xi \Big|_0^L - \int_0^L x y'^2 dx \right),$$

$$W_{w_c} = \frac{w_c}{2} \left(L \int_0^L y'^2 dx - \int_0^L x y'^2 dx \right),$$

$$W_{w_c} = \int_0^L \frac{1}{2} w_c (L - x) y'^2 dx. \tag{4.12}$$

To calculate the work done by w_s, an infinitesimal element of length dx displaced laterally by the amount $y(x)$ is considered, as shown in Figure (4.4). The work done by the lateral body forces in this element is given by

$$dW_{w_s} = (w_s dx) y(x),$$

and the total work done by w_s is

$$W_{w_s} = \int_0^L w_s y dx. \tag{4.13}$$

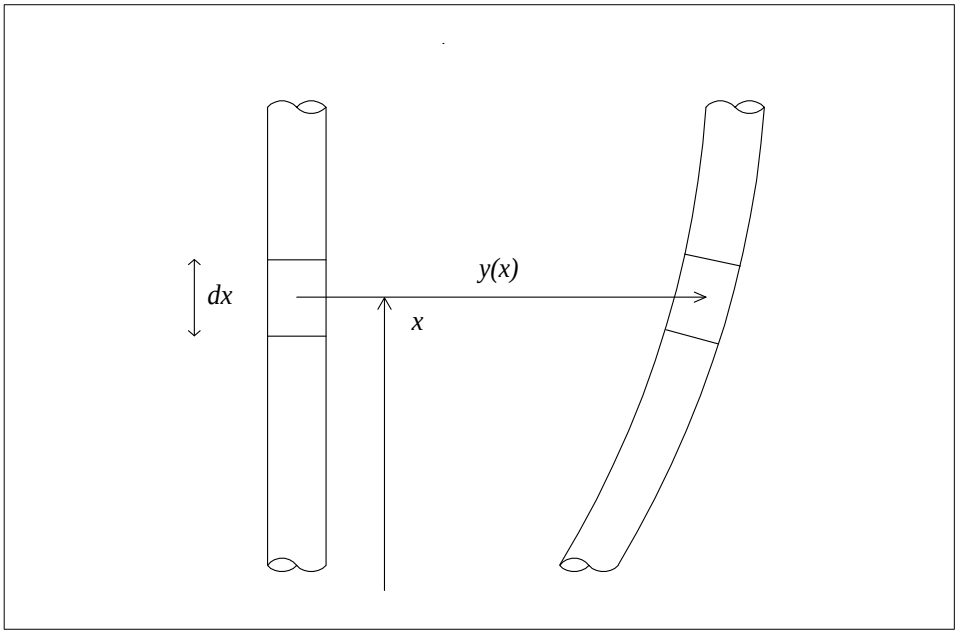

Figure 4.4: Lateral displacement of an infinitesimal element of the beam

4.2.3 Strain Energy

The strain energy V is composed solely of the bending term V_{b} since the terms due to compression and to shear do not need to be considered. The expression of V_{rmb} is given in terms of the moment $M(x)$ by

$$V_{\mathrm{b}} = \int_0^L \frac{M^2}{2EI} dx.$$

For small lateral displacements and strains, the moment is given by

$$M(x) = -Eiy''.$$

Combining the last two expressions results in

$$V = V_{\mathrm{b}} = \int_0^L \frac{EI}{2} y''^2 dx. \tag{4.14}$$

4.2.4 Total Potential Energy

The work done by the external and body forces represents a decrease in the potential energy of these forces. Since the potential energy depends on a referential, it is suitable to assume that the potential energy of the external forces is zero at the beginning of the buckling process. Therefore, the potential energy U_w of the external forces and body forces is given by the negative of the work done by these forces, that is

$$U_{\mathrm{w}} = -(W_{\mathrm{P}} + W_{w_{\mathrm{c}}} + W_{w_{\mathrm{s}}}). \tag{4.15}$$

Substituting Equation (4.14) (strain energy) and Equation (4.15) (potential energy) into Equation (4.8) results in

$$U(y) = \int_0^L \left\{ \frac{EI}{2} y''^2 - \frac{1}{2} \left[P + w_{\mathrm{c}}(L-x) \right] y'^2 - w_{\mathrm{s}} y \right\} dx. \tag{4.16}$$

The expression of the total potential energy as given by Equation (4.16) can be used to calculate the total potential energy for *any* configuration that the column may have. The notation $U(y)$ for the total potential energy emphasizes its dependence on the function $y(x)$. The purpose now is to determine for what function $y(x)$ the total potential energy becomes stationary. This is a typical problem of calculus of variations.

4.2.5 Differential Equation of the Generalized Beam-Column

One of the advantages of the variational method is that, in addition to furnishing the differential equation, it provides the types of boundary conditions that are appropriate to the problem at hand. Expressions like Equation (4.16) are called *functionals* in calculus of variations. For a given function $y(x)$, the integral in Equation (4.16) evaluates a scalar, in this case representing energy.

The integrand in Equation (4.16) is a function of the independent variable x, and of the function $y(x)$ and its first and second derivatives. So it can be written as

$$U(y) = \int_0^L F(x, y, y', y'') dx,$$

where

$$F(x,y,y',y'') = \frac{EI}{2}y''^2 - \frac{1}{2}\left[P + w_c(L-x)\right]y'^2 - w_s y. \tag{4.17}$$

The second order *Euler-Lagrange differential equation* and the set of boundary terms are given by (see Appendix C):

$$\text{D.E.:} \qquad \frac{d^2}{dx^2}\left(\frac{\partial F}{\partial y''}\right) - \frac{d}{dx}\left(\frac{\partial F}{\partial y'}\right) + \frac{\partial F}{\partial y} = 0, \tag{4.18}$$

$$\text{B.C.:} \quad \begin{cases} y & or \quad \dfrac{\partial F}{\partial y'} - \dfrac{d}{dx}\left(\dfrac{\partial F}{\partial y''}\right), \\ y' & or \quad \dfrac{\partial F}{\partial y''}. \end{cases}$$

For a pinned-ends problem, the displacement at the ends, which are *essential boundary conditions,* are prescribed. That is,

$$y(0) = 0 \qquad \text{and} \qquad \text{y(L)} = 0.$$

Therefore, the second pair of boundary conditions are the *natural* ones given by $\partial F/\partial y''$ evaluated at $x = 0$ and $x = L$. Using Equation (4.17), the partial derivatives required by Equation (4.18) are calculated:

$$\frac{\partial F}{y''} = EIy'',$$

$$\frac{\partial F}{\partial y'} = -[P + w_{\mathrm{c}}(L - x)]y',$$

$$\frac{\partial F}{\partial y} = -w_{\mathrm{s}}.$$

Substituting these expressions into Equation (4.18) the differential equation and the boundary conditions which compose the boundary value problem are

$$\begin{cases} \dfrac{d^2}{dx^2}(EIy'') + \dfrac{d}{dx}\{[P + w_{\mathrm{c}}(L - x)]y'\} - w_{\mathrm{s}} = 0 \\ y(0) = y(L) = EIy''(0) = EIy''(L) = 0 \end{cases} \tag{4.19}$$

4.2.6 Rearranging the Differential Equation

Before the boundary value problem given by Equation (4.19) is solved, some rearranging is required to make it easier to handle. The differential equation may be written in the following form:

$$\frac{d}{dx}\left\{\frac{d}{dx}(EIy'') + [P + w_{\mathrm{c}}(L - x)]y'\right\} = w_{\mathrm{s}}.$$

Since w_{s} is constant, this equation can be integrated immediately and a constant of integration *c* introduced:

$$\frac{d}{dx}(EIy'')+[P+w_{\mathrm{c}}(L-x)]y'=w_{\mathrm{s}}x+c.$$

Since EI is assumed constant, this expression can be written as

$$y'''+\frac{1}{EI}[P+w_{\mathrm{c}}(L-x)]y'=\frac{w_{\mathrm{s}}}{EI}x+\frac{c}{EI}. \tag{4.20}$$

Now a linear change of variable is made to the independent variable x to simplify the coefficient of the term in y'. The change of variable is given by

$$x=aX+b \rightarrow X=\frac{x-b}{a}$$

where a and b are parameters to be determined. Applying the chain rule the derivatives are given by

$$\frac{dy}{dx}=\frac{dy}{dX}\frac{dX}{dx}=\frac{1}{a}\frac{dy}{dX}, \tag{4.21-a}$$

$$\frac{d^2y}{dx^2}=\frac{1}{a^2}\frac{d^2y}{dX^2}, \tag{4.21-b}$$

$$\frac{d^3y}{dx^3}=\frac{1}{a^3}\frac{d^3y}{dX^3}. \tag{4.21-c}$$

Substituting these results in Equation (4.20) yields to

$$\frac{d^3y}{dX^3}+\frac{1}{EI}[P+w_{\mathrm{c}}(L-aX-b)]a^2\frac{dy}{dX}=a^3\frac{w_{\mathrm{s}}}{EI}(aX+b)+a^3\frac{c}{EI}. \tag{4.22}$$

The parameters a and b are chosen such that the coefficient of y' becomes -X.[6] That is

$$\frac{1}{EI}[P+w_{\mathrm{c}}(L-aX-b)]a^2=-X$$

Expanding this expression and collecting terms dependent and independent of X gives

$$(w_{\mathrm{c}}a^3-EI)X-a^2[P+w_{\mathrm{c}}(L-b)]=0$$

Since this expression must be valid for any possible value of X, it is required that $(w_{\mathrm{c}}a^3-EI)=0$ and $[P+w_{\mathrm{c}}(L-b)]=0$. Therefore, the constants of the linear transformation are

$$\begin{cases} a=\left(\dfrac{EI}{w_{\mathrm{c}}}\right)^{\frac{1}{3}}, \\ b=\dfrac{P}{w_{\mathrm{c}}}+L. \end{cases}$$

The constant a is a positive parameter which depends on the geometry of the column, on the inclination, and on the material the column is made. The positive parameter b has dimension of length in which the term P/w_{c} may be interpreted as an "extension" of the column corresponding to the axial force *P*. Therefore, the change of variable and the inverse transform are given by

6 The reason for this choice is justified in Section 4.2.7.

$$x = X\left(\frac{EI}{w_c}\right)^{\frac{1}{3}} + \left(\frac{P}{w_c} + L\right), \tag{4.23-a}$$

and

$$X = -\left(\frac{EI}{w_c}\right)^{-\frac{1}{3}}\left(\frac{P}{w_c} + L - x\right). \tag{4.23-b}$$

Applying the change of variable to the differential Equation (4.20), rearranging, and using the results of Equation (4.9) yields to

$$y''' - Xy' = \left[\left(\frac{EI}{w_c}\right)^{\frac{1}{3}} \tan\theta\right] X + \left[\left(\frac{P}{w_c} + L\right)\tan\theta + \frac{c}{w_c}\right].$$

Defining the constants

$$\begin{cases} \alpha = \left(\dfrac{EI}{w_c}\right)^{\frac{1}{3}} \tan\theta, \\ b_3 = \dfrac{1}{2}\left[\left(\dfrac{P}{w_c} + L\right)\tan\theta + \dfrac{c}{w_c}\right], \end{cases} \tag{4.24}$$

The differential equation becomes

$$y''' - Xy' = \alpha X + 2b_3. \tag{4.25}$$

The constant α is known from given data. The parameter b_3 is still undetermined because of the integration constant c, which depends on P.

The change of variable resulted in an equivalent but more convenient equation. This equation is classified as a *non-homogeneous linear differential equation of third order with non-constant coefficients*. The same change of variable must be applied to the boundary conditions. If X_1 is the value for $x=0$ (the lower end of the column) and X_2 is the value for $x=L$ (the upper end of the column) the boundaries are now given by

$$\begin{cases} X_1 = -\left(\dfrac{EI}{w_c}\right)^{-\frac{1}{3}} \left(\dfrac{P}{w_c}+L\right), \\ \\ X_2 = -\left(\dfrac{EI}{w_c}\right)^{-\dfrac{1}{3}} \left(\dfrac{P}{w_c}\right). \end{cases} \tag{4.26}$$

In the new scale of the variable X, the length of the column is

$$L_D = X_2 - X_1 = -\left(\frac{EI}{w_c}\right)^{-\frac{1}{3}} L. \tag{4.27}$$

A dimensional analysis shows that the new independent variable X is dimensionless. Since the change of variable affects only the independent variable, the values of y at the boundaries remain unchanged. The values of y'' at the boundaries also remain unchanged because they are homogeneous. Therefore the boundary problem after the change of variable transforms into the following:

$$\begin{cases} y''' - Xy' = \alpha X + 2b_3, \\ \\ y(X_1) = y(X_2) = y''(X_1) = y''(X_2) = 0. \end{cases} \tag{4.28}$$

4.2.7 General Solution of the Differential Equation

The differential equation in Equation (4.28) does not include a term in *y*(*X*), allowing the differential equation to be written as

$$(y')'' - Xy' = \alpha X + 2b_3.$$

Making $z(X) = y'(X)$ results in[7]

$$z'' - Xz = \alpha X + 2b_3. \tag{4.29}$$

This differential equation does not have solutions expressed in terms of elementary functions. The homogeneous form of the Equation (4.29) is known as Airy's differential equation[8] whose solutions are written in terms of the Airy functions $\mathrm{Ai}(X)$ and $\mathrm{Bi}(X)$ as follows:

$$z(X) = c_1 \mathrm{Ai}(X) + c_2 \mathrm{Bi}(X).$$

The solution of the non-homogeneous form can be obtained using variation of parameters. The Wronskian *W*(Ai,Bi) is constant and equal to 1/π and the solution can be written as

$$z(X) = \left[\pi \int_X^D (\alpha x + 2b_3)\mathrm{Bi}(x)dx\right]\mathrm{Ai}(X) + \left[\pi \int_U^X (\alpha x + 2b_3)\mathrm{Ai}(x)dx\right]\mathrm{Bi}(X),$$

7 Here, z is **not** a complex variable but rather the function $z(x) = y'(x)$.
8 The reason for choosing the coefficient of *y*′ equal to -*X* in Equation (4.22).

where b_3, D and E are constants to be determined. The function $z(X)$ must be integrated to determine $y(X)$. This introduces the fourth integration constant required by the initial fourth order differential equation.

Another approach is to obtain a solution from Equation (4.25) by power series taking advantage of the fact that any point $X \neq \infty$ is an ordinary point. The process to obtain the solution is presented in Appendix D. The solution is expressed in closed form in terms of some members of the generalized hypergeometric functions. The general solution and its first and second derivative are written as:

$$y(X) = b_1 M_1(X) + b_2 M_2(X) + b_3 M_4(X) + b_4 - \alpha X, \tag{4.30}$$

$$y'(X) = b_1 R_1(X) + b_2 R_2(X) + b_3 R_4(X) - \alpha, \tag{4.31}$$

$$y''(X) = b_1 N_1(X) + b_2 N_2(X) + b_3 N_4(X). \tag{4.32}$$

The functions M_i, R_i and N_i, for i=1..3 are given by

$$M_1(X) = X\,{}_1F_2\left(\frac{1}{3}; \frac{2}{3}, \frac{4}{3}; \frac{X^3}{9}\right)$$
$$M_2(X) = \frac{X^2}{2}\,{}_1F_2\left(\frac{2}{3}; \frac{4}{3}, \frac{5}{3}; \frac{X^3}{9}\right)$$
$$M_3(X) = \frac{X^3}{3}\,{}_2F_3\left(1, 1; \frac{4}{3}; \frac{5}{3}, 2; \frac{X^3}{9}\right)$$

$$R_1(X) = {}_0F_1\left(\frac{2}{3}; \frac{X^3}{9}\right)$$
$$R_2(X) = X\,{}_0F_1\left(\frac{4}{3}; \frac{X^3}{9}\right)$$
$$R_3(X) = X^2\,{}_1F_2\left(1; \frac{4}{3}, \frac{5}{3}; \frac{X^3}{9}\right)$$

$$N_1(X) = \frac{X^2}{2}\,{}_0F_1\left(\frac{5}{3}; \frac{X^3}{9}\right)$$
$$N_2(X) = {}_0F_1\left(\frac{1}{3}; \frac{X^3}{9}\right)$$
$$N_3(X) = 2X\,{}_0F_1\left(1; \frac{2}{3}, \frac{4}{3}; \frac{X^3}{9}\right)$$

where the functions ${}_pF_q(\alpha_p; \beta_q; x)$ are generalized hypergeometric functions (Erdélyi 1953 - vol. I). The functions $R_1(x)$ and $R_2(x)$ are two independent linear combinations of the Airy functions $\mathrm{Ai}(x)$ and $\mathrm{Bi}(x)$.

4.2.8 Imposing the Boundary Conditions to the General Solution

The final step for the solution of the generalized beam-column problem is the imposition of the boundary conditions. For this particular case (pinned-ends), the boundary conditions given by Equation (4.28) are

$$y(X_1) = y(X_2) = y''(X_1) = y''(X_2) = 0.$$

Using Equations (4.30) and (4.32), the four boundary conditions are written as

$$\begin{cases} y(X_1) = b_1 M_1(X_1) + b_2 M_2(X_1) + b_3 M_4(X_1) + b_4 - \alpha X_1 = 0, \\ y(X_2) = b_1 M_1(X_2) + b_2 M_2(X_2) + b_3 M_4(X_2) + b_4 - \alpha X_2 = 0, \\ y''(X_1) = b_1 N_1(X_1) + b_2 N_2(X_1) + b_3 N_4(X_1) = 0, \\ y''(X_2) = b_1 N_1(X_2) + b_2 N_2(X_2) + b_3 N_4(X_2) = 0. \end{cases}$$

This leads to a non-homogeneous system of linear equations that can be put in matrix form:

$$\begin{bmatrix} M_1(X_1) & M_2(X_1) & M_3(X_1) & 1 \\ M_1(X_2) & M_2(X_2) & M_3(X_2) & 1 \\ N_1(X_1) & N_2(X_1) & N_3(X_1) & 0 \\ N_1(X_2) & N_2(X_2) & N_3(X_2) & 0 \end{bmatrix} \begin{Bmatrix} b_1 \\ b_2 \\ b_3 \\ b_4 \end{Bmatrix} = \alpha \begin{Bmatrix} X_1 \\ X_2 \\ 0 \\ 0 \end{Bmatrix}. \tag{4.33}$$

From linear algebra it is known that a non-homogeneous system does not have a trivial solution, which proves the claim presented in Section (4.2). In addition, the non-trivial solution is unique as long as the matrix of the system is non-singular.

Given the angle θ, the geometry, and the composition of the column, the end points X_1 and X_2 are linear functions of the axial force P as given by Equation (4.27). In addition, X_1 and X_2 are related by Equation (4.27), which implies that X_2-X_1 is constant and represents the length of the inclined beam-column. Changing the axial force P, the interval $[X_1, X_2]$ slides along the negative semi-axis of X. Therefore, the system above can be written as

$$\mathbf{S}(P)\mathbf{b} \;=\; \mathbf{X}.$$

In general, for a given P, the *boundary matrix* $\mathbf{S}(P)$ is non-singular and the system can be solved uniquely for the vector of coefficients $\mathbf{b}$. Consequently, the final configuration of the column (displacement, slope and curvature) is known at any point of its length. However, there may be distinct values for the force P (maybe infinitely many), called critical values, in which the matrix $\mathbf{S}(P)$ becomes singular and no solution exists. At these critical values the displacement at any point becomes unbounded and the structure collapses. No equilibrium (even unstable) exists at all.

4.3 The Solution Using Superposition

The differential equation for the flagpole with pinned-ends, Equation (4.2), and the differential equation for the beam-column, Equation (4.4), can easily be obtained by setting the angle[9] θ equal to 90° respectively in Equation (4.19). Equation (4.19) comprises the two differential equations as special cases.

Someone may conjecture that one could use superposition to obtain the solution of the generalized beam-column using the solutions for the flagpole and the beam-column. It would be as simple as performing the same load decomposition as shown in Figure (4.2), solving the two cases, and then adding the two solutions. However, it will be proved that this is *not* the case.

If $y_{\mathrm{fp}}(x)$ and $y_{\mathrm{bc}}(x)$ are the solutions for the flagpole and the beam-column problems respectively, with regard to the load decomposition of Figure (4.2), the next two expressions are true. From Equation (4.2)

$$Eiy_{\mathrm{fp}}^{(iv)} + [w_{\mathrm{c}}(L-x)y'_{\mathrm{fp}}]' = 0,$$

9 Incorporated in the terms w_{c} and w_{s}.

and from Equation (4.4)

$$EIy_{\mathrm{bc}}^{(iv)} + Py_{\mathrm{bc}}'' = w_{\mathrm{s}}.$$

The solutions $y_{\mathrm{fp}}(x)$ and $y_{\mathrm{bc}}(x)$ are independent because one is dependent on P and the other is not. Making $y_{\mathrm{sp}}(x) = Ay_{\mathrm{fp}}(x) + By_{\mathrm{bc}}(x)$ and assuming that $y_{\mathrm{sp}}(x)$ solves Equation (4.19) for either $A \neq 0$ or $B \neq 0$. Substituting $y_{\mathrm{fp}}(x)$ into Equation (4.19) gives

$$EI(Ay_{\mathrm{fp}} + By_{\mathrm{bc}})^{(iv)} + \frac{d}{dx}\left\{[P + w_{\mathrm{c}}(L-x)](Ay_{\mathrm{fp}} + By_{\mathrm{bc}})'\right\} - w_{\mathrm{s}} = 0$$

Rearranging gives:

$$EI(Ay_{\mathrm{fp}} + By_{\mathrm{bc}})^{(iv)} + \frac{d}{dx}\left\{[P + w_{\mathrm{c}}(L-x)](Ay_{\mathrm{fp}} + By_{\mathrm{bc}})'\right\} - w_{\mathrm{s}} = 0$$

$$A\left\{EIy_{\mathrm{fp}}^{(iv)} + \frac{d}{dx}\left\{[P + w_{\mathrm{c}}(L-x)]y_{\mathrm{fp}}'e\right\}\right\} + \mathrm{B}\left\{EIy_{\mathrm{bc}}^{(iv)} + \frac{d}{dx}\left\{[P + w_{\mathrm{c}}(L-x)]y_{\mathrm{bc}}'\right\}\right\} = w_{\mathrm{s}}$$

$$A\left\{EIy_{\mathrm{fp}}^{(iv)} + \frac{d}{dx}[w_{\mathrm{c}}(L-x)y_{\mathrm{fp}}']\right\} + APy_{\mathrm{fp}}'' + \mathrm{B}\left\{EIy_{\mathrm{bc}}^{(iv)} + Py_{\mathrm{bc}}''\right\} - Bw_{\mathrm{c}}y_{\mathrm{bc}}' = w_{\mathrm{s}}$$

The expressions between braces are null because they solved differential equations for the flagpole and the beam column respectively.

$$APy_{\mathrm{fp}}'' - Bw_{\mathrm{c}}y_{\mathrm{bc}}' = 0$$

To have an identity, the last expression must be true for any x. But this establishes a contradiction because, since the two solutions are independent, the last expression

above can only hold identically for $A = B = 0$. Therefore, the assumption that $y_{\mathrm{sp}}(x) = Ay_{\mathrm{f}}(x) + By_{\mathrm{b}}(x)$ is solution of Equation (4.20) is false.

4.4 Conclusions of the Chapter

In this chapter a model that represents the behavior of a generalized beam-column element was developed. This phenomenon is characterized by a singular behavior instead of an eigenvalue behavior.

The differential equation and the boundary conditions required to make the problem well posed were obtained. The solution of the problem was presented in closed form in terms of some members of the generalized hypergeometric functions. It was also proved that the solution cannot be written as a superposition of the solution for the flagpole and the beam-column problems.

This model will be used in the same fashion as the Euler column solution to determine the buckling force of a drillstring under circular constraints. However, before this problem can be addressed, a detailed analysis of the behavior of the solution is required.

Chapter 5

Analysis Of The Behavior Of A Generalized Beam Column

In this chapter, an analysis of the solution of a generalized beam-column is made. The purpose of this analysis is to determine the general shape of the center line of the element and to characterize the behavior and change of the behavior when combinations of the parameters L, EI, w, θ, and P put the beam-column close to critical values. Due to the diversity of behaviors, a specific terminology will be introduced during the development of the chapter to classify these behaviors.

5.1 Evaluation of the Generalized Hypergeometric Functions

The first problem considered is the evaluation of the hypergeometric functions which comprise the general solution. They must be numerically generated for large negative values of the independent argument X. It is expected that the third buckling mode will require large values for the axial force P which is reflected in large negative values for the dimensionless variables X_1 and X_2. This is analogous to the trigonometric model. In addition, the argument X in the hypergeometric functions occurs in the cubic power.

Three different numerical methods are used to evaluate these functions: series expansion, path integration of differential equation, and asymptotic expansion. The reasons for the use of these methods are described in Appendix E.

5.2 Determining the Singularities of the Boundary Matrix

The change of variable applied to the differential equation introduced the dimensionless parameter L_{D} which accounts for the length L , the stiffness EI, and the distributed weight *w* of the beam-column, and the inclination θ. In addition, the value of the parameter α is also defined. Thus, the only parameters that need to be dealt with for a given configuration are L_{D} and P.

To analyze the solution, a column with fixed L_{D} and α will be selected. If the other parameters are fixed, P and X_2 are linearly related as shown in Equation (4.25). Therefore P and X_2 may be used interchangeably and the reference will be made to the most appropriate for the context. The variable P will be used when dealing with force and the variable X_2 will be used when dealing with the solution of the differential equation.

The first step in analyzing the behavior of the solution is to determine the critical forces for a given configuration. These critical forces occur when the determinant of the boundary matrix $\mathbf{S}$ vanishes. The boundary determinant is defined in Chapter 4 as

$$\mathbf{S}(P) = \mathbf{S}(X_1, X_2) = \begin{bmatrix} M_1(X_1) & M_2(X_1) & M_3(X_1) & 1 \\ M_1(X_2) & M_2(X_2) & M_3(X_2) & 1 \\ N_1(X_1) & N_2(X_1) & N_3(X_1) & 0 \\ N_1(X_2) & N_2(X_2) & N_3(X_2) & 0 \end{bmatrix}.$$

Points X_1 and X_2 are related to L_{D} by Equation (4 27)

$$L_D = X_2 - X_1 = -\left(\frac{EI}{w_{\mathrm{c}}}\right)^{-\frac{1}{3}} L. \tag{4 27}$$

For a given configuration (L, EI, w, and θ) L_{D} is constant and the boundary matrix can be written as a function of X_2, namely

$$\mathbf{S}(X_2) = \begin{bmatrix} M_1(X_2 - L_{\mathrm{D}}) & M_2(X_2 - L_{\mathrm{D}}) & M_3(X_2 - L_{\mathrm{D}}) & 1 \\ M_1(X_2) & M_2(X_2) & M_3(X_2) & 1 \\ N_1(X_2 - L_{\mathrm{D}}) & N_2(X_2 - L_{\mathrm{D}}) & N_3(X_2 - L_{\mathrm{D}}) & 0 \\ N_1(X_2) & N_2(X_2) & N_3(X_2) & 0 \end{bmatrix}$$

The determinant of $\mathbf{S}(X_2)$ can be obtained expanding the fourth column which results in

$$\begin{aligned} \det[\mathbf{S}(X_2)] = & \\ & [M_1(X_2-L_{\mathrm{D}})-M_1(X_2)][N_2(X_2-L_{\mathrm{D}})N_3(X_2)-N_3(X_2-L_{\mathrm{D}})N_2(X_2)] \\ +&[M_2(X_2-L_{\mathrm{D}})-M_2(X_2)][N_3(X_2-L_{\mathrm{D}})N_1(X_2)-N_1(X_2-L_{\mathrm{D}})N_3(X_2)] \\ +&[M_3(X_2-L_{\mathrm{D}})-M_3(X_2)][N_1(X_2-L_{\mathrm{D}})N_2(X_2)-N_2(X_2-L_{\mathrm{D}})N_1(X_2)] \end{aligned}$$

For a given L_{D}, the function $\det[\mathbf{S}(X_2)]$ may be plotted to show the distribution of the roots. Figure (5.1) shows the four first roots for $L_{\mathrm{D}} = 2.0$. The root spacing is not constant and increases for higher roots as can be seen from the plot in Figure (5.1). This is analogous to Euler column theory in which the critical forces are proportional to the square of the order (i.e. n^2). No attempt is made here to obtain a relationship between the roots of $\det[\mathbf{S}(X_2)]$. The maximum amplitude of the waves decreases for increasing X.

For $L_{\mathrm{D}} = 2.0$ all roots are negative. Consequently, such a configuration requires compressive forces to cause buckling. That is not the case when $L_{\mathrm{D}} > 2.64806$. For these configuration one or more roots are positive, which means that the beam-column will buckle even if submitted to a limited axial tension.

In these cases, it is said that the beam-column buckles under the self weight. Figure (5.2) shows the five first roots for $L_{\mathrm{D}} = 2.8$ in which a positive root occurs.

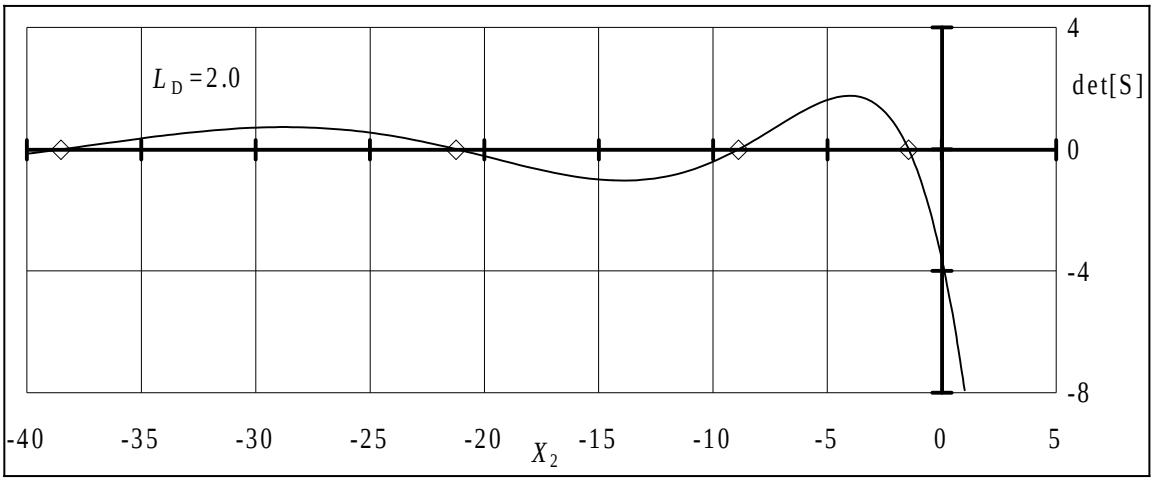

Figure 5.1: Roots of the boundary determinant for L_D=2.0

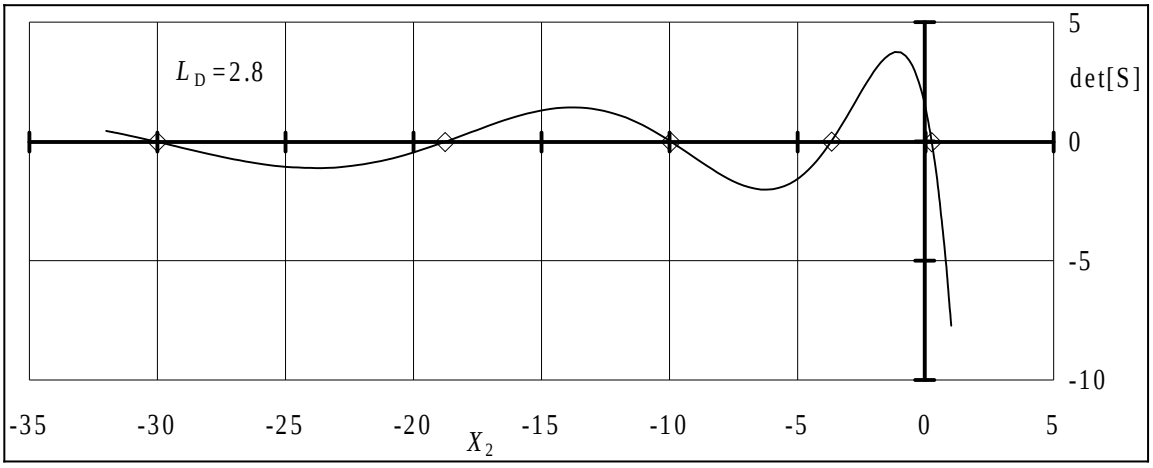

Figure 5.2: Roots of the boundary determinant for L_D=2.8

The dimensionless length of 2.64806 should be compared with the value of 2.65 found by Lubinski for the maximum length for stands of drill pipes or drill collars vertically stacked (Lubinski 1987 - vol. I - pg. 49). The difference corresponds to the precision attained. The dimensionless length 2.64806, however, is not restricted to vertical columns.

Table (5.1) presents roots of det[$\mathbf{S}(X_2)$] for a large range of L_D. For small values of L_D, the roots have large absolute values meaning that the critical forces are very high. Depending upon the material the beam-column is made, it may crush by compression before buckling occurs. Also, there are cases in which the first roots are positive, representing buckling under self weight. The next step is to determine the behavior of the solution close to the critical points.

5.3 Behavior in the Neighborhood of Critical Points

The purpose of this section is to generate the solutions for a specific beam-column configuration under different loading. Finding the solutions and plotting the center line gives an insight into the beam-column behavior.

5.3.1 Generalized Beam-Column Example

The dimensions of the beam-column to be analyzed are that for a regular API 5 in drill pipe. The geometric and mechanical characteristics used are:

L_D	1st root	2nd root	3rd root	4th root	5th root	6th root
0.6	-27.115	-109.363	-246.435	-438.341	-685.148	-986.751
0.7	-19.792	-80.219	-180.930	-321.912	-503.185	-724.742
0.8	-15.021	-61.286	-138.390	-246.338	-385.144	-554.784
0.9	-11.734	-48.289	-109.212	-194.508	-304.172	-438.206
1.0	-9.368	-38.972	-88.327	-157.414	-246.240	-354.806
1.1	-7.604	-32.078	-72.861	-126.956	-203.365	-293.088
1.2	-6.251	-26.817	-61.086	-109.063	-170.748	-246.142
1.3	-5.185	-22.712	-51.911	-92.790	-145.350	-209.589
1.4	-4.329	-19.445	-44.621	-79.869	-125.188	-180.580
1.5	-3.629	-16.800	-38.730	-69.435	-108.913	-157.164
1.6	-3.044	-14.627	-33.900	-60.886	-95.584	-137.991
1.7	-2.551	-12.817	-29.888	-53.793	-84.528	-122.094
1.8	-2.129	-11.293	-26.519	-47.840	-75.255	-108.763
1.9	-1.762	-9.996	-23.659	-42.795	-67.400	-97.473
2.0	-1.440	-8.883	-21.211	-38.481	-60.687	-87.828
2.1	-1.155	-7.918	-19.098	-34.761	-54.902	-79.512
2.2	-0.900	-7.076	-17.259	-31.530	-49.882	-72.312
2.3	-0.669	-6.335	-15.649	-28.706	-45.495	-66.017
2.4	-0.458	-5.680	-14.231	-26.221	-41.640	-60.487
2.5	-0.263	-5.098	-12.973	-24.022	-38.232	-55.601
2.6	-0.082	-4.576	-11.853	-22.067	-35.204	-51.263
2.7	0.086	-4.107	-10.850	-20.320	-32.501	-47.392
2.8	0.244	-3.683	-9.947	-18.751	-30.078	-43.924
2.9	0.295	-3.300	-9.132	-17.338	-27.895	-40.80
3.0	0.539	-2.948	-8.392	-16.058	-25.923	-37.983

Table 5.1: Roots of det[$\mathbf{S}(X_2)$]

E	30.0×10^{6} *psi*
OD	5 *in*
ID	4.276 *in*
L	90 *ft*
w	19.5 *lbf/ft*
θ	31 °
I	6.881×10^{-4} ft^4

Using these numbers, the values of L_D and α are

L_D	1.60
α	33.790 *ft*

The choice for the dimensions above was made without any particular purpose. The angle of 31° was chosen because the resulting value for L_D is in Table (5.1). If the angle is selected as 45° the value would be L_D=1.50. For other values of L_D the resulting numbers would clearly be different, but the behavior would essentially be the same.

5.3.2 Singular Behavior of a Generalized Beam-Column

The generalized beam-column problem has a finite equilibrium solution for any value of the axial force P except for an infinite number of discrete values for which no solution exists. Equilibrium solutions for axial forces less than the first critical force are stable solutions and equilibrium solutions for axial forces greater than the first critical force are unstable solutions. The limitation of small displacements imposes restrictions on how close the force can be to the critical values. In addition, the compressive limit of the beam-column puts restrictions on how intense an axial force can be.

For a given axial force P, the equilibrium configuration is found by solving the system in Equation (4.32) for the coefficient vector $\mathbf{b}$. With $\mathbf{b}$, the solution $y(X)$ and its

first and second derivatives are determined. Figure (5.3) shows solutions for values of X_2 less than the first critical value. The abscissa was chosen X-X_2 to superimpose the curves for different values of X_2.

For $X_2 = 0$ $(P = 0)$, the solution represents the condition in which the beam-column is supported at its ends, and bends due to self weight. As expected, the displacements along the column increase as the value of X_2 is decreased (increased P). These solutions are stable in the sense that if a beam-column is perturbed from its equilibrium state, it will return to equilibrium when the perturbation is removed. In addition, if the axial force changes, the displacements adjust to the equilibrium.

Figure (5.3) also shows the catastrophic behavior when the axial force approaches the singularity. It should be considered that, long before the critical force is reached, the system collapses and the model is no longer valid because the assumption of small displacement is violated. The behavior shown in Figure (5.3) is called *subcritical buckling of first mode* because the axial force P is smaller than the first critical force.

The singularity can be observed for X_2 approaching the first critical force from

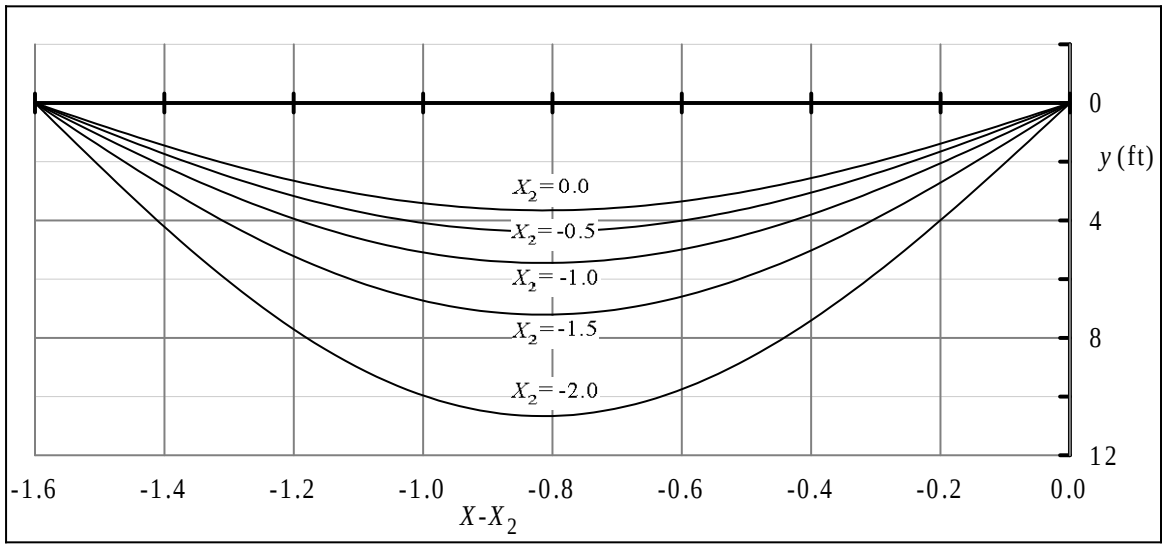

Figure 5.3: Configuration for $P \rightarrow P_1^-$

the right $(X_2 \to 3.0440^{+})$. A plot of the maximum displacement $y_{\max}$ versus X_2 is shown in Figure (5.4). This graph should be compared with the graph shown in Figure (3.3).

Without constraints, the axial force cannot be increased to cross the first critical force without collapsing the beam-column. However, it is expected to have equilibrium configurations for axial forces larger than the first critical force. The solutions will correspond to the shapes the center line must have in order to give equilibrium to the beam-column. The equilibrium for axial forces larger than the first critical force are unstable.

To understand this unstable equilibrium, one may consider that the beam-column is sufficiently supported along its length to prevent collapse when the axial force P is beyond the first critical force $(P_1 < P \ll P_2)$. Then, for an arbitrary initial shape of the center line, the reactions acting on these supports will not be zero. This means that if one support is removed, the center line will change shape. Now, consider moving the supports until the shape of the center line becomes identical to the shape of the equilibrium solution. The closer the center line is to the solution, the smaller the reactions on the supports, and when a perfect fit is reached all reactions will be zero. This means that if

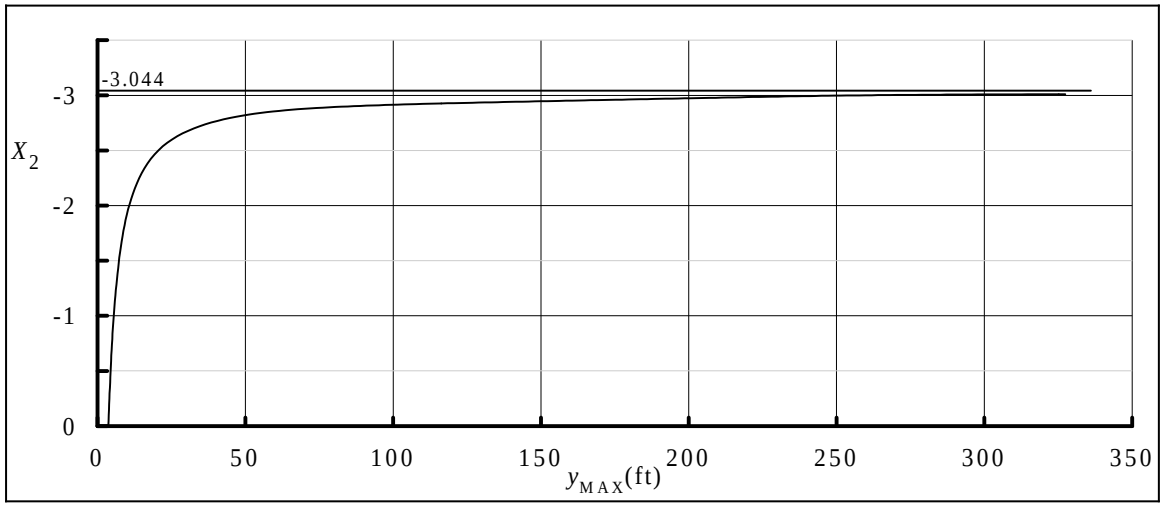

Figure 5.4: Maximum lateral displacement for $P \to P_1^{-}$

the supports are all removed, the center line will remain steady and a state of equilibrium is obtained. Intuitively this equilibrium is unstable in the sense that any slight perturbation of this configuration will cause an immediate collapse of the beam-column.

For X_2 approaching the first root from the left $(X_2 \to 3.0440^{-})$, the equilibrium configurations are those shown in Figure (5.5). The reason for this shape of the center line, in contrast with the subcritical shape, is that the moment generated by the distributed weight acts in opposition to the moment generated by the axial force, helping the bending moment keep the balance. Due to the shape of the center line and to the fact that the force is above the critical, this behavior is called *supercritical buckling of first mode*.

The plot of the maximum lateral displacement $y_{\max}$ versus X_2 is shown in Figure (5.6) where the same behavior as the previous case exists in a symmetric fashion. It seems unnatural that the maximum displacement is smaller for a larger axial force. However this is not a process of increasing the axial force, but a process of finding the equilibrium for a larger force. It becomes clear when one considers that the equilibrium

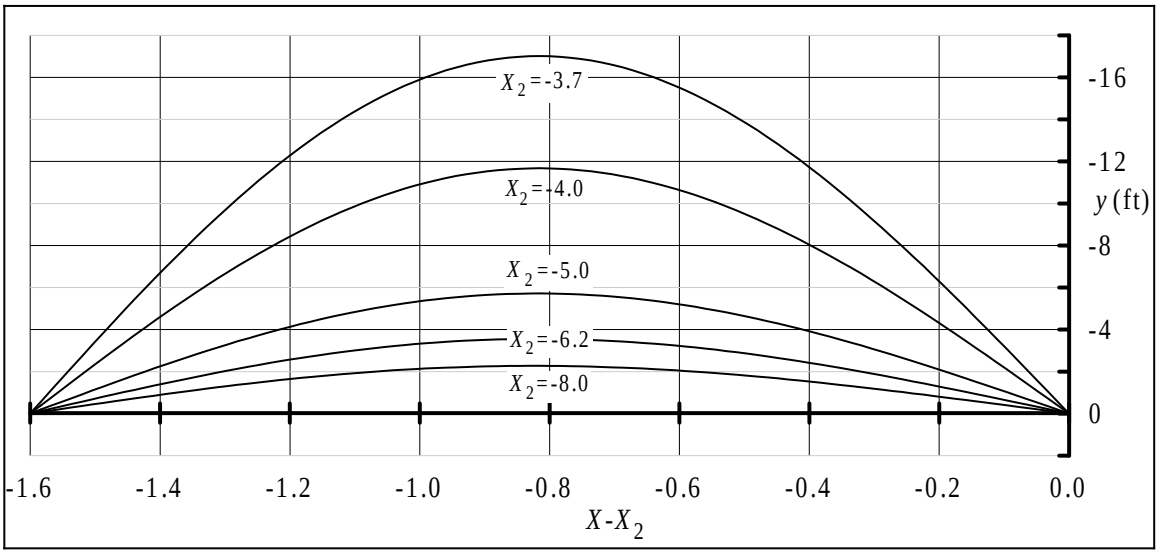

Figure 5.5: Configuration for $P \to P_1^{+}$

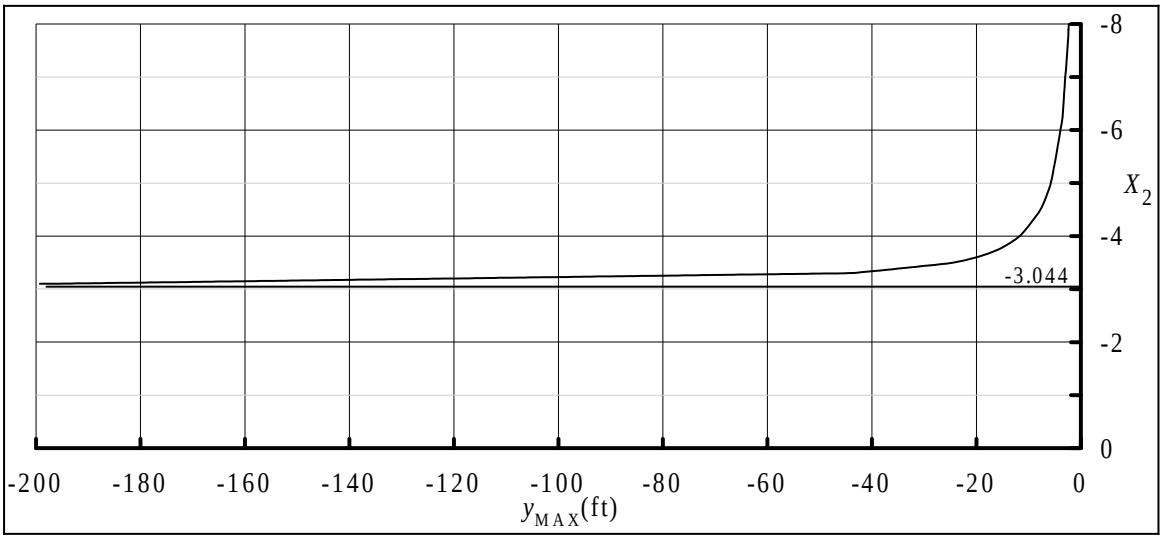

Figure 5.6: Maximum lateral displacement for $P \rightarrow P_1^+$

involves a balance between the moment distribution and the curvature along the beam-column, and how this balance changes with a change of the center line.

The moment distribution due to the distributed weight is fairly insensitive to the shape of the center line. However, the moment distribution due to the axial force is highly dependent on this shape. If the axial force increases there are two ways to reestablish the equilibrium: (1) increasing the curvature, as occurred in the subcritical case, or (2) decreasing the moment. In this case, to compensate for the larger axial force, a decrease in the displacement along the length of the beam-column is required, resulting in a decrease in moment. One cannot increase the curvature and decrease the displacements simultaneously without changing the buckling mode.

Figure (5.7) shows the center line of the beam-column for several values of X_2 as the axial force P increases. As P increases, X_2 moves closer to the second critical value represented by the dimensionless number $X_2 = -14.627$. The graph shows that, for the first time (excluding the ends), the center line crosses the axis. The mode number is given by N+1, where N is the number of times the center line crosses the axis.

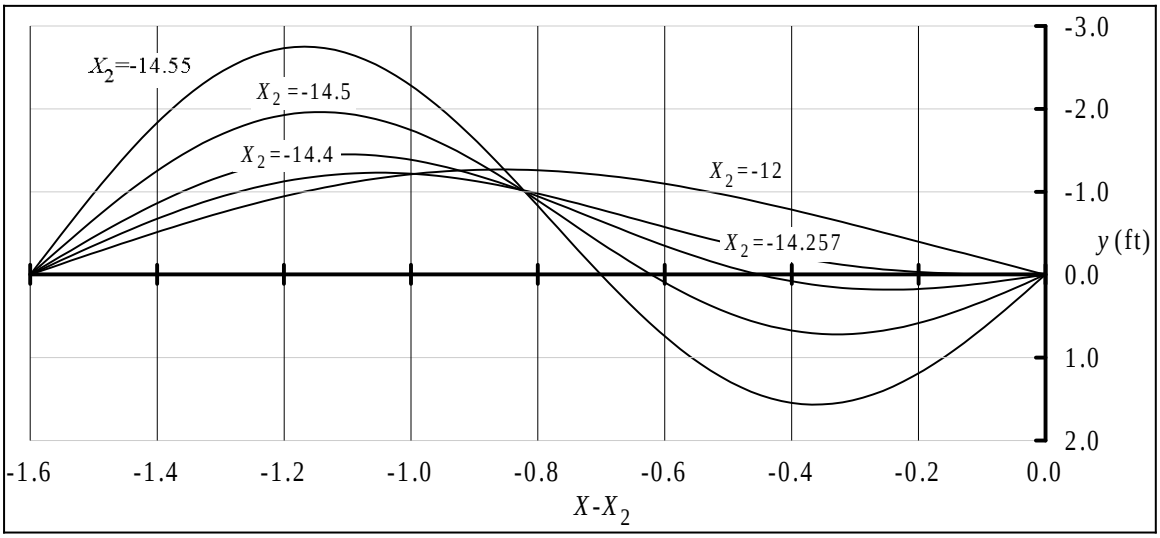

Figure 5.7: Configuration for $P \rightarrow P_2^-$

The value of X_2 where the number of crossing points changes is used to define the limit between two buckling modes. The first change is called the *lower limit* of the second mode and occurs at $X_2 = -14.257$ for this case. It coincides with the *upper limit* of the first mode. This limit is obtained for the value of X_2 at which the derivative at the upper end of the column $X\text{-}X_2 = 0$ vanishes. The region between the lower limit of the second mode and the second critical value is called the *subcritical buckling of second mode*. The effect of the singularity when $X_2 \rightarrow -14.627^+$ is seen in Figure (5.8) for the displacement at (X-X_2=-1.2). This graph represents a continuation of the graph in Figure (5.6) however corresponding to different points along the beam-column.

The next step is the analysis of the behavior when X_2 approaches the second critical force from the left ($X_2 \rightarrow -14.627^-$). A reverse behavior similar to the subcritical case is shown in Figure (5.9). The upper limit for the second mode is found to be $X_2 = -14.985$. At this value, the derivative at the lower end of the column vanishes $X - X_2 = L_D = -1.6$. Analogously, this region is called the *supercritical buckling of second mode.*

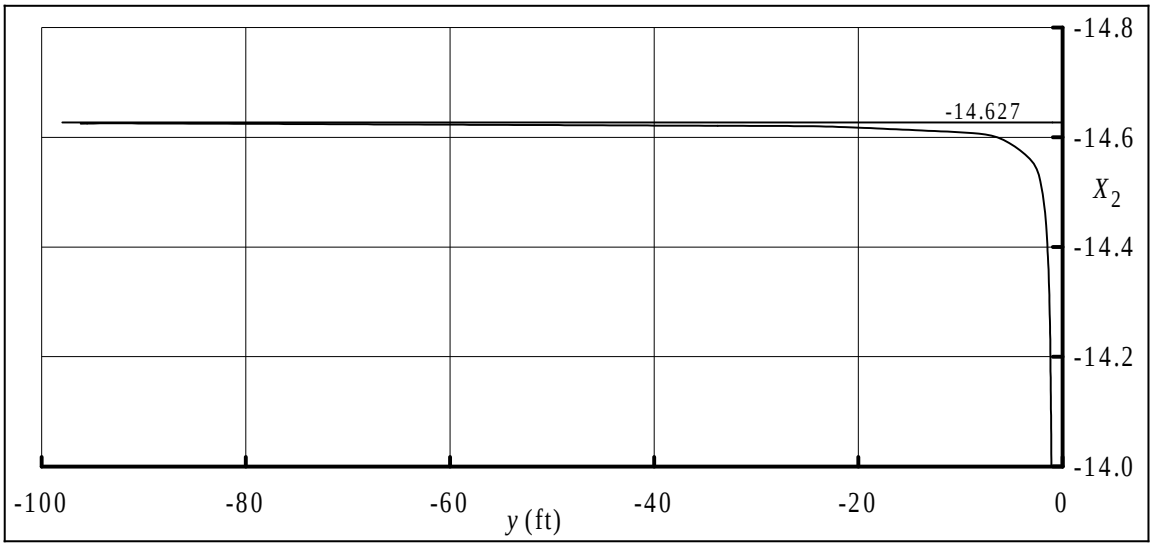

Figure 5.8: Maximum lateral displacement for $P \rightarrow P_2^-$ and X-X_2=-1.2

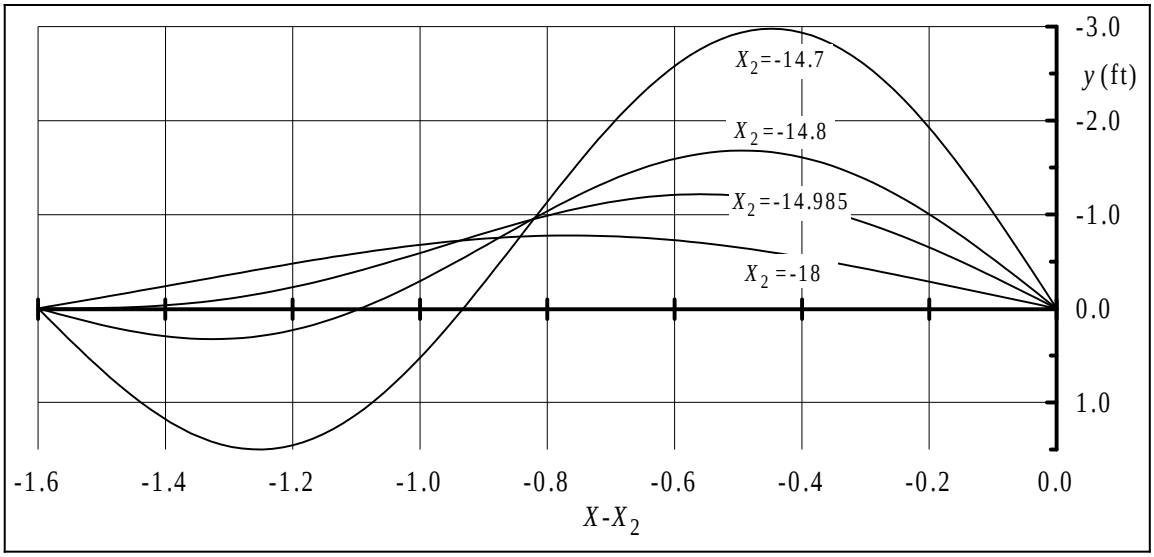

Figure 5.9: Configuration for $P \rightarrow P_2^+$

The lower and upper limits for the second mode define the region of the second buckling mode. For the beam-column in this example, this region is the interval (-14.985,-14.257) with a singularity at $X_2 = -14.627$. Since the derivative never vanishes at the ends of the beam-column in the subcritical region of first mode, (the beam-column can never be made straight, even under tension), there is no corresponding lower limit for the first buckling mode.

For $X_2 = -18$ in Figure (5.9), the curve has a shape resembling those of the first mode. For values larger (up to a point) than the upper limit of the second mode the curve does not cross the axis which could erroneously indicate buckling of first mode. The axial force, however, is far beyond the limits for first mode buckling and even beyond the second mode. The equilibrium in this region is called *pseudo buckling of first mode*. Regions like this occur again in higher modes.

The final step in this analysis is to approach the third singularity at $X_2 = -33.900$. Figure (5.10) illustrates this process for X_2 approaching the singularity from the right ($X_2 \rightarrow -33.900^{+}$). For values far below the singularity ($X_2 = -20$), the beam-column is in

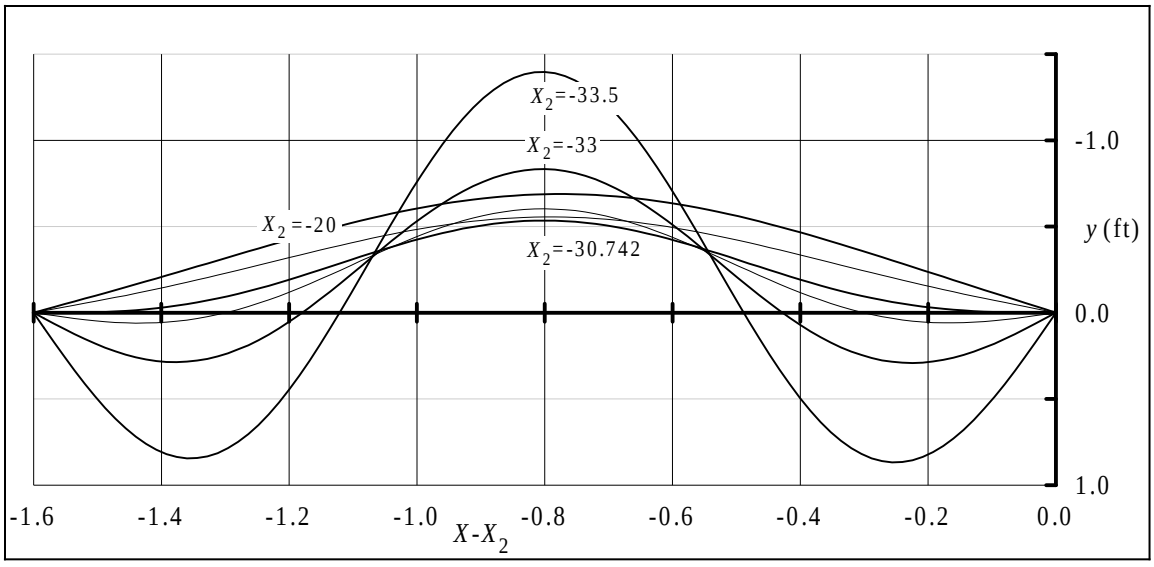

Figure 5.10: Configuration for $P \rightarrow P_3^{-}$

the region of pseudo buckling of first mode. Reaching $X_2 = -30.676$ the derivative at X_1 vanishes (but not at X_2) and the beam-column enters the region of pseudo buckling of second mode. This region is very narrow and at $X_2 = -30.742$ the derivative at X_2 vanishes and the beam-column enters the region of subcritical buckling of third mode. This value, $X_2 = -30.742$, represents the lower limit for the third mode. The curve resembles the 1½-periods of a sine curve as in Chapter 2. The curve, however, is slightly asymmetrical, and the most important characteristic is the difference between the amplitude of the central wave and the amplitude of the external waves.

The interval (-33.900, -30.742) defines the region of subcritical buckling of third mode. This region will be used to determine the buckling force in the same way as the third mode of the Euler column solution in Chapter 3. The characteristics of curves in the region of subcritical buckling of third mode indicate that this buckling mode should be used for curved bore-holes with build gradients. This is because the external waves grow downward and the central wave grows upward.

To complete the analysis, the process for X_2 approaching the third singularity from the left $(X_2 \rightarrow -33.900^{-})$ is shown in Figure (5.11). The curves also resemble the 1½-periods of a sine curve like the curves in the subcritical region. In this case, however, the direction of the displacements is reversed. This indicates that this buckling mode should be used for curved bore-holes with drop gradients.

The region of supercritical buckling of third mode ends when the central wave of the curve crosses the axis, here at $X_2 = -35.085$. After this value, the beam-column enters in another region of pseudo buckling of first mode. It is beyond the scope of this investigation to analyze and describe the behavior for axial forces above the third critical mode.

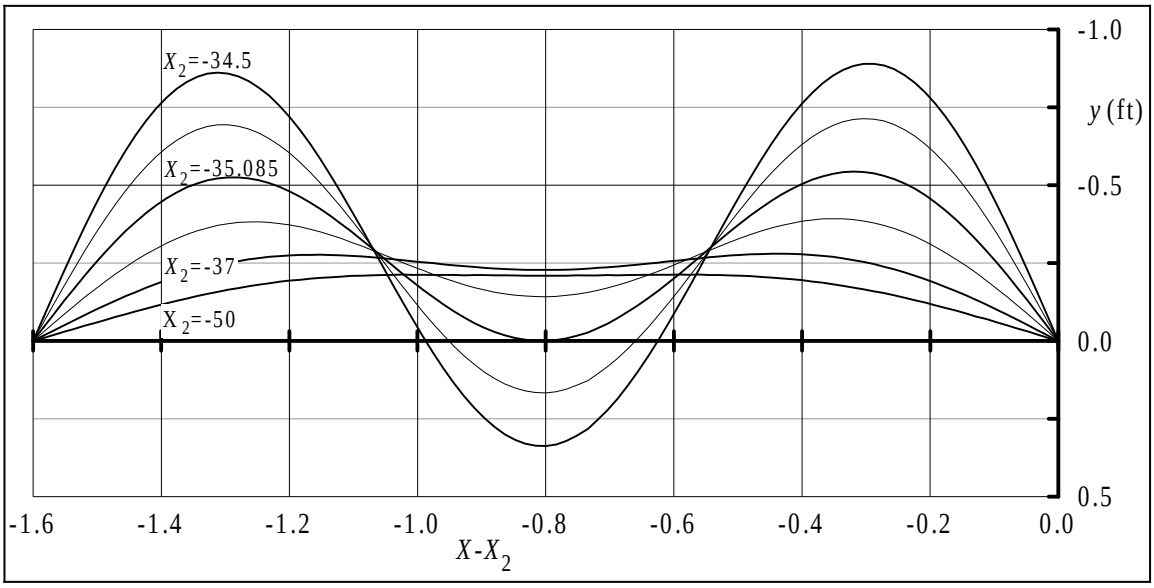

Figure 5.11: Configuration for $P \rightarrow P_3^+$

5.4 Conclusions of the Chapter

The analysis made in this chapter shows the behavior and characteristics of a generalized beam-column up to the third mode based on the model developed in Chapter 4. Although several assumptions have been made to obtain the differential equation, this analysis shows that the model furnishes a very accurate description of the expected behavior of a generalized beam-column. That is, no trivial solution exists, the solutions have infinitely many singularities which correspond to different modes of buckling, and the deflection curves resemble those for the Euler column in which the number of half-periods is equal to the buckling mode number.

The region of subcritical buckling of third mode should be used to model the buckling of drillstrings within curved bore-holes with build gradients. The region of supercritical buckling of third mode should be used to model the buckling of drillstrings within curved bore-holes with drop gradients.

Chapter 6

The Hypergeometric Model

The procedure to determine the buckling force of a weighted drillstring within two concentric circular constraints uses the same idea applied to the weightless case.

The curved bore-hole theory will be associated with the generalized beam-column theory. In this process, a new parameter must be considered: the change of inclination of the drillstring along the bore-hole. Since the inclination affects the buckling force of a beam-column, it is expected that the buckling force changes along the bore-hole. Therefore, in contrast with the trigonometric model, in which only one buckling force is determined, the hypergeometric model will determine a distribution of buckling force. Also, since the shape of the buckled beam-column is not periodic (Chapter 5), parameters as wave-length and maximum amplitude cannot be explored. In particular, from the analysis made in Chapter 5, it is known that the amplitudes of the inner and outer waves in the subcritical and supercritical buckling of third mode are different in a buckled beam-column. However, the same concept of the center of curvature will be applied.

The increased number of variables and the functions that have to be evaluated suggest that the computational effort to find the solution will be larger using the hypergeometric model than using the trigonometric model.

The buckling force at the point of inclination θ is called the *local buckling force* and denoted by P'_{θ}. This is to differentiate from the *causational buckling force*, denoted by ${}_{\theta 1}P_{\theta 2}$, which represents the axial force that must be applied at the point of inclination θ_1 to buckle the drillstring about the point of inclination θ_2, for $\theta_2 \geq \theta_1$.

6.1 Differences Between Building and Dropping Bore-Holes

The difference in the buckling behavior between a building bore-hole and a dropping bore-hole is due to two factors. The first is the expected shape of the buckled portion, and the second is the sequence of events during the buckling process.

In a building bore-hole, the buckling process occurs in the region of subcritical buckling of third mode, whereas in a dropping bore-hole, the buckling process occurs in the region of supercritical buckling of third mode. This does not mean that, under the same mechanical conditions, the critical force in a dropping bore-hole will be larger than the critical force in a building bore-hole.

In a building bore-hole, the buckling process starts with the drillstring lying on the lower generatrix of the curved bore-hole which is identical to the outer constraint of the problem. This means that the constraints will immediately lend resistance to the drillstring. In a dropping bore-hole, the buckling process will also start with the drillstring lying on the lower generatrix of the curved bore-hole. But now this generatrix is identical to the inner constraint of the problem. Depending on the distributed weight, stiffness of the drillstring, and drop gradient, the drillstring may be pushed against the outer constraint and acquire resistance or it may start buckling even without touching the outer constraint. Because of the importance of building bore-holes in the petroleum industry, especially in horizontal drilling, this work deals only with building-angle of bore-holes.

6.2 Analysis of the Build Section of a Curved Bore-hole

In a building bore-hole, it is assumed that the weight is applied by thick-walled drill collars positioned in the vertical section of the bore-hole at the top of the curved section called the *kickoff point* (KOP). The point of application of the weight can be made

more general as will be seen in Section 6.3.1. Of concern is the maximum permissible weight that can be applied at the kickoff point (*WKOP*$_{max}$) without putting the drillstring at risk of buckling. The maximum permissible weight applied at the KOP determines the maximum weight available to be applied on the drill bit, *WOB*$_{max}$. For simplicity, since the inclination at the KOP is zero, the causational buckling force will be denoted by $P_\theta = {}_0P_\theta$. For a given *BG*[1] and the inclination at the position of the drill bit β, the maximum weight on bit[2] is given by

$$WOB_{\max} = WKOP_{\max} + \frac{w}{BG}\sin\beta. \tag{6.1}$$

The deeper the point along the curved section, the more inclined the bore-hole and, consequently, the higher the buckling force becomes. However, the compressive axial force down the drillstring increases because of the accumulation of the distributed weight. Therefore, the point of buckling depends on the gradient of the buckling force and the gradient of the compressive force along the drillstring.

The causational buckling force is related to the local buckling force by

$${}_{\theta 1}P_{\theta 2} = P'_{\theta_2} - \frac{w}{BG}\left(\sin\theta_2 - \sin\theta_1\right) \tag{6.2}$$

and, therefore, to calculate *WKOP*$_{max}$ it is necessary to determine the angle θ_2 with minimum P_{θ_2}. *WKOP*$_{max}$ is given by

$$WKOP_{\max} = \min(P_{\theta_2}) \qquad 0 \le \theta_2 \le \beta \tag{6.3}$$

---

1 Usually in degrees/100 ft, degrees/30m, degrees/10ft converted to radians/length.
2 Not including the drag along the curved section of the bore-hole

Algebraic manipulation of Equations (6.1), (6.2), and (6.3) results in

$$WOB_{\max} = \min\left[P'_{\theta_2} + \frac{w}{BG}(\sin\beta - \sin\theta_2)\right] \qquad 0 \le \theta_2 \le \beta \tag{6.4}$$

6.2.1 Frictional Effects

The above formulas do not consider the friction between the drillstring and the bore-hole wall. To introduce friction, the following aspects are considered:

1- Friction exists where contact exists. In a 2D model only point or line contacts exist. The buckled portion of the drillstring has contact with the bore-hole wall only at its extremes. The contact the column makes with the inner constraint does not produce any friction force because the normal force is zero. This implies that the local buckling force P' is free of any frictional effect.

2- The distributed force along the contact line will produce friction forces for the unbuckled portions of the drillstring. These friction forces will affect the causational buckling force and, consequently, the $WKOP_{max}$ and WOB_{max}.

3- The distributed force along the contact line is not constant and depends on the stiffness of the drillstring, the curvature of the bore-hole, and the distribution of the axial force.

The axial force increases from the KOP toward the bit. If P is the axial force applied at the point of inclination θ_1, then the average value for the axial force between this point and the point of inclination θ_2 is

$$\bar{P}(\theta_1, \theta_2) = P + \frac{180}{\pi}\frac{w}{BG}\left[\frac{\cos\theta_1 - \cos\theta_2}{\theta_2 - \theta_1} - \sin\theta_1\right].$$

Neglecting the stiffness effects of the drillstring, the average radial distributed force along the contact line is

$$\bar{w}_{\text{rad}}(q_1, q_2) = \frac{p}{18000} P\,BG + \frac{1}{2}\left[\sin(q_2) - \sin(q_1)\right] w\,.$$

Consequently, the average friction force acting along the contact line between θ_1 and θ_2 is

$$\bar{F}_f(\theta_1, \theta_2) = \mu(\theta_2 - \theta_1)\left\{ P + \frac{9000}{\pi BG}\left[\sin(\theta_2) - \sin(\theta_1)\right] w \right\} \tag{6.5}$$

The friction force should be added to Equation (6.2) and (6.3) to obtain the correct values for ${}_{\theta 1}P_{\theta 2}$ and $WKOP_{\max}$. The friction force should be subtracted from Equation (6.4) to obtain the correct values for $WOB_{\max}$. In this case, the angle θ_2 plays the role of θ_1, and the angle at the bit β plays the role of θ_2 in Equation (6.5). The correction for friction cannot be applied directly to Equation (6.1).

In this investigation, no correction will be made to account for friction. The reason is that this model is a *theoretical model* which depends on experimental results to validate the theory. Experiments dealing with friction are time consuming because they require several repetitions for averaging purposes. In addition, the large number of variables affecting the friction coefficients (lubricant type, contact surface finish and heterogeneity, and others), and their uncertainties, make the experiments difficult to control. Using high frequency vibration is the best way to minimize or even eliminate the effects of friction upon the experiments. With this approach, a frictionless model can be validated and the effects of friction introduced later. Friction was minimized in the experiments and not considered in the predictions for Chapter 7. In addition, the simulations presented in Chapter 7 for field dimensions do not include any correction for friction.

6.2.2 Local Buckling Force at a Given Angle θ

The kernel of the hypergeometric model is the calculation of the local buckling force for any given angle θ along the curved section. Figure (6.1) shows a schematic of a buckled drillstring, with the parameters concerned with the determination of the local buckling force. The concepts of the curved bore-hole theory are applied in the same fashion as for the trigonometric model.

Three buckling conditions have to be satisfied. The buckled portion must be tangent to the outer constraint at both ends; the curvature at the ends must be equal to the curvature of the circle; and the central wave must be tangent to the inner constraint. These three conditions will impose a fit of the buckled element between the two concentric circular constraints.

From the generalized beam-column theory, two variables can be handled to obtain the fit: the complementary length of the buckled portion L', and the axial force which should impose a buckling on the element in the region of subcritical buckling of third mode. The goal is to satisfy the above three conditions by adjusting these two variables.

6.2.3 Functional Measurement of the Fit

The three conditions for the fit, as stated in the previous section, are quite formal and an alternate functional form is required. The fit must be expressed in a way that permits mathematical handling.

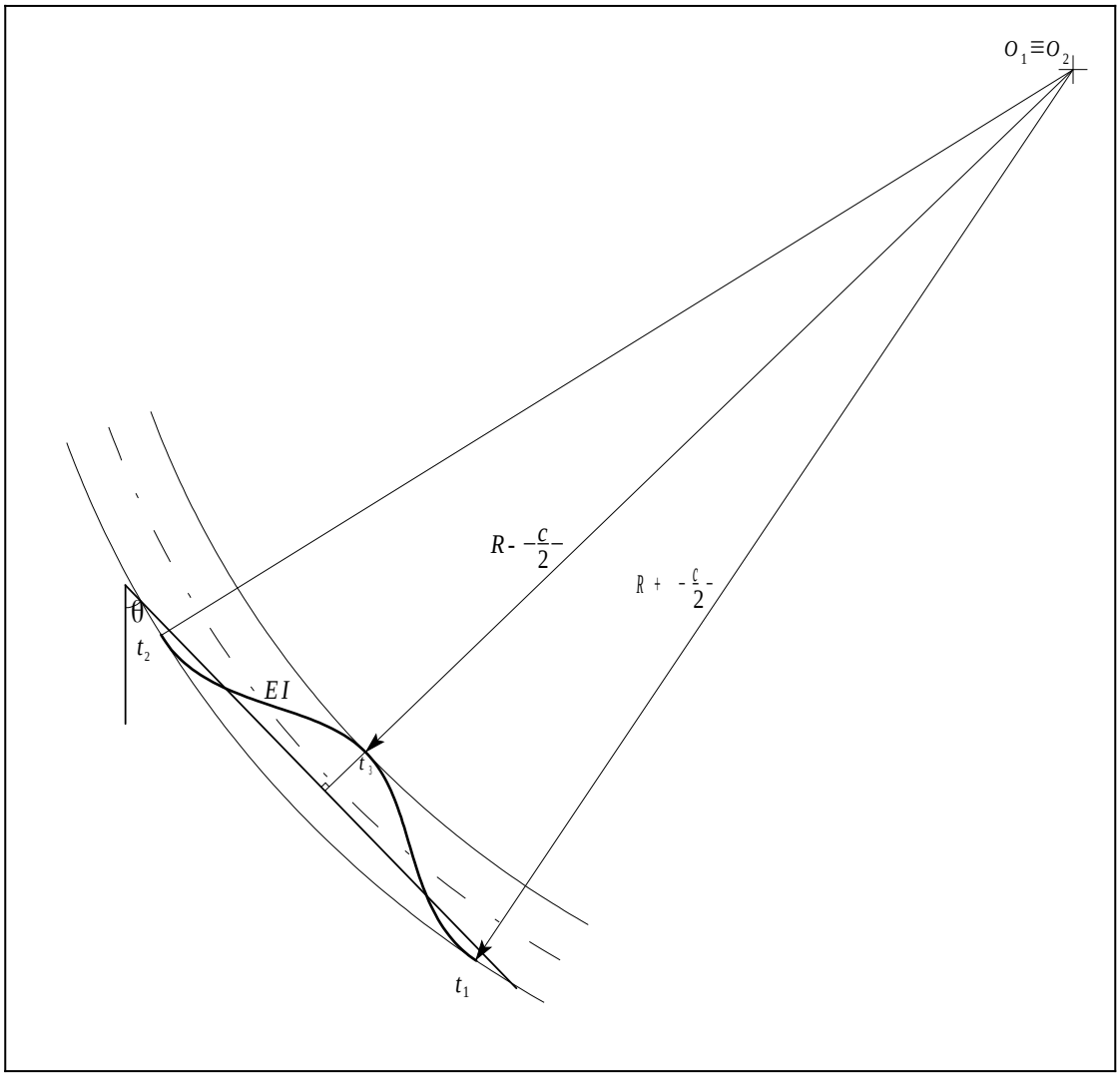

Figure 6.1: A generic buckled portion of a drillstring

For a complementary length L' and a force P in the region of subcritical buckling of third mode, the center line of the drillstring has the shape of a $1^1/_2$-waves. If a fit exists, it is possible to find one and only one point at each one-sixth end portion of the element, t_1 and t_2, whose radii of curvature satisfy (see Figure [6.1]):

$$\rho_1 = \rho_2 = R + \frac{c}{2}, \tag{6.6}$$

and the centers of curvature O_1 and O_2 coincide. R is the radius of the center line of the curved bore-hole and *c* is the diametrical clearance between the bore-hole wall and the outside diameter of the drillstring. The coincidence between the two centers is expressed by

$$O_1 \equiv O_2 \Leftrightarrow \begin{cases} x_{O1} = x_{O2} \\ y_{O1} = y_{O2} \end{cases} \tag{6.7}$$

In addition, the circle with center at $O_1 \equiv O$ and radius of curvature $R - \frac{c}{2}$ is tangent to the central wave at t_3. This is expressed by

$$\sqrt{(x_3 - x_o)^2 + (y_3 - y_o)^2} = R - \frac{c}{2}. \tag{6.8}$$

Equations (6.7) and (6.8) give the three quantities that can be measured to assess the goodness of the fit. Residuals of these three measures are obtained and an appropriate normalization applied. The normalizations used are the clearance *c* for the residual of the radii of curvature and the bore-hole radius R for the residuals of the coordinates of the

centers of curvature. These three normalized residuals are functions of the complementary length L' and the axial force P. They are, then, expressed by

$$f_1(L', P) = \frac{\sqrt{(x_3 - x_O)^2 + (y_3 - y_O)^2} - (R - \frac{c}{2})}{c}, \tag{6.9-a}$$

$$f_2(L', P) = \frac{x_{c1} - x_{c2}}{R}, \tag{6.9-b}$$

$$f_3(L', P) = \frac{y_{c1} - y_{c2}}{R}. \tag{6.9-c}$$

A fit exists if one can find L'_{fit} and P_{fit} such that

$$f(L'_{\text{fit}}, P_{\text{fit}}) = \begin{Bmatrix} f_1(L'_{\text{fit}}, P_{\text{fit}}) \\ f_2(L'_{\text{fit}}, P_{\text{fit}}) \\ f_3(L'_{\text{fit}}, P_{\text{fit}}) \end{Bmatrix} = \begin{Bmatrix} 0 \\ 0 \\ 0 \end{Bmatrix}.$$

Since L' and P correspond uniquely to the pair of dimensionless variables X_1 and X_2, the problem of fit can be written in the form

$$f(X_1, X_2) = \begin{Bmatrix} f_1(X_1, X_2) \\ f_2(X_1, X_2) \\ f_3(X_1, X_2) \end{Bmatrix} = \begin{Bmatrix} 0 \\ 0 \\ 0 \end{Bmatrix}. \tag{6.10}$$

6.2.3.1 Numerical Evaluation of the Vector Fit Function *f*(X_1,X_2)

For almost any arbitrary pair (X_1, X_2), and the mechanical and geometrical properties of the drillstring, the boundary system of Equation (4.33) may be solved for the coefficient vector $\mathbf{b}$:

$$\mathbf{S}(X_1, X_2)\mathbf{b} = \alpha \begin{Bmatrix} X_1 \\ X_2 \\ 0 \\ 0 \end{Bmatrix}$$

With $\mathbf{b}$, the expressions for the displacement, the first derivative, and the second derivative can be calculated using (see Chapter 4)

$$y(X) = b_1 M_1(X) + b_2 M_2(X) + b_3 M_4(X) + b_4 - \alpha X, \tag{4.30}$$

$$y'(X) = b_1 R_1(X) + b_2 R_2(X) + b_3 R_4(X) - \alpha, \tag{4.31}$$

$$y''(X) = b_1 N_1(X) + b_2 N_2(X) + b_3 N_4(X). \tag{4.32}$$

The first step is to find the two points X_{t1} and X_{t2} in the interval between X_1 and X_2, where the radii of curvature are equal $R + \frac{c}{2}$ to . To calculate the radius of curvature, the following expression is used: (See Appendix B, eq. [B.1].)

$$\rho(X) = \frac{\left[1 + y'^2(X)\right]^{\frac{3}{2}}}{y''(X)}.$$

Therefore, the two points X_{t1} and X_{t2} solve the equation

$$\rho(X) - \left(R + \frac{c}{2}\right) = 0. \tag{6.11}$$

There may be zero, two, four or six points in the interval between X_1 and X_2 that satisfy this equation as shown in Figure (6.2). If the shape of the center line is too flat so that the minimum radius of curvature in one of the half-waves is larger than $R+c/2$, then no point in this half-wave satisfies Equation (6.11). Only points in the two extreme sixths are acceptable. The search process to find the two points should avoid the internal solutions because they do not represent acceptable tangency points. The process should also avoid selecting points outside the interval (X_1, X_2). A *Modified Newton-Raphson* method (one which permits limited backtracking) is used to find these roots, with the numerical derivative calculated using the *Richardson's deferred approach to the limit* technique. These two numerical methods are presented and analyzed by Press et. al. (1992). The use of simple finite differences proved to be unstable in prototype tests.

When a new case is run, no other information is available and a fixed initial guess is required for the Newton-Raphson method. However, after the first two points are found additional information is available for the next iteration.

The initial guess is controlled by two variables, a fraction and an eccentricity, defined as follows:

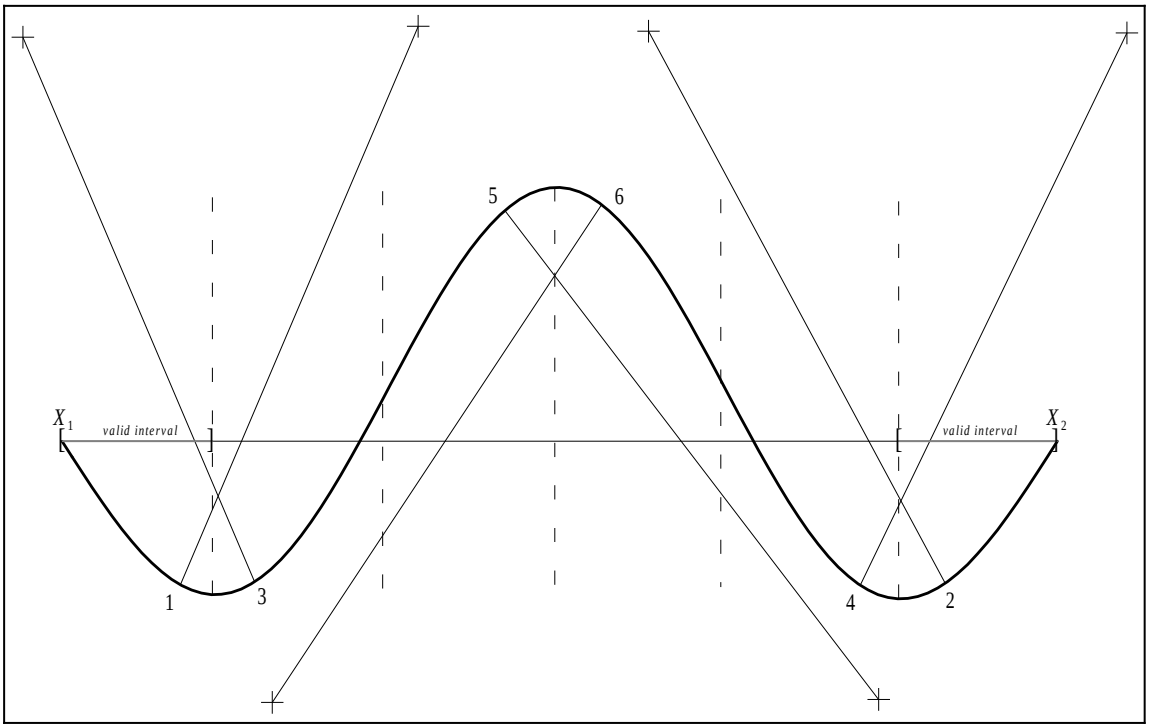

Figure 6.2: Six quarter of wave with six points that satisfy Equation (6.2)

$$f_{\mathrm{g}} = \frac{X_{\mathrm{t}2} - X_{\mathrm{t}1}}{X_2 - X_1},$$

$$e_{\mathrm{g}} = \frac{(X_2 - X_{\mathrm{t}2}) - (X_{\mathrm{t}1} - X_1)}{(X_2 - X_{\mathrm{t}2}) + (X_{\mathrm{t}1} - X_1)}. \tag{6.12-a}$$

Inverting these expressions yields to

$$X_{\mathrm{t}1} = \frac{1}{2}\left(1 + e_{\mathrm{g}} + f_{\mathrm{g}} - e_{\mathrm{g}} f_{\mathrm{g}}\right) X_1 + \frac{1}{2}\left(1 - e_{\mathrm{g}} - f_{\mathrm{g}} + e_{\mathrm{g}} f_{\mathrm{g}}\right) X_2,$$

$$X_{\mathrm{t}2} = \frac{1}{2}\left(1 + e_{\mathrm{g}} - f_{\mathrm{g}} - e_{\mathrm{g}} f_{\mathrm{g}}\right) X_1 + \frac{1}{2}\left(1 - e_{\mathrm{g}} + f_{\mathrm{g}} + e_{\mathrm{g}} f_{\mathrm{g}}\right) X_2. \tag{6.12-b}$$

In prototype tests, the fraction varied between 0.95 and 0.97 and the eccentricity is always close to zero, revealing a very small asymmetry in the shape of the center line. Based on these prototype tests, f_{g}=0.96 and e_{g}=0 are good starting points for new runs. When, or if, the pair of points X_{t1} and X_{t2} is found, the fraction and eccentricity are recalculated and saved for the next iteration.

The second step is to find the centers of curvature. This is done using Equation (B.2):

$$\begin{cases} x_{\mathrm{c}}(x) = x - \left[1 + y'(x)^2\right] \frac{y'(x)}{y''(x)}, \\ y_{\mathrm{c}}(x) = y(x) + \left[1 + y'(x)^2\right] \frac{1}{y''(x)}. \end{cases} \tag{B.2}$$

Care must be taken when performing these calculations in order to assure that the coordinates are homogeneous. Using the expressions for the derivatives in Equations (4.21-a,b) we obtain:

$$y'(x) = \left(\frac{w_{\mathrm{c}}}{EI}\right)^{\frac{1}{3}} y'(X),$$
$$y''(x) = \left(\frac{w_{\mathrm{c}}}{EI}\right)^{\frac{2}{3}} y''(X).$$

With the centers of curvature, the test functions f_2 and f_3 are calculated from Equations (6.9-b,c).

The third step is to calculate the component f_1. By definition, this component exists only when the two centers O_1 and O_2 coincide. However, f_1 is required for the fit search process. A possible solution uses the average center O given by

$$O = (x_O, y_O) = \frac{O_1 + O_1}{2} = \left(\frac{x_{c1} + x_{c2}}{2}, \frac{y_{c1} + y_{c2}}{2} \right).$$

When the fit is found the centers O_1 and O_2 coalesce, and the component f_1 defines. Finally, the fraction f_g and the eccentricity e_g may be recalculated for the next iteration using Equation (6.12).

6.2.4 Searching for the Fit

The search for the fit is the process of finding X_1 and X_2 which satisfy Equation (6.10). The first problem becomes evident: this is a nonlinear overdetermined system with three equations and two variables. Nonlinear problems like this are usually difficult to solve. There is no theorem for existence and uniqueness of solutions. However, by the nature of the problem, it is expected that a unique solution exists which satisfies the constraints.

The system is linearized using truncation of the Taylor's series expansion for the fit function $\mathbf{f} = (f_1, f_2, f_3)$, and a modified Newton-Raphson procedure[3] is employed to search for the root. The overdetermined linear system used in the Newton-Raphson procedure is

$$\begin{bmatrix} f_{1,1}(X_{1,n}, X_{2,n}) & f_{1,2}(X_{1,n}, X_{2,n}) \\ f_{2,1}(X_{1,n}, X_{2,n}) & f_{2,2}(X_{1,n}, X_{2,n}) \\ f_{3,1}(X_{1,n}, X_{2,n}) & f_{3,2}(X_{1,n}, X_{2,n}) \end{bmatrix} \begin{Bmatrix} \delta X_{1,n+1} \\ \delta X_{2,n+1} \end{Bmatrix} = - \begin{Bmatrix} f_1(X_{1,n}, X_{2,n}) \\ f_2(X_{1,n}, X_{2,n}) \\ f_3(X_{1,n}, X_{2,n}) \end{Bmatrix}. \quad (6.13)$$

where

3 See Appendix F for derivation of the Newton-Raphson expression for a non-square system of nonlinear equations.

$$\delta X_{i,n+1} = X_{i,n+1} - X_{i,n} \tag{6.14}$$

Two approaches are used to solve this problem. The first approach reduces the order of the problem by neglecting one of three equations and working with a 2×2 system. The second uses the *full rank least square* method. The choice of the approach rests on the state of the fit during the process and is explained in Section (6.2.4.3).

6.2.4.1 Reducing the Order of the System

The less sensitive component of the fit is f_3 which measures the distance between the two centers of curvature in the y-direction. The component f_3 approaches zero when the other two components approach zero because of the constraints imposed on the solution. In most cases, the magnitude of f_3 is smaller than that of f_1 and f_2 (away from the limits $\theta = 0^\circ$ and $\theta = 90^\circ$), even when no control is imposed on it. Therefore, neglecting the third equation of the linearized system in Equation (6.13) the problem reduces to

$$\begin{bmatrix} f_{1,1} & f_{1,2} \\ f_{2,1} & f_{2,2} \end{bmatrix} \begin{Bmatrix} \delta X_{1,n+1} \\ \delta X_{2,n+1} \end{Bmatrix} = - \begin{Bmatrix} f_1 \\ f_2 \end{Bmatrix}. \tag{6.15}$$

At each iteration, this system is first solved for $\delta X_{1,n+1}$ and $\delta X_{2,n+1}$ and then for $X_{1,n+1}$ and $X_{2,n+1}$, the next candidates in the iteration process.

6.2.4.2 Full Rank Least Square Method

For a given overdetermined system of linear equations of the form

$$\mathbf{A}\mathbf{x} = \mathbf{b},$$

the idea is to find $\mathbf{x}$ which minimizes the norm $\|\mathbf{A}\mathbf{x} - \mathbf{b}\|_p$ for some suitable choice of p. In general, p assumes one of the values 1, 2 or ∞. Norm minimization for $p=2$, or 2-norm, is known as *least squares* and is much more tractable then the 1-norm or the ∞-norm[4]. It can be shown (Golub, Van Loan - pg. 222) that if $\mathbf{A}$ has full column rank (rank 2 in this case), there is an unique least square solution $\mathbf{x}_{\mathrm{LS}}$ and it solves the symmetric positive definite linear system, called *normal equations*,

$$\mathbf{A}^{\mathrm{T}}\mathbf{A}\mathbf{x}_{\mathrm{LS}} = \mathbf{A}^{\mathrm{T}}\mathbf{b}.$$

Applying this formula to the system to Equation (6.13) yields to

$$\begin{bmatrix} f_{1,1} & f_{2,1} & f_{3,1} \\ f_{1,2} & f_{2,2} & f_{3,2} \end{bmatrix} \begin{bmatrix} f_{1,1} & f_{1,2} \\ f_{2,1} & f_{2,2} \\ f_{3,1} & f_{3,2} \end{bmatrix}_n \begin{Bmatrix} \delta X_{1,n+1} \\ \delta X_{2,n+1} \end{Bmatrix} = - \begin{bmatrix} f_{1,1} & f_{2,1} & f_{3,1} \\ f_{1,2} & f_{2,2} & f_{3,2} \end{bmatrix} \begin{Bmatrix} f_1 \\ f_2 \\ f_3 \end{Bmatrix}_n .$$

Expanding, the following 2×2 system is obtained

$$\begin{bmatrix} A & C \\ C & B \end{bmatrix}_n \begin{Bmatrix} \delta X_{1,n+1} \\ \delta X_{2,n+1} \end{Bmatrix} = - \begin{Bmatrix} U \\ V \end{Bmatrix}_n . \tag{6.16-a}$$

where

4 The 1-norm and the ∞-norm are not differentiable.

$$
\begin{aligned}
A &= f_{1,1}^2 + f_{2,1}^2 + f_{3,1}^2 \\
B &= f_{1,2}^2 + f_{2,2}^2 + f_{3,2}^2 \\
C &= f_{1,1}f_{1,2} + f_{2,1}f_{2,2} + f_{3,1}f_{3,2} \\
U &= f_{1,1}f_1 + f_{2,1}f_2 + f_{3,1}f_3 \\
V &= f_{1,2}f_1 + f_{2,2}f_2 + f_{3,2}f_3
\end{aligned}
\tag{6.16-b}
$$

Again, at each iteration, this system is solved for $\delta X_{1,n+1}$ and $\delta X_{2,n+1}$ and then for $X_{1,n+1}$ and $X_{2,n+1}$.

6.2.4.3 Advancing One Step and Stop Criteria

When the vector $\delta\mathbf{X}_{n+1} = (\delta X_{1,n+1}, \delta X_{2,n+1})$ is determined by solving Equations (6.15) or (6.16), the original Newton-Raphson method calculates the $X_{1,n+1}$ and $\mathbf{X}_{2,n+1}$ from Equation (6.14). The vector $\delta\mathbf{X}_{n+1}$ is a *descent direction* which means that when sufficient close enough to the solution , the vector $\delta\mathbf{X}_{n+1}$ points toward a direction which minimize the scalar product $\mathbf{X}\cdot\mathbf{X}$. However, the new point may overshoot. The strategy is to apply the full step $\delta\mathbf{X}_{n+1}$, and to test if this results in an improvement in the search. If not, the process backtracks in the descent direction by a relaxation λ in the form of

$$
\begin{aligned}
&\mathbf{X}_{n+1} = \mathbf{X}_n + \lambda\delta\mathbf{X}_{n+1}, \\
&\lambda_{\min} \leq \lambda < 1.
\end{aligned}
\tag{6.17}
$$

The value $\lambda_{\min}$ is an arbitrary limit to prevent the steps from becoming too small.

Stop criteria are individually applied to each of the components of $\mathbf{f}(X_1, X_2)$. Each component has its own tolerance ε and the test is made for

$$|f_i(X_{1,n}, X_{2,n}) \leq \varepsilon_i| \qquad i = 1, 2, 3.$$

If the test proves true for the three components the procedure stops. The magnitude of the tolerances ε_i are not fixed and depend on the parameters being used. Although not absolute, good accuracy is obtained for $\varepsilon_1 = 10^{-5}$ and $\varepsilon_2 = \varepsilon_3 = 10^{-6}$.

The choice between reducing the order of the system and the use of the full rank least square method considers the magnitude of f_2 and f_3. In most cases the reduced system is used. However, if the magnitude of one of them is much larger than the magnitude of the other (in the order of 10^2 if<1), the full range least square method is used in the attempt to reduce the difference.

6.2.4.4 Initial Guess and Process Guidance During Search

To avoid crash and increase the chance of convergence to the correct solution, it is important that the pair of dimensionless variables X_1 and X_2 remain inside certain limits. This is valid not only for the initial guess, but also during the whole process including all sub-processes, particularly the intervals used to calculate derivatives. These restrictions impose a relationship between X_1 and X_2. For a given X_2, there exists an interval in which X_1 must fall to assure that the buckled portion of the drillstring is in the region of subcritical buckling of third mode.

The limits for the various regions of buckling and the definition of these limits were discussed in Chapter 5. The subcritical buckling of third mode is bounded by the lower limit of the third mode and the third critical value. The third critical value is the third root of the determinant of $\mathbf{S}(X_2)$. The lower limit occurs when the derivative at X_2 vanishes.

In this case it is more appropriate to work with L_{D} and X_2. For a given L_{D}, the lower limit and the critical value are found as defined in Chapter 5. Figure (6.3) shows the plot of the lower limit and critical value for a range of L_{D}. The two sets of points

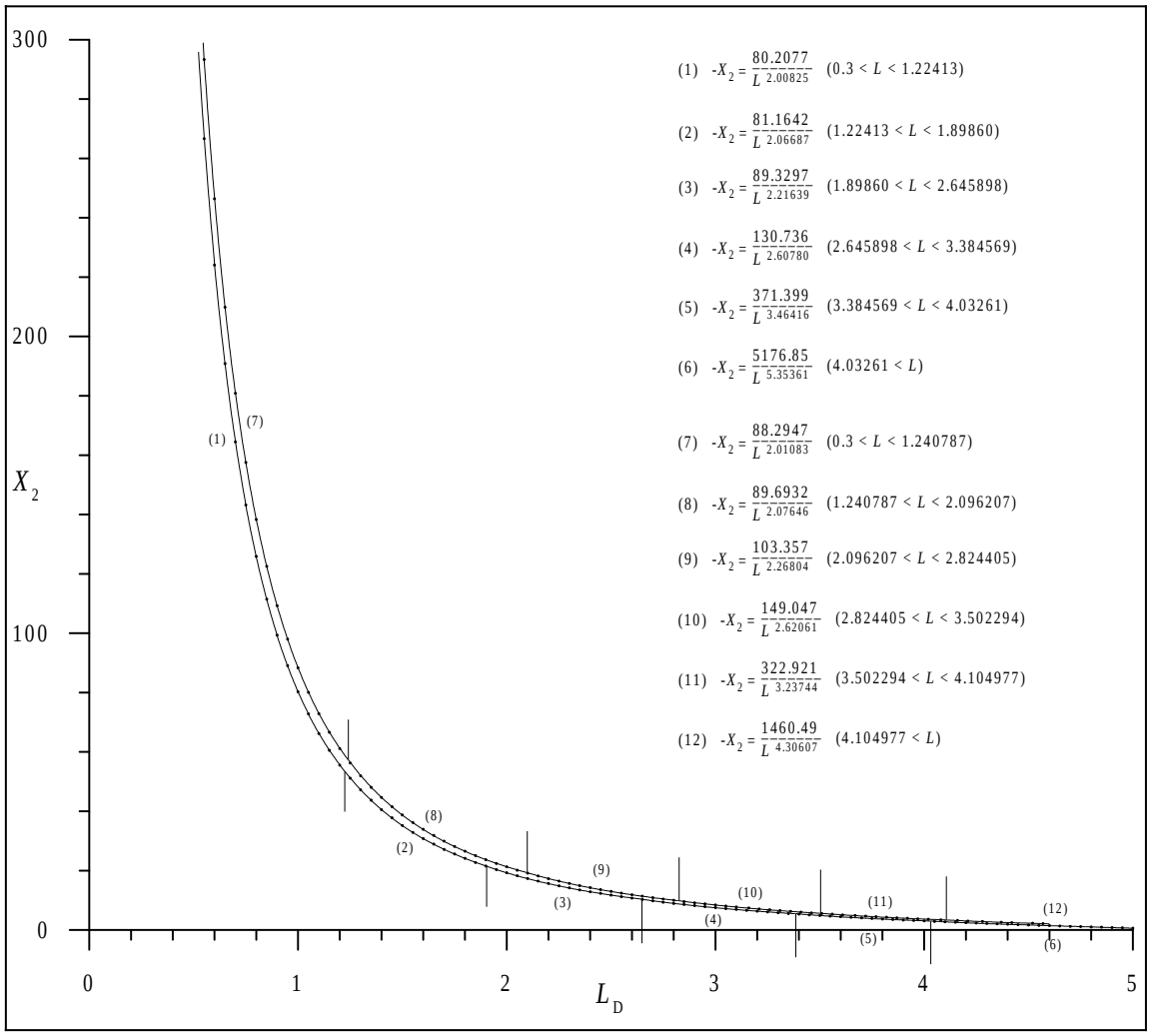

Figure 6.3: Strip for the subcritical buckling of 3rd mode

define a strip which constitutes the domain of the search. Several segments (1 to 12) were obtained by power-law least square fit. These segment fits are not used to determine the boundary points, but to serve as limiting values for a more successful iterative procedure.

Before a new pair of variables X_1 and X_2 is accepted during the search for fit, a check is made to assure that they are inside the valid strip. If not, the parameter λ in Equation (6.17) is decreased to force the new point to be in the domain of the solutions.

No previous information exists when a new case begins. The order of magnitude for the length of the buckled column is obtained using the trigonometric model presented in Chapter 3. It is expected that the hypergeometric model result in a shorter beam-column length than that determined by the trigonometric model. Therefore, a fraction of the length given by the trigonometric model is used as the initial value L_{D}. The value for the fraction varies between 0.7 and 0.98 and is found by trial-and-error until the process is triggered.

In addition to the initial length L_{D}, an initial value for X_2 must be entered. This value should be within in the valid strip of Figure (6.3). A fraction g given by

$$g = \frac{X_2 - X_{\mathrm{L}}}{X_{\mathrm{U}} - X_{\mathrm{L}}},$$

where X_{L} and X_{U} are the lower and upper limit for the chosen L_{D}, may be used to control the initial guess. The stability of the search process is quite independent of the initial value for g however, a good initial guess for g lessens the number of iterations needed to converge. In general the value $g = 0.75$ furnishes quite good rates of convergence.

When a fit is found in terms of X_1 and X_2, the pertinent parameters may be obtained using the formulas presented in Chapter 4, in particular, the local buckling force. The length and position of the buckled portion of the column (between tangency points) can be directly calculated using Equation (6.12).

6.2.5 Spotting the Buckling Point Region

The procedure showed in Sections 6.2.2 trough 6.2.4 can be repeated to find the angle which minimizes the vertical force P_θ. Use of a numerical process for minimization is not recommended because of the narrow range of stability of the fit procedure.

Using brute force is more reliable than using a minimization process to find the angle that minimizes the vertical force P_θ. The curves for the local and positional buckling force are plotted from a sample of points which cover a large range for the inclination θ. The range extends from as low as 2° up to as high as 89° in 1° or 2° intervals.

Linear and quadratic extrapolations for the parameters f_g and e_g of Equation (6.12-a) are used to help to cover the range of inclinations. These extrapolations make the process much more robust, and fits are normally obtained with few iterations.

6.3 Graphical Representation of the Results

There are several ways to apply the hypergeometric model. It can be used to determine the buckling force at a given point along the bore-hole. It can also be used to determine the maximum axial force that can be applied at any one point in the bore-hole. Another important application is in the design of drillstrings. All these tasks are better performed if the analysis covers the entire range of the inclination. The data required for an analysis are the outside and inside drillstring diameters, the distributed weight and modulus of elasticity of the drillstring, and the diameter and build gradient of the bore-hole. The distributed weight should account for the buoyancy when the drillstring is submersed in the drilling fluid.

For each angle θ the following parameters are calculated: the local buckling force

P'_θ, the causational buckling force P_θ with respect to the KOP, the length of the buckled portion of the drillstring, and other pertinent parameters. Both P'_θ and P_θ are used to construct the *buckling graph* of the drillstring–bore-hole configuration. The causational buckling force can also be considered a measure of the *buckling risk* of a drillstring. The smaller the causational buckling force of a point in a drillstring, the higher the risk of the drillstring to buckle at this point.

6.3.1 Buckling Graphs Structure.

The buckling graphs are composed of one pair of curves as shown in Figure (4). The upper or P'-curve is the plot of the local buckling force P'_θ, and the lower or P-curve is the plot of the causational buckling force P_θ. From the definitions of P'_θ and P_θ, the two curves cross at $\theta = 0^\circ$. The P-curve can be generated for points other than the KOP. However, the resulting curve is just the P-curve vertically shifted enough to make it coincide with the P'-curve at the angle of application of the force. An example is shown as the dotted curve in Figure (6.4) for axial forces applied at $\theta = 10^\circ$. There is no meaning in plotting the points to the left of the intersection of the curves.

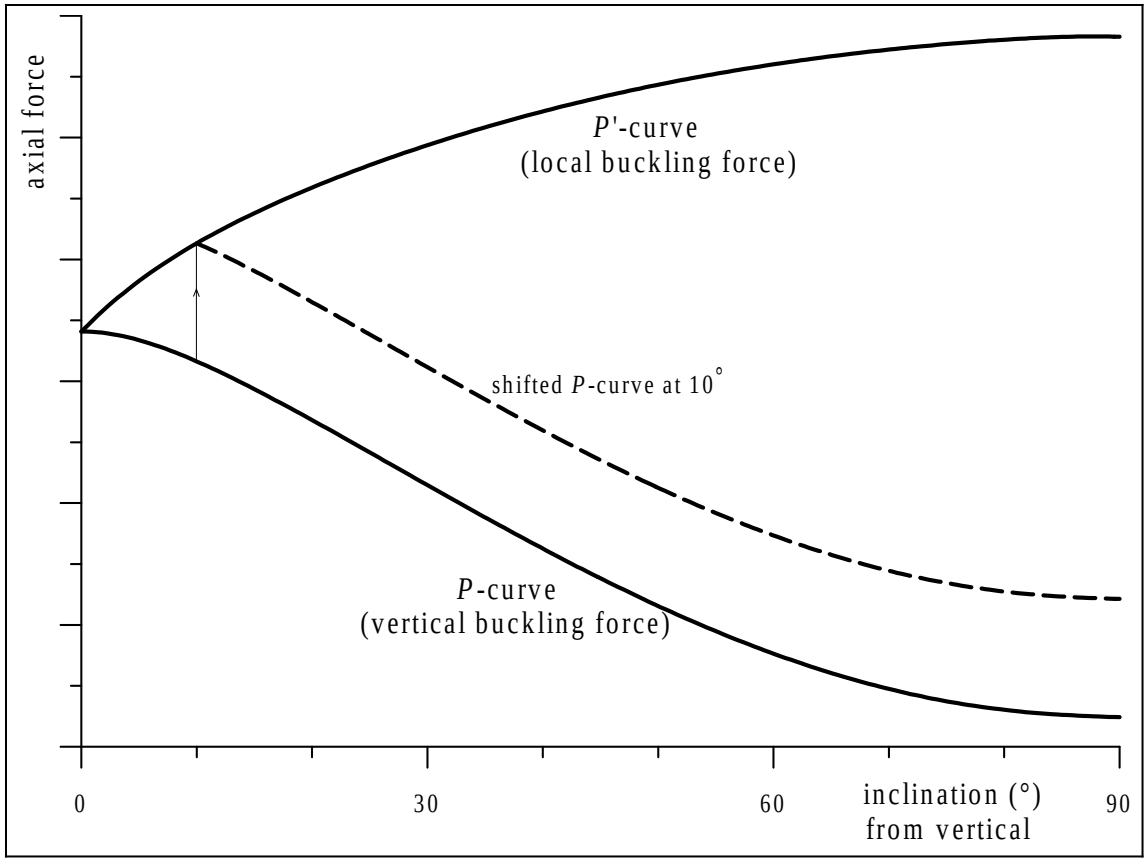

Figure 6.4: Structure of the buckling graph with a shift of the *P*-curve at 10 deg.

6.3.2 Tapered Drillstrings and The *P*-curve shifting method

The hypergeometric model was developed assuming a constant cross-sectional drillstring throughout the curved section of the bore-hole. If a tapered drillstring must be analyzed, the same results for the constant cross section can be applied. For that, the concept and process of shifting the *P*-curve is used. This process is called the *P-curve shifting method.*

To analyze a drillstring with two different cross sections, two pairs of curves, one for each of the cross sections of the tapered drillstring, are generated. It is assumed for now that the curvature and the diameter of the bore-hole are constant along the entire curved section. The two pairs of curves are plotted on the same graph, as shown in Figure (6.5).

The tapered drillstring in Figure (6.5) is composed of a lower section of API 5 *in* drill pipe and an upper section of API $4^1/_2$ *in* drill pipe. The build gradient is $2^\circ/100ft$ and the bore-hole diameter is $12^1/_4$ *in*. Additional data are printed in Figure (6.5). The upper set of curves belongs to the API 5 *in* drill pipe and the lower set to the API $4\frac{1}{2}$ *in* drill pipe.

The position of the crossover (where the drillstring changes diameter) determines where buckling occurs and, consequently, the maximum force that can be applied on bit. Initially, the crossover is positioned at the point in the bore-hole with 35.8° of inclination. For this angle, the P-curve for the 5 *in* drill pipe is vertically shifted (at 1) to determine the force that must be applied at the crossover to buckle the drillstring at the bottom of the curved section (at 90°). To determine this force, a *buckling line* is constructed by drawing a horizontal line through the point at 90° in the shifted *P*-curve. In this case the force found is P_{90}=31,326 *lb*. This force is also the local buckling force (P'-curve) for the $4^1/_2$ *in* at the crossover. This means that the drillstring will buckle simultaneously at the

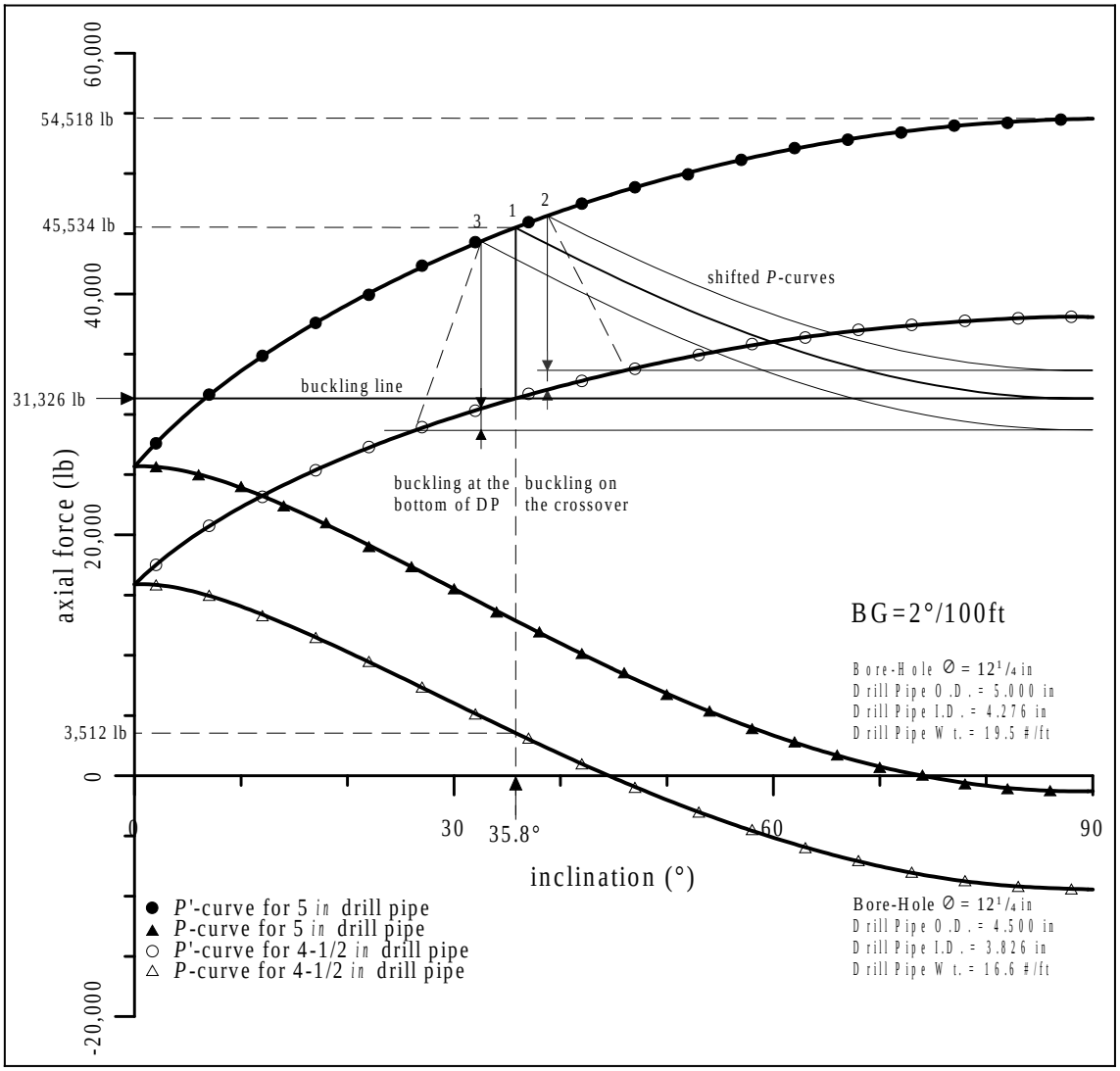

Figure 6.5: Buckling analysis for a tapered drillstring

crossover and at the bottom of the drillstring. The angle of 35.8° is a characteristic angle for this tapered drillstring. The angle is found by shifting the P-curve together with the horizontal buckling line (by trial-and-error or numerical search), until they cross the P'-curves for both drill pipes at the same vertical. This vertical line divides the graph into two regions.

If the crossover is positioned to the right of the vertical line at 1, as depicted by the shifted curve at 2, buckling occurs only at the crossover. This is not desirable because it reduces the maximum force that can be applied at the bit. This reduction in force is given by the amount between the arrows at the vertical line at 2.

On the other hand, if the crossover is positioned to the left of the vertical line at 1, as depicted by the shifted curve at 3, buckling occurs only at the bottom of the drillstring. This is desirable because the available force at the bit is the maximum possible (dictated by the 5 *in* drill pipe and not the $4^1/_2$ *in* drill pipe), and buckling is prevented on the crossover. Buckling on the crossover causes stress concentrations and likely failure of the drillstring at the crossover. Positioning the crossover to the left of the vertical line requires a longer section of 5 *in* drill pipes.

The analysis above was made for the drill bit at 90°. For other angles the horizontal buckling line should be drawn at the corresponding position (angle where the bit is located) and proceed in the same way.

The project engineer needs to consider the cost of running a heavier column. This includes the increased rental costs of a heavier column, and costs associated with the increase in torque, drag, and power for trips and pumping, and even the possible need of a larger rig. The vertical line at 1 is, therefore, a limit for optimal positioning of the crossover. The project engineer also needs to consider that the end of the curved section changes during drilling. Considering this, the expected performance of the bit is required to determine the starting position of the crossover.

This analysis can be extended to drillstrings with more complex configuration. In

this case, the analysis should be made from the bottom of the drillstring towards the top. The same procedure is also valid for constant cross-sectional drillstrings inside bore-holes with different diameters (which influences the positioning of casing shoes), or constant cross-sectional drillstrings inside bore-holes with two or more different radii of curvature (which influences the point of change of curvature in multi-curved well projects). In these cases what is needed is the buckling graphs for each set of parameters.

6.4 Conclusions of the Chapter

This chapter presents the *hypergeometric model*. It consolidates all the knowledge and methods developed in the previous chapters.

A comper code was written in FORTRAN to process the numerical calculations to solve any practical case.

The analysis for tapered drillstring gives the industry a new tool to optimize drilling in horizontal and high inclination bore-holes.

The next chapter will exhibit the predictions made for the experimental validation tests performed in laboratory, and predictions for a sample of parameters found in actual drilling operations.

Chapter 7

Experimental And Numerical Results

The purpose of this chapter is to present the numerical predictions using the trigonometric and hypergeometric models for the medium-scale experiment run within the facilities of the Petroleum Engineering Department at Colorado School of Mines, and compare them with the experimental results. The description of the apparatus, along with the procedure for running the experiments, buckling criteria, data acquisition, and additional details are described by Gurakin (Gurakin - 1996). Also this chapter includes predictions made using two other models available in the literature. In addition, simulations for a sample of dimensions commonly used in the oil industry were performed, although this set of simulated results cannot be considered as a field or design *grimoire*.

7.1 Predictions for the Experiments

The experiments were run using combinations of two bore-hole diameters, three build gradients, three rod diameters, and two different rod materials (steel and aluminium). A total of seventeen combinations were used. Certain combinations were not run, for instance, $^1/_4$ *in* steel rod inside a bore-hole with a curvature of 40 *ft* (for both 1 *in* and 2 *in* bore-hole diameters), because the expected buckling forces were beyond the limitations of the equipment. In addition, $^1/_8$ *in* steel rod inside a bore-hole with a curvature of 113 *ft* and a diameter of 2 *in* was not run because the expected buckling

force would be too low for the resolution of the equipment.

The experimental buckling forces were reported as *intervals* in which the actual buckling force should fall, rather than as *definite values*. This is because the primary (controlled) parameter in the experiment is the axial force, applied with standard weights with discrete resolution, through a system of pulleys. The displacement is a secondary parameter (resultant) which is a consequence of the applied axial force. In the experiment, the information of highest importance is the buckling force, and an accurate control of the magnitude of the force being applied to the rod is needed. In experiments where the controlled parameter is the displacement (in general applied by means of a screw mounting), the force is not controlled but measured instead, usually with load cells. The final force for a given displacement is a function of the displacement and the final configuration of the rod inside the constraints. The shape of the buckled drillstring may be different when the experiment is repeated, or when the rod is perturbed (to induce buckling for example). In addition, the load cell requires frequent calibrations. Additional detail can be obtained in the work of Gurakin (1996). The resulting intervals are plotted in the graphs as *Hi-Low* marks (⌡).

During the experiments, only the trigonometric model was operational and predictions based on this reduced model were used for comparison with the results. The trigonometric model is independent of the inclination and the predictions are represented by horizontal lines. To avoid crowding the graphs, only one point (symbol ✳) is shown for each prediction. The trigonometric model predictions are always close to the cusp formed by the P-curve and the P'-curve at $\theta = 0^{\circ}$.

It is expected that the trigonometric model can reasonably predict buckling forces for those cases with high curvature because the distributed weight would represent a small fraction of the axial force. On the other hand, for small curvature, the distributed weight causes a deviation toward values above those predicted by the trigonometric model. This was noted during the experiments, and later, when the hypergeometric model

became operational, the predictions with this enhanced model showed very good agreement with the observed experimental results. The predictions using the hypergeometric model, and experimental results (Hi-Low intervals) are presented as buckling graphs in Figures (7.1) to (7.7),[1,2] and have the same structure of the buckling graphs presented in Chapter 6.

Where experimental results are available, shifted *P*-curves are plotted to correct for the position of application of the force. In the experiments, axial forces and buckled portions occurred at predetermined angles. Table (7.1) shows for each radius of curvature used in the experiment, the equivalent build gradients, the inclinations at the position where the axial force is applied, and where the buckled portion is induced. In certain cases the shifted curves barely differs from the *P′*-curves.

radius of curvature	equivalent build gradient	inclination of the applied force	inclination of the buckled portion
113 ft	50.70 °/100 ft	82.4°	87.5°
58 ft	98.79 °/100 ft	75.2°	85.0°
40 ft	143.24 °/100 ft	68.5°	82.8°

Table 7.1: Angular positions for axial forces and buckled portions.

From the seventeen predictions made, only two show significant deviation from the experiment results. The other fifteen are accurate predictions or within acceptable experimental errors.

The experimental results shown in Figure (7.7) for aluminium rods, and radii of curvature of 40 *ft* and 58 *ft* are far below the predictions. Later, when the apparatus was being set up for a radius of curvature of 113 *ft*, it was found that the aluminium rods used were bent, probably due either to mishandling of the rods or to permanent deformation

1 See Appendix A for tables containing the numerical results for all graphs presented in this chapter.
2 Figures with experimental results are shown in sequence in the end of this section.

during the tests. A new set of rods with certified straightness was used in the experiment for 113 *ft.* After the tests, the rods remained straight indicating that no permanent deformation had occurred. The result matched the prediction.

In Figure (7.5) the buckling force interval for 40 *ft* is 5% below the prediction. This can be credited to experimental errors due to eccentricity of the axial force and tortuosity of the rod which becomes more evident at high buckling forces. It is expected to obtain buckling forces smaller than the predicted due to the impossibility of obtaining perfectly straight rods, accurate alignment and centralization of the forces. After analyzing the graphs, I conclude that the experimental results were accurately predicted and that they validate the hypergeometric model.

Two other models exist in the literature which predict buckling forces for drillstrings in curved bore-holes, the model presented by Schuh (1991), and the model presented by He and Kyllingstad (1993). These models were discussed in the literature review (Chapter 2). Predictions for each experiment were made using the formulations in the papers and are included in the graphs for comparison. The resulting curves represent the same parameter of the P'-curves of the hypergeometric model, that is, the local buckling force. The curves are labeled S-# for the predictions with Schuh's model, and H-# for the predictions with He and Kyllingstad's model. The symbol # represents the value, in feet, of the radius of curvature used in the prediction. Both models use fundamentals taken from straight bore-hole theory. The models are based on the formula for critical force by Dawson and Paslay (1984) which does not correctly account for the effect of inclination, as explained in Chapter 2.

Schuh's model mixes Dawson and Paslay's formula (unloading buckling force), with Lubinski's formula for the pitch (weightless column), and an incorrect interpretation for the boundary effects of the curved bore-hole in the drillstring. He and Kyllingstad's model also uses Dawson and Paslay's formula (unloading buckling force) with a

adjusting factor to correct for the effect of the curvature.

Both models failed to predict the unloading buckling force for all experiments. Those models are able to detect the influence of the inclination in the behavior of the buckling force, but seem to miss something. I cogitate that those models do not appropriately account for the effects of the curved constraints.

The hypergeometric model effectively predicts the unloading buckling force which prevents helical buckling of drillstrings within curved bore-holes. This allows a more efficient use of drillstrings.

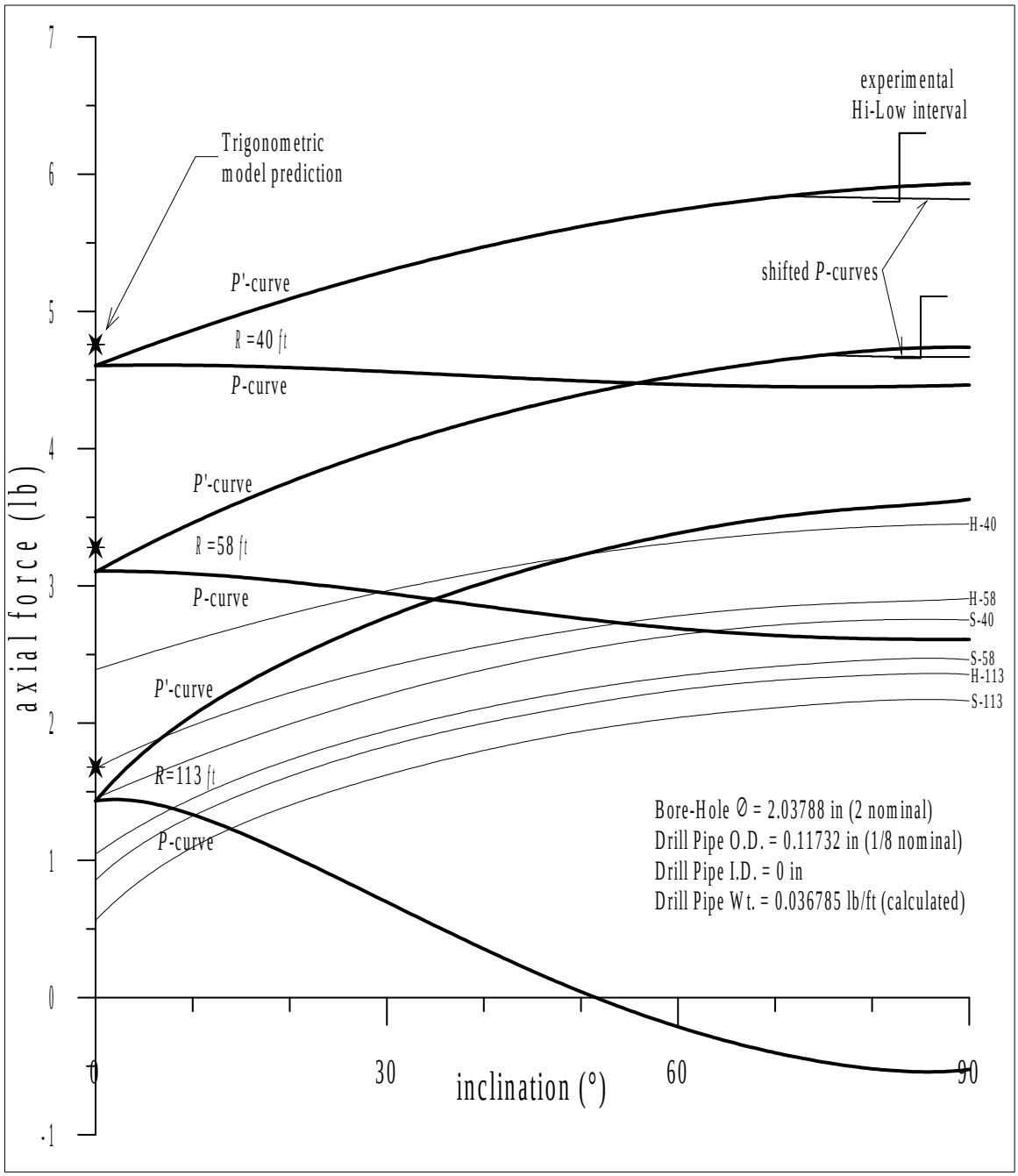

Figure 7.1: Predictions and experimental results for $\frac{1}{8}$ in steel rod - 2 in well

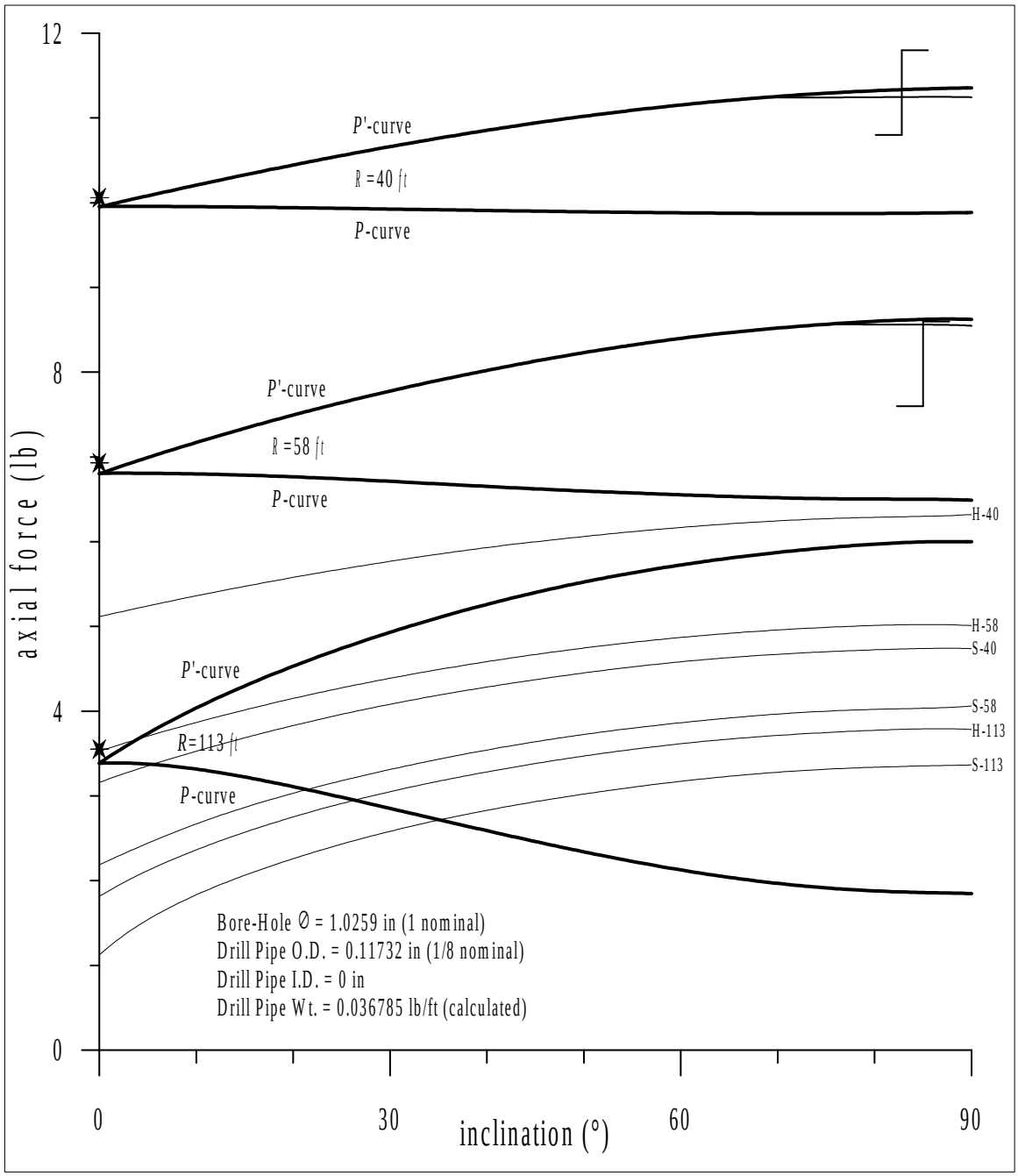

Figure 7.2: Predictions and experimental results for $\frac{1}{8}$ in steel rod - 1 in well

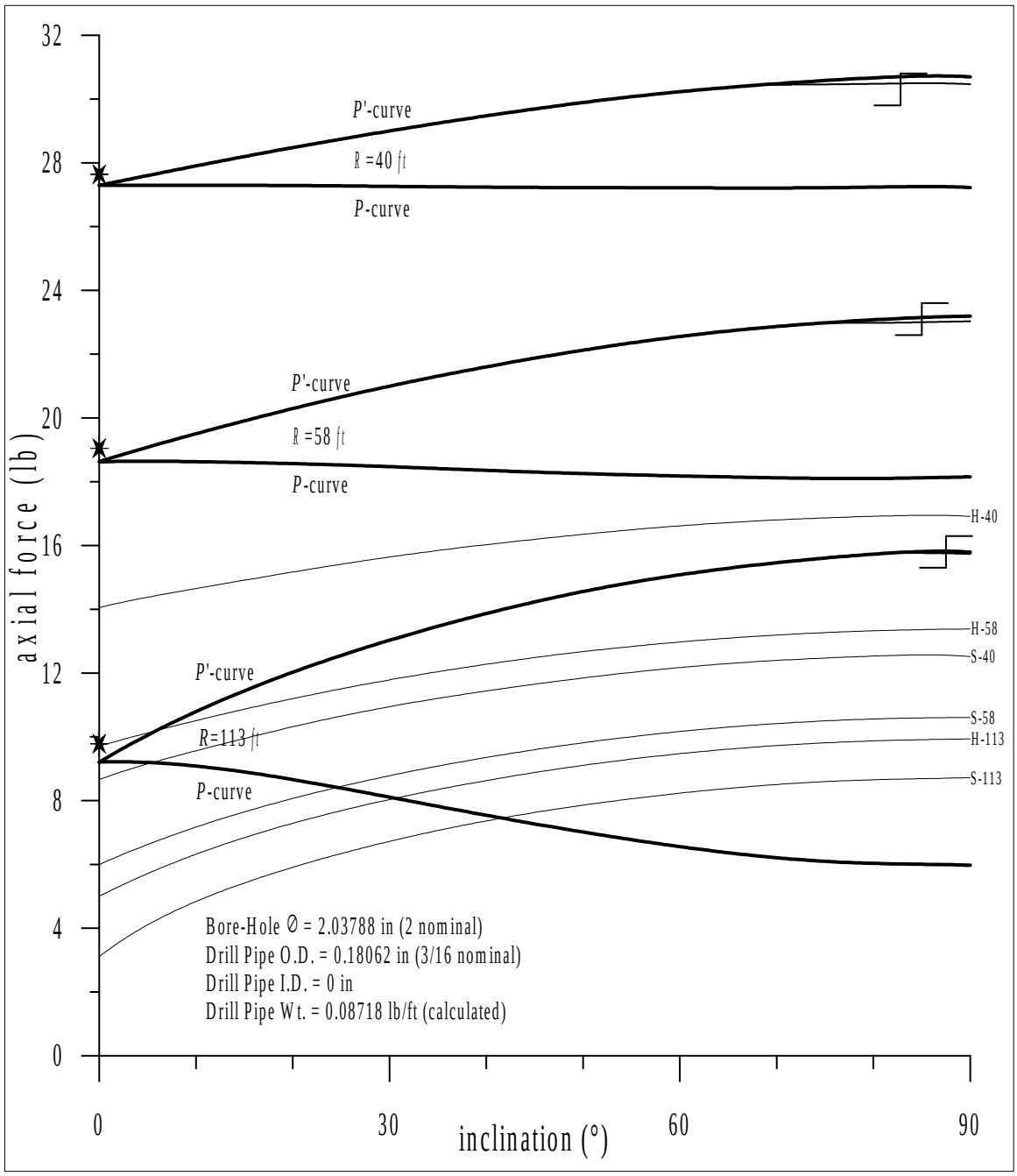

Figure 7.3: Predictions and experimental results for $\frac{3}{16}$ in steel rod - 2 in well

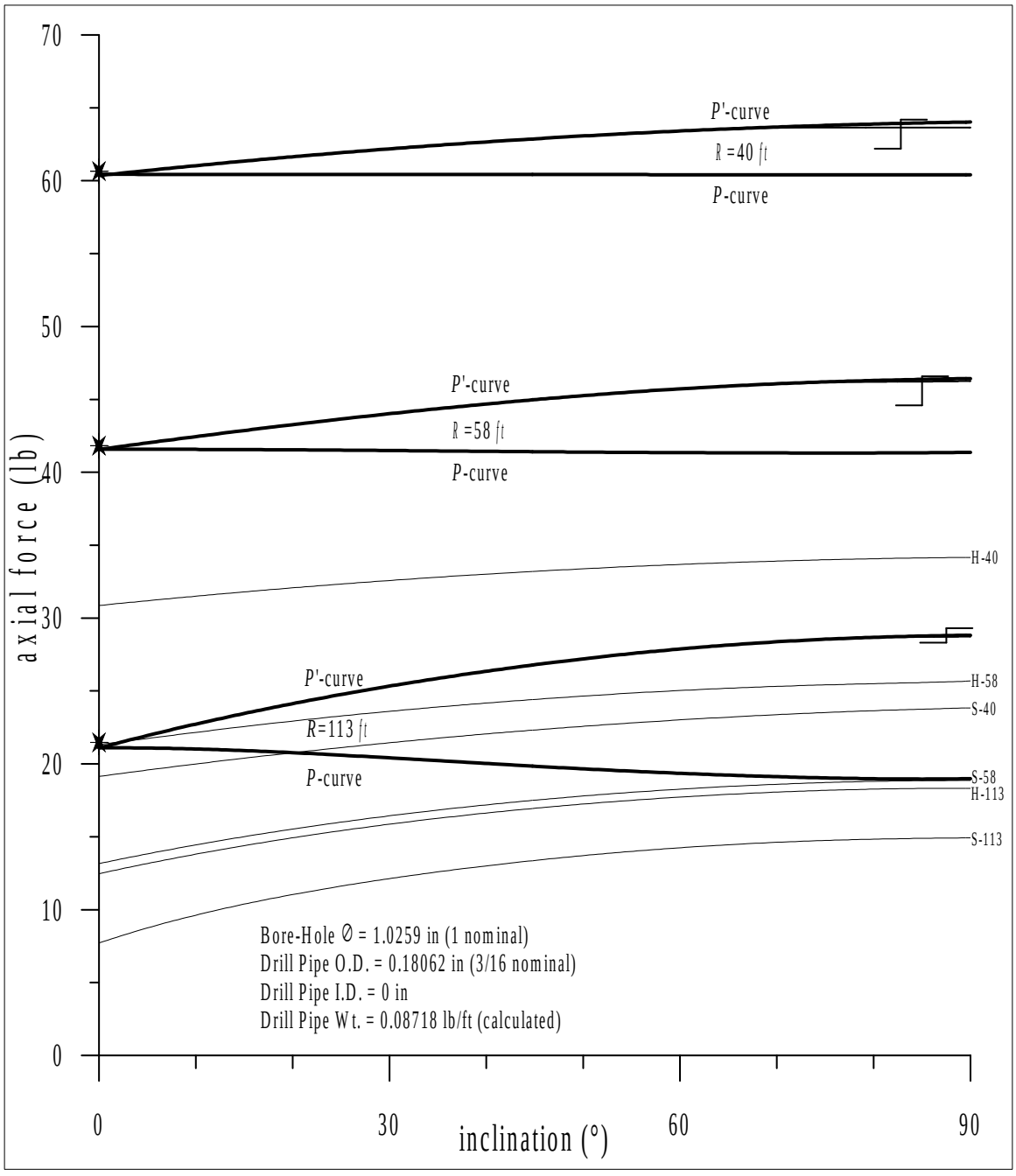

Figure 7.4: Predictions and experimental results for $\frac{3}{16}$ in steel rod - 1 in well

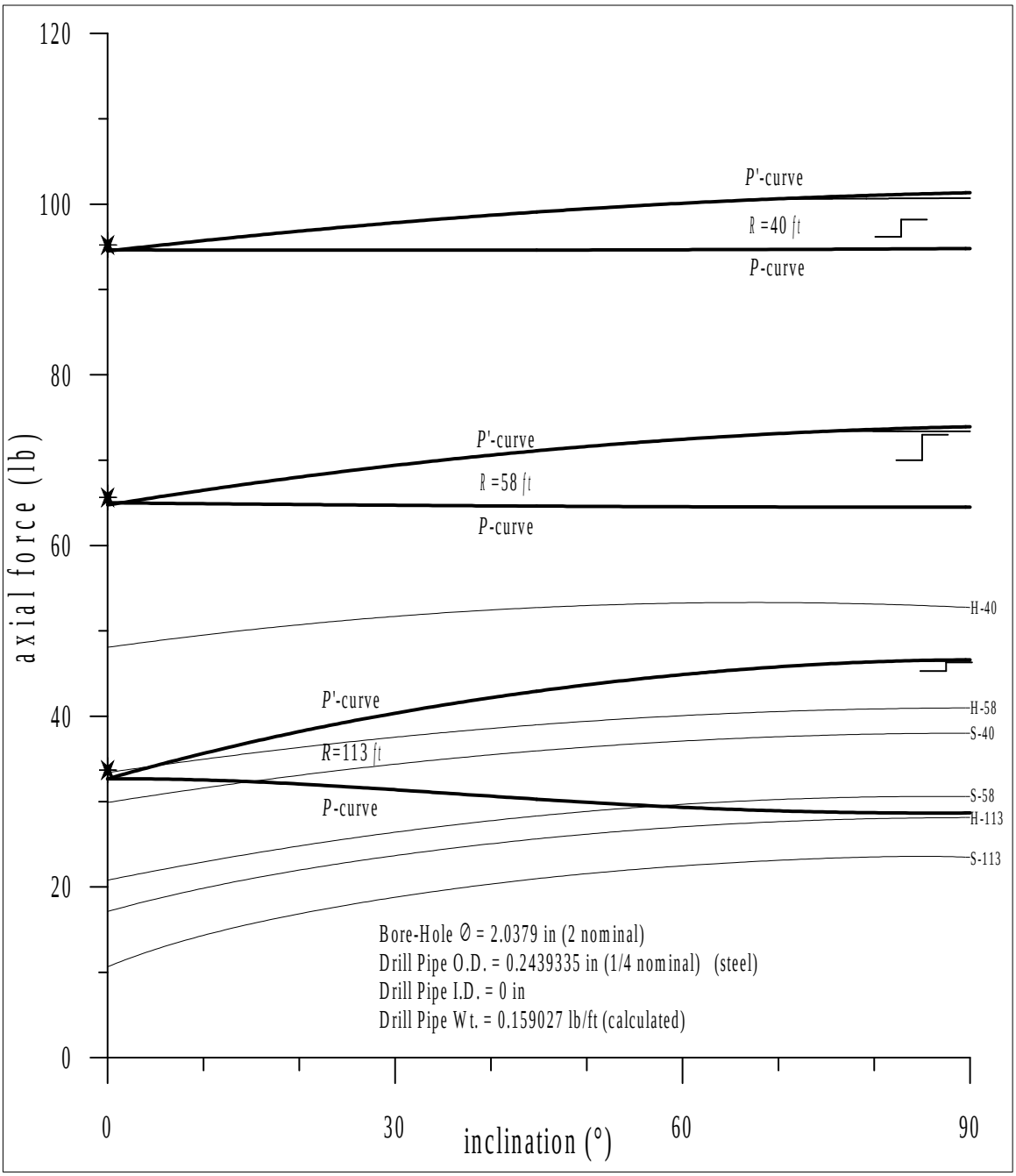

Figure 7.5: Predictions and experimental results for $\frac{1}{4}$ in steel rod - 2 in well

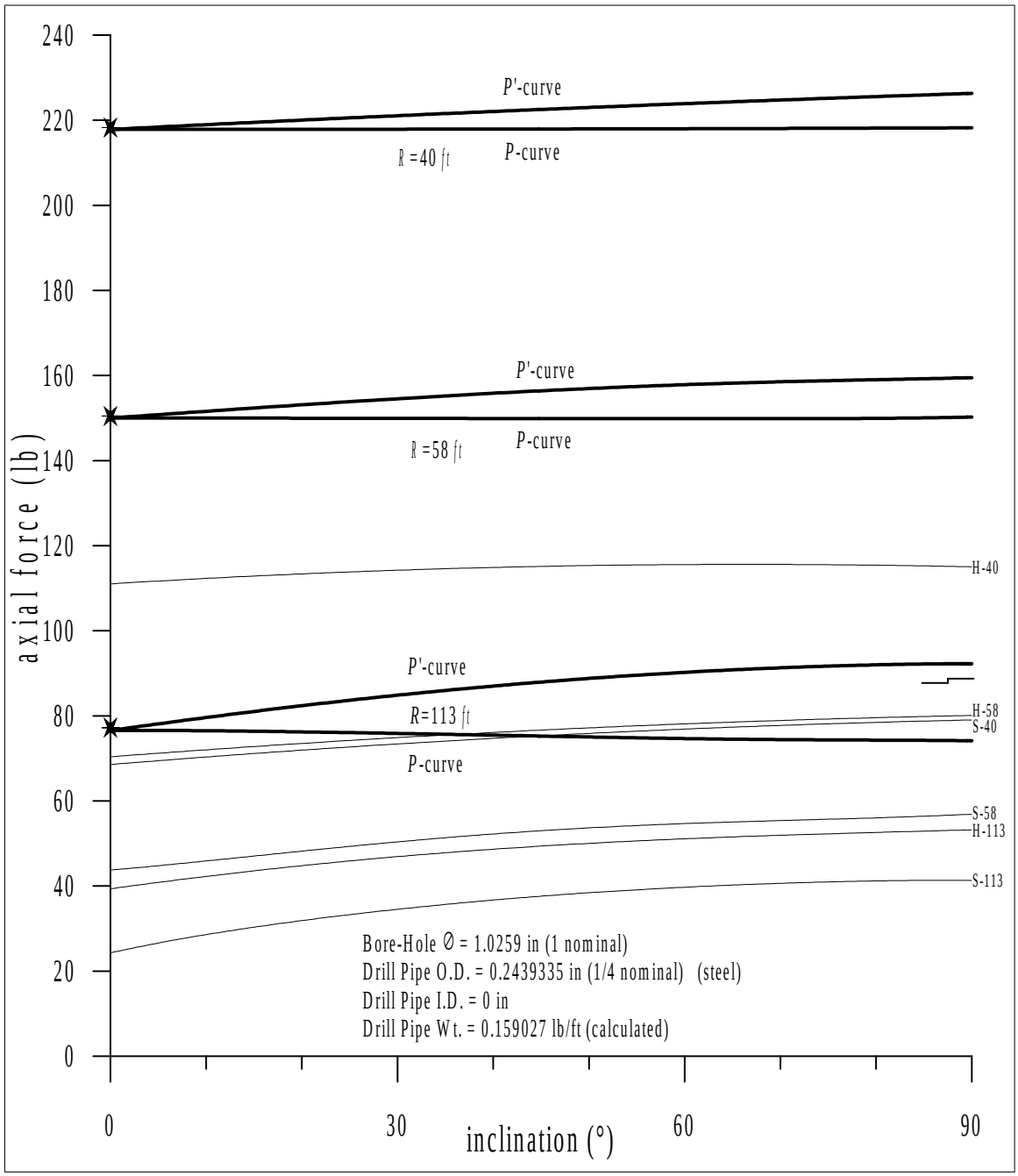

Figure 7.6: Predictions and experimental results for $\frac{1}{4}$ in steel rod - 1 in well

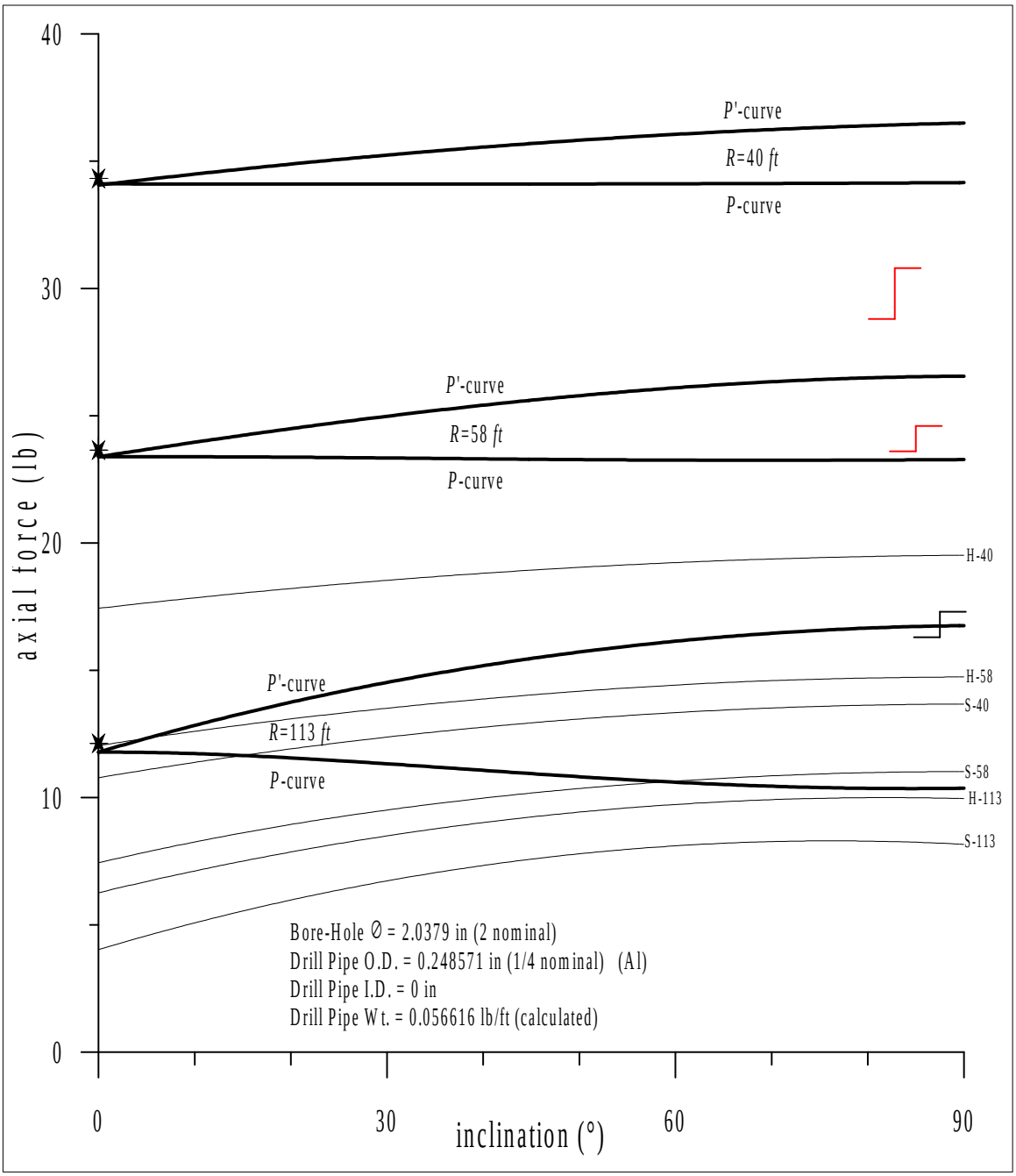

Figure 7.7: Predictions and experimental results for $\frac{1}{4}$ in aluminium rod - 2 in well

7.2 Field Simulations

Three common bore-hole diameters were chosen for simulation: $17^1/_2$ *in*, $12^1/_4$ *in* and 6 *in*. These diameters are commonly used in horizontal and extended reach drilling. The drill pipe used for the $17^1/_2$ *in* bore-hole is the API 5 *in*-19.5 *lb*/*ft*. Two drill pipe diameters are used for the $12^1/_4$ *in* bore-hole, API 5 *in*-19.5 *lb*/*ft*, and API $4^1/_2$ *in*-16.6 *lb*/*ft*. The drill pipe used for the 6 *in* is the API $3^1/_2$ *in*-13.3 *lb*/*ft* (11.285 *lb*/*ft* with 9.5 *lb*/*gal* mud). The build gradients used vary from 2°/100*ft* to 7°/100*ft*. These rates cover the normal range for directional and horizontal drilling. Higher build gradients were also used with the 6 *in* case.

The simulations do not include the effect of the tool joints. API 5 *in* drill pipes have tool joints with $6^1/_2$ *in* of external diameter. The influence of the tool joints is to decrease the clearance between the drillstring and the bore-hole wall. The length of tool joint is 18 *in* and they occur approximately every 30 *ft* of the drillstring. Smaller clearances increase the buckling load. Therefore, simulations neglecting the tool joints are conservative. The effect of the tool joints is more relevant for tight bore-holes.

In all cases listed above, with the exception of the 6 *in* bore-hole with API $3^1/_2$ *in* drill pipe with 7°/100*ft* or higher gradients, the length of the buckled portion *L* is longer than the distance between the tool joints. The contact points occur at the tool joints which indicates that the decrease in the clearance is effective. When *L* is shorter than 30 *ft*, however, the tool joints still contact the bore-hole wall, but the assumption that the drillstring is tangent to the bore-hole wall is no longer valid as depicted in Figure (7.8).[3] For these cases, the results are conservative if one neglects the external diameter of the tool joints.

---

3 In this schematic, dimensions were chosen to highlight the effects of the tool joints.

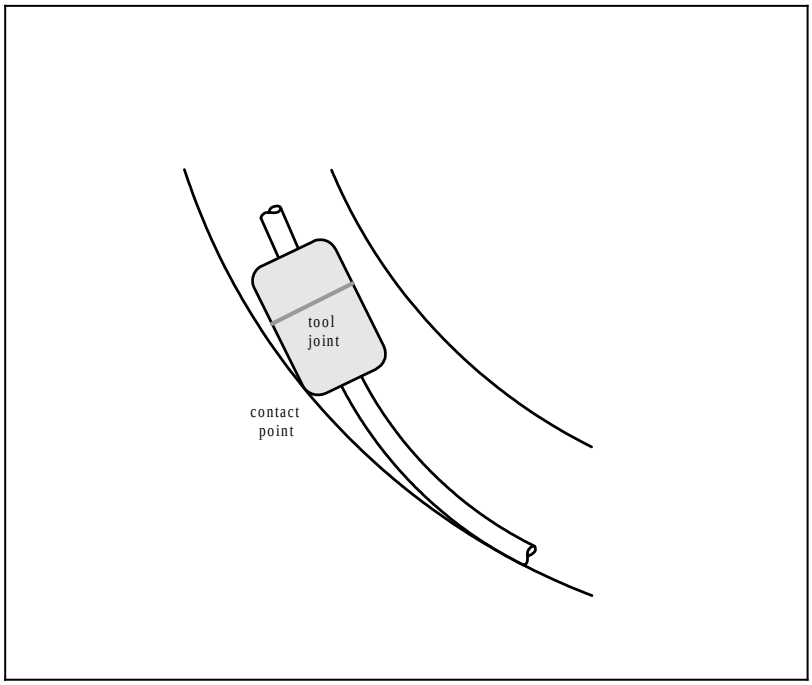

Figure 7.8: Contact between a tool joint and the bore-hole wall

7.2.1 Case No.1: $17^1/_2$ *in* Bore-Hole - API 5 *in* Drill Pipe

Using the procedure described in the previous chapter, Case No.1 was run with BG=2˚/100ft. The results for the local buckling force P' and vertical buckling force P were obtained for angles ranging from 2˚ to 88˚ in 1˚ intervals, and plotted in Figure (7.10).[4] The curves shown were obtained with a polynomial curve fit.

The P'-curve shows that the local buckling force increases with the inclination from P'=14,086 *lb* at θ=0˚ to P'=38,318 *lb* at θ=90˚. This increase in the buckling force with the angle is expected from the theoretical model. On the other hand, the positional

4 Figures with simulated results are shown in sequence in the end of this chapter.

buckling force at the KOP decreases from P = 14,086 *lb* at θ=0° to P = -17,511 *lb* at θ=90°. The graph clearly indicates that the least resistance to buckling occurs at the bottom of the drillstring when the drill pipe at the KOP is under a traction of 17,511 *lb*. The buckling force at θ=0° should be compared to the buckling force obtained using the trigonometric model. Using the same geometric parameters it is found:

L'	L	P
129.94 *ft*	123.90 *ft*	15,638 *lb*

Note that P=15,638 *lb* is the buckling force (3rd mode) for an Euler column with the same stiffness, and length equal to the complementary length L'=129.94 *ft*. The axial force 14,086 *lb* is the buckling force for a vertical weighted column of the same length obtained from the case θ=0° in the general beam-column model (which is identical to the flagpole model with pinned ends). The difference between the two forces is roughly half the weight of the column.[5] Therefore, a first calculation based on the trigonometric model results in

$$P_{weighted} \cong 15{,}638 lb - \frac{1}{2} \cdot 130\, ft \cdot 19.5 lb/ft = 14{,}370.5 lb\,,$$

which compares reasonably well (±2%) with the prediction based on the hypergeometric model for low angles.

Although the trigonometric and hypergeometric models are related for low angles, they differ considerably at high inclinations. Based on the trigonometric model, the

5 This expedite calculation considers that the weight of the column contributes to a decrease in the buckling force given by Euler column theory. Since the weight is distributed along the column, an element of column on the top has a bigger effect than its symmetrical at the bottom and, in average, only half of the weight contributes to decrease the buckling force.

maximum weight on bit that could be applied at the beginning of the horizontal section would be limited to 14,087 *lb*, whereas based on the hypergeometric model this limit is 38,319 *lb*.

Case No.1 was repeated for additional values of the build gradient and the results are presented in Figure (7.10). Several conclusions may be extracted from this graph. The effect of the build gradient is readily seen; the higher the build gradient the higher the buckling force.

For higher build gradients, the general shape of the curves does not change. The P'-curve shows an increase in the local buckling force which is less steep at higher build gradients. A flattening of the *P*-curve is evident at higher build gradients. This flattening implies that the effect of the distributed weight decreases with increasing build gradient. This results from the fact that the distributed weight is constant, whereas the local buckling force increases with build gradient. In the limit as the build gradient increases, the P'-curve and the P-curve approach a horizontal line. This means that the column buckles along the whole length not only at the bottom.

Under no circumstances, even using unrealistic values for distributed weight, radius of curvature, or stiffness, did buckling occur at points other than the bottom of the drillstring. It can be concluded that, for a homogeneous drillstring in the absence of friction, buckling always occurs at the bottom of the drillstring.

Note that the derivative of both the P'-curve and the *P*-curve vanishes at 90°. This is an expected result for a frictionless model. The values of the axial force are identical for supplementary angles. Therefore both curves are symmetric with respect to 90°. Since there is no reason for discontinuity in the derivative at 90°, the derivatives must vanish there. This is analogous to pressure in a hydrostatic U-tube. When friction is present, buckling may occur at an intermediary point along the bore-hole or even at the top of the curved section as shown in Figure (7.9). Build gradient and friction coefficients

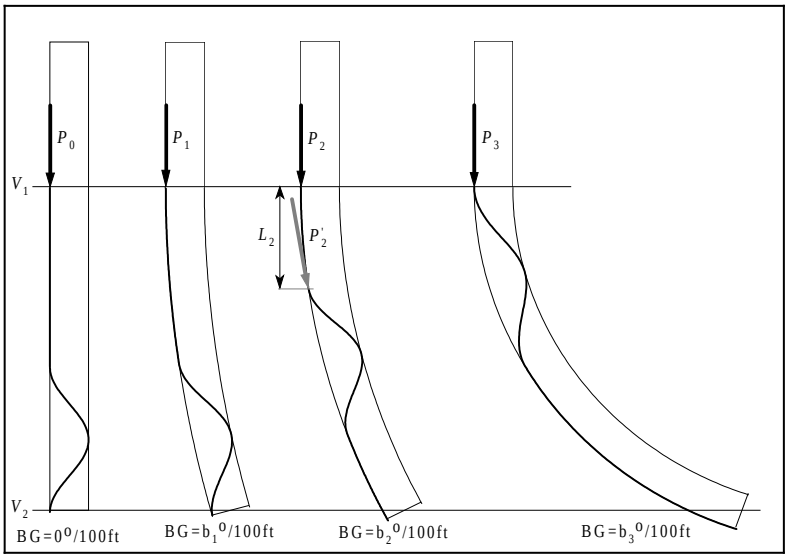

Figure 7.9: Position of the buckled portion of the drillstring

determine the position of the buckled portion. This is analogous to pressure in a viscous flowing U-tube.

7.2.2 Case No.2: $12^1/_4$ *in* Bore-Hole - API 5 *in* Drill Pipe

The results of Case No.2 are useful in comparing the clearance effect on the buckling behavior of the column. The clearance changes when either the bore-hole diameter or the outside diameter of the drillstring change. By changing only the bore-hole diameter, the stiffness of the drillstring is preserved. Figure (7.11) shows the results of the analysis for 6 build gradients.

The first thing observed is that the general behavior does not change substantially from the previous case. The shapes of the curves remain essentially the same, but the values for the buckling forces change. A decrease of the clearance caused by changing the bore-hole diameter, and keeping the other mechanical and geometric parameters fixed,

causes an increase in the buckling force. This too, is an expected result as a tighter constraint gives more support to the drillstring. In fact, in the limit, when the clearance is zero, the buckling limit is theoretically infinite and the load capacity of the drillstring is limited by the force that causes failure by compression.

7.2.3 Case No.3: $12^{1}/_{4}$ *in* Bore-Hole - API $4^{1}/_{2}$ *in* Drill Pipe

In Case No.3 the increase of the clearance results from the decrease of the outside diameter of the drillstring. This also causes a decrease in the stiffness and the distributed weight which affects the column behavior. The buckling force decreased in average 50% with respect to Case No.2. The results are shown in Figure (7.12). Again, the curve shapes are essentially the same as displayed in previous cases.

7.2.4 Case No.4: 6 *in* Bore-Hole - API $3^{1}/_{2}$ *in* Drill Pipe

The final case uses a set of diameters known as a slim hole. The clearance is very small which highlights its effects upon the buckling force. The results are shown in Figure (7.13). Since slim holes tend to have higher curvatures, runs were made for build gradients up to $12^{\circ}/100ft$. At this rate the curves are rather flat revealing that the distributed weight has minimum importance in the final behavior. In addition, the buckling force is more than 50% of the compressive limit for a drill pipe grade E (yield strength of 75,000 *psi*).

A comparison between this case with Case No.1 reveals the clearance effects on the buckling resistance of the drillstring. The local buckling load for Case No.4 is always larger than that of Case No.1 for the same build gradient, even though the stiffness of the drillstring is 3.17 times smaller.

7.3 Conclusions of the Chapter

This chapter validates the *hypergeometric model* by comparing the model with experimental results and shows the limitations of previously existing models. The comparison between the experimental results and the predictions supports the entire mathematical model for buckling in curved bore-holes which includes the trigonometric model, the curved bore-hole theory, and the generalized beam-column theory.

The hypergeometric model became operational during the summer of 1996 one year after the experimental results were obtained (summer of 1995). The model does not use *any* information from the experiments since it is purely physical and mathematical with *no* coefficient or factor to adjust to the experimental results. The close agreement is an indication that, not only does the model successfully describe the physical phenomenon, but also that the experiments were consistently designed and run. It can also be concluded that *all* the assumptions made are sound.

Two models available in the literature were used to predict the unloading buckling force for the experiments. Both presented results too conservative.

The field simulations are far from covering the entire range of diameters and build gradients usually found in the industry. The purpose of this work was to develop a model for curved bore-holes. In addition, the results obtained and presented are industry instrumental in the understanding of the effect of the curvature upon the buckling resistance of a drillstring.

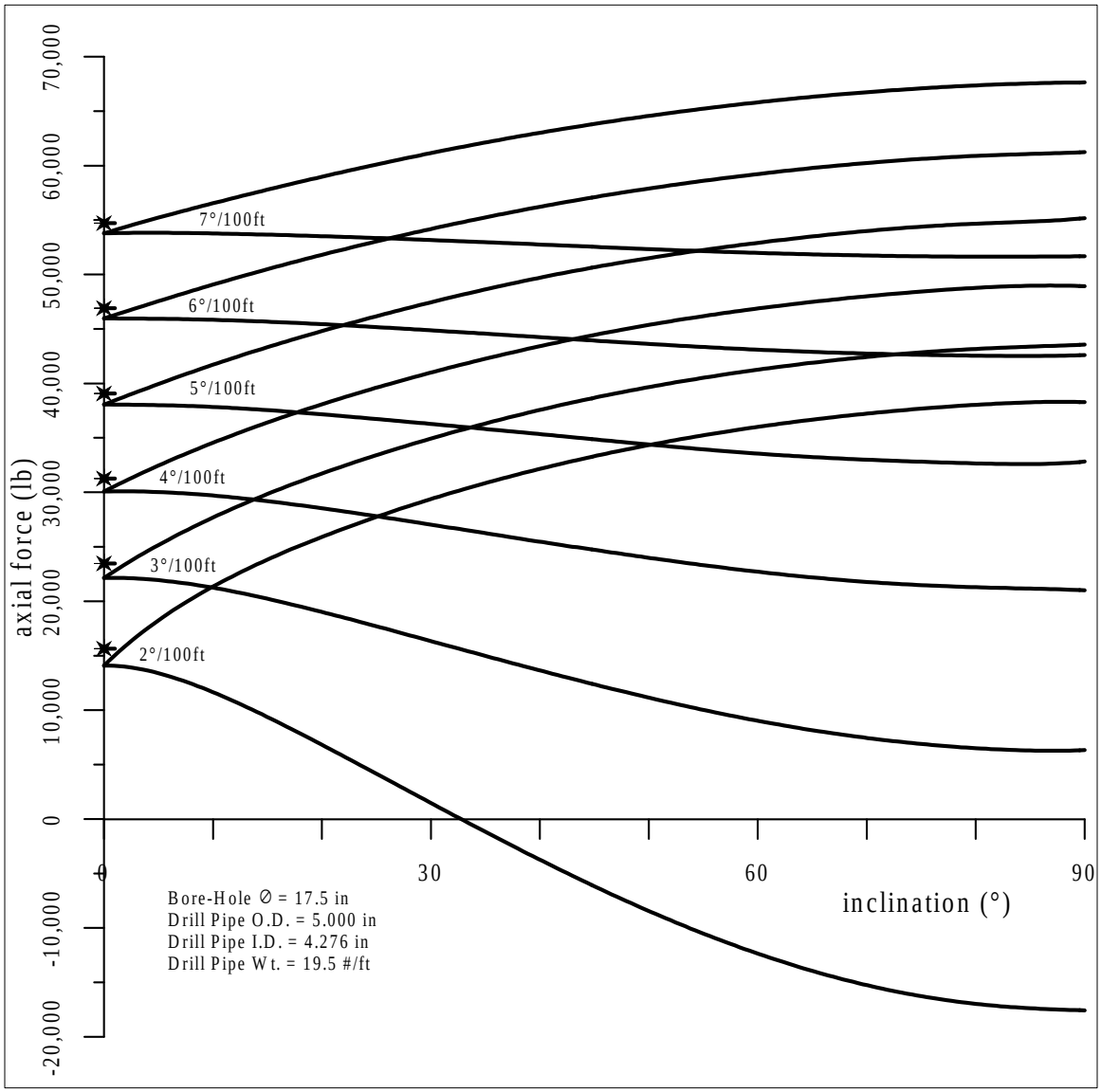

Figure 7.10: Case No.1 with multiple build gradients

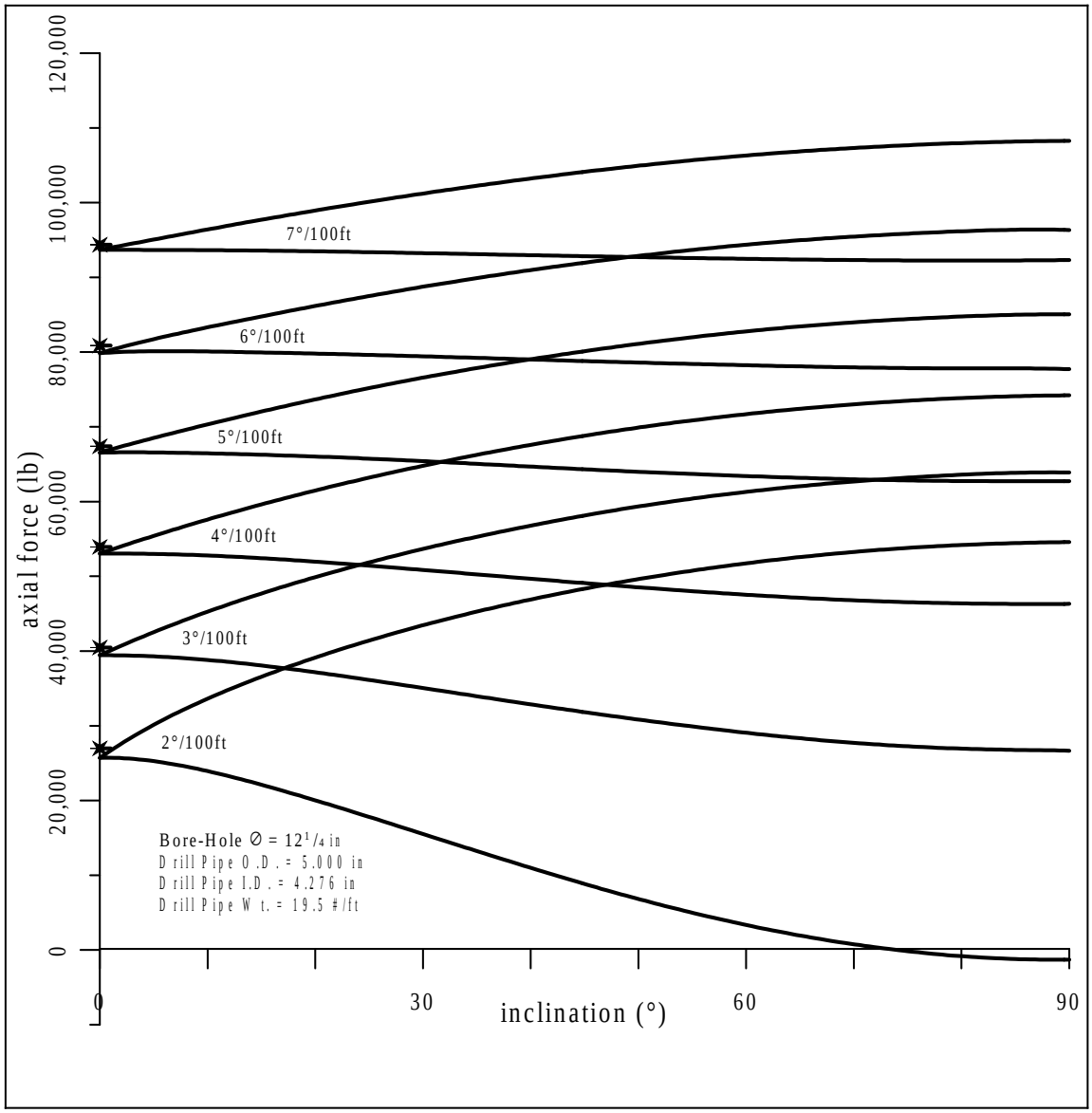

Figure 7.11: Case No.2 with multiple build gradients

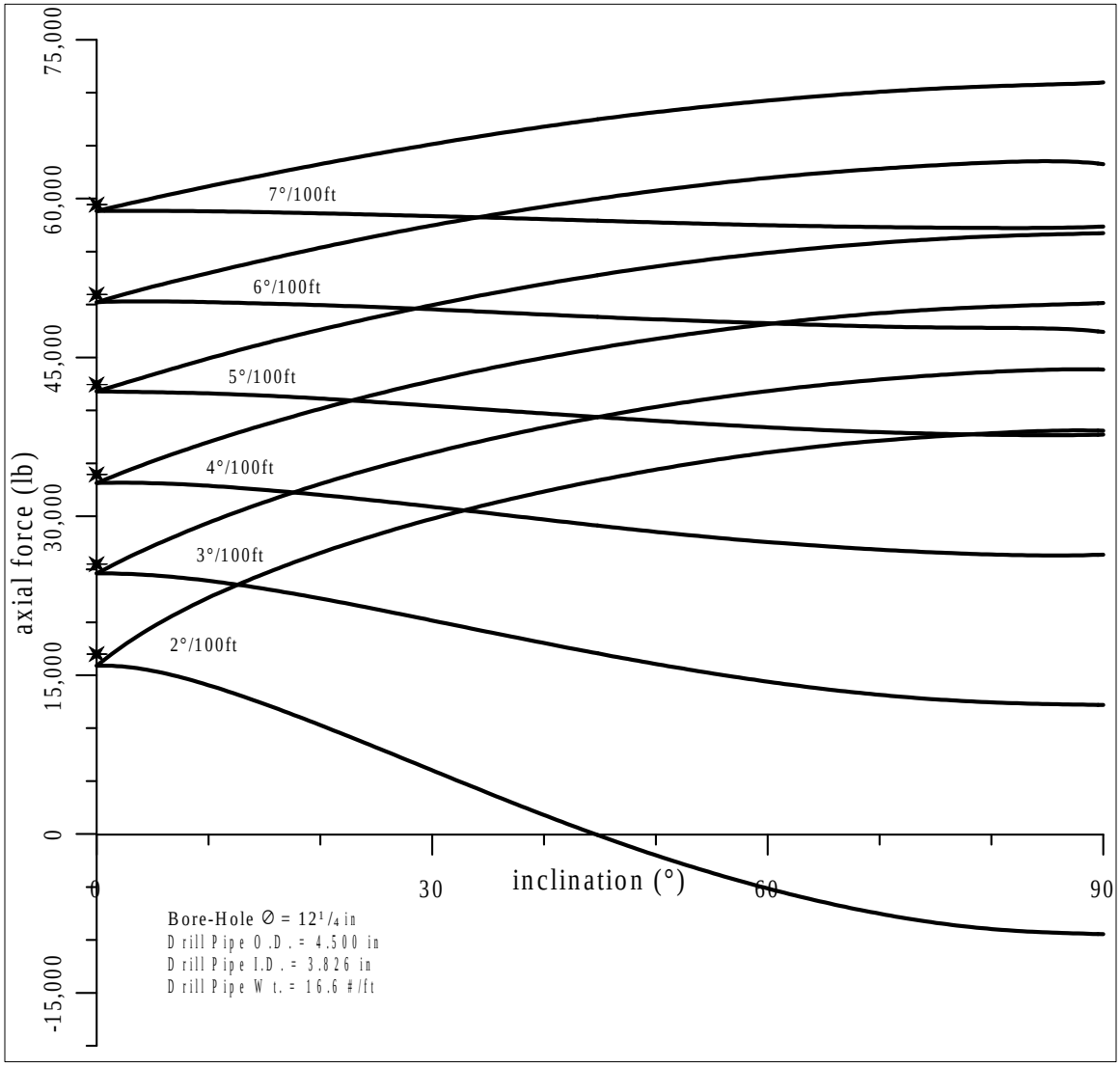

Figure 7.12: Case No.3 with multiple build gradients

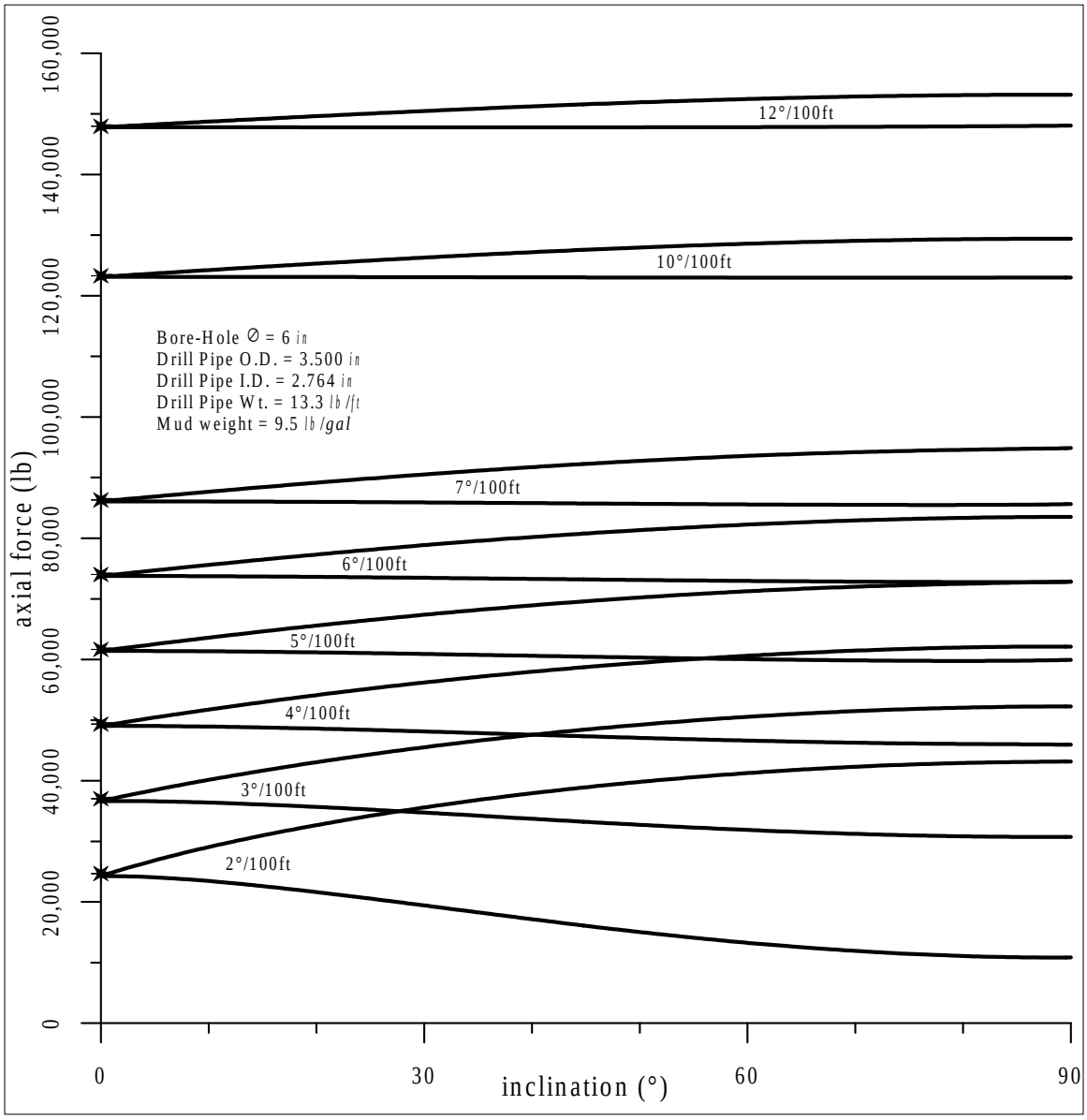

Figure 7.13: Case No.4 with multiple build gradients

Chapter 8

Conclusions

The *hypergeometric model* is a new tool available in bore-hole drilling.

*

For the first time the buckling behavior of drillstrings within curved bore-holes can be determined using a *fully analytical* model. Every detail of the *hypergeometric model* formulation was developed with the specific goal of solving the problem of buckling of drillstrings within curved bore-holes. It is entirely self-contained and does not resort to any result or formulation from buckling in straight bore-holes or to any kind of adjustable factors to fit field results. The mathematical and physical fundamentals of this model, along with its experimental validation make this model unique in its area.

**

This model results from the integration of several areas of knowledge with the purpose of understanding an important, and so far unsolved, problem of the drilling of bore-holes. This work has many facets. Other areas of engineering, sciences, and mathematics will profit from the intermediary results developed and presented here.

The model for the generalized beam-column is, as far as I know, original. The development of this model became imperative when it was realized that it would be the kernel to solve the problem of buckling for curved bore-holes, in which the changing inclination is an important parameter. No such theory existed.

The solutions for the generalized beam-column are no more complex than that for the Euler column or for the flagpole. The solution for the first uses trigonometric functions, and the solution for the second uses Bessel functions. The solution for the

generalized beam-column uses generalized hypergeometric functions.

The representation of the solution in a closed form using hypergeometric functions and the evaluation of these functions using asymptotic expansions were fundamental to an efficient and accurate implementation of the generalized beam-column model.

The implementation of the hypergeometric model revealed that the behavior for the drillstring, as predicted by the model, agrees with the intuitive behavior expected for the phenomenon. The development of the *buckling graphs* and the *P-curve shifting method* permit precise predictions and accurate comparisons with experimental results. The successful comparisons with experimental results opened a wide horizon for practical applications.

One immediate application is in horizontal oil, gas and geothermal well design and drilling. The increase in the buckling resistance of the drillstring as a result of the curvature of the bore-hole allows larger weights on the drill bit in horizontal sections, which consequently increases the maximum length of these bore-hole sections. Another practical application is the design and optimization of tapered drillstrings. This will result in an additional savings in the cost of horizontal wells.

***

8.1 Conclusions

Two categories of conclusions exist: conclusions concerned with the model and conclusions concerned with the buckling behavior of drillstrings constrained within curved bore-holes. From the presentation in the previous chapters, it is concluded that the model has strong physical and mathematical foundations, excellent experimental support, and can properly predict the buckling behavior of drillstrings constrained within curved

bore-holes. The results of several examples allow the following conclusions concerned with the behavior of drillstrings constrained within curved bore-holes:

1- The local buckling force increases with inclination for building bore-holes. The curve that describes the local buckling force (P'-curve) is concave, with slope (derivative) zero at the angle of ninety degrees.
2- The buckling force increases with build gradient. The shape of the P'-curve retains its same characteristics but a flattening becomes evident, revealing that the distributed weight has less influence for higher build gradients.
3- It follows that for higher build gradients, the trigonometric model furnishes acceptable predictions.
4- The P-curve shows that, for frictionless cases, the highest risk of buckling occurs at the lowest part of the curved section. The KOP is as a reference point for comparing buckling forces along the drillstring. Vertically shifting the P-curve allows the calculation of the axial force using any other reference point along the drillstring.
5- The P-curve flattens with an increase in the build gradient. This characteristic indicates that at higher build gradients the risk of buckling is the same along the entire length of the drillstring.
6- The buckling force increases as the diameter of the bore-hole decreases.
7- Buckling force increases with the stiffness of the drillstring.
8- Friction does not influence in the P'-curve but it does affect the P-curve. Although friction had not been implemented in this model, it may be easily included for field applications following the discussion in Chapter 6. The inclusion of friction affects the position along the curved section of the bore-hole at which buckling will occur, and consequently, the maximum force which can be applied on the bit.
9- The model is not restricted to homogeneous drillstrings. Tapered drillstrings, tapered bore-holes, and multi-curved bore-holes can be analyzed using the P-curve shifting

method.

I conjecture that this does exhaust neither all the conclusions of this work nor other possibilities, and the experience obtained with the *hypergeometric model* will expose more conclusions and guide investigators toward additional improvements.

****

8.2 Future Work

There are several points in this work that deserve further investigations or implementations. These points are concerned with the list of assumptions presented in Chapter 1.

A 3D model needs to be developed. I anticipate that such a model requires different methods than those applied in the *hypergeometric model*. Only a 3D model will be able to determine the loading buckling force of a drillstring. This is important in drilling operations using PDM in which the drillstring does not rotate. If rotation is used the maximum weight on bit should be calculated considering the *hypergeometric model*.

The torque developed along the drillstring during drilling operations is an important parameter to be analyzed. There are experimental studies indicating that the direction of the torque dictates the direction of the helix in helical buckling. This implies that two possible stable states exist and that the final state of the drillstring is that which requires less energy to buckle and, consequently, a lower axial force. This force is smaller than the axial force required when the drillstring is free of torque.

For practical applications, friction effects must be implemented. This concerns more with the completeness of the model than with the expected final numbers. During drilling, the drillstrings rotates and vibrates, and most of the frictional forces are released. In this case, dynamic friction coefficients must be used.

There exist two ways of using this model. The first is the direct use of a numerical code implemented in a computer. The advantage of using a numerical code is that the exact value for the parameters can be used. The second way is the use of *buckling graphs*. Graphs covering the wide range of parameters used in the industry can be generated and made accessible to project engineers. Numerical tables or curve fits can also substitute these graphs.

*****

Cited References

Abramowitz, M., I. A. Stegun 1972. Handbook of mathematical functions. New York, NY: Dover Publications.

Adrichem, W., K. R. Newman 1992. Validation of coiled-tubing penetration predictions in horizontal wells. SPE paper No 24765 read at the 67th Annual Technical Conference and Exhibition of the Society of Petroleum Engineers, 4-7 October. Washington, DC.

Bleich, F. 1952. Buckling strength of metal structures. New York, NY: McGraw-Hill Book Company, Inc.

Cheatham, J. B., P. D. Pattillo 1984. Helical postbuckling configuration of a weightless column under the action of an axial load. Society of Petroleum Engineers Journal (August): 467-472.

Chen, Y., Y. Lin, J. B. Cheatham 1990. Tubing and casing buckling in horizontal wells. Journal of Petroleum Technology (February): 140-141,191.

Dawson, R., P. R. Paslay 1984. Drillpipe buckling in inclined holes. Journal of Petroleum Technology (October): 1734-1738.

De Bruijn, N. G. 1981. Asymptotic methods in analysis. New York, NY: Dover Publications.

Erdélyi, A. 1953. Higher transcendental functions - 3 vol.'s. New York, NY: McGraw-Hill Book Company, Inc.

Euler, L. 1744. Methodus inveniendi lineas curvas maximi minimive proprietate gaudentes. Lausanne and Geneva.

Golub, G. H., C. F. V. Loan 1989. Matrix computations - 2nd edition. Baltimore, MD: The John Hopkins University Press.

Gurakin, G. 1996. A laboratory demonstration of the buckling of rods contained within

curved tubes. MSc Thesis No. T-4770, Colorado School of Mines, Golden, CO.

Hartog, J. P. D. 1949. Strength of materials. New York, NY: McGraw-Hill Book Company, Inc..

_____ 1952. Advanced strength of materials. New York, NY: McGraw-Hill Book Company, Inc..

He, X., A. Kyllingstad 1993. Helical buckling and lock-up conditions for coiled tubing in curved wells. SPE paper No 25370 read at the SPE Asia Pacific Oil & Gas Conference & Exhibition, 8-10 February. Singapore.

Heisig, G., 1995. Postbuckling analysis of drillstrings using the finite element method. PD-Vol. 65, Drilling Technology ASME: 91-98.

Kwon, Y. W. 1988. Analysis of helical buckling. SPE Drilling Engineering (June): 211-216.

Lai, W. M., D. Rubin, E. Krempl 1993. Introduction to continuum mechanics - 3rd edition. Tarrytown, NY: Pergamon Press Inc..

Lebedev, N. N. 1972. Special functions and their applications. New York, NY: Dover Publications.

Langhaar, H. L. 1989. Energy methods in applied mechanics. Malabar, FL: Robert E. Krieger Publishing Co., Inc..

Love, A. E. H. 1944. A treatise on the mathematical theory of elasticity - 4th edition. New York, NY: Dover Publications.

Lubinski, A. 1950. A study of the buckling of rotary drilling strings. Drilling and Production Practice, American Petroleum Institute, New York: 178-214.

_____ 1951. Influence of tension and compression on straightness and buckling of tubular goods in oil wells. Proceedings of the 31st Annual Meeting API, Prod. Bul. 237, New York: 31-49.

_____ 1987. Developments in petroleum engineering - 2 vol.'s. Houston, TX: Gulf Publishing Company. Edited by Stefan Miska.

Lubinski, A., K. A. Blenkarn 1957. Buckling of tubing in pumping wells, its effects and means for controlling it. Transactions of AIME 210, 73.

Lubinski, A., W. S. Althouse, J. L. Logan 1962. Helical buckling of tubing sealed in packers. Journal of Petroleum Technology (June): 625-670.

Luke, Y. L. 1962. Integral of Bessel functions. New York, NY: McGraw-Hill Book Company, Inc..

_____ 1969. The special functions and their approximations - 2 vol.'s. New York, NY: Academic Press.

Meijer, C. S. 1946. Nederl. Akad. Wetensch. Proc. Ser. A.49, 344-356, 457-469, 632-641, 765-722,936-943, 1063-1072, 1165-1175.

Mitchell, R. F. 1982. Buckling behavior of well tubing: the packer effect. SPEJ (October): 616-624.

_____ 1988. New concepts for helical buckling. SPE Drilling Engineering (September): 303-310.

Paslay, P. R., D. B. Bogy 1964. The stability of a circular rod laterally constrained to be in contact with an inclined circular cylinder. Journal of Applied Mechanics (December): 605-610.

Press, W. H., S. A. Teukolsky, W. T. Vetterling, B. P. Flannery. 1992. Numerical recipes - 2nd edition. New York, NY: Cambridge University Press.

Reddy, J. N. 1993. An introduction to the finite element model - 2nd edition. New York, NY: McGraw-Hill, Inc..

Salies, J. B., J. J. Azar, J. R. Sorem, Jr. 1995. Experimental and mathematical modeling of helical buckling of pipes in horizontal wellbores. PD-Vol. 65, Drilling Technology ASME: 79-89.

Segel, L. A., G. H. Handelman 1977. Mathematics applied to continuum mechanics. New York, NY: Macmillan Publishing Company.

Schuh, F. J. 1991. The critical buckling force and stresses for pipe in inclined curved

boreholes. SPE paper No 21942 read at SPE/IADC Drilling Conference, 11-14 March. Amsterdam.

Simitses, G. J. 1986. An introduction to the elastic stability of structures. Malabar, FL: Robert E. Krieger Publishing Co., Inc..

Struik, D. J. 1961. Lectures on classical differential geometry. 2nd ed.. Reading, MA: Addison-Wesley Publishing Company, Inc..

Surayanarayana, P. V. R., R. C. McCann 1995. An experimental study of buckling and post-buckling of laterally constrained rods. Journal of Energy Resources Technology (June): Vol. 117 115-124.

Timoshenko, S. P. 1958. Strength of materials - 3rd edition - 2 vol.'s. New York, NY: Van Nostrand Reinhold Company.

Timoshenko, S. P., J. E. Gere. 1988. Theory of elastic stability - 2nd edition. New York, NY: McGraw-Hill Publishing Company.

Wu, J., H. C. Juvkam-Wold 1990. Discussion on tubing and casing in horizontal wells. Journal of Petroleum Technology (August): 1062-1063.

_____ 1993. Study of helical buckling of pipes in horizontal wells. SPE paper No 25503 read at Production Operations Symposium, 21-23 March. Oklahoma City, OK.

Appendix A

Tables Of Numeric Results
(Abridged)

The tables presented here are excerpts of the tables used to plot the graphics in Chapter 7. Originally the tables were generated in intervals of 1°. However, to save space, they were reproduced in intervals of 5°. These intervals are not strict at the ends where the minimum and maximum angles were also included.

The tables also include the data read by the FORTRAN program. These data are:

ID of the Well
OD of the Pipe
ID of the Pipe
Weight of the Pipe
Modulus of Elasticity
Radius of Curvature (Negative for Build)
Error in the radius of curvature
Error in the clearance
Error in the X-coordinate of the center of curvature
Error in the Y-coordinate of the center of curvature
λ_{min}
Maximum number of iterations

Additional information required by the program and not printed are the initial and final angle, the step interval, and the initial stepsize *h* used in the Richardson's method for derivative calculations. The stepsizes are plotted in each line of the table. The program also prints the results obtained using the trigonometric model. Hi-Low values obtained in the experiments are also included whenever available.

2.0379	in	ID of the Well
0.1173	in	OD of the Pipe
0	in	ID of the Pipe
0.0368	lb/ft	Weight of the Pipe
3E+7	lb/in^2	Modulus of Elasticity
-112.915	ft	Radius of Curvature (Negative for Build)
0.00001	(fraction)	Error in the radius of curvature
0.000001	(fraction)	Error in the clearance
0.000001	(fraction)	Error in the X-coordinate of the center of curvature
0.0001	(fraction)	Error in the Y-coordinate of the center of curvature
0.125		λ_{min}
100		Maximum number of iterations
Simple model results		
Lp	L	P
10.11	9.64	1.68
Hi-Low experimental results		
angle	high value	low value
-none-	-none-	-none-

θ ($^\circ$)	P_c (lb)	P_v (lb)	L_d	L_i (ft)	g_i	L_f (ft)	g_f	L_t (ft)	$\#_{it}$	h
1	**1.51**	**1.44**	**2.6823**	**10.02**	**0.9566**	**10.05**	**0.9569**	**9.60**	**5**	**0.0001**
5	**1.79**	**1.43**	**2.4787**	**9.30**	**0.8364**	**9.30**	**0.8368**	**8.93**	**4**	**0.0001**
10	**2.05**	**1.32**	**2.3189**	**8.82**	**0.7256**	**8.73**	**0.7411**	**8.42**	**5**	**0.0001**
15	**2.26**	**1.18**	**2.1987**	**8.35**	**0.6661**	**8.33**	**0.6763**	**8.06**	**5**	**0.0001**
20	**2.45**	**1.03**	**2.0950**	**7.97**	**0.6336**	**8.01**	**0.6301**	**7.77**	**11**	**0.0001**
25	**2.64**	**0.89**	**1.9984**	**7.71**	**0.6038**	**7.74**	**0.6026**	**7.51**	**8**	**0.0001**
30	**2.77**	**0.69**	**1.9235**	**7.16**	**0.6000**	**7.56**	**0.5760**	**7.35**	**8**	**0.0001**
35	**2.90**	**0.51**	**1.8496**	**7.45**	**0.5480**	**7.41**	**0.5452**	**7.21**	**14**	**0.0001**
40	**3.01**	**0.34**	**1.7757**	**7.19**	**0.5346**	**7.27**	**0.5324**	**7.08**	**8**	**0.0001**
45	**3.12**	**0.18**	**1.7013**	**7.04**	**0.4974**	**7.16**	**0.5144**	**6.98**	**8**	**0.0001**
50	**3.24**	**0.06**	**1.6190**	**7.12**	**0.4926**	**7.03**	**0.5009**	**6.86**	**10**	**0.0001**
55	**3.32**	**-0.08**	**1.5414**	**6.90**	**0.4873**	**6.95**	**0.4936**	**6.79**	**12**	**0.0001**
60	**3.39**	**-0.21**	**1.4588**	**6.89**	**0.4871**	**6.89**	**0.4864**	**6.73**	**5**	**0.0001**
65	**3.43**	**-0.33**	**1.3729**	**6.86**	**0.4769**	**6.86**	**0.4770**	**6.70**	**6**	**0.0001**
70	**3.51**	**-0.39**	**1.2669**	**6.79**	**0.4834**	**6.79**	**0.4739**	**6.63**	**3**	**0.0001**
75	**3.53**	**-0.48**	**1.1523**	**6.78**	**0.4625**	**6.78**	**0.4627**	**6.62**	**2**	**0.0001**
80	**3.56**	**-0.53**	**1.0056**	**6.75**	**0.4753**	**6.75**	**0.4640**	**6.60**	**101**	**0.0001**
85	**3.60**	**-0.54**	**0.7969**	**6.71**	**0.4725**	**6.73**	**0.4607**	**6.58**	**9**	**0.0001**
88	**3.61**	**-0.54**	**0.5868**	**6.75**	**0.4602**	**6.73**	**0.4618**	**6.58**	**66**	**0.0001**

Table A.1: $^1/_8$ *in* steel rod - 2 *in* bore-hole - 113 *ft* radius of curvature.

2.0379	in	ID of the Well
0.1173	in	OD of the Pipe
0	in	ID of the Pipe
0.0368	lb/ft	Weight of the Pipe
3E+7	lb/in^2	Modulus of Elasticity
-57.915	ft	Radius of Curvature (Negative for Build)
0.00001	(fraction)	Error in the radius of curvature
0.000001	(fraction)	Error in the clearance
0.000001	(fraction)	Error in the X-coordinate of the center of curvature
0.0001	(fraction)	Error in the Y-coordinate of the center of curvature
0.125		λ_{min}
100		Maximum number of iterations
Simple model results		
Lp	L	P
7.24	6.91	3.28
Hi-Low experimental results		
angle	high value	low value
85	5.11	4.66

θ (°)	P_c (lb)	P_v (lb)	L_d	L_i (ft)	g_i	L_f (ft)	g_f	L_t (ft)	$\#_{it}$	h
2	**3.18**	**3.11**	**1.9205**	**7.19**	**0.9784**	**7.20**	**0.9776**	**6.87**	**46**	**0.0001**
5	**3.29**	**3.10**	**1.8863**	**7.08**	**0.9458**	**7.08**	**0.9465**	**6.76**	**4**	**0.0001**
10	**3.46**	**3.09**	**1.8306**	**6.89**	**0.9040**	**6.89**	**0.9035**	**6.60**	**3**	**0.0001**
15	**3.62**	**3.07**	**1.7774**	**6.72**	**0.8716**	**6.74**	**0.8689**	**6.46**	**4**	**0.0001**
20	**3.76**	**3.03**	**1.7294**	**6.66**	**0.8396**	**6.62**	**0.8391**	**6.35**	**4**	**0.0001**
25	**3.89**	**2.99**	**1.6792**	**6.47**	**0.8078**	**6.50**	**0.8103**	**6.25**	**5**	**0.0001**
30	**4.00**	**2.94**	**1.6310**	**7.00**	**0.8000**	**6.41**	**0.7907**	**6.17**	**11**	**0.0001**
35	**4.11**	**2.89**	**1.5794**	**6.27**	**0.7629**	**6.33**	**0.7698**	**6.09**	**5**	**0.0001**
40	**4.21**	**2.84**	**1.5272**	**6.22**	**0.7441**	**6.25**	**0.7539**	**6.03**	**13**	**0.0001**
45	**4.30**	**2.80**	**1.4715**	**6.16**	**0.7491**	**6.19**	**0.7385**	**5.97**	**9**	**0.0001**
50	**4.41**	**2.78**	**1.4094**	**6.10**	**0.7279**	**6.12**	**0.7275**	**5.91**	**4**	**0.0001**
55	**4.47**	**2.72**	**1.3487**	**6.08**	**0.7154**	**6.08**	**0.7157**	**5.87**	**4**	**0.0001**
60	**4.54**	**2.69**	**1.2792**	**6.00**	**0.7180**	**6.04**	**0.7104**	**5.84**	**10**	**0.0001**
65	**4.59**	**2.65**	**1.2037**	**6.05**	**0.6935**	**6.01**	**0.7009**	**5.81**	**5**	**0.0001**
70	**4.65**	**2.65**	**1.1147**	**5.97**	**0.7062**	**5.97**	**0.6968**	**5.77**	**6**	**0.0001**
75	**4.68**	**2.62**	**1.0135**	**5.94**	**0.6883**	**5.96**	**0.6932**	**5.76**	**12**	**0.0001**
80	**4.71**	**2.61**	**0.8850**	**5.95**	**0.6866**	**5.94**	**0.6892**	**5.75**	**8**	**0.0001**
85	**4.74**	**2.61**	**0.7022**	**5.92**	**0.6878**	**5.93**	**0.6872**	**5.74**	**6**	**0.0001**
88	**4.74**	**2.61**	**0.5174**	**5.93**	**0.6843**	**5.93**	**0.6877**	**5.74**	**6**	**0.0001**

Table A.2: $^1/_8$ *in* steel rod - 2 *in* bore-hole - 58 *ft* radius of curvature.

2.0379	in	ID of the Well
0.1173	in	OD of the Pipe
0	in	ID of the Pipe
0.0368	lb/ft	Weight of the Pipe
3E+7	lb/in^2	Modulus of Elasticity
-39.915	ft	Radius of Curvature (Negative for Build)
0.00001	(fraction)	Error in the radius of curvature
0.000001	(fraction)	Error in the clearance
0.000001	(fraction)	Error in the X-coordinate of the center of curvature
0.0001	(fraction)	Error in the Y-coordinate of the center of curvature
0.125		λ_{min}
100		Maximum number of iterations
Simple model results		
Lp	L	P
6.01	5.73	4.76
Hi-Low experimental results		
angle	high value	low value
82.8	6.3	5.8

θ (°)	P_c (lb)	P_v (lb)	L_d	L_i (ft)	g_i	L_f (ft)	g_f	L_t (ft)	$\#_{it}$	h
3	**4.69**	**4.61**	**1.5957**	**5.90**	**0.9853**	**5.98**	**0.9840**	**5.71**	**6**	**0.0001**
5	**4.74**	**4.61**	**1.5854**	**5.77**	**0.9753**	**5.95**	**0.9734**	**5.68**	**101**	**0.0001**
10	**4.87**	**4.61**	**1.5580**	**5.86**	**0.9491**	**5.87**	**0.9497**	**5.61**	**3**	**0.0001**
15	**4.99**	**4.61**	**1.5287**	**5.79**	**0.9290**	**5.79**	**0.9288**	**5.54**	**3**	**0.0001**
20	**5.09**	**4.58**	**1.4991**	**5.73**	**0.9098**	**5.74**	**0.9104**	**5.49**	**4**	**0.0001**
25	**5.20**	**4.57**	**1.4654**	**5.69**	**0.8962**	**5.67**	**0.8923**	**5.44**	**4**	**0.0001**
30	**5.29**	**4.56**	**1.4302**	**5.80**	**0.8000**	**5.62**	**0.8766**	**5.39**	**5**	**0.0001**
35	**5.39**	**4.55**	**1.3905**	**5.58**	**0.8618**	**5.57**	**0.8643**	**5.34**	**4**	**0.0001**
40	**5.48**	**4.54**	**1.3493**	**5.51**	**0.8544**	**5.53**	**0.8511**	**5.30**	**8**	**0.0001**
45	**5.54**	**4.50**	**1.3066**	**5.51**	**0.8458**	**5.50**	**0.8407**	**5.28**	**4**	**0.0001**
50	**5.62**	**4.50**	**1.2568**	**5.46**	**0.8326**	**5.46**	**0.8329**	**5.24**	**4**	**0.0001**
55	**5.69**	**4.48**	**1.2036**	**5.41**	**0.8249**	**5.43**	**0.8235**	**5.22**	**6**	**0.0001**
60	**5.74**	**4.47**	**1.1446**	**5.40**	**0.8198**	**5.40**	**0.8163**	**5.19**	**3**	**0.0001**
65	**5.78**	**4.45**	**1.0787**	**5.36**	**0.8084**	**5.39**	**0.8104**	**5.18**	**6**	**0.0001**
70	**5.83**	**4.45**	**1.0020**	**5.38**	**0.8071**	**5.37**	**0.8065**	**5.16**	**4**	**0.0001**
75	**5.87**	**4.45**	**0.9101**	**5.33**	**0.8040**	**5.35**	**0.8032**	**5.15**	**13**	**0.0001**
80	**5.90**	**4.45**	**0.7954**	**5.34**	**0.8044**	**5.34**	**0.8015**	**5.14**	**4**	**0.0001**
85	**5.92**	**4.46**	**0.6313**	**5.33**	**0.8015**	**5.34**	**0.7998**	**5.13**	**5**	**0.0001**
88	**5.93**	**4.46**	**0.4653**	**5.33**	**0.8002**	**5.34**	**0.7992**	**5.13**	**72**	**0.0001**

Table A.3: $^1/_8$ in steel rod - 2 *in* bore-hole - 40 *ft* radius of curvature.

1.0259	in	ID of the Well
0.1173	in	OD of the Pipe
0	in	ID of the Pipe
0.0368	lb/ft	Weight of the Pipe
3E+7	lb/in^2	Modulus of Elasticity
-112.957	ft	Radius of Curvature (Negative for Build)
0.00001	(fraction)	Error in the radius of curvature
0.000001	(fraction)	Error in the clearance
0.000001	(fraction)	Error in the X-coordinate of the center of curvature
0.0001	(fraction)	Error in the Y-coordinate of the center of curvature
0.125		λ_{min}
100		Maximum number of iterations
Simple model results		
Lp	L	P
6.96	6.63	3.55
Hi-Low experimental results		
angle	high value	low value
-none-	-none-	-none-

θ (°)	P_c (lb)	P_v (lb)	L_d	L_i (ft)	g_i	L_f (ft)	g_f	L_t (ft)	$\#_{it}$	h
1	**3.46**	**3.39**	**1.8463**	**6.90**	**0.9788**	**6.92**	**0.9794**	**6.60**	**4**	**0.0001**
5	**3.74**	**3.37**	**1.7725**	**6.68**	**0.9092**	**6.65**	**0.9126**	**6.37**	**25**	**0.00001**
10	**4.03**	**3.31**	**1.6977**	**6.43**	**0.8492**	**6.39**	**0.8492**	**6.14**	**11**	**0.00001**
15	**4.29**	**3.22**	**1.6339**	**6.21**	**0.8039**	**6.19**	**0.7998**	**5.96**	**8**	**0.00001**
20	**4.52**	**3.10**	**1.5772**	**5.98**	**0.7623**	**6.03**	**0.7604**	**5.82**	**7**	**0.00001**
25	**4.75**	**2.99**	**1.5195**	**5.92**	**0.7123**	**5.88**	**0.7307**	**5.68**	**15**	**0.00001**
30	**4.92**	**2.84**	**1.4700**	**6.70**	**0.8000**	**5.78**	**0.6999**	**5.59**	**15**	**0.0001**
35	**5.09**	**2.71**	**1.4180**	**5.72**	**0.6629**	**5.68**	**0.6810**	**5.49**	**5**	**0.0001**
40	**5.27**	**2.60**	**1.3635**	**5.58**	**0.6570**	**5.58**	**0.6598**	**5.41**	**4**	**0.0001**
45	**5.41**	**2.47**	**1.3105**	**5.51**	**0.6436**	**5.51**	**0.6443**	**5.34**	**5**	**0.0001**
50	**5.53**	**2.35**	**1.2558**	**5.45**	**0.6344**	**5.45**	**0.6346**	**5.29**	**4**	**0.0001**
55	**5.62**	**2.21**	**1.1995**	**5.37**	**0.6187**	**5.41**	**0.6208**	**5.25**	**9**	**0.0001**
60	**5.73**	**2.14**	**1.1347**	**5.36**	**0.6189**	**5.36**	**0.6131**	**5.20**	**4**	**0.0001**
65	**5.79**	**2.02**	**1.0680**	**5.30**	**0.6101**	**5.33**	**0.6018**	**5.18**	**16**	**0.0001**
70	**5.87**	**1.96**	**0.9891**	**5.29**	**0.6067**	**5.30**	**0.5977**	**5.15**	**16**	**0.0001**
75	**5.92**	**1.90**	**0.8980**	**5.29**	**0.5984**	**5.28**	**0.5917**	**5.13**	**10**	**0.0001**
80	**5.97**	**1.88**	**0.7831**	**5.26**	**0.5897**	**5.26**	**0.5894**	**5.11**	**48**	**0.0001**
85	**6.00**	**1.86**	**0.6209**	**5.25**	**0.5925**	**5.25**	**0.5892**	**5.10**	**101**	**0.0001**
88	**6.00**	**1.85**	**0.4578**	**5.25**	**0.5887**	**5.25**	**0.5878**	**5.10**	**26**	**0.0001**

Table A.4: 1/8 in steel rod - 1 in bore-hole - 113 ft radius of curvature.

1.0259	in	ID of the Well
0.1173	in	OD of the Pipe
0	in	ID of the Pipe
0.0368	lb/ft	Weight of the Pipe
3E+7	lb/in^2	Modulus of Elasticity
-57.957	ft	Radius of Curvature (Negative for Build)
0.000001	(fraction)	Error in the radius of curvature
0.000001	(fraction)	Error in the clearance
0.000001	(fraction)	Error in the X-coordinate of the center of curvature
0.0001	(fraction)	Error in the Y-coordinate of the center of curvature
0.125		λ_{min}
100		Maximum number of iterations
Simple model results		
Lp	L	P
4.98	4.75	6.93
Hi-Low experimental results		
angle	high value	low value
85	8.6	7.6

θ (°)	P_c (lb)	P_v (lb)	L_d	L_i (ft)	g_i	L_f (ft)	g_f	L_t (ft)	$\#_{it}$	h
2	**6.88**	**6.81**	**1.3241**	**4.96**	**0.9887**	**4.96**	**0.9892**	**4.73**	**4**	**0.00001**
5	**7.00**	**6.81**	**1.3116**	**4.92**	**0.9729**	**4.92**	**0.9739**	**4.70**	**3**	**0.00001**
10	**7.17**	**6.80**	**1.2897**	**4.85**	**0.9492**	**4.86**	**0.9508**	**4.64**	**4**	**0.00001**
15	**7.34**	**6.79**	**1.2653**	**4.81**	**0.9264**	**4.80**	**0.9298**	**4.59**	**3**	**0.0001**
20	**7.49**	**6.76**	**1.2408**	**4.73**	**0.9144**	**4.75**	**0.9101**	**4.54**	**4**	**0.0001**
25	**7.64**	**6.73**	**1.2136**	**4.70**	**0.8964**	**4.70**	**0.8936**	**4.50**	**3**	**0.0001**
30	**7.78**	**6.72**	**1.1835**	**4.80**	**0.8000**	**4.65**	**0.8781**	**4.46**	**6**	**0.0001**
35	**7.90**	**6.68**	**1.1528**	**4.61**	**0.8638**	**4.62**	**0.8642**	**4.43**	**4**	**0.0001**
40	**8.02**	**6.65**	**1.1185**	**4.58**	**0.8532**	**4.58**	**0.8532**	**4.40**	**3**	**0.0001**
45	**8.14**	**6.63**	**1.0814**	**4.54**	**0.8455**	**4.55**	**0.8430**	**4.37**	**7**	**0.0001**
50	**8.23**	**6.60**	**1.0416**	**4.54**	**0.8323**	**4.52**	**0.8325**	**4.34**	**7**	**0.0001**
55	**8.33**	**6.58**	**0.9967**	**4.50**	**0.8241**	**4.49**	**0.8256**	**4.32**	**5**	**0.0001**
60	**8.40**	**6.56**	**0.9480**	**4.48**	**0.8153**	**4.48**	**0.8175**	**4.30**	**3**	**0.0001**
65	**8.47**	**6.54**	**0.8928**	**4.46**	**0.8161**	**4.46**	**0.8119**	**4.29**	**18**	**0.0001**
70	**8.53**	**6.52**	**0.8294**	**4.44**	**0.8076**	**4.44**	**0.8084**	**4.27**	**19**	**0.0001**
75	**8.57**	**6.51**	**0.7541**	**4.44**	**0.8042**	**4.43**	**0.8043**	**4.27**	**12**	**0.0001**
80	**8.60**	**6.50**	**0.6592**	**4.43**	**0.8037**	**4.43**	**0.8021**	**4.26**	**4**	**0.0001**
85	**8.63**	**6.51**	**0.5232**	**4.42**	**0.8002**	**4.42**	**0.8004**	**4.25**	**24**	**0.0001**
87	**8.63**	**6.50**	**0.4414**	**4.43**	**0.8003**	**4.42**	**0.7999**	**4.25**	**77**	**0.0001**

Table A.5: 1/8 in steel rod - 1 in bore-hole - 58 ft radius of curvature.

1.0259	in	ID of the Well
0.1173	in	OD of the Pipe
0	in	ID of the Pipe
0.0368	lb/ft	Weight of the Pipe
3E+7	lb/in^2	Modulus of Elasticity
-39.957	ft	Radius of Curvature (Negative for Build)
0.000001	(fraction)	Error in the radius of curvature
0.000001	(fraction)	Error in the clearance
0.000001	(fraction)	Error in the X-coordinate of the center of curvature
0.0001	(fraction)	Error in the Y-coordinate of the center of curvature
0.125		λ_{min}
100		Maximum number of iterations
Simple model results		
Lp	L	P
4.14	3.94	10.06
Hi-Low experimental results		
angle	high value	low value
82.8	11.8	10.8

θ (°)	P_c (lb)	P_v (lb)	L_d	L_i (ft)	g_i	L_f (ft)	g_f	L_t (ft)	$\#_{it}$	h
1	**9.98**	**9.96**	**1.1034**	**4.13**	**0.9973**	**4.13**	**0.9974**	**3.94**	**5**	**0.000001**
5	**10.08**	**9.96**	**1.0959**	**4.11**	**0.9877**	**4.11**	**0.9873**	**3.92**	**7**	**0.0001**
10	**10.21**	**9.96**	**1.0845**	**4.09**	**0.9761**	**4.08**	**0.9753**	**0**	**4**	**0.0001**
15	**10.33**	**9.95**	**1.0710**	**4.06**	**0.9631**	**4.06**	**0.9642**	**3.88**	**4**	**0.0001**
20	**10.44**	**9.94**	**1.0549**	**4.04**	**0.9525**	**4.04**	**0.9536**	**3.86**	**3**	**0.0001**
25	**10.55**	**9.93**	**1.0366**	**4.01**	**0.9440**	**4.01**	**0.9437**	**3.84**	**3**	**0.0001**
30	**10.66**	**9.92**	**1.0158**	**4.00**	**0.9000**	**3.99**	**0.9347**	**3.82**	**77**	**0.0001**
35	**10.76**	**9.91**	**0.9923**	**3.98**	**0.9267**	**3.97**	**0.9268**	**3.80**	**5**	**0.0001**
40	**10.86**	**9.92**	**0.9656**	**3.96**	**0.9189**	**3.95**	**0.9190**	**3.78**	**7**	**0.0001**
45	**10.94**	**9.90**	**0.9367**	**3.94**	**0.9137**	**3.94**	**0.9125**	**3.77**	**4**	**0.0001**
50	**11.02**	**9.90**	**0.9040**	**3.93**	**0.9061**	**3.92**	**0.9060**	**3.76**	**5**	**0.0001**
55	**11.09**	**9.88**	**0.8678**	**3.91**	**0.9013**	**3.91**	**0.9012**	**3.75**	**4**	**0.0001**
60	**11.15**	**9.88**	**0.8267**	**3.90**	**0.8967**	**3.90**	**0.8961**	**3.74**	**6**	**0.0001**
65	**11.21**	**9.88**	**0.7796**	**3.90**	**0.8912**	**3.89**	**0.8925**	**3.73**	**7**	**0.0001**
70	**11.26**	**9.88**	**0.7250**	**3.88**	**0.8883**	**3.88**	**0.8894**	**3.72**	**10**	**0.0001**
75	**11.30**	**9.88**	**0.6597**	**3.88**	**0.8863**	**3.88**	**0.8868**	**3.72**	**27**	**0.0001**
80	**11.33**	**9.88**	**0.5768**	**3.88**	**0.8856**	**3.87**	**0.8851**	**3.71**	**18**	**0.0001**
85	**11.34**	**9.88**	**0.4582**	**3.87**	**0.8847**	**3.87**	**0.8843**	**3.71**	**8**	**0.0001**
88	**11.35**	**9.88**	**0.3376**	**3.87**	**0.8838**	**3.87**	**0.8840**	**3.71**	**18**	**0.0001**

Table A.6 1/8 in steel rod - 1 in bore-hole - 40 ft radius of curvature.

2.03788	in	ID of the Well
0.180615	in	OD of the Pipe
0	in	ID of the Pipe
0.08718	lb/ft	Weight of the Pipe
3E+7	lb/in^2	Modulus of Elasticity
-112.915	ft	Radius of Curvature (Negative for Build)
0.000001	(fraction)	Error in the radius of curvature
0.000001	(fraction)	Error in the clearance
0.000001	(fraction)	Error in the X-coordinate of the center of curvature
0.0001	(fraction)	Error in the Y-coordinate of the center of curvature
0.125		λ_{min}
100		Maximum number of iterations
Simple model results		
Lp	L	P
9.94	9.48	9.78
Hi-Low experimental results		
angle	high value	low value
87.5	16.3	15.3

θ (°)	P_c (lb)	P_v (lb)	L_d	L_i (ft)	g_i	L_f (ft)	g_f	L_t (ft)	$\#_{it}$	h
1	**9.38**	**9.21**	**1.9843**	**9.90**	**0.9835**	**9.92**	**0.9824**	**9.46**	**4**	**0.0001**
5	**10.07**	**9.21**	**1.9124**	**9.55**	**0.9222**	**9.57**	**0.9224**	**9.16**	**4**	**0.0001**
10	**10.76**	**9.06**	**1.8413**	**9.26**	**0.8602**	**9.25**	**0.8620**	**8.87**	**3**	**0.0001**
15	**11.47**	**8.92**	**1.7721**	**8.93**	**0.8103**	**8.96**	**0.8201**	**8.61**	**4**	**0.0001**
20	**11.99**	**8.62**	**1.7172**	**8.72**	**0.7774**	**8.76**	**0.7791**	**8.44**	**53**	**0.00001**
25	**12.54**	**8.38**	**1.6587**	**8.63**	**0.7437**	**8.57**	**0.7526**	**8.26**	**9**	**0.00001**
30	**13.03**	**8.11**	**1.6029**	**9.50**	**0.9000**	**8.40**	**0.7264**	**8.11**	**7**	**0.0001**
35	**13.43**	**7.79**	**1.5500**	**8.19**	**0.6945**	**8.28**	**0.7041**	**8.00**	**8**	**0.0001**
40	**13.89**	**7.56**	**1.4910**	**8.23**	**0.6860**	**8.14**	**0.6838**	**7.88**	**5**	**0.0001**
45	**14.23**	**7.27**	**1.4349**	**8.12**	**0.6507**	**8.05**	**0.6704**	**7.79**	**5**	**0.0001**
50	**14.57**	**7.03**	**1.3742**	**7.96**	**0.6580**	**7.96**	**0.6581**	**7.71**	**3**	**0.0001**
55	**14.86**	**6.80**	**1.3105**	**7.88**	**0.6453**	**7.88**	**0.6446**	**7.64**	**3**	**0.0001**
60	**15.05**	**6.53**	**1.2446**	**7.78**	**0.6502**	**7.84**	**0.6381**	**7.60**	**27**	**0.0001**
65	**15.27**	**6.35**	**1.1691**	**7.78**	**0.6267**	**7.79**	**0.6275**	**7.55**	**3**	**0.0001**
70	**15.50**	**6.25**	**1.0821**	**7.76**	**0.6227**	**7.73**	**0.6252**	**7.50**	**23**	**0.001**
75	**15.62**	**6.11**	**0.9830**	**7.71**	**0.6218**	**7.71**	**0.6192**	**7.48**	**5**	**0.0001**
80	**15.74**	**6.04**	**0.8580**	**7.69**	**0.6194**	**7.69**	**0.6173**	**7.46**	**3**	**0.0001**
85	**15.78**	**5.97**	**0.6814**	**7.68**	**0.6135**	**7.68**	**0.6131**	**7.46**	**101**	**0.0001**
88	**15.82**	**5.99**	**0.5018**	**7.68**	**0.6150**	**7.67**	**0.6132**	**7.45**	**11**	**0.0001**

Table A.7: 3/16 in steel rod - 2 in bore-hole - 113 ft radius of curvature.

2.03788	in	ID of the Well
0.180615	in	OD of the Pipe
0	in	ID of the Pipe
0.08718	lb/ft	Weight of the Pipe
3E+7	lb/in^2	Modulus of Elasticity
-57.915	ft	Radius of Curvature (Negative for Build)
0.000001	(fraction)	Error in the radius of curvature
0.000001	(fraction)	Error in the clearance
0.000001	(fraction)	Error in the X-coordinate of the center of curvature
0.0001	(fraction)	Error in the Y-coordinate of the center of curvature
0.125		λ_{min}
100		Maximum number of iterations
Simple model results		
Lp	L	P
7.12	6.79	19.05
Hi-Low experimental results		
angle	high value	low value
85	23.6	22.6

θ (°)	P_c (lb)	P_v (lb)	L_d	L_i (ft)	g_i	L_f (ft)	g_f	L_t (ft)	$\#_{it}$	h
1	**18.73**	**18.64**	**1.4253**	**7.12**	**0.9952**	**7.12**	**0.9953**	**6.79**	**4**	**0.00001**
5	**19.09**	**18.65**	**1.4094**	**7.05**	**0.9770**	**7.05**	**0.9773**	**6.73**	**3**	**0.00001**
10	**19.50**	**18.62**	**1.3883**	**6.97**	**0.9576**	**6.97**	**0.9569**	**6.66**	**3**	**0.00001**
15	**19.92**	**18.61**	**1.3641**	**6.91**	**0.9370**	**6.90**	**0.9376**	**6.59**	**4**	**0.00001**
20	**20.31**	**18.58**	**1.3382**	**6.85**	**0.9177**	**6.83**	**0.9209**	**6.53**	**4**	**0.00001**
25	**20.64**	**18.51**	**1.3110**	**6.74**	**0.9082**	**6.77**	**0.9053**	**6.48**	**4**	**0.00001**
30	**21.00**	**18.48**	**1.2799**	**6.70**	**0.9000**	**6.71**	**0.8923**	**6.43**	**4**	**0.0001**
35	**21.29**	**18.40**	**1.2476**	**6.66**	**0.8805**	**6.66**	**0.8795**	**6.39**	**4**	**0.0001**
40	**21.59**	**18.34**	**1.2116**	**6.62**	**0.8653**	**6.62**	**0.8675**	**6.35**	**4**	**0.0001**
45	**21.86**	**18.29**	**1.1724**	**6.58**	**0.8587**	**6.58**	**0.8590**	**6.31**	**3**	**0.0001**
50	**22.16**	**18.29**	**1.1282**	**6.54**	**0.8483**	**6.53**	**0.8501**	**6.27**	**5**	**0.0001**
55	**22.36**	**18.22**	**1.0814**	**6.49**	**0.8404**	**6.50**	**0.8432**	**6.25**	**5**	**0.0001**
60	**22.55**	**18.18**	**1.0288**	**6.47**	**0.8367**	**6.48**	**0.8365**	**6.22**	**4**	**0.0001**
65	**22.75**	**18.17**	**0.9688**	**6.46**	**0.8298**	**6.45**	**0.8311**	**6.20**	**5**	**0.0001**
70	**22.87**	**18.13**	**0.9006**	**6.43**	**0.8237**	**6.43**	**0.8260**	**6.18**	**3**	**0.0001**
75	**22.99**	**18.11**	**0.8190**	**6.43**	**0.8231**	**6.42**	**0.8227**	**6.17**	**5**	**0.0001**
80	**23.10**	**18.13**	**0.7155**	**6.41**	**0.8208**	**6.41**	**0.8205**	**6.16**	**4**	**0.0001**
85	**23.14**	**18.11**	**0.5684**	**6.41**	**0.8195**	**6.41**	**0.8193**	**6.16**	**5**	**0.0001**
88	**23.20**	**18.16**	**0.4185**	**6.40**	**0.8191**	**6.40**	**0.8194**	**6.15**	**101**	**0.0001**

Table A.8: 3/16 in steel rod - 2 in bore-hole - 58 ft radius of curvature.

2.03788	in	ID of the Well
0.180615	in	OD of the Pipe
0	in	ID of the Pipe
0.08718	lb/ft	Weight of the Pipe
3E+7	lb/in^2	Modulus of Elasticity
-39.915	ft	Radius of Curvature (Negative for Build)
0.000001	(fraction)	Error in the radius of curvature
0.000001	(fraction)	Error in the clearance
0.000001	(fraction)	Error in the X-coordinate of the center of curvature
0.0001	(fraction)	Error in the Y-coordinate of the center of curvature
0.125		λ_{min}
100		Maximum number of iterations
Simple model results		
Lp	L	P
5.91	5.64	27.64
Hi-Low experimental results		
angle	high value	low value
82.8	30.8	29.8

θ (°)	P_c (lb)	P_v (lb)	L_d	L_i (ft)	g_i	L_f (ft)	g_f	L_t (ft)	#it	h
1	**27.36**	**27.30**	**1.1835**	**5.91**	**0.9977**	**5.91**	**0.9978**	**5.64**	**4**	**0.000001**
5	**27.61**	**27.31**	**1.1764**	**5.88**	**0.9888**	**5.89**	**0.9890**	**5.61**	**4**	**0.00001**
10	**27.90**	**27.30**	**1.1653**	**5.85**	**0.9793**	**5.85**	**0.9786**	**5.59**	**4**	**0.00001**
15	**28.19**	**27.29**	**1.1515**	**5.82**	**0.9699**	**5.82**	**0.9686**	**5.56**	**4**	**0.00001**
20	**28.49**	**27.30**	**1.1347**	**5.60**	**0.9900**	**5.79**	**0.9596**	**5.53**	**6**	**0.00001**
25	**28.76**	**27.29**	**1.1156**	**5.76**	**0.9523**	**5.76**	**0.9507**	**5.50**	**4**	**0.0001**
30	**29.01**	**27.27**	**1.0939**	**5.73**	**0.9434**	**5.73**	**0.9431**	**5.48**	**3**	**0.0001**
35	**29.24**	**27.24**	**1.0696**	**5.71**	**0.9361**	**5.71**	**0.9357**	**5.46**	**3**	**0.0001**
40	**29.48**	**27.24**	**1.0417**	**5.69**	**0.9285**	**5.69**	**0.9286**	**5.44**	**3**	**0.00001**
45	**29.68**	**27.22**	**1.0107**	**5.66**	**0.9211**	**5.67**	**0.9226**	**5.42**	**4**	**0.00001**
50	**29.90**	**27.24**	**0.9755**	**5.65**	**0.9178**	**5.65**	**0.9176**	**5.41**	**3**	**0.00001**
55	**30.07**	**27.22**	**0.9367**	**5.64**	**0.9116**	**5.63**	**0.9126**	**5.39**	**6**	**0.00001**
60	**30.25**	**27.23**	**0.8922**	**5.61**	**0.9082**	**5.62**	**0.9081**	**5.38**	**4**	**0.00001**
65	**30.36**	**27.21**	**0.8421**	**5.61**	**0.9031**	**5.61**	**0.9051**	**5.37**	**3**	**0.00001**
70	**30.50**	**27.23**	**0.7831**	**5.60**	**0.9018**	**5.60**	**0.9018**	**5.36**	**4**	**0.00001**
75	**30.58**	**27.22**	**0.7129**	**5.59**	**0.8983**	**5.59**	**0.8997**	**5.35**	**11**	**0.00001**
80	**30.67**	**27.25**	**0.6233**	**5.59**	**0.8991**	**5.58**	**0.8984**	**5.35**	**11**	**0.00001**
85	**30.72**	**27.26**	**0.4951**	**5.58**	**0.8976**	**5.58**	**0.8973**	**5.34**	**5**	**0.0001**
86	**30.73**	**27.26**	**0.4597**	**5.58**	**0.8973**	**5.58**	**0.8973**	**5.34**	**4**	**0.0001**

Table A.9: 3/16 in steel rod - 2 in bore-hole - 40 ft radius of curvature.

1.0259	in	ID of the Well
0.180615	in	OD of the Pipe
0	in	ID of the Pipe
0.08718	lb/ft	Weight of the Pipe
3E+7	lb/in^2	Modulus of Elasticity
-112.957	ft	Radius of Curvature (Negative for Build)
0.000001	(fraction)	Error in the radius of curvature
0.000001	(fraction)	Error in the clearance
0.000001	(fraction)	Error in the X-coordinate of the center of curvature
0.0001	(fraction)	Error in the Y-coordinate of the center of curvature
0.125		λ_{min}
100		Maximum number of iterations
Simple model results		
Lp	L	P
6.71	6.4	21.46
Hi-Low experimental results		
angle	high value	low value
87.5	29.3	28.3

θ (°)	P_c (lb)	P_v (lb)	L_d	L_i (ft)	g_i	L_f (ft)	g_f	L_t (ft)	$\#_{it}$	h
1	**21.26**	**21.09**	**1.3395**	**6.69**	**0.9911**	**6.69**	**0.9919**	**6.38**	**4**	**0.00001**
5	**21.93**	**21.07**	**1.3159**	**6.58**	**0.9604**	**6.58**	**0.9623**	**6.29**	**4**	**0.00001**
10	**22.73**	**21.02**	**1.2864**	**6.47**	**0.9308**	**6.46**	**0.9292**	**6.18**	**4**	**0.00001**
15	**23.43**	**20.88**	**1.2578**	**6.36**	**0.8969**	**6.36**	**0.9014**	**6.09**	**4**	**0.00001**
20	**24.12**	**20.76**	**1.2272**	**6.27**	**0.8728**	**6.26**	**0.8767**	**6.00**	**4**	**0.00001**
25	**24.74**	**20.58**	**1.1965**	**6.18**	**0.8563**	**6.18**	**0.8555**	**5.93**	**3**	**0.00001**
30	**25.30**	**20.38**	**1.1648**	**6.50**	**0.9000**	**6.11**	**0.8363**	**5.87**	**10**	**0.0001**
35	**25.84**	**20.19**	**1.1310**	**6.04**	**0.8184**	**6.04**	**0.8183**	**5.81**	**2**	**0.0001**
40	**26.34**	**20.01**	**1.0952**	**5.99**	**0.8040**	**5.98**	**0.8048**	**5.75**	**5**	**0.0001**
45	**26.76**	**19.80**	**1.0576**	**5.91**	**0.7979**	**5.93**	**0.7917**	**5.71**	**10**	**0.0001**
50	**27.16**	**19.62**	**1.0168**	**5.90**	**0.7786**	**5.89**	**0.7799**	**5.67**	**4**	**0.0001**
55	**27.56**	**19.49**	**0.9719**	**5.86**	**0.7723**	**5.84**	**0.7724**	**5.63**	**10**	**0.000001**
60	**27.83**	**19.31**	**0.9238**	**5.82**	**0.7617**	**5.82**	**0.7638**	**5.61**	**14**	**0.000001**
65	**28.11**	**19.19**	**0.8691**	**5.80**	**0.7560**	**5.79**	**0.7560**	**5.58**	**21**	**0.000001**
70	**28.37**	**19.12**	**0.8064**	**5.76**	**0.7531**	**5.76**	**0.7525**	**5.56**	**13**	**0.000001**
75	**28.52**	**19.01**	**0.7330**	**5.75**	**0.7462**	**5.75**	**0.7474**	**5.54**	**30**	**0.000001**
80	**28.64**	**18.94**	**0.6405**	**5.74**	**0.7434**	**5.74**	**0.7443**	**5.53**	**101**	**0.000001**
84	**28.75**	**18.96**	**0.5399**	**5.73**	**0.7421**	**5.73**	**0.7430**	**5.53**	**45**	**0.001**
88	**28.80**	**18.96**	**0.3743**	**5.72**	**0.7433**	**5.72**	**0.7430**	**5.52**	**14**	**0.001**

Table A.10: 3/16 in steel rod - 1 in bore-hole - 113 ft radius of curvature.

1.0259	in	ID of the Well
0.180615	in	OD of the Pipe
0	in	ID of the Pipe
0.08718	lb/ft	Weight of the Pipe
3E+7	lb/in^2	Modulus of Elasticity
-57.957	ft	Radius of Curvature (Negative for Build)
0.000001	(fraction)	Error in the radius of curvature
0.000001	(fraction)	Error in the clearance
0.000001	(fraction)	Error in the X-coordinate of the center of curvature
0.0001	(fraction)	Error in the Y-coordinate of the center of curvature
0.125		λ_{min}
100		Maximum number of iterations
Simple model results		
Lp	L	P
4.81	4.58	41.83
Hi-Low experimental results		
angle	high value	low value
85	46.6	44.6

θ (°)	P_c (lb)	P_v (lb)	L_d	L_i (ft)	g_i	L_f (ft)	g_f	L_t (ft)	$\#_{it}$	h
1	**41.67**	**41.59**	**0.9612**	**4.80**	**0.9980**	**4.80**	**0.9979**	**4.58**	**7**	**0.000001**
5	**42.03**	**41.59**	**0.9556**	**4.78**	**0.9897**	**4.78**	**0.9895**	**4.56**	**7**	**0.00001**
10	**42.46**	**41.58**	**0.9467**	**4.76**	**0.9790**	**4.75**	**0.9796**	**4.54**	**3**	**0.0001**
15	**42.87**	**41.56**	**0.9358**	**4.73**	**0.9702**	**4.73**	**0.9701**	**4.52**	**3**	**0.0001**
20	**43.29**	**41.56**	**0.9225**	**4.71**	**0.9612**	**4.71**	**0.9612**	**4.50**	**2**	**0.0001**
25	**43.65**	**41.52**	**0.9074**	**4.68**	**0.9528**	**4.69**	**0.9528**	**4.48**	**3**	**0.0001**
30	**44.02**	**41.49**	**0.8898**	**4.67**	**0.9461**	**4.66**	**0.9449**	**4.46**	**4**	**0.0001**
35	**44.37**	**41.47**	**0.8698**	**4.65**	**0.9383**	**4.65**	**0.9381**	**4.44**	**3**	**0.0001**
40	**44.70**	**41.46**	**0.8473**	**4.63**	**0.9313**	**4.63**	**0.9315**	**4.43**	**5**	**0.0001**
45	**44.98**	**41.41**	**0.8223**	**4.70**	**0.9000**	**4.61**	**0.9254**	**4.41**	**7**	**0.00001**
50	**45.28**	**41.41**	**0.7939**	**4.59**	**0.9203**	**4.60**	**0.9205**	**4.40**	**5**	**0.00001**
55	**45.50**	**41.36**	**0.7624**	**4.59**	**0.9153**	**4.59**	**0.9158**	**4.39**	**11**	**0.00001**
60	**45.72**	**41.35**	**0.7265**	**4.58**	**0.9120**	**4.57**	**0.9118**	**4.38**	**8**	**0.00001**
65	**45.94**	**41.36**	**0.6853**	**4.56**	**0.9072**	**4.56**	**0.9080**	**4.37**	**14**	**0.00001**
70	**46.06**	**41.32**	**0.6378**	**4.55**	**0.9054**	**4.56**	**0.9056**	**4.36**	**8**	**0.00001**
75	**46.22**	**41.34**	**0.5803**	**4.55**	**0.9037**	**4.55**	**0.9032**	**4.36**	**13**	**0.00009**
80	**46.30**	**41.32**	**0.5076**	**4.55**	**0.9022**	**4.55**	**0.9018**	**4.35**	**17**	**0.00009**
85	**46.38**	**41.35**	**0.4031**	**4.54**	**0.9000**	**4.54**	**0.9008**	**4.35**	**10**	**0.001**

Table A.11: 3/16 in steel rod - 1 in bore-hole - 58 ft radius of curvature.

1.0259	in	ID of the Well
0.180615	in	OD of the Pipe
0	in	ID of the Pipe
0.08718	lb/ft	Weight of the Pipe
3E+7	lb/in^2	Modulus of Elasticity
-39.957	ft	Radius of Curvature (Negative for Build)
0.000001	(fraction)	Error in the radius of curvature
0.000001	(fraction)	Error in the clearance
0.000001	(fraction)	Error in the X-coordinate of the center of curvature
0.0001	(fraction)	Error in the Y-coordinate of the center of curvature
0.125		λ_{min}
100		Maximum number of iterations
Simple model results		
Lp	L	P
3.99	3.81	60.67
Hi-Low experimental results		
angle	high value	low value
82.8	64.2	62.2

θ (°)	P_c (lb)	P_v (lb)	L_d	L_i (ft)	g_i	L_f (ft)	g_f	L_t (ft)	$\#_{it}$	h
3	**60.63**	**60.44**	**0.7974**	**3.99**	**0.9969**	**3.99**	**0.9970**	**3.80**	**8**	**0.000001**
5	**60.75**	**60.44**	**0.7959**	**3.98**	**0.9948**	**3.98**	**0.9950**	**3.80**	**5**	**0.000001**
10	**61.05**	**60.45**	**0.7907**	**3.97**	**0.9901**	**3.97**	**0.9901**	**3.79**	**3**	**0.000001**
15	**61.34**	**60.44**	**0.7836**	**3.96**	**0.9854**	**3.96**	**0.9853**	**3.78**	**3**	**0.00001**
20	**61.63**	**60.44**	**0.7745**	**3.95**	**0.9809**	**3.95**	**0.9808**	**3.77**	**3**	**0.00001**
25	**61.90**	**60.43**	**0.7634**	**3.94**	**0.9757**	**3.94**	**0.9765**	**3.76**	**6**	**0.00001**
30	**62.18**	**60.44**	**0.7502**	**3.93**	**0.9721**	**3.93**	**0.9723**	**3.75**	**6**	**0.0001**
35	**62.42**	**60.43**	**0.7349**	**3.92**	**0.9688**	**3.92**	**0.9686**	**3.75**	**3**	**0.0001**
40	**62.67**	**60.43**	**0.7172**	**3.92**	**0.9646**	**3.92**	**0.9651**	**3.74**	**3**	**0.0001**
45	**62.88**	**60.42**	**0.6971**	**3.91**	**0.9622**	**3.91**	**0.9617**	**3.73**	**5**	**0.0001**
50	**63.10**	**60.43**	**0.6740**	**3.90**	**0.9587**	**3.90**	**0.9588**	**3.73**	**3**	**0.0001**
55	**63.29**	**60.44**	**0.6480**	**3.90**	**0.9562**	**3.90**	**0.9563**	**3.72**	**5**	**0.0001**
60	**63.45**	**60.43**	**0.6182**	**3.89**	**0.9540**	**3.89**	**0.9541**	**3.72**	**6**	**0.0001**
65	**63.60**	**60.44**	**0.5838**	**3.89**	**0.9521**	**3.89**	**0.9521**	**3.71**	**5**	**0.0001**
70	**63.71**	**60.44**	**0.5436**	**3.88**	**0.9505**	**3.88**	**0.9504**	**3.71**	**12**	**0.0001**
75	**63.80**	**60.44**	**0.4950**	**3.88**	**0.9492**	**3.88**	**0.9492**	**3.71**	**101**	**0.0001**
80	**63.61**	**60.17**	**0.4341**	**3.88**	**0.9483**	**3.89**	**0.9482**	**3.72**	**101**	**0.0001**

Table A.12: 3/16 in steel rod - 1 in bore-hole - 40 ft radius of curvature.

2.0379	in	ID of the Well
0.243935	in	OD of the Pipe
0	in	ID of the Pipe
0.15903	lb/ft	Weight of the Pipe
3E+7	lb/in^2	Modulus of Elasticity
-112.915	ft	Radius of Curvature (Negative for Build)
0.000001	(fraction)	Error in the radius of curvature
0.000001	(fraction)	Error in the clearance
0.000001	(fraction)	Error in the X-coordinate of the center of curvature
0.0001	(fraction)	Error in the Y-coordinate of the center of curvature
0.125		λ_{min}
100		Maximum number of iterations
Simple model results		
Lp	L	P
9.77	9.32	33.67
Hi-Low experimental results		
angle	high value	low value
87.5	46.3	45.3

θ (°)	P_c (lb)	P_v (lb)	L_d	L_i (ft)	g_i	L_f (ft)	g_f	L_t (ft)	$\#_{it}$	h
2	**33.28**	**32.65**	**1.5900**	**9.71**	**0.9804**	**9.71**	**0.9814**	**9.27**	**4**	**0.0001**
5	**34.19**	**32.62**	**1.5660**	**9.58**	**0.9545**	**9.57**	**0.9562**	**9.15**	**8**	**0.0001**
10	**35.65**	**32.54**	**1.5263**	**9.40**	**0.9228**	**9.37**	**0.9195**	**8.96**	**4**	**0.0001**
15	**37.01**	**32.36**	**1.4874**	**9.22**	**0.8885**	**9.19**	**0.8872**	**8.81**	**5**	**0.0001**
20	**38.23**	**32.09**	**1.4493**	**9.09**	**0.8597**	**9.04**	**0.8599**	**8.67**	**7**	**0.0001**
25	**39.27**	**31.68**	**1.4122**	**8.86**	**0.8464**	**8.91**	**0.8361**	**8.56**	**5**	**0.0001**
30	**40.41**	**31.43**	**1.3709**	**8.50**	**0.9000**	**8.78**	**0.8183**	**8.44**	**7**	**0.0001**
35	**41.33**	**31.03**	**1.3303**	**8.73**	**0.8021**	**8.68**	**0.8000**	**8.35**	**9**	**0.0001**
40	**42.26**	**30.72**	**1.2865**	**8.58**	**0.7817**	**8.59**	**0.7833**	**8.27**	**5**	**0.0001**
45	**42.93**	**30.23**	**1.2428**	**8.52**	**0.7701**	**8.52**	**0.7699**	**8.21**	**3**	**0.0001**
50	**43.75**	**29.99**	**1.1927**	**8.40**	**0.7546**	**8.44**	**0.7579**	**8.14**	**6**	**0.0001**
55	**44.32**	**29.61**	**1.1410**	**8.43**	**0.7426**	**8.39**	**0.7501**	**8.09**	**14**	**0.0001**
60	**44.96**	**29.41**	**1.0824**	**8.33**	**0.7379**	**8.33**	**0.7417**	**8.04**	**5**	**0.0001**
65	**45.34**	**29.06**	**1.0194**	**8.29**	**0.7414**	**8.30**	**0.7342**	**8.01**	**6**	**0.0001**
70	**45.71**	**28.84**	**0.9464**	**8.23**	**0.7327**	**8.26**	**0.7291**	**7.98**	**26**	**0.0001**
75	**46.09**	**28.75**	**0.8593**	**8.20**	**0.7245**	**8.23**	**0.7234**	**7.95**	**6**	**0.0001**
80	**46.36**	**28.67**	**0.7504**	**8.22**	**0.7177**	**8.21**	**0.7207**	**7.93**	**6**	**0.0001**
85	**46.55**	**28.66**	**0.5955**	**8.20**	**0.7196**	**8.20**	**0.7200**	**7.92**	**3**	**0.001**
88	**46.59**	**28.65**	**0.4388**	**8.20**	**0.7205**	**8.20**	**0.7190**	**7.92**	**18**	**0.001**

Table A.13: 1/4 in steel rod - 2 in bore-hole - 113 ft radius of curvature.

2.0379	in	ID of the Well
0.243935	in	OD of the Pipe
0	in	ID of the Pipe
0.15903	lb/ft	Weight of the Pipe
3E+7	lb/in^2	Modulus of Elasticity
-57.915	ft	Radius of Curvature (Negative for Build)
0.000001	(fraction)	Error in the radius of curvature
0.000001	(fraction)	Error in the clearance
0.000001	(fraction)	Error in the X-coordinate of the center of curvature
0.0001	(fraction)	Error in the Y-coordinate of the center of curvature
0.125		λ_{min}
100		Maximum number of iterations
Simple model results		
Lp	L	P
7	6.67	65.64
Hi-Low experimental results		
angle	high value	low value
85	73	70

θ (°)	P_c (lb)	P_v (lb)	L_d	L_i (ft)	g_i	L_f (ft)	g_f	L_t (ft)	$\#_{it}$	h
3	**65.41**	**64.92**	**1.1427**	**6.98**	**0.9928**	**6.98**	**0.9926**	**6.66**	**32**	**0.00001**
5	**65.71**	**64.91**	**1.1389**	**6.96**	**0.9875**	**6.96**	**0.9878**	**6.64**	**3**	**0.00001**
10	**66.51**	**64.91**	**1.1273**	**6.92**	**0.9764**	**6.92**	**0.9764**	**6.60**	**3**	**0.00001**
15	**67.25**	**64.87**	**1.1134**	**6.87**	**0.9644**	**6.88**	**0.9656**	**6.57**	**5**	**0.00001**
20	**67.99**	**64.84**	**1.0969**	**6.83**	**0.9559**	**6.84**	**0.9551**	**6.53**	**6**	**0.00001**
25	**68.74**	**64.85**	**1.0776**	**6.80**	**0.9446**	**6.80**	**0.9458**	**6.50**	**7**	**0.0001**
30	**69.39**	**64.78**	**1.0562**	**6.60**	**0.9000**	**6.77**	**0.9368**	**6.47**	**39**	**0.0001**
35	**69.98**	**64.69**	**1.0323**	**6.74**	**0.9292**	**6.74**	**0.9293**	**6.44**	**4**	**0.0001**
40	**70.63**	**64.71**	**1.0047**	**6.71**	**0.9221**	**6.71**	**0.9221**	**6.42**	**5**	**0.0001**
45	**71.14**	**64.62**	**0.9747**	**6.69**	**0.9149**	**6.68**	**0.9150**	**6.39**	**6**	**0.0001**
50	**71.69**	**64.63**	**0.9405**	**6.66**	**0.9090**	**6.65**	**0.9093**	**6.37**	**5**	**0.0001**
55	**72.06**	**64.52**	**0.9032**	**6.63**	**0.9064**	**6.64**	**0.9040**	**6.36**	**6**	**0.0001**
60	**72.53**	**64.55**	**0.8601**	**6.62**	**0.8978**	**6.62**	**0.9000**	**6.34**	**4**	**0.0001**
65	**72.84**	**64.50**	**0.8115**	**6.60**	**0.8959**	**6.60**	**0.8960**	**6.33**	**6**	**0.0001**
70	**73.18**	**64.53**	**0.7546**	**6.60**	**0.8935**	**6.59**	**0.8927**	**6.31**	**16**	**0.0001**
75	**73.38**	**64.48**	**0.6869**	**6.58**	**0.8904**	**6.58**	**0.8906**	**6.31**	**30**	**0.0001**
80	**73.59**	**64.52**	**0.6006**	**6.57**	**0.8892**	**6.57**	**0.8888**	**6.30**	**11**	**0.0001**
85	**73.73**	**64.55**	**0.4770**	**6.57**	**0.8880**	**6.57**	**0.8879**	**6.30**	**8**	**0.0002**
86	**73.77**	**64.58**	**0.4428**	**6.57**	**0.8878**	**6.57**	**0.8877**	**6.29**	**18**	**0.0002**

Table A.14: 1/4 in steel rod - 2 in bore-hole - 58 ft radius of curvature.

2.0379	in	ID of the Well
0.243935	in	OD of the Pipe
0	in	ID of the Pipe
0.15903	lb/ft	Weight of the Pipe
3E+7	lb/in^2	Modulus of Elasticity
-39.915	ft	Radius of Curvature (Negative for Build)
0.000001	(fraction)	Error in the radius of curvature
0.000001	(fraction)	Error in the clearance
0.000001	(fraction)	Error in the X-coordinate of the center of curvature
0.0001	(fraction)	Error in the Y-coordinate of the center of curvature
0.125		λ_{min}
100		Maximum number of iterations
Simple model results		
Lp	L	P
5.81	5.54	95.24
Hi-Low experimental results		
angle	high value	low value
82.8	98.2	96.2

θ ($^\circ$)	P_c (lb)	P_v (lb)	L_d	L_i (ft)	g_i	L_f (ft)	g_f	L_t (ft)	$\#_{it}$	h
1	**94.75**	**94.63**	**0.9517**	**5.81**	**0.9988**	**5.81**	**0.9988**	**5.54**	**4**	**0.000005**
5	**95.19**	**94.63**	**0.9482**	**5.80**	**0.9941**	**5.80**	**0.9941**	**5.53**	**6**	**0.000005**
10	**95.74**	**94.64**	**0.9417**	**5.78**	**0.9887**	**5.78**	**0.9884**	**5.51**	**6**	**0.00001**
15	**96.28**	**94.63**	**0.9328**	**5.76**	**0.9832**	**5.76**	**0.9831**	**5.50**	**4**	**0.00001**
20	**96.80**	**94.63**	**0.9217**	**5.75**	**0.9776**	**5.75**	**0.9777**	**5.48**	**4**	**0.00001**
25	**97.31**	**94.63**	**0.9081**	**5.73**	**0.9729**	**5.73**	**0.9729**	**5.47**	**3**	**0.0001**
30	**97.82**	**94.65**	**0.8920**	**5.80**	**0.9000**	**5.71**	**0.9681**	**5.46**	**7**	**0.00001**
35	**98.29**	**94.65**	**0.8734**	**5.70**	**0.9642**	**5.70**	**0.9638**	**5.44**	**3**	**0.00001**
40	**98.72**	**94.64**	**0.8522**	**5.69**	**0.9597**	**5.69**	**0.9597**	**5.43**	**5**	**0.00001**
45	**99.15**	**94.66**	**0.8280**	**5.67**	**0.9556**	**5.68**	**0.9562**	**5.42**	**6**	**0.00001**
50	**99.49**	**94.62**	**0.8007**	**5.66**	**0.9530**	**5.67**	**0.9529**	**5.41**	**10**	**0.00001**
55	**99.87**	**94.67**	**0.7694**	**5.65**	**0.9501**	**5.65**	**0.9499**	**5.40**	**5**	**0.00001**
60	**100.14**	**94.64**	**0.7341**	**5.64**	**0.9479**	**5.65**	**0.9473**	**5.40**	**6**	**0.00001**
65	**100.43**	**94.68**	**0.6931**	**5.64**	**0.9451**	**5.64**	**0.9450**	**5.39**	**5**	**0.00001**
70	**100.66**	**94.69**	**0.6452**	**5.64**	**0.9431**	**5.63**	**0.9434**	**5.38**	**29**	**0.00001**
75	**100.87**	**94.74**	**0.5874**	**5.63**	**0.9424**	**5.63**	**0.9420**	**5.38**	**11**	**0.00002**
80	**101.01**	**94.76**	**0.5140**	**5.63**	**0.9410**	**5.63**	**0.9408**	**5.38**	**5**	**0.0001**
84	**101.11**	**94.80**	**0.4338**	**5.62**	**0.9404**	**5.62**	**0.9404**	**5.38**	**10**	**0.0001**

Table A.15: 1/4 in steel rod - 2 in bore-hole - 40 ft radius of curvature.

1.0259	in	ID of the Well
0.243935	in	OD of the Pipe
0	in	ID of the Pipe
0.15903	lb/ft	Weight of the Pipe
3E+7	lb/in^2	Modulus of Elasticity
-112.957	ft	Radius of Curvature (Negative for Build)
0.000001	(fraction)	Error in the radius of curvature
0.000001	(fraction)	Error in the clearance
0.000001	(fraction)	Error in the X-coordinate of the center of curvature
0.0001	(fraction)	Error in the Y-coordinate of the center of curvature
0.125		λ_{min}
100		Maximum number of iterations
Simple model results		
Lp	L	P
6.45	6.15	77.22
Hi-Low experimental results		
angle	high value	low value
87.5	88.7	87.7

θ (°)	P_c (lb)	P_v (lb)	L_d	L_i (ft)	g_i	L_f (ft)	g_f	L_t (ft)	$\#_{it}$	h
1	**76.87**	**76.56**	**1.0555**	**6.46**	**0.9961**	**6.45**	**0.9959**	**6.15**	**4**	**0.00001**
5	**78.12**	**76.55**	**1.0452**	**6.39**	**0.9804**	**6.39**	**0.9801**	**6.10**	**4**	**0.00001**
10	**79.61**	**76.49**	**1.0307**	**6.32**	**0.9621**	**6.33**	**0.9617**	**6.04**	**3**	**0.00001**
15	**81.05**	**76.40**	**1.0142**	**6.26**	**0.9458**	**6.27**	**0.9453**	**5.99**	**4**	**0.00001**
20	**82.34**	**76.19**	**0.9965**	**6.21**	**0.9301**	**6.21**	**0.9300**	**5.94**	**3**	**0.00001**
25	**83.68**	**76.09**	**0.9762**	**6.16**	**0.9162**	**6.16**	**0.9162**	**5.90**	**4**	**0.00001**
30	**84.83**	**75.85**	**0.9546**	**6.30**	**0.9900**	**6.12**	**0.9031**	**5.86**	**12**	**0.0001**
35	**85.99**	**75.68**	**0.9304**	**6.08**	**0.8919**	**6.07**	**0.8919**	**5.82**	**6**	**0.0001**
40	**86.92**	**75.38**	**0.9047**	**6.04**	**0.8820**	**6.04**	**0.8817**	**5.79**	**3**	**0.0001**
45	**87.88**	**75.17**	**0.8759**	**5.99**	**0.8724**	**6.00**	**0.8723**	**5.76**	**8**	**0.0001**
50	**88.73**	**74.97**	**0.8442**	**5.97**	**0.8646**	**5.97**	**0.8646**	**5.73**	**2**	**0.0001**
55	**89.59**	**74.87**	**0.8088**	**5.95**	**0.8549**	**5.94**	**0.8573**	**5.70**	**7**	**0.0001**
60	**90.22**	**74.66**	**0.7698**	**5.93**	**0.8499**	**5.92**	**0.8516**	**5.69**	**7**	**0.0001**
65	**90.81**	**74.52**	**0.7255**	**5.92**	**0.8477**	**5.90**	**0.8464**	**5.67**	**8**	**0.0001**
70	**91.32**	**74.44**	**0.6742**	**5.89**	**0.8422**	**5.89**	**0.8419**	**5.65**	**30**	**0.0001**
75	**91.68**	**74.32**	**0.6132**	**5.88**	**0.8390**	**5.88**	**0.8393**	**5.64**	**48**	**0.0001**
80	**91.96**	**74.27**	**0.5361**	**5.87**	**0.8372**	**5.87**	**0.8370**	**5.64**	**15**	**0.00001**
83	**92.09**	**74.26**	**0.4761**	**5.86**	**0.8363**	**5.86**	**0.8359**	**5.63**	**5**	**0.0002**

Table A.16: 1/4 in steel rod - 1 in bore-hole - 113 ft radius of curvature.

1.0259	in	ID of the Well
0.243935	in	OD of the Pipe
0	in	ID of the Pipe
0.15903	lb/ft	Weight of the Pipe
3E+7	lb/in^2	Modulus of Elasticity
-57.957	ft	Radius of Curvature (Negative for Build)
0.000001	(fraction)	Error in the radius of curvature
0.000001	(fraction)	Error in the clearance
0.000001	(fraction)	Error in the X-coordinate of the center of curvature
0.0001	(fraction)	Error in the Y-coordinate of the center of curvature
0.125		λ_{min}
100		Maximum number of iterations
Simple model results		
Lp	L	P
4.62	4.41	150.5
Hi-Low experimental results		
angle	high value	low value
-none-	-none-	-none-

θ (°)	P_c (lb)	P_v (lb)	L_d	L_i (ft)	g_i	L_f (ft)	g_f	L_t (ft)	$\#_{it}$	h
3	**150.51**	**150.02**	**0.7557**	**4.62**	**0.9968**	**4.62**	**0.9968**	**4.40**	**11**	**0.000001**
5	**150.82**	**150.02**	**0.7542**	**4.61**	**0.9945**	**4.61**	**0.9946**	**4.40**	**3**	**0.000001**
10	**151.61**	**150.01**	**0.7492**	**4.60**	**0.9894**	**4.60**	**0.9894**	**4.39**	**3**	**0.000001**
15	**152.40**	**150.02**	**0.7423**	**4.59**	**0.9842**	**4.59**	**0.9843**	**4.38**	**8**	**0.00001**
20	**153.16**	**150.01**	**0.7336**	**4.57**	**0.9798**	**4.57**	**0.9796**	**4.36**	**6**	**0.00001**
25	**153.88**	**149.99**	**0.7230**	**4.56**	**0.9749**	**4.56**	**0.9750**	**4.35**	**5**	**0.00001**
30	**154.57**	**149.97**	**0.7104**	**4.55**	**0.9900**	**4.55**	**0.9707**	**4.34**	**7**	**0.0001**
35	**155.26**	**149.97**	**0.6957**	**4.54**	**0.9665**	**4.54**	**0.9667**	**4.34**	**19**	**0.0001**
40	**155.88**	**149.96**	**0.6789**	**4.53**	**0.9626**	**4.53**	**0.9629**	**4.33**	**4**	**0.0001**
45	**156.46**	**149.94**	**0.6597**	**4.52**	**0.9590**	**4.52**	**0.9594**	**4.32**	**5**	**0.0001**
50	**156.95**	**149.89**	**0.6381**	**4.51**	**0.9564**	**4.51**	**0.9563**	**4.31**	**8**	**0.0001**
55	**157.46**	**149.91**	**0.6133**	**4.51**	**0.9534**	**4.51**	**0.9537**	**4.31**	**3**	**0.0001**
60	**157.89**	**149.91**	**0.5850**	**4.50**	**0.9513**	**4.50**	**0.9512**	**4.30**	**13**	**0.0001**
65	**158.23**	**149.87**	**0.5525**	**4.50**	**0.9495**	**4.50**	**0.9491**	**4.30**	**11**	**0.0001**
70	**158.54**	**149.88**	**0.5144**	**4.49**	**0.9473**	**4.49**	**0.9475**	**4.29**	**4**	**0.0001**
75	**158.80**	**149.89**	**0.4684**	**4.49**	**0.9461**	**4.49**	**0.9461**	**4.29**	**36**	**0.0001**
79	**158.99**	**149.94**	**0.4229**	**4.48**	**0.9450**	**4.49**	**0.9453**	**4.29**	**28**	**0.0001**

Table A.17: 1/4 in steel rod - 1 in bore-hole - 58 ft radius of curvature.

1.0259	in	ID of the Well
0.243935	in	OD of the Pipe
0	in	ID of the Pipe
0.15903	lb/ft	Weight of the Pipe
3E+7	lb/in^2	Modulus of Elasticity
-39.957	ft	Radius of Curvature (Negative for Build)
0.000001	(fraction)	Error in the radius of curvature
0.000001	(fraction)	Error in the clearance
0.000001	(fraction)	Error in the X-coordinate of the center of curvature
0.0001	(fraction)	Error in the Y-coordinate of the center of curvature
0.125		λ_{min}
100		Maximum number of iterations
Simple model results		
Lp	L	P
3.84	3.66	218.3
Hi-Low experimental results		
angle	high value	low value
-none-	-none-	-none-

θ (°)	P_c (lb)	P_v (lb)	L_d	L_i (ft)	g_i	L_f (ft)	g_f	L_t (ft)	$\#_{it}$	h
4	**218.34**	**217.90**	**0.6275**	**3.84**	**0.9979**	**3.84**	**0.9979**	**3.66**	**3**	**0.00001**
6	**218.56**	**217.90**	**0.6266**	**3.83**	**0.9969**	**3.83**	**0.9969**	**3.65**	**7**	**0.00001**
8	**218.78**	**217.90**	**0.6253**	**3.83**	**0.9954**	**3.83**	**0.9959**	**3.65**	**9**	**0.00001**
10	**218.78**	**217.68**	**0.6241**	**3.83**	**0.9949**	**3.83**	**0.9949**	**3.65**	**101**	**0.000001**
12	**219.22**	**217.90**	**0.6221**	**3.83**	**0.9939**	**3.83**	**0.9939**	**3.65**	**15**	**0.000001**
14	**219.43**	**217.90**	**0.6201**	**3.82**	**0.9930**	**3.82**	**0.9930**	**3.65**	**11**	**0.000001**
16	**219.65**	**217.90**	**0.6178**	**3.82**	**0.9920**	**3.82**	**0.9920**	**3.65**	**66**	**0.000001**
18	**219.86**	**217.90**	**0.6153**	**3.82**	**0.9910**	**3.82**	**0.9910**	**3.64**	**25**	**0.000001**
20	**220.07**	**217.90**	**0.6125**	**3.82**	**0.9901**	**3.82**	**0.9901**	**3.64**	**6**	**0.000001**
22	**220.29**	**217.91**	**0.6095**	**3.82**	**0.9892**	**3.82**	**0.9891**	**3.64**	**8**	**0.000001**
24	**220.48**	**217.90**	**0.6062**	**3.81**	**0.9882**	**3.81**	**0.9883**	**3.64**	**11**	**0.000001**
26	**220.69**	**217.90**	**0.6026**	**3.81**	**0.9872**	**3.81**	**0.9874**	**3.64**	**25**	**0.000001**
28	**220.88**	**217.90**	**0.5988**	**3.81**	**0.9865**	**3.81**	**0.9865**	**3.64**	**2**	**0.000001**
30	**221.10**	**217.92**	**0.5946**	**3.81**	**0.9856**	**3.81**	**0.9856**	**3.63**	**30**	**0.000001**

Table A.18: 1/4 in steel rod - 1 in bore-hole - 40 ft radius of curvature.

2.0379	in	ID of the Well
0.248571	in	OD of the Pipe
0	in	ID of the Pipe
0.056626	lb/ft	Weight of the Pipe
1E+7	lb/in^2	Modulus of Elasticity
-112.915	ft	Radius of Curvature (Negative for Build)
0.000001	(fraction)	Error in the radius of curvature
0.000001	(fraction)	Error in the clearance
0.000001	(fraction)	Error in the X-coordinate of the center of curvature
0.0001	(fraction)	Error in the Y-coordinate of the center of curvature
0.125		λ_{min}
100		Maximum number of iterations
Simple model results		
Lp	L	P
9.76	9.31	12.13
Hi-Low experimental results		
angle	high value	low value
87.5	17.3	16.3

θ (°)	P_c (lb)	P_v (lb)	L_d	L_i (ft)	g_i	L_f (ft)	g_f	L_t (ft)	$\#_{it}$	h
1	**11.88**	**11.77**	**1.5912**	**9.75**	**0.9900**	**9.75**	**0.9907**	**9.30**	**4**	**0.00001**
5	**12.33**	**11.77**	**1.5589**	**9.54**	**0.9553**	**9.56**	**0.9563**	**9.13**	**4**	**0.00001**
10	**12.82**	**11.71**	**1.5213**	**9.36**	**0.9190**	**9.37**	**0.9206**	**8.96**	**3**	**0.00001**
15	**13.30**	**11.64**	**1.4831**	**9.21**	**0.8931**	**9.19**	**0.8889**	**8.81**	**3**	**0.00001**
20	**13.73**	**11.54**	**1.4456**	**9.02**	**0.8685**	**9.04**	**0.8614**	**8.67**	**4**	**0.00001**
25	**14.13**	**11.43**	**1.4073**	**8.89**	**0.8377**	**8.91**	**0.8388**	**8.56**	**8**	**0.00001**
30	**14.50**	**11.30**	**1.3679**	**9.30**	**0.8000**	**8.79**	**0.8183**	**8.45**	**10**	**0.0001**
35	**14.83**	**11.16**	**1.3275**	**8.67**	**0.7953**	**8.69**	**0.8017**	**8.36**	**5**	**0.0001**
40	**15.17**	**11.06**	**1.2836**	**8.58**	**0.7812**	**8.59**	**0.7843**	**8.27**	**4**	**0.0001**
45	**15.48**	**10.96**	**1.2370**	**8.51**	**0.7721**	**8.50**	**0.7730**	**8.19**	**3**	**0.0001**
50	**15.68**	**10.78**	**1.1907**	**8.45**	**0.7603**	**8.45**	**0.7604**	**8.15**	**3**	**0.0001**
55	**15.97**	**10.73**	**1.1363**	**8.36**	**0.7586**	**8.38**	**0.7504**	**8.08**	**12**	**0.0001**
60	**16.11**	**10.57**	**1.0807**	**8.34**	**0.7448**	**8.34**	**0.7430**	**8.05**	**3**	**0.0001**
65	**16.31**	**10.52**	**1.0158**	**8.29**	**0.7352**	**8.29**	**0.7351**	**8.00**	**2**	**0.0001**
70	**16.43**	**10.43**	**0.9435**	**8.28**	**0.7292**	**8.26**	**0.7305**	**7.98**	**20**	**0.0001**
75	**16.55**	**10.38**	**0.8570**	**8.21**	**0.7261**	**8.24**	**0.7251**	**7.95**	**8**	**0.0001**
80	**16.68**	**10.38**	**0.7477**	**8.20**	**0.7189**	**8.21**	**0.7228**	**7.93**	**4**	**0.0002**
85	**16.72**	**10.35**	**0.5938**	**8.21**	**0.7186**	**8.20**	**0.7219**	**7.92**	**27**	**0.0002**
87	**16.74**	**10.36**	**0.5008**	**8.20**	**0.7217**	**8.20**	**0.7209**	**7.92**	**40**	**0.00001**

Table A.19: 1/4 in aluminium rod - 2 in bore-hole - 113 ft radius of curvature.

2.0379	in	ID of the Well
0.248571	in	OD of the Pipe
0	in	ID of the Pipe
0.056626	lb/ft	Weight of the Pipe
1E+7	lb/in^2	Modulus of Elasticity
-57.915	ft	Radius of Curvature (Negative for Build)
0.000001	(fraction)	Error in the radius of curvature
0.000001	(fraction)	Error in the clearance
0.000001	(fraction)	Error in the X-coordinate of the center of curvature
0.0001	(fraction)	Error in the Y-coordinate of the center of curvature
0.125		λ_{min}
100		Maximum number of iterations
Simple model results		
Lp	L	P
6.99	6.66	23.65
Hi-Low experimental results		
angle	high value	low value
85	24.6	23.6

θ ($^\circ$)	P_c (lb)	P_v (lb)	L_d	L_i (ft)	g_i	L_f (ft)	g_f	L_t (ft)	$\#_{it}$	h
1	**23.45**	**23.40**	**1.1412**	**6.99**	**0.9977**	**6.99**	**0.9976**	**6.67**	**4**	**0.000001**
5	**23.68**	**23.40**	**1.1339**	**6.96**	**0.9881**	**6.95**	**0.9880**	**6.63**	**4**	**0.00001**
10	**23.97**	**23.40**	**1.1224**	**6.92**	**0.9772**	**6.91**	**0.9765**	**6.59**	**4**	**0.00001**
15	**24.23**	**23.38**	**1.1087**	**6.86**	**0.9666**	**6.87**	**0.9657**	**6.56**	**4**	**0.00001**
20	**24.50**	**23.38**	**1.0922**	**6.82**	**0.9571**	**6.83**	**0.9557**	**6.53**	**4**	**0.00001**
25	**24.75**	**23.36**	**1.0733**	**6.80**	**0.9466**	**6.79**	**0.9462**	**6.49**	**3**	**0.00001**
30	**24.99**	**23.35**	**1.0519**	**6.80**	**0.9000**	**6.76**	**0.9376**	**6.46**	**7**	**0.0001**
35	**25.20**	**23.32**	**1.0281**	**6.73**	**0.9301**	**6.73**	**0.9301**	**6.44**	**3**	**0.00001**
40	**25.43**	**23.32**	**1.0008**	**6.70**	**0.9228**	**6.70**	**0.9229**	**6.41**	**4**	**0.00001**
45	**25.60**	**23.29**	**0.9710**	**6.69**	**0.9152**	**6.68**	**0.9160**	**6.39**	**6**	**0.00001**
50	**25.80**	**23.29**	**0.9370**	**6.65**	**0.9105**	**6.65**	**0.9103**	**6.37**	**3**	**0.00001**
55	**25.97**	**23.28**	**0.8992**	**6.63**	**0.9045**	**6.63**	**0.9055**	**6.35**	**4**	**0.00001**
60	**26.10**	**23.26**	**0.8569**	**6.61**	**0.9004**	**6.61**	**0.9005**	**6.33**	**4**	**0.00001**
65	**26.22**	**23.25**	**0.8084**	**6.59**	**0.8976**	**6.60**	**0.8972**	**6.32**	**8**	**0.00001**
70	**26.33**	**23.24**	**0.7520**	**6.58**	**0.8950**	**6.59**	**0.8939**	**6.31**	**11**	**0.00001**
75	**26.43**	**23.27**	**0.6840**	**6.57**	**0.8923**	**6.57**	**0.8917**	**6.30**	**5**	**0.00001**
80	**26.50**	**23.27**	**0.5982**	**6.57**	**0.8890**	**6.57**	**0.8901**	**6.29**	**7**	**0.00001**
85	**26.53**	**23.27**	**0.4752**	**6.57**	**0.8890**	**6.57**	**0.8889**	**6.29**	**101**	**0.00001**
86	**26.55**	**23.28**	**0.4411**	**6.57**	**0.8889**	**6.56**	**0.8889**	**6.29**	**101**	**0.00001**

Table A.20: 1/4 in aluminium rod - 2 in bore-hole - 58 ft radius of curvature.

2.0379	in	ID of the Well
0.248571	in	OD of the Pipe
0	in	ID of the Pipe
0.056626	lb/ft	Weight of the Pipe
1E+7	lb/in^2	Modulus of Elasticity
-39.915	ft	Radius of Curvature (Negative for Build)
0.000001	(fraction)	Error in the radius of curvature
0.000001	(fraction)	Error in the clearance
0.000001	(fraction)	Error in the X-coordinate of the center of curvature
0.0001	(fraction)	Error in the Y-coordinate of the center of curvature
0.125		λ_{min}
100		Maximum number of iterations
Simple model results		
Lp	L	P
5.8	5.53	34.32
Hi-Low experimental results		
angle	high value	low value
82.8	30.8	28.8

θ (°)	P_c (lb)	P_v (lb)	L_d	L_i (ft)	g_i	L_f (ft)	g_f	L_t (ft)	$\#_{it}$	h
2	**34.18**	**34.10**	**0.9468**	**5.80**	**0.9977**	**5.80**	**0.9977**	**5.53**	**3**	**0.000001**
5	**34.30**	**34.11**	**0.9440**	**5.79**	**0.9944**	**5.79**	**0.9942**	**5.52**	**4**	**0.000001**
10	**34.5**	**34.11**	**0.9375**	**5.77**	**0.9889**	**5.77**	**0.9886**	**5.51**	**5**	**0.00001**
15	**34.69**	**34.11**	**0.9287**	**5.75**	**0.9835**	**5.75**	**0.9832**	**5.49**	**4**	**0.00001**
20	**34.88**	**34.11**	**0.9176**	**5.74**	**0.9781**	**5.74**	**0.9781**	**5.48**	**3**	**0.00001**
25	**35.06**	**34.11**	**0.9042**	**5.72**	**0.9732**	**5.72**	**0.9731**	**5.46**	**3**	**0.00001**
30	**35.23**	**34.10**	**0.8884**	**5.71**	**0.9686**	**5.71**	**0.9686**	**5.45**	**3**	**0.00001**
35	**35.40**	**34.11**	**0.8698**	**5.69**	**0.9646**	**5.69**	**0.9643**	**5.44**	**4**	**0.00001**
40	**35.56**	**34.11**	**0.8486**	**5.68**	**0.9607**	**5.68**	**0.9604**	**5.43**	**5**	**0.00001**
45	**35.71**	**34.11**	**0.8246**	**5.50**	**0.9000**	**5.67**	**0.9565**	**5.42**	**9**	**0.00001**
50	**35.83**	**34.10**	**0.7974**	**5.66**	**0.9537**	**5.66**	**0.9534**	**5.41**	**4**	**0.00001**
55	**35.95**	**34.10**	**0.7664**	**5.65**	**0.9504**	**5.65**	**0.9505**	**5.40**	**6**	**0.00001**
60	**36.07**	**34.11**	**0.7310**	**5.64**	**0.9472**	**5.64**	**0.9478**	**5.39**	**8**	**0.00001**
65	**36.16**	**34.11**	**0.6903**	**5.63**	**0.9456**	**5.63**	**0.9457**	**5.39**	**6**	**0.00001**
70	**36.25**	**34.13**	**0.6426**	**5.63**	**0.9442**	**5.63**	**0.9438**	**5.38**	**16**	**0.00001**
75	**36.32**	**34.13**	**0.5851**	**5.62**	**0.9426**	**5.62**	**0.9425**	**5.38**	**20**	**0.00001**
80	**36.37**	**34.15**	**0.5119**	**5.62**	**0.9416**	**5.62**	**0.9415**	**5.37**	**16**	**0.00001**
81	**36.39**	**34.16**	**0.4943**	**5.62**	**0.9415**	**5.62**	**0.9414**	**5.37**	**7**	**0.0001**

Table A.21: 1/4 in aluminium rod - 2 in bore-hole - 40 ft radius of curvature.

17.5	in	ID of the Well
5	in	OD of the Pipe
4.276	in	ID of the Pipe
19.5	lb/ft	Weight of the Pipe
3E+7	lb/in^2	Modulus of Elasticity
-2864.789	ft	Radius of Curvature (Negative for Build)
0.0000001	(fraction)	Error in the radius of curvature
0.0000001	(fraction)	Error in the clearance
0.0000001	(fraction)	Error in the X-coordinate of the center of curvature
0.000013	(fraction)	Error in the Y-coordinate of the center of curvature
0.125		λ_{min}
100		Maximum number of iterations
Simple model results		
Lp	L	P
129.94	123.9	15638.3

θ (°)	P_c (lb)	P_v (lb)	L_d	L_i (ft)	g_i	L_f (ft)	g_f	L_t (ft)	$\#_{it}$	h
2	**15,876**	**13,926**	**2.3164**	**120.00**	**0.8559**	**123.77**	**0.8919**	**118.56**	**5**	**0.00001**
5	**18,335**	**13,466**	**2.1581**	**117.07**	**0.7978**	**115.43**	**0.7935**	**111.08**	**5**	**0.0001**
10	**21,354**	**11,654**	**1.9947**	**108.78**	**0.6947**	**107.10**	**0.6909**	**103.57**	**5**	**0.0001**
15	**23,825**	**9,367**	**1.8776**	**103.08**	**0.6363**	**101.47**	**0.6233**	**98.43**	**8**	**0.0001**
20	**25,933**	**6,827**	**1.7842**	**98.79**	**0.5912**	**97.31**	**0.5743**	**94.60**	**6**	**0.0001**
25	**27,731**	**4,122**	**1.7054**	**94.25**	**0.5577**	**94.14**	**0.5373**	**91.68**	**4**	**0.0001**
30	**29,255**	**1,323**	**1.6360**	**91.00**	**0.5000**	**91.69**	**0.5097**	**89.41**	**6**	**0.0001**
35	**30,940**	**-1,102**	**1.5626**	**90.53**	**0.4816**	**89.21**	**0.4866**	**87.09**	**6**	**0.0001**
40	**32,293**	**-3,615**	**1.4965**	**87.93**	**0.4700**	**87.37**	**0.4740**	**85.36**	**5**	**0.0001**
45	**33,279**	**-6,222**	**1.4358**	**87.13**	**0.4287**	**86.10**	**0.4568**	**84.19**	**10**	**0.0001**
50	**34,267**	**-8,527**	**1.3714**	**85.17**	**0.4471**	**84.89**	**0.4457**	**83.06**	**5**	**0.0001**
55	**35,127**	**-10,634**	**1.3048**	**83.90**	**0.4326**	**83.89**	**0.4329**	**82.13**	**3**	**0.0001**
60	**35,995**	**-12,384**	**1.2321**	**82.89**	**0.4283**	**82.93**	**0.4220**	**81.21**	**4**	**0.0001**
65	**36,586**	**-14,043**	**1.1562**	**82.26**	**0.4205**	**82.30**	**0.4195**	**80.63**	**9**	**0.000005**
70	**37,186**	**-15,308**	**1.0695**	**81.69**	**0.4207**	**81.70**	**0.4143**	**80.06**	**9**	**0.000005**
75	**37,663**	**-16,296**	**0.9691**	**81.19**	**0.4153**	**81.24**	**0.4085**	**79.62**	**8**	**0.000005**
80	**38,072**	**-16,943**	**0.8445**	**80.94**	**0.4144**	**80.86**	**0.4081**	**79.27**	**78**	**0.000005**
85	**38,268**	**-17,383**	**0.6700**	**80.81**	**0.4096**	**80.72**	**0.4048**	**79.14**	**32**	**0.0001**
88	**38,318**	**-17,511**	**0.4937**	**80.86**	**0.4036**	**80.71**	**0.4050**	**79.13**	**19**	**0.0001**

Table A.22: 5 in 19.5 lb/ft drill-pipe - 171/2 in bore-hole - 2°/100ft BG.

17.5	in	ID of the Well
5	in	OD of the Pipe
4.276	in	ID of the Pipe
19.5	lb/ft	Weight of the Pipe
3E+7	lb/in^2	Modulus of Elasticity
-1909.859	ft	Radius of Curvature (Negative for Build)
0.0000001	(fraction)	Error in the radius of curvature
0.0000001	(fraction)	Error in the clearance
0.0000001	(fraction)	Error in the X-coordinate of the center of curvature
0.000013	(fraction)	Error in the Y-coordinate of the center of curvature
0.125		λ_{min}
100		Maximum number of iterations
Simple model results		
Lp	L	P
106.1	101.17	23457.17

θ (°)	P_c (lb)	P_v (lb)	L_d	L_i (ft)	g_i	L_f (ft)	g_f	L_t (ft)	$\#_{it}$	h
2	**23,386**	**22,087**	**1.9427**	**103.43**	**0.9482**	**103.8**	**0.9475**	**99.20**	**6**	**0.00001**
5	**25,218**	**21,972**	**1.8679**	**99.94**	**0.8847**	**99.91**	**0.8875**	**95.75**	**4**	**0.001**
10	**27,771**	**21,304**	**1.7718**	**95.13**	**0.8131**	**95.13**	**0.8131**	**91.49**	**3**	**0.001**
15	**29,923**	**20,284**	**1.6949**	**92.04**	**0.7436**	**91.60**	**0.7582**	**88.31**	**5**	**0.001**
20	**31,765**	**19,028**	**1.6293**	**88.38**	**0.7034**	**88.86**	**0.7154**	**85.84**	**6**	**0.001**
25	**33,336**	**17,597**	**1.5709**	**85.72**	**0.6785**	**86.71**	**0.6808**	**83.90**	**9**	**0.001**
30	**35,054**	**16,432**	**1.5089**	**85.54**	**0.6602**	**84.56**	**0.6495**	**81.93**	**7**	**0.001**
35	**36,464**	**15,102**	**1.4523**	**82.65**	**0.6152**	**82.91**	**0.6279**	**80.42**	**5**	**0.001**
40	**37,581**	**13,642**	**1.3989**	**82.04**	**0.5991**	**81.67**	**0.6083**	**79.29**	**26**	**0.001**
45	**38,706**	**12,372**	**1.3424**	**80.45**	**0.5989**	**80.49**	**0.5955**	**78.20**	**3**	**0.001**
50	**39,746**	**11,216**	**1.2836**	**79.45**	**0.5779**	**79.45**	**0.5778**	**77.24**	**3**	**0.001**
55	**40,570**	**10,063**	**1.2235**	**78.90**	**0.5675**	**78.66**	**0.5692**	**76.51**	**6**	**0.001**
60	**41,304**	**9,051**	**1.1587**	**77.70**	**0.5621**	**77.99**	**0.5580**	**75.89**	**6**	**0.001**
65	**41,899**	**8,146**	**1.0882**	**77.67**	**0.5472**	**77.46**	**0.5528**	**75.41**	**5**	**0.001**
70	**42,521**	**7,525**	**1.0072**	**76.71**	**0.5498**	**76.94**	**0.5441**	**74.92**	**7**	**0.001**
75	**42,834**	**6,861**	**0.9149**	**76.66**	**0.5422**	**76.69**	**0.5405**	**74.70**	**4**	**0.001**
79	**43,116**	**6,558**	**0.8242**	**76.64**	**0.5462**	**76.48**	**0.5381**	**74.50**	**14**	**0.001**
85	**43,378**	**6,278**	**0.6333**	**76.47**	**0.5306**	**76.30**	**0.5352**	**74.34**	**13**	**0.001**
88	**43,488**	**6,268**	**0.4664**	**76.23**	**0.5343**	**76.24**	**0.5364**	**74.28**	**29**	**0.001**

Table A.23: 5 in 19.5 lb/ft drill-pipe - 171/2 in bore-hole - 3°/100ft BG.

17.5	in	ID of the Well
5	in	OD of the Pipe
4.276	in	ID of the Pipe
19.5	lb/ft	Weight of the Pipe
3E+7	lb/in^2	Modulus of Elasticity
-1432.324	ft	Radius of Curvature (Negative for Build)
0.0000001	(fraction)	Error in the radius of curvature
0.0000001	(fraction)	Error in the clearance
0.0000001	(fraction)	Error in the X-coordinate of the center of curvature
0.000013	(fraction)	Error in the Y-coordinate of the center of curvature
0.125		λ_{min}
100		Maximum number of iterations
Simple model results		
Lp	L	P
91.88	87.61	31277.4

θ (°)	P_c (lb)	P_v (lb)	L_d	L_i (ft)	g_i	L_f (ft)	g_f	L_t (ft)	$\#_{it}$	h
5	**32,478**	**30,044**	**1.6587**	**88.42**	**0.9287**	**88.72**	**0.9308**	**84.86**	**5**	**0.001**
10	**34,592**	**29,742**	**1.5992**	**85.62**	**0.8767**	**85.87**	**0.8777**	**82.33**	**4**	**0.001**
15	**36,501**	**29,272**	**1.5455**	**83.94**	**0.8292**	**83.52**	**0.8354**	**80.24**	**9**	**0.001**
20	**38,123**	**28,570**	**1.4975**	**82.11**	**0.7865**	**81.67**	**0.8002**	**78.59**	**7**	**0.001**
25	**39,551**	**27,747**	**1.4518**	**80.18**	**0.7787**	**80.14**	**0.7682**	**77.22**	**5**	**0.001**
30	**40,932**	**26,967**	**1.4052**	**85.00**	**0.7500**	**78.75**	**0.7456**	**75.97**	**7**	**0.001**
35	**42,191**	**26,171**	**1.3583**	**77.20**	**0.7233**	**77.55**	**0.7244**	**74.89**	**8**	**0.001**
40	**43,337**	**25,384**	**1.3105**	**76.98**	**0.6934**	**76.51**	**0.7039**	**73.94**	**9**	**0.001**
45	**44,526**	**24,776**	**1.2589**	**75.49**	**0.6903**	**75.49**	**0.6909**	**73.00**	**3**	**0.001**
50	**45,262**	**23,866**	**1.2096**	**74.89**	**0.6759**	**74.87**	**0.6763**	**72.46**	**4**	**0.001**
55	**46,306**	**23,427**	**1.1515**	**73.92**	**0.6776**	**74.04**	**0.6658**	**71.68**	**5**	**0.001**
60	**46,883**	**22,694**	**1.0934**	**73.59**	**0.6620**	**73.60**	**0.6589**	**71.29**	**6**	**0.001**
65	**47,444**	**22,130**	**1.0280**	**73.26**	**0.6506**	**73.18**	**0.6511**	**70.91**	**4**	**0.001**
70	**48,011**	**21,765**	**0.9527**	**72.50**	**0.6475**	**72.77**	**0.6443**	**70.54**	**18**	**0.001**
75	**48,447**	**21,468**	**0.8646**	**72.58**	**0.6456**	**72.47**	**0.6390**	**70.26**	**15**	**0.001**
80	**48,799**	**21,293**	**0.7545**	**72.28**	**0.6419**	**72.25**	**0.6358**	**70.05**	**7**	**0.001**
85	**49,008**	**21,184**	**0.5987**	**72.12**	**0.6353**	**72.13**	**0.6357**	**69.95**	**4**	**0.0001**
87	**49,003**	**21,111**	**0.5052**	**72.29**	**0.6326**	**72.15**	**0.6338**	**69.97**	**15**	**0.0001**

Table A.24: 5 in 19.5 lb/ft drill-pipe - 171/2 in bore-hole - 4°/100ft BG.

17.5	in	ID of the Well
5	in	OD of the Pipe
4.276	in	ID of the Pipe
19.5	lb/ft	Weight of the Pipe
3E+7	lb/in^2	Modulus of Elasticity
-1145.952	ft	Radius of Curvature (Negative for Build)
0.0000001	(fraction)	Error in the radius of curvature
0.0000001	(fraction)	Error in the clearance
0.0000001	(fraction)	Error in the X-coordinate of the center of curvature
0.000013	(fraction)	Error in the Y-coordinate of the center of curvature
0.125		λ_{min}
100		Maximum number of iterations
Simple model results		
Lp	L	P
82.19	78.36	39093.15

θ (°)	P_c (lb)	P_v (lb)	L_d	L_i (ft)	g_i	L_f (ft)	g_f	L_t (ft)	$\#_{it}$	h
2	**38,822**	**38,042**	**1.5266**	**81.61**	**0.9815**	**81.57**	**0.9803**	**77.84**	**4**	**0.0001**
5	**39,940**	**37,992**	**1.5024**	**80.23**	**0.9546**	**80.36**	**0.9535**	**76.78**	**3**	**0.0001**
10	**41,679**	**37,799**	**1.4635**	**78.30**	**0.9185**	**78.58**	**0.9143**	**75.22**	**4**	**0.0001**
15	**43,311**	**37,527**	**1.4253**	**76.74**	**0.8856**	**77.02**	**0.8816**	**73.83**	**5**	**0.0001**
20	**44,872**	**37,229**	**1.3866**	**75.98**	**0.8456**	**75.62**	**0.8546**	**72.59**	**5**	**0.0001**
25	**46,249**	**36,805**	**1.3487**	**74.83**	**0.8337**	**74.45**	**0.8284**	**71.54**	**6**	**0.0001**
30	**47,549**	**36,376**	**1.3096**	**73.40**	**0.8073**	**73.40**	**0.8073**	**70.60**	**3**	**0.0001**
35	**48,532**	**35,715**	**1.2721**	**72.78**	**0.7938**	**72.63**	**0.7886**	**69.92**	**4**	**0.0001**
40	**49,765**	**35,401**	**1.2283**	**71.71**	**0.7734**	**71.71**	**0.7742**	**69.08**	**3**	**0.0001**
45	**50,686**	**34,885**	**1.1849**	**71.05**	**0.7594**	**71.05**	**0.7593**	**68.49**	**3**	**0.0001**
50	**51,397**	**34,279**	**1.1398**	**70.67**	**0.7477**	**70.55**	**0.7491**	**68.05**	**4**	**0.0001**
55	**52,334**	**34,030**	**1.0876**	**69.91**	**0.7423**	**69.93**	**0.7400**	**67.48**	**4**	**0.0001**
60	**52,970**	**33,618**	**1.0328**	**69.67**	**0.7286**	**69.52**	**0.7314**	**67.11**	**9**	**0.0001**
65	**53,421**	**33,169**	**0.9726**	**68.97**	**0.7294**	**69.23**	**0.7234**	**66.86**	**10**	**0.0001**
70	**54,039**	**33,040**	**0.9014**	**68.85**	**0.7231**	**68.86**	**0.7174**	**66.51**	**4**	**0.0001**
75	**54,435**	**32,851**	**0.8187**	**68.50**	**0.7152**	**68.63**	**0.7127**	**66.30**	**4**	**0.0001**
80	**54,639**	**32,632**	**0.7157**	**68.61**	**0.7119**	**68.53**	**0.7102**	**66.22**	**8**	**0.0001**
85	**54,907**	**32,646**	**0.5676**	**68.47**	**0.7093**	**68.39**	**0.7087**	**66.09**	**26**	**0.0001**
86	**54,904**	**32,612**	**0.5271**	**68.26**	**0.7096**	**68.40**	**0.7090**	**66.10**	**58**	**0.0001**

Table A.25: 5 in 19.5 lb/ft drill-pipe - 171/2 in bore-hole - 5°/100ft BG.

17.5	in	ID of the Well
5	in	OD of the Pipe
4.276	in	ID of the Pipe
19.5	lb/ft	Weight of the Pipe
3E+7	lb/in^2	Modulus of Elasticity
-954.9297	ft	Radius of Curvature (Negative for Build)
0.0000001	(fraction)	Error in the radius of curvature
0.0000001	(fraction)	Error in the clearance
0.0000001	(fraction)	Error in the X-coordinate of the center of curvature
0.000013	(fraction)	Error in the Y-coordinate of the center of curvature
0.125		λ_{min}
100		Maximum number of iterations
Simple model results		
Lp	L	P
75.02	71.53	46912.71

θ (°)	P_c (lb)	P_v (lb)	L_d	L_i (ft)	g_i	L_f (ft)	g_f	L_t (ft)	$\#_{it}$	h
2	**46,618**	**45,968**	**1.3968**	**74.64**	**0.9854**	**74.64**	**0.9861**	**71.21**	**4**	**0.0001**
5	**47,582**	**45,959**	**1.3803**	**73.93**	**0.9658**	**73.83**	**0.9666**	**70.50**	**4**	**0.0001**
10	**49,108**	**45,874**	**1.3523**	**72.81**	**0.9349**	**72.61**	**0.9376**	**69.43**	**5**	**0.0001**
15	**50,483**	**45,664**	**1.3242**	**71.51**	**0.9122**	**71.56**	**0.9119**	**68.50**	**4**	**0.0001**
20	**51,860**	**45,492**	**1.2938**	**70.83**	**0.8909**	**70.56**	**0.8897**	**67.62**	**13**	**0.0001**
25	**53,062**	**45,192**	**1.2631**	**69.90**	**0.8730**	**69.72**	**0.8692**	**66.87**	**5**	**0.0001**
30	**54,207**	**44,896**	**1.2304**	**68.00**	**0.7500**	**68.96**	**0.8515**	**66.19**	**6**	**0.0001**
35	**55,247**	**44,566**	**1.1961**	**68.24**	**0.8381**	**68.29**	**0.8372**	**65.60**	**4**	**0.0001**
40	**56,251**	**44,282**	**1.1589**	**67.66**	**0.8225**	**67.66**	**0.8226**	**65.04**	**3**	**0.0001**
45	**57,139**	**43,972**	**1.1195**	**66.89**	**0.8157**	**67.13**	**0.8120**	**64.56**	**7**	**0.0001**
50	**57,818**	**43,554**	**1.0780**	**66.44**	**0.7982**	**66.73**	**0.7999**	**64.20**	**5**	**0.0001**
55	**58,602**	**43,349**	**1.0309**	**66.28**	**0.7903**	**66.28**	**0.7907**	**63.80**	**3**	**0.0001**
60	**59,247**	**43,121**	**0.9795**	**65.90**	**0.7819**	**65.93**	**0.7849**	**63.48**	**3**	**0.0001**
65	**59,758**	**42,882**	**0.9223**	**65.64**	**0.7744**	**65.65**	**0.7772**	**63.24**	**3**	**0.0001**
70	**60,177**	**42,678**	**0.8567**	**65.34**	**0.7764**	**65.44**	**0.7723**	**63.05**	**30**	**0.0001**
75	**60,621**	**42,635**	**0.7780**	**65.30**	**0.7712**	**65.22**	**0.7688**	**62.84**	**5**	**0.001**
80	**60,886**	**42,547**	**0.6798**	**65.14**	**0.7686**	**65.09**	**0.7661**	**62.74**	**7**	**0.001**
85	**61,071**	**42,521**	**0.5396**	**65.01**	**0.7619**	**65.02**	**0.7649**	**62.67**	**4**	**0.001**
88	**61,142**	**42,532**	**0.3976**	**65.01**	**0.7634**	**65.00**	**0.7645**	**62.65**	**16**	**0.001**

Table A.26: 5 in 19.5 lb/ft drill-pipe - 171/2 in bore-hole - 6°/100ft BG.

17.5	in	ID of the Well
5	in	OD of the Pipe
4.276	in	ID of the Pipe
19.5	lb/ft	Weight of the Pipe
3E+7	lb/in^2	Modulus of Elasticity
-818.5111	ft	Radius of Curvature (Negative for Build)
0.0000001	(fraction)	Error in the radius of curvature
0.0000001	(fraction)	Error in the clearance
0.0000001	(fraction)	Error in the X-coordinate of the center of curvature
0.000013	(fraction)	Error in the Y-coordinate of the center of curvature
0.125		λ_{min}
100		Maximum number of iterations
Simple model results		
Lp	L	P
69.46	66.23	54730.87

θ (°)	P_c (lb)	P_v (lb)	L_d	L_i (ft)	g_i	L_f (ft)	g_f	L_t (ft)	$\#_{it}$	h
3	**54,677**	**53,842**	**1.2915**	**68.98**	**0.9853**	**69.02**	**0.9849**	**65.86**	**4**	**0.00001**
5	**55,223**	**53,832**	**1.2836**	**68.70**	**0.9756**	**68.66**	**0.9751**	**65.54**	**4**	**0.00001**
10	**56,542**	**53,770**	**1.2628**	**67.82**	**0.9528**	**67.80**	**0.9526**	**64.79**	**3**	**0.00001**
15	**57,772**	**53,641**	**1.2405**	**66.93**	**0.9358**	**67.04**	**0.9323**	**64.11**	**5**	**0.00001**
20	**58,968**	**53,509**	**1.2160**	**66.13**	**0.9124**	**66.32**	**0.9150**	**63.48**	**5**	**0.00001**
25	**60,045**	**53,299**	**1.1901**	**65.76**	**0.8972**	**65.69**	**0.8984**	**62.93**	**5**	**0.00001**
30	**61,123**	**53,143**	**1.1614**	**65.00**	**0.7500**	**65.09**	**0.8832**	**62.39**	**10**	**0.0001**
35	**62,171**	**53,016**	**1.1301**	**64.53**	**0.8696**	**64.52**	**0.8699**	**61.88**	**7**	**0.0001**
40	**62,970**	**52,710**	**1.0979**	**64.10**	**0.8582**	**64.10**	**0.8581**	**61.51**	**4**	**0.0001**
45	**63,837**	**52,551**	**1.0616**	**63.71**	**0.8489**	**63.65**	**0.8477**	**61.11**	**4**	**0.0001**
50	**64,595**	**52,368**	**1.0222**	**63.26**	**0.8360**	**63.28**	**0.8393**	**60.78**	**3**	**0.0001**
55	**65,297**	**52,222**	**0.9789**	**63.05**	**0.8313**	**62.94**	**0.8315**	**60.47**	**6**	**0.0001**
60	**65,878**	**52,056**	**0.9310**	**62.72**	**0.8238**	**62.66**	**0.8244**	**60.23**	**10**	**0.0001**
65	**66,268**	**51,803**	**0.8778**	**62.33**	**0.8220**	**62.48**	**0.8196**	**60.07**	**9**	**0.0001**
70	**66,732**	**51,734**	**0.8153**	**62.28**	**0.8157**	**62.28**	**0.8145**	**59.89**	**3**	**0.001**
75	**67,109**	**51,691**	**0.7410**	**62.04**	**0.8111**	**62.12**	**0.8107**	**59.74**	**5**	**0.001**
80	**67,387**	**51,668**	**0.6476**	**62.01**	**0.8097**	**62.00**	**0.8088**	**59.64**	**3**	**0.001**
85	**67,563**	**51,663**	**0.5141**	**61.94**	**0.8060**	**61.94**	**0.8075**	**59.58**	**5**	**0.001**
88	**67,618**	**51,667**	**0.3789**	**61.93**	**0.8072**	**61.93**	**0.8068**	**59.57**	**17**	**0.001**

Table A.27: 5 in 19.5 lb/ft drill-pipe - 171/2 in bore-hole - 7°/100ft BG.

12.25	in	ID of the Well
5	in	OD of the Pipe
4.276	in	ID of the Pipe
19.5	lb/ft	Weight of the Pipe
3E+7	lb/in^2	Modulus of Elasticity
-2864.789	ft	Radius of Curvature (Negative for Build)
0.000001	(fraction)	Error in the radius of curvature
0.0000001	(fraction)	Error in the clearance
0.0000001	(fraction)	Error in the X-coordinate of the center of curvature
0.000013	(fraction)	Error in the Y-coordinate of the center of curvature
0.125		λ_{min}
100		Maximum number of iterations
Simple model results		
Lp	L	P
98.96	94.36	26962.2

θ (°)	P_c (lb)	P_v (lb)	L_d	L_i (ft)	g_i	L_f (ft)	g_f	L_t (ft)	$\#_{it}$	h
2	**27,612**	**25,663**	**1.7948**	**95.00**	**0.9000**	**95.90**	**0.9336**	**91.71**		
5	**30,141**	**25,272**	**1.7139**	**91.41**	**0.8608**	**91.67**	**0.8596**	**87.96**		
10	**33,707**	**24,007**	**1.6120**	**86.60**	**0.7786**	**86.55**	**0.7742**	**83.37**		
15	**36,639**	**22,181**	**1.5344**	**83.57**	**0.7147**	**82.92**	**0.7138**	**80.10**		
20	**39,143**	**20,036**	**1.4697**	**80.96**	**0.6637**	**80.16**	**0.6684**	**77.59**		
25	**41,267**	**17,658**	**1.4133**	**77.71**	**0.6438**	**78.01**	**0.6319**	**75.65**		
30	**43,449**	**15,518**	**1.3561**	**75.72**	**0.6209**	**76.00**	**0.6092**	**73.79**		
35	**45,222**	**13,180**	**1.3044**	**74.20**	**0.5842**	**74.47**	**0.5844**	**72.39**		
40	**46,963**	**11,055**	**1.2516**	**73.07**	**0.5620**	**73.07**	**0.5619**	**71.09**		
45	**48,179**	**8,677**	**1.2029**	**72.14**	**0.5448**	**72.13**	**0.5448**	**70.23**		
50	**49,528**	**6,734**	**1.1493**	**71.46**	**0.5367**	**71.14**	**0.5354**	**69.31**		
55	**50,789**	**5,028**	**1.0928**	**70.25**	**0.5260**	**70.26**	**0.5248**	**68.49**		
60	**51,656**	**3,276**	**1.0352**	**69.27**	**0.5076**	**69.68**	**0.5120**	**67.95**		
65	**52,570**	**1,940**	**0.9705**	**69.25**	**0.5051**	**69.08**	**0.5048**	**67.40**		
70	**53,168**	**674**	**0.8995**	**68.71**	**0.5116**	**68.71**	**0.5019**	**67.05**		
75	**53,773**	**-187**	**0.8154**	**68.33**	**0.4981**	**68.35**	**0.4967**	**66.71**		
80	**54,259**	**-756**	**0.7109**	**67.97**	**0.4888**	**68.07**	**0.4926**	**66.45**		
85	**54,399**	**-1,252**	**0.5644**	**68.04**	**0.4931**	**68.01**	**0.4905**	**66.40**		
88	**54,518**	**-1,311**	**0.4157**	**67.98**	**0.4880**	**67.95**	**0.4917**	**66.35**		

Table A.28: 5 in 19.5 lb/ft drill-pipe - 171/2 in bore-hole - 2°/100ft BG.

12.25	in	ID of the Well
5	in	OD of the Pipe
4.276	in	ID of the Pipe
19.5	lb/ft	Weight of the Pipe
3E+7	lb/in^2	Modulus of Elasticity
-1909.859	ft	Radius of Curvature (Negative for Build)
0.0000001	(fraction)	Error in the radius of curvature
0.000001	(fraction)	Error in the clearance
0.000001	(fraction)	Error in the X-coordinate of the center of curvature
0.00001	(fraction)	Error in the Y-coordinate of the center of curvature
0.125		λ_{min}
100		Maximum number of iterations
Simple model results		
Lp	L	P
80.8	77.05	40444

θ (°)	P_c (lb)	P_v (lb)	L_d	L_i (ft)	g_i	L_f (ft)	g_f	L_t (ft)	$\#_{it}$	h
1	**40,059**	**39,409**	**1.5040**	**80.36**	**0.9839**	**80.35**	**0.9840**	**76.67**	**3**	**0.00001**
5	**42,564**	**39,318**	**1.4550**	**77.93**	**0.9264**	**77.82**	**0.9291**	**74.44**		
10	**45,303**	**38,836**	**1.4027**	**75.58**	**0.8700**	**75.31**	**0.8752**	**72.22**		
15	**47,690**	**38,051**	**1.3566**	**73.69**	**0.8268**	**73.31**	**0.8319**	**70.44**		
20	**49,784**	**37,046**	**1.3143**	**71.48**	**0.7919**	**71.68**	**0.7962**	**68.99**		
25	**51,832**	**36,093**	**1.2717**	**70.54**	**0.7662**	**70.20**	**0.7646**	**67.65**		
30	**53,578**	**34,957**	**1.2312**	**69.30**	**0.7311**	**69.00**	**0.7389**	**66.58**		
35	**55,284**	**33,922**	**1.1892**	**67.90**	**0.7203**	**67.90**	**0.7206**	**65.58**		
40	**56,894**	**32,955**	**1.1460**	**66.59**	**0.7023**	**66.91**	**0.7009**	**64.68**		
45	**58,267**	**31,932**	**1.1024**	**66.45**	**0.6830**	**66.10**	**0.6857**	**63.94**		
50	**59,356**	**30,826**	**1.0578**	**65.20**	**0.6743**	**65.48**	**0.6735**	**63.38**		
55	**60,490**	**29,983**	**1.0088**	**65.01**	**0.6606**	**64.86**	**0.6631**	**62.81**		
60	**61,360**	**29,108**	**0.9568**	**64.18**	**0.6542**	**64.40**	**0.6542**	**62.39**		
65	**61,973**	**28,220**	**0.9002**	**64.08**	**0.6425**	**64.08**	**0.6446**	**62.11**		
70	**62,738**	**27,742**	**0.8339**	**63.49**	**0.6404**	**63.70**	**0.6402**	**61.76**		
75	**63,256**	**27,283**	**0.7569**	**63.60**	**0.6330**	**63.45**	**0.6346**	**61.53**		
80	**63,554**	**26,877**	**0.6613**	**63.31**	**0.6295**	**63.32**	**0.6305**	**61.41**		
85	**63,877**	**26,777**	**0.5244**	**63.21**	**0.6316**	**63.18**	**0.6292**	**61.28**		
88	**63,918**	**26,698**	**0.3865**	**63.20**	**0.6279**	**63.17**	**0.6288**	**61.28**		

Table A.29: 5 in 19.5 lb/ft drill-pipe - 121/4 in bore-hole - 3°/100ft BG.

12.25	in	ID of the Well
5	in	OD of the Pipe
4.276	in	ID of the Pipe
19.5	lb/ft	Weight of the Pipe
3E+7	lb/in^2	Modulus of Elasticity
-1432.324	ft	Radius of Curvature (Negative for Build)
0.0000001	(fraction)	Error in the radius of curvature
0.000001	(fraction)	Error in the clearance
0.000001	(fraction)	Error in the X-coordinate of the center of curvature
0.00001	(fraction)	Error in the Y-coordinate of the center of curvature
0.125		λ_{min}
100		Maximum number of iterations
Simple model results		
Lp	L	P
69.98	66.72	53927.59

θ (°)	P_c (lb)	P_v (lb)	L_d	L_i (ft)	g_i	L_f (ft)	g_f	L_t (ft)	$\#_{it}$	h
1.5	**53,762**	**53,031**	**1.3028**	**69.60**	**0.9866**	**69.60**	**0.9865**	**66.41**	**3**	**0.00001**
5	**55,393**	**52,959**	**1.2807**	**68.42**	**0.9572**	**68.50**	**0.9576**	**65.44**		
10	**57,567**	**52,717**	**1.2499**	**67.00**	**0.9244**	**67.11**	**0.9213**	**64.22**		
15	**59,675**	**52,446**	**1.2185**	**65.73**	**0.8946**	**65.85**	**0.8909**	**63.10**		
20	**61,452**	**51,899**	**1.1888**	**64.99**	**0.8638**	**64.84**	**0.8650**	**62.20**		
25	**63,151**	**51,347**	**1.1578**	**64.02**	**0.8445**	**63.91**	**0.8413**	**61.38**		
30	**64,789**	**50,824**	**1.1253**	**63.06**	**0.8218**	**63.06**	**0.8215**	**60.62**		
35	**66,370**	**50,349**	**1.0909**	**62.12**	**0.8007**	**62.28**	**0.8030**	**59.92**		
40	**67,520**	**49,566**	**1.0572**	**61.84**	**0.7858**	**61.72**	**0.7876**	**59.43**		
45	**68,934**	**49,184**	**1.0185**	**61.04**	**0.7750**	**61.07**	**0.7763**	**58.84**		
50	**69,988**	**48,592**	**0.9790**	**60.66**	**0.7636**	**60.60**	**0.7640**	**58.41**		
55	**70,931**	**48,052**	**0.9361**	**60.08**	**0.7520**	**60.19**	**0.7548**	**58.04**		
60	**71,672**	**47,483**	**0.8896**	**60.06**	**0.7435**	**59.87**	**0.7447**	**57.76**		
65	**72,348**	**47,034**	**0.8371**	**59.60**	**0.7339**	**59.59**	**0.7376**	**57.51**		
70	**73,019**	**46,773**	**0.7766**	**59.32**	**0.7344**	**59.32**	**0.7326**	**57.26**		
75	**73,512**	**46,534**	**0.7054**	**59.00**	**0.7336**	**59.13**	**0.7285**	**57.09**		
80	**73,885**	**46,379**	**0.6161**	**58.99**	**0.7276**	**58.99**	**0.7256**	**56.96**		
85	**74,082**	**46,258**	**0.4891**	**58.94**	**0.7249**	**58.93**	**0.7240**	**56.91**		
88	**74,183**	**46,270**	**0.3603**	**58.89**	**0.7283**	**58.90**	**0.7241**	**56.88**		

Table A.30: 5 in 19.5 lb/ft drill-pipe - 121/4 in bore-hole - 4°/100ft BG.

12.25	in	ID of the Well
5	in	OD of the Pipe
4.276	in	ID of the Pipe
19.5	lb/ft	Weight of the Pipe
3E+7	lb/in^2	Modulus of Elasticity
-1145.952	ft	Radius of Curvature (Negative for Build)
0.000001	(fraction)	Error in the radius of curvature
0.0000001	(fraction)	Error in the clearance
0.0000001	(fraction)	Error in the X-coordinate of the center of curvature
0.00001	(fraction)	Error in the Y-coordinate of the center of curvature
0.125		λ_{min}
100		Maximum number of iterations
Simple model results		
Lp	L	P
62.59	59.68	67404

θ (°)	P_c (lb)	P_v (lb)	L_d	L_i (ft)	g_i	L_f (ft)	g_f	L_t (ft)	$\#_{it}$	h
2	**67,380**	**66,600**	**1.1658**	**62.27**	**0.9883**	**62.29**	**0.9884**	**59.42**	**3**	**0.00005**
5	**68,546**	**66,598**	**1.1539**	**61.75**	**0.9726**	**61.72**	**0.9721**	**58.92**		
10	**70,380**	**66,500**	**1.1334**	**60.86**	**0.9465**	**60.85**	**0.9475**	**58.16**		
15	**72,028**	**66,245**	**1.1122**	**60.14**	**0.9262**	**60.11**	**0.9252**	**57.51**		
20	**73,641**	**65,999**	**1.0892**	**59.41**	**0.9052**	**59.40**	**0.9050**	**56.89**		
25	**75,235**	**65,792**	**1.0641**	**58.74**	**0.8879**	**58.74**	**0.8879**	**56.29**		
30	**76,529**	**65,356**	**1.0387**	**55.00**	**0.9000**	**58.21**	**0.8717**	**55.83**		
35	**77,950**	**65,133**	**1.0098**	**57.74**	**0.8565**	**57.66**	**0.8579**	**55.33**		
40	**79,154**	**64,790**	**0.9797**	**57.10**	**0.8424**	**57.20**	**0.8455**	**54.93**		
45	**80,096**	**64,295**	**0.9480**	**56.84**	**0.8325**	**56.84**	**0.8330**	**54.61**		
50	**81,064**	**63,946**	**0.9127**	**56.34**	**0.8236**	**56.49**	**0.8233**	**54.30**		
55	**81,972**	**63,667**	**0.8737**	**56.03**	**0.8178**	**56.17**	**0.8153**	**54.01**		
60	**82,725**	**63,373**	**0.8307**	**55.78**	**0.8086**	**55.91**	**0.8079**	**53.78**		
65	**83,452**	**63,200**	**0.7820**	**55.73**	**0.8060**	**55.67**	**0.8031**	**53.56**		
70	**84,059**	**63,060**	**0.7262**	**55.44**	**0.7976**	**55.47**	**0.7980**	**53.38**		
75	**84,420**	**62,836**	**0.6604**	**55.34**	**0.7951**	**55.36**	**0.7939**	**53.28**		
80	**84,764**	**62,757**	**0.5770**	**55.25**	**0.7927**	**55.25**	**0.7919**	**53.19**		
85	**85,023**	**62,762**	**0.4580**	**55.18**	**0.7885**	**55.18**	**0.7903**	**53.12**		
88	**85,077**	**62,745**	**0.3375**	**55.17**	**0.7894**	**55.17**	**0.7896**	**53.12**		

Table A.31: 5 in 19.5 lb/ft drill-pipe - 121/4 in bore-hole - 5°/100ft BG.

12.25	in	ID of the Well
5	in	OD of the Pipe
4.276	in	ID of the Pipe
19.5	lb/ft	Weight of the Pipe
3E+7	lb/in^2	Modulus of Elasticity
-954.9297	ft	Radius of Curvature (Negative for Build)
0.0000001	(fraction)	Error in the radius of curvature
0.0000001	(fraction)	Error in the clearance
0.0000001	(fraction)	Error in the X-coordinate of the center of curvature
0.00001	(fraction)	Error in the Y-coordinate of the center of curvature
0.125		λ_{min}
100		Maximum number of iterations
Simple model results		
Lp	L	P
57.14	54.48	80886.35

θ (°)	P_c (lb)	P_v (lb)	L_d	L_i (ft)	g_i	L_f (ft)	g_f	L_t (ft)	$\#_{it}$	h
2	**80,596**	**79,946**	**1.0672**	**56.83**	**0.9880**	**57.02**	**0.9919**	**54.38**	**101**	**0.00001**
5	**81,766**	**80,143**	**1.0579**	**56.59**	**0.9804**	**56.59**	**0.9804**	**54.00**	**3**	**0.00005**
10	**83,311**	**80,077**	**1.0434**	**55.99**	**0.9619**	**56.02**	**0.9624**	**53.51**	**4**	**0.0001**
15	**84,827**	**80,008**	**1.0267**	**55.48**	**0.9462**	**55.49**	**0.9455**	**53.04**	**5**	**0.0005**
20	**86,202**	**79,833**	**1.0087**	**55.01**	**0.9307**	**55.01**	**0.9306**	**52.62**	**3**	**0.0005**
25	**87,491**	**79,621**	**0.9887**	**54.59**	**0.9163**	**54.58**	**0.9167**	**52.24**	**4**	**0.0005**
30	**88,704**	**79,393**	**0.9668**	**54.18**	**0.9036**	**54.18**	**0.9036**	**51.89**	**3**	**0.0005**
35	**89,953**	**79,272**	**0.9421**	**53.91**	**0.8933**	**53.79**	**0.8927**	**51.54**	**6**	**0.0005**
40	**90,980**	**79,011**	**0.9158**	**53.47**	**0.8812**	**53.47**	**0.8820**	**51.26**	**4**	**0.0005**
45	**91,923**	**78,756**	**0.8869**	**53.24**	**0.8734**	**53.18**	**0.8729**	**51.00**	**6**	**0.0005**
50	**92,884**	**78,619**	**0.8546**	**52.90**	**0.8638**	**52.90**	**0.8650**	**50.75**	**3**	**0.0005**
55	**93,721**	**78,468**	**0.8190**	**52.68**	**0.8563**	**52.66**	**0.8581**	**50.53**	**7**	**0.0005**
60	**94,376**	**78,250**	**0.7796**	**52.52**	**0.8498**	**52.47**	**0.8523**	**50.37**	**7**	**0.0005**
65	**95,032**	**78,156**	**0.7345**	**52.29**	**0.8471**	**52.29**	**0.8471**	**50.20**	**4**	**0.001**
70	**95,449**	**77,951**	**0.6830**	**52.25**	**0.8429**	**52.17**	**0.8434**	**50.11**	**7**	**0.001**
75	**95,883**	**77,896**	**0.6211**	**52.10**	**0.8394**	**52.06**	**0.8401**	**50.00**	**28**	**0.001**
80	**96,177**	**77,838**	**0.5429**	**52.00**	**0.8385**	**51.99**	**0.8377**	**49.94**	**60**	**0.0025**
85	**96,365**	**77,815**	**0.4311**	**51.94**	**0.8357**	**51.95**	**0.8369**	**49.90**	**30**	**0.001**
87	**96,420**	**77,824**	**0.3637**	**51.93**	**0.8363**	**51.93**	**0.8364**	**49.89**	**101**	**0.0001**

Table A.32: 5 in 19.5 lb/ft drill-pipe - 121/4 in bore-hole - 6°/100ft BG.

12.25	in	ID of the Well
5	in	OD of the Pipe
4.276	in	ID of the Pipe
19.5	lb/ft	Weight of the Pipe
3E+7	lb/in^2	Modulus of Elasticity
-818.5111	ft	Radius of Curvature (Negative for Build)
0.0000001	(fraction)	Error in the radius of curvature
0.000001	(fraction)	Error in the clearance
0.000001	(fraction)	Error in the X-coordinate of the center of curvature
0.00001	(fraction)	Error in the Y-coordinate of the center of curvature
0.125		λ_{min}
100		Maximum number of iterations
Simple model results		
Lp	L	P
52.9	50.44	94366.78

θ (°)	P_c (lb)	P_v (lb)	L_d	L_i (ft)	g_i	L_f (ft)	g_f	L_t (ft)	$\#_{it}$	h
2	**94,247**	**93,690**	**0.9877**	**52.77**	**0.9939**	**52.77**	**0.9941**	**50.33**	**5**	**0.0001**
5	**95,086**	**93,695**	**0.9819**	**52.53**	**0.9856**	**52.52**	**0.9853**	**50.11**	**4**	**0.0001**
10	**96,429**	**93,657**	**0.9708**	**52.10**	**0.9723**	**52.13**	**0.9717**	**49.77**	**5**	**0.0001**
15	**97,740**	**93,609**	**0.9576**	**51.75**	**0.9592**	**51.75**	**0.9590**	**49.44**	**3**	**0.0001**
20	**98,955**	**93,496**	**0.9426**	**51.41**	**0.9473**	**51.41**	**0.9473**	**49.14**	**11**	**0.0005**
25	**100,085**	**93,339**	**0.9257**	**51.08**	**0.9359**	**51.10**	**0.9362**	**48.87**	**5**	**0.001**
30	**101,190**	**93,210**	**0.9065**	**52.00**	**0.9000**	**50.80**	**0.9258**	**48.60**	**11**	**0.001**
35	**102,279**	**93,124**	**0.8849**	**50.49**	**0.9155**	**50.52**	**0.9167**	**48.35**	**23**	**0.002**
40	**103,299**	**93,039**	**0.8608**	**50.29**	**0.9083**	**50.26**	**0.9088**	**48.12**	**30**	**0.002**
45	**104,143**	**92,857**	**0.8346**	**50.01**	**0.9029**	**50.04**	**0.9009**	**47.93**	**9**	**0.002**
50	**104,965**	**92,738**	**0.8052**	**49.92**	**0.8947**	**49.84**	**0.8943**	**47.75**	**6**	**0.002**
55	**105,675**	**92,601**	**0.7725**	**49.64**	**0.8897**	**49.67**	**0.8888**	**47.60**	**41**	**0.002**
60	**106,350**	**92,527**	**0.7356**	**49.54**	**0.8820**	**49.51**	**0.8835**	**47.46**	**17**	**0.0025**
65	**106,889**	**92,423**	**0.6937**	**49.38**	**0.8796**	**49.38**	**0.8794**	**47.35**	**15**	**0.0025**
70	**107,284**	**92,286**	**0.6453**	**49.31**	**0.8762**	**49.29**	**0.8758**	**47.27**	**13**	**0.003**
75	**107,708**	**92,291**	**0.5869**	**49.20**	**0.8735**	**49.20**	**0.8735**	**47.18**	**3**	**0.0005**
80	**107,996**	**92,277**	**0.5132**	**49.15**	**0.8715**	**49.14**	**0.8715**	**47.13**	**46**	**0.0001**
85	**108,204**	**92,303**	**0.4075**	**49.09**	**0.8698**	**49.10**	**0.8704**	**47.09**	**101**	**0.0001**
87.5	**108,253**	**92,307**	**0.3235**	**49.09**	**0.8699**	**49.09**	**0.8701**	**47.09**	**50**	**0.0001**

Table A.33: 5 in 19.5 lb/ft drill-pipe - 121/4 in bore-hole - 7°/100ft BG.

12.25	in	ID of the Well
4.5	in	OD of the Pipe
3.826	in	ID of the Pipe
16.6	lb/ft	Weight of the Pipe
3E+7	lb/in^2	Modulus of Elasticity
-2864.789	ft	Radius of Curvature (Negative for Build)
0.000001	(fraction)	Error in the radius of curvature
0.0000001	(fraction)	Error in the clearance
0.0000001	(fraction)	Error in the X-coordinate of the center of curvature
0.00001	(fraction)	Error in the Y-coordinate of the center of curvature
0.125		λ_{min}
100		Maximum number of iterations
Simple model results		
Lp	L	P
102.32	97.56	16988.26

θ (°)	P_c (lb)	P_v (lb)	L_d	L_i (ft)	g_i	L_f (ft)	g_f	L_t (ft)	$\#_{it}$	h
2	**17,492**	**15,832**	**1.9870**	**98.73**	**0.9095**	**98.19**	**0.9150**	**93.99**	**4**	**0.0001**
5	**19,493**	**15,349**	**1.8790**	**93.02**	**0.8112**	**92.96**	**0.8255**	**89.33**	**4**	**0.0001**
10	**22,229**	**13,971**	**1.7514**	**85.92**	**0.7485**	**86.98**	**0.7265**	**83.96**	**7**	**0.0001**
15	**24,586**	**12,277**	**1.6538**	**82.07**	**0.6675**	**82.66**	**0.6670**	**80.03**	**10**	**0.0001**
20	**26,631**	**10,366**	**1.5739**	**80.30**	**0.6046**	**79.39**	**0.6219**	**77.03**	**7**	**0.0001**
25	**28,380**	**8,283**	**1.5059**	**77.70**	**0.5860**	**76.88**	**0.5830**	**74.72**	**8**	**0.0001**
30	**29,873**	**6,095**	**1.4454**	**74.92**	**0.5533**	**74.92**	**0.5533**	**72.92**	**3**	**0.0001**
35	**31,058**	**3,781**	**1.3912**	**73.17**	**0.5331**	**73.46**	**0.5303**	**71.58**	**6**	**0.0001**
40	**32,275**	**1,707**	**1.3346**	**72.70**	**0.5037**	**72.07**	**0.5085**	**70.28**	**5**	**0.0001**
45	**33,444**	**-182**	**1.2767**	**70.81**	**0.4984**	**70.81**	**0.4980**	**69.11**	**3**	**0.0001**
50	**34,477**	**-1,953**	**1.2184**	**69.18**	**0.4805**	**69.75**	**0.4834**	**68.12**	**13**	**0.0001**
55	**35,239**	**-3,716**	**1.1604**	**69.18**	**0.4738**	**69.00**	**0.4696**	**67.43**	**17**	**0.0001**
60	**36,087**	**-5,097**	**1.0958**	**68.21**	**0.4629**	**68.21**	**0.4635**	**66.68**	**3**	**0.0001**
65	**36,656**	**-6,444**	**1.0283**	**67.70**	**0.4683**	**67.70**	**0.4590**	**66.20**	**4**	**0.0001**
70	**37,060**	**-7,628**	**0.9534**	**67.36**	**0.4532**	**67.35**	**0.4527**	**65.89**	**3**	**0.0001**
75	**37,559**	**-8,376**	**0.8634**	**67.06**	**0.4461**	**66.94**	**0.4476**	**65.49**	**16**	**0.0001**
80	**37,803**	**-9,030**	**0.7538**	**66.79**	**0.4489**	**66.75**	**0.4452**	**65.32**	**5**	**0.0001**
85	**38,072**	**-9,303**	**0.5972**	**66.56**	**0.4405**	**66.56**	**0.4423**	**65.13**	**5**	**0.0001**
88	**38,115**	**-9,412**	**0.4401**	**66.55**	**0.4465**	**66.54**	**0.4418**	**65.12**	**12**	**0.0001**

Table A.34: 41/2 in 16.6 lb/ft drill-pipe - 121/4 in bore-hole - 2°/100ft BG.

12.25	in	ID of the Well
4.5	in	OD of the Pipe
3.826	in	ID of the Pipe
16.6	lb/ft	Weight of the Pipe
3E+7	lb/in^2	Modulus of Elasticity
-1909.859	ft	Radius of Curvature (Negative for Build)
0.000001	(fraction)	Error in the radius of curvature
0.0000001	(fraction)	Error in the clearance
0.0000001	(fraction)	Error in the X-coordinate of the center of curvature
0.00001	(fraction)	Error in the Y-coordinate of the center of curvature
0.125		λ_{min}
100		Maximum number of iterations
Simple model results		
Lp	L	P
83.54	79.66	25482.21

θ (°)	P_c (lb)	P_v (lb)	L_d	L_i (ft)	g_i	L_f (ft)	g_f	L_t (ft)	$\#_{it}$	h
3	**26,184**	**24,525**	**1.6419**	**80.94**	**0.9408**	**81.16**	**0.9399**	**77.59**	**9**	**0.0001**
5	**27,156**	**24,393**	**1.6096**	**79.36**	**0.9095**	**79.63**	**0.9070**	**76.25**	**4**	**0.0001**
10	**29,384**	**23,879**	**1.5391**	**75.90**	**0.8494**	**76.43**	**0.8414**	**73.41**	**4**	**0.0001**
15	**31,371**	**23,165**	**1.4783**	**73.72**	**0.7827**	**73.89**	**0.7932**	**71.13**	**4**	**0.0001**
20	**33,110**	**22,267**	**1.4246**	**71.72**	**0.7454**	**71.86**	**0.7525**	**69.30**	**4**	**0.0001**
25	**34,597**	**21,198**	**1.3760**	**69.79**	**0.7110**	**70.25**	**0.7190**	**67.85**	**7**	**0.0001**
30	**36,120**	**20,269**	**1.3258**	**70.00**	**0.6000**	**68.72**	**0.6939**	**66.45**	**9**	**0.0001**
35	**37,377**	**19,193**	**1.2789**	**67.53**	**0.6748**	**67.53**	**0.6726**	**65.37**	**4**	**0.0001**
40	**38,314**	**17,936**	**1.2348**	**66.67**	**0.6527**	**66.68**	**0.6526**	**64.61**	**4**	**0.0001**
45	**39,437**	**17,019**	**1.1850**	**65.90**	**0.6357**	**65.72**	**0.6334**	**63.72**	**6**	**0.0001**
50	**40,368**	**16,081**	**1.1345**	**65.15**	**0.6174**	**64.95**	**0.6232**	**63.02**	**16**	**0.0001**
55	**41,218**	**15,248**	**1.0810**	**64.28**	**0.6142**	**64.28**	**0.6125**	**62.40**	**3**	**0.0001**
60	**41,775**	**14,319**	**1.0258**	**63.51**	**0.5967**	**63.86**	**0.5992**	**62.02**	**15**	**0.0001**
65	**42,357**	**13,623**	**0.9634**	**63.13**	**0.5950**	**63.43**	**0.5926**	**61.62**	**7**	**0.0001**
70	**42,855**	**13,064**	**0.8927**	**62.88**	**0.5871**	**63.07**	**0.5858**	**61.30**	**5**	**0.0001**
75	**43,274**	**12,651**	**0.8098**	**62.80**	**0.5835**	**62.79**	**0.5838**	**61.03**	**4**	**0.0001**
80	**43,541**	**12,319**	**0.7070**	**62.00**	**0.5791**	**62.62**	**0.5805**	**60.88**	**101**	**0.0001**
85	**43,796**	**12,213**	**0.5605**	**62.47**	**0.5779**	**62.46**	**0.5775**	**60.73**	**5**	**0.0001**
87.2	**43,819**	**12,153**	**0.4621**	**62.45**	**0.5781**	**62.46**	**0.5773**	**60.73**	**20**	**0.001**

Table A.35: 41/2 in 16.6 lb/ft drill-pipe - 121/4 in bore-hole - 3°/100ft BG.

12.25	in	ID of the Well
4.5	in	OD of the Pipe
3.826	in	ID of the Pipe
16.6	lb/ft	Weight of the Pipe
3E+7	lb/in^2	Modulus of Elasticity
-1432.324	ft	Radius of Curvature (Negative for Build)
0.0000001	(fraction)	Error in the radius of curvature
0.0000001	(fraction)	Error in the clearance
0.0000001	(fraction)	Error in the X-coordinate of the center of curvature
0.00001	(fraction)	Error in the Y-coordinate of the center of curvature
0.125		λ_{min}
100		Maximum number of iterations
Simple model results		
Lp	L	P
72.35	68.98	33977.69

θ (°)	P_c (lb)	P_v (lb)	L_d	L_i (ft)	g_i	L_f (ft)	g_f	L_t (ft)	$\#_{it}$	h
2	**34,014**	**33,184**	**1.4491**	**71.52**	**0.9782**	**71.61**	**0.9759**	**68.35**	**4**	**0.0001**
5	**35,216**	**33,144**	**1.4212**	**70.32**	**0.9406**	**70.31**	**0.9445**	**67.21**	**4**	**0.0001**
10	**37,062**	**32,933**	**1.3782**	**68.74**	**0.9025**	**68.44**	**0.8986**	**65.56**	**7**	**0.0001**
15	**38,687**	**32,533**	**1.3388**	**67.20**	**0.8640**	**66.92**	**0.8618**	**64.21**	**5**	**0.0001**
20	**40,235**	**32,103**	**1.2997**	**65.71**	**0.8326**	**65.56**	**0.8308**	**62.99**	**5**	**0.0001**
25	**41,495**	**31,447**	**1.2635**	**64.60**	**0.8024**	**64.51**	**0.8030**	**62.06**	**4**	**0.0001**
30	**42,755**	**30,867**	**1.2253**	**62.00**	**0.7500**	**63.52**	**0.7821**	**61.17**	**6**	**0.0001**
35	**44,005**	**30,367**	**1.1852**	**62.58**	**0.7604**	**62.58**	**0.7605**	**60.33**	**3**	**0.0001**
40	**44,924**	**29,641**	**1.1466**	**61.92**	**0.7445**	**61.92**	**0.7444**	**59.73**	**3**	**0.0001**
45	**45,966**	**29,153**	**1.1035**	**61.33**	**0.7311**	**61.20**	**0.7289**	**59.08**	**6**	**0.0001**
50	**46,756**	**28,543**	**1.0598**	**60.93**	**0.7173**	**60.67**	**0.7181**	**58.60**	**7**	**0.0001**
56	**47,652**	**27,940**	**1.0021**	**60.00**	**0.7090**	**60.10**	**0.7047**	**58.08**	**6**	**0.0001**
60	**48,245**	**27,654**	**0.9595**	**59.71**	**0.7052**	**59.73**	**0.6976**	**57.74**	**6**	**0.0001**
65	**48,736**	**27,187**	**0.9027**	**59.27**	**0.6938**	**59.43**	**0.6915**	**57.48**	**21**	**0.0001**
70	**49,178**	**26,836**	**0.8375**	**59.26**	**0.6901**	**59.17**	**0.6851**	**57.24**	**22**	**0.0001**
75	**49,557**	**26,590**	**0.7604**	**59.04**	**0.6818**	**58.96**	**0.6804**	**57.05**	**5**	**0.001**
80	**49,802**	**26,386**	**0.6643**	**58.83**	**0.6793**	**58.83**	**0.6779**	**56.93**	**3**	**0.001**
85	**49,983**	**26,296**	**0.5271**	**58.71**	**0.6797**	**58.74**	**0.6760**	**56.85**	**7**	**0.001**
88	**50,088**	**26,326**	**0.3882**	**58.70**	**0.6759**	**58.69**	**0.6752**	**56.81**	**14**	**0.001**

Table A.36: 41/2 in 16.6 lb/ft drill-pipe - 121/4 in bore-hole - 4°/100ft BG.

12.25	in	ID of the Well
4.5	in	OD of the Pipe
3.826	in	ID of the Pipe
16.6	lb/ft	Weight of the Pipe
3E+7	lb/in^2	Modulus of Elasticity
-1145.952	ft	Radius of Curvature (Negative for Build)
0.000001	(fraction)	Error in the radius of curvature
0.0000001	(fraction)	Error in the clearance
0.0000001	(fraction)	Error in the X-coordinate of the center of curvature
0.00001	(fraction)	Error in the Y-coordinate of the center of curvature
0.125		λ_{min}
100		Maximum number of iterations
Simple model results		
Lp	L	P
64.71	61.7	42468.4

θ (°)	P_c (lb)	P_v (lb)	L_d	L_i (ft)	g_i	L_f (ft)	g_f	L_t (ft)	$\#_{it}$	h
2	**42,431**	**41,767**	**1.301**	**64.28**	**0.9834**	**64.29**	**0.9845**	**61.35**	**4**	**0.00001**
5	**43,401**	**41,743**	**1.2841**	**63.52**	**0.9648**	**63.52**	**0.9627**	**60.67**	**4**	**0.00001**
10	**44,945**	**41,642**	**1.2556**	**62.52**	**0.9279**	**62.36**	**0.9313**	**59.64**	**21**	**0.0001**
15	**46,364**	**41,441**	**1.2272**	**61.46**	**0.9000**	**61.34**	**0.9034**	**58.74**	**4**	**0.0001**
20	**47,648**	**41,141**	**1.1986**	**60.31**	**0.8770**	**60.46**	**0.8792**	**57.97**	**6**	**0.0001**
25	**48,900**	**40,860**	**1.1682**	**59.59**	**0.8556**	**59.65**	**0.8569**	**57.24**	**4**	**0.0001**
30	**49,924**	**40,413**	**1.1382**	**59.00**	**0.8379**	**59.00**	**0.8379**	**56.67**	**3**	**0.0001**
35	**51,054**	**40,142**	**1.1044**	**58.38**	**0.8226**	**58.32**	**0.8219**	**56.06**	**7**	**0.0001**
40	**52,006**	**39,778**	**1.0698**	**57.81**	**0.8081**	**57.76**	**0.8088**	**55.56**	**5**	**0.0001**
45	**52,897**	**39,446**	**1.0325**	**57.13**	**0.7918**	**57.26**	**0.7962**	**55.11**	**20**	**0.0001**
50	**53,563**	**38,990**	**0.9938**	**56.90**	**0.7827**	**56.90**	**0.7836**	**54.79**	**3**	**0.0001**
55	**54,363**	**38,780**	**0.9497**	**56.36**	**0.7719**	**56.47**	**0.7760**	**54.40**	**16**	**0.0001**
60	**54,864**	**38,390**	**0.9030**	**56.29**	**0.7669**	**56.21**	**0.7669**	**54.17**	**14**	**0.0001**
65	**55,354**	**38,114**	**0.8500**	**55.96**	**0.7649**	**55.96**	**0.7596**	**53.95**	**5**	**0.0001**
70	**55,809**	**37,933**	**0.7890**	**55.60**	**0.7567**	**55.74**	**0.7557**	**53.75**	**15**	**0.0001**
75	**56,245**	**37,870**	**0.7163**	**55.51**	**0.7497**	**55.54**	**0.7512**	**53.56**	**5**	**0.001**
80	**56,461**	**37,727**	**0.6260**	**55.41**	**0.7481**	**55.44**	**0.7489**	**53.48**	**56**	**0.001**
85	**56,610**	**37,660**	**0.4970**	**55.40**	**0.7468**	**55.38**	**0.7464**	**53.43**	**34**	**0.0015**
88	**56,689**	**37,678**	**0.3661**	**55.35**	**0.7463**	**55.35**	**0.7461**	**53.40**	**22**	**0.0015**

Table A.37: 41/2 in 16.6 lb/ft drill-pipe - 121/4 in bore-hole - 5°/100ft BG.

12.25	in	ID of the Well
4.5	in	OD of the Pipe
3.826	in	ID of the Pipe
16.6	lb/ft	Weight of the Pipe
3E+7	lb/in^2	Modulus of Elasticity
-954.9297	ft	Radius of Curvature (Negative for Build)
0.0000001	(fraction)	Error in the radius of curvature
0.0000001	(fraction)	Error in the clearance
0.0000001	(fraction)	Error in the X-coordinate of the center of curvature
0.00001	(fraction)	Error in the Y-coordinate of the center of curvature
0.125		λ_{min}
100		Maximum number of iterations
Simple model results		
Lp	L	P
59.07	56.33	50963.32

θ (°)	P_c (lb)	P_v (lb)	L_d	L_i (ft)	g_i	L_f (ft)	g_f	L_t (ft)	$\#_{it}$	h
3	**51,143**	**50,314**	**1.1865**	**58.60**	**0.9835**	**58.65**	**0.9839**	**55.96**	**4**	**0.00001**
5	**51,678**	**50,296**	**1.1789**	**58.25**	**0.9729**	**58.32**	**0.9738**	**55.68**	**4**	**0.00001**
10	**52,998**	**50,246**	**1.1587**	**57.51**	**0.9506**	**57.54**	**0.9500**	**54.99**	**3**	**0.00001**
15	**54,214**	**50,111**	**1.1375**	**56.75**	**0.9299**	**56.85**	**0.9286**	**54.38**	**5**	**0.00001**
20	**55,408**	**49,986**	**1.1142**	**56.23**	**0.9084**	**56.20**	**0.9102**	**53.81**	**5**	**0.00001**
25	**56,485**	**49,786**	**1.0897**	**55.63**	**0.8928**	**55.63**	**0.8927**	**53.31**	**3**	**0.00001**
30	**57,498**	**49,572**	**1.0633**	**55.12**	**0.8778**	**55.12**	**0.8778**	**52.85**	**3**	**0.00001**
35	**58,440**	**49,347**	**1.0350**	**54.58**	**0.8621**	**54.65**	**0.8637**	**52.43**	**6**	**0.00001**
40	**59,253**	**49,063**	**1.0048**	**54.29**	**0.8521**	**54.26**	**0.8524**	**52.09**	**4**	**0.00001**
45	**60,054**	**48,845**	**0.9716**	**53.88**	**0.8415**	**53.88**	**0.8417**	**51.75**	**3**	**0.00001**
50	**60,720**	**48,576**	**0.9359**	**53.60**	**0.8340**	**53.58**	**0.8323**	**51.48**	**4**	**0.001**
55	**61,436**	**48,451**	**0.8957**	**53.10**	**0.8252**	**53.26**	**0.8233**	**51.20**	**8**	**0.001**
60	**61,910**	**48,182**	**0.8523**	**53.05**	**0.8152**	**53.06**	**0.8161**	**51.01**	**3**	**0.001**
65	**62,476**	**48,109**	**0.8022**	**52.90**	**0.8102**	**52.82**	**0.8107**	**50.80**	**5**	**0.001**
70	**62,837**	**47,941**	**0.7455**	**52.67**	**0.8066**	**52.67**	**0.8068**	**50.67**	**6**	**0.00001**
75	**63,160**	**47,848**	**0.6777**	**52.45**	**0.8032**	**52.54**	**0.8025**	**50.55**	**17**	**0.00001**
80	**63,385**	**47,774**	**0.5923**	**52.40**	**0.7981**	**52.46**	**0.8002**	**50.48**	**46**	**0.00001**
85	**63,544**	**47,753**	**0.4702**	**52.40**	**0.7989**	**52.40**	**0.7988**	**50.43**	**49**	**0.00001**

Table A.38: 41/2 in 16.6 lb/ft drill-pipe - 121/4 in bore-hole - 6°/100ft BG.

12.25	in	ID of the Well
4.5	in	OD of the Pipe
3.826	in	ID of the Pipe
16.6	lb/ft	Weight of the Pipe
3E+7	lb/in^2	Modulus of Elasticity
-818.5111	ft	Radius of Curvature (Negative for Build)
0.000001	(fraction)	Error in the radius of curvature
0.0000001	(fraction)	Error in the clearance
0.0000001	(fraction)	Error in the X-coordinate of the center of curvature
0.00001	(fraction)	Error in the Y-coordinate of the center of curvature
0.125		λ_{min}
100		Maximum number of iterations
Simple model results		
Lp	L	P
54.69	52.15	59456.78

θ (°)	P_c (lb)	P_v (lb)	L_d	L_i (ft)	g_i	L_f (ft)	g_f	L_t (ft)	$\#_{it}$	h
2	**59,335**	**58,861**	**1.1033**	**54.30**	**0.9890**	**54.52**	**0.9919**	**52.00**	**9**	**0.000001**
5	**60,051**	**58,867**	**1.0950**	**54.21**	**0.9805**	**54.17**	**0.9805**	**51.70**	**4**	**0.00001**
10	**61,156**	**58,797**	**1.0802**	**53.66**	**0.9634**	**53.64**	**0.9624**	**51.23**	**4**	**0.00001**
15	**62,275**	**58,759**	**1.0629**	**53.15**	**0.9468**	**53.13**	**0.9459**	**50.78**	**4**	**0.00001**
20	**63,278**	**58,631**	**1.0443**	**52.69**	**0.9306**	**52.68**	**0.9309**	**50.39**	**4**	**0.00001**
25	**64,225**	**58,483**	**1.0237**	**52.26**	**0.9174**	**52.26**	**0.9173**	**50.02**	**3**	**0.00001**
30	**65,200**	**58,407**	**1.0004**	**51.85**	**0.9050**	**51.85**	**0.9050**	**49.66**	**3**	**0.00001**
35	**66,008**	**58,215**	**0.9756**	**51.60**	**0.8940**	**51.52**	**0.8937**	**49.36**	**6**	**0.00001**
40	**66,834**	**58,101**	**0.9479**	**51.13**	**0.8847**	**51.19**	**0.8828**	**49.07**	**8**	**0.00001**
45	**67,508**	**57,900**	**0.9182**	**50.92**	**0.8738**	**50.92**	**0.8738**	**48.83**	**9**	**0.00001**
50	**68,161**	**57,753**	**0.8851**	**50.65**	**0.8651**	**50.67**	**0.8661**	**48.61**	**7**	**0.00001**
55	**68,763**	**57,633**	**0.8483**	**50.50**	**0.8606**	**50.44**	**0.8589**	**48.41**	**26**	**0.0001**
60	**69,316**	**57,549**	**0.8071**	**50.25**	**0.8539**	**50.24**	**0.8531**	**48.23**	**5**	**0.0001**
65	**69,753**	**57,439**	**0.7607**	**50.09**	**0.8468**	**50.08**	**0.8487**	**48.09**	**5**	**0.0001**
70	**70,086**	**57,318**	**0.7072**	**49.93**	**0.8450**	**49.97**	**0.8443**	**47.98**	**16**	**0.001**
75	**70,400**	**57,275**	**0.6431**	**49.85**	**0.8408**	**49.86**	**0.8410**	**47.89**	**7**	**0.001**
80	**70,610**	**57,229**	**0.5622**	**49.78**	**0.8391**	**49.79**	**0.8386**	**47.83**	**34**	**0.0001**
85	**70,781**	**57,245**	**0.4464**	**49.75**	**0.8373**	**49.74**	**0.8377**	**47.78**	**87**	**0.00001**

Table A.39: 41/2 in 16.6 lb/ft drill-pipe - 121/4 in bore-hole - 7°/100ft BG.

6	in	ID of the Well
3.5	in	OD of the Pipe
2.764	in	ID of the Pipe
11.2851	lb/ft	Weight of the Pipe - 13.3 lb/ft with 9.5 lb/gal mud
3E+7	lb/in^2	Modulus of Elasticity
-2864.789	ft	Radius of Curvature (Negative for Build)
0.000001	(fraction)	Error in the radius of curvature
0.0000001	(fraction)	Error in the clearance
0.0000001	(fraction)	Error in the X-coordinate of the center of curvature
0.00001	(fraction)	Error in the Y-coordinate of the center of curvature
0.125		λ_{min}
100		Maximum number of iterations
Simple model results		
Lp	L	P
58.11	55.41	24664.82

θ (°)	P_c (lb)	P_v (lb)	L_d	L_i (ft)	g_i	L_f (ft)	g_f	L_t (ft)	$\#_{it}$	h
1	**24,803**	**24,239**	**1.3180**	**57.52**	**0.9776**	**57.52**	**0.9776**	**54.90**	**3**	**0.00001**
5	**26,861**	**24,043**	**1.2617**	**55.06**	**0.9030**	**55.13**	**0.9037**	**52.80**	**5**	**0.00001**
10	**29,074**	**23,460**	**1.2052**	**52.73**	**0.8395**	**52.86**	**0.8375**	**50.78**	**7**	**0.00001**
15	**31,002**	**22,635**	**1.1576**	**50.98**	**0.7861**	**51.10**	**0.7861**	**49.21**	**18**	**0.00001**
20	**32,668**	**21,610**	**1.1158**	**49.79**	**0.7441**	**49.71**	**0.7443**	**47.96**	**35**	**0.00001**
25	**34,241**	**20,578**	**1.0756**	**48.63**	**0.7107**	**48.50**	**0.7139**	**46.86**	**8**	**0.0001**
30	**35,533**	**19,368**	**1.0390**	**47.35**	**0.6810**	**47.57**	**0.6854**	**46.02**	**8**	**0.0001**
35	**36,860**	**18,317**	**1.0007**	**46.66**	**0.6677**	**46.67**	**0.6642**	**45.20**	**4**	**0.0001**
40	**37,836**	**17,055**	**0.9653**	**46.04**	**0.6423**	**46.03**	**0.6432**	**44.62**	**4**	**0.0001**
45	**38,854**	**15,994**	**0.9270**	**45.22**	**0.6275**	**45.41**	**0.6274**	**44.05**	**17**	**0.0001**
50	**39,813**	**15,047**	**0.8868**	**44.84**	**0.6110**	**44.84**	**0.6128**	**43.53**	**3**	**0.0001**
55	**40,530**	**14,048**	**0.8460**	**44.35**	**0.5986**	**44.43**	**0.6010**	**43.15**	**10**	**0.0001**
60	**41,174**	**13,176**	**0.8016**	**44.08**	**0.5923**	**44.07**	**0.5919**	**42.82**	**4**	**0.0001**
65	**41,771**	**12,471**	**0.7524**	**43.75**	**0.5834**	**43.75**	**0.5857**	**42.53**	**4**	**0.0001**
70	**42,300**	**11,920**	**0.6968**	**43.47**	**0.5796**	**43.48**	**0.5794**	**42.27**	**3**	**0.0001**
75	**42,622**	**11,394**	**0.6325**	**43.27**	**0.5788**	**43.31**	**0.5733**	**42.12**	**10**	**0.0001**
80	**42,867**	**11,029**	**0.5522**	**43.23**	**0.5731**	**43.19**	**0.5702**	**42.01**	**8**	**0.0001**
85	**43,054**	**10,847**	**0.4380**	**43.13**	**0.5718**	**43.11**	**0.5692**	**41.93**	**23**	**0.0001**
86.25	**43,079**	**10,819**	**0.3979**	**43.10**	**0.5700**	**43.10**	**0.5686**	**41.92**	**10**	**0.001**

Table A.40: 31/2 in 13.3 lb/ft drill-pipe - 6 in bore-hole - 2°/100ft BG.

6	in	ID of the Well
3.5	in	OD of the Pipe
2.764	in	ID of the Pipe
11.2851	lb/ft	Weight of the Pipe - 13.3 lb/ft with 9.5 lb/gal mud
3E+7	lb/in^2	Modulus of Elasticity
-1909.859	ft	Radius of Curvature (Negative for Build)
0.000001	(fraction)	Error in the radius of curvature
0.0000001	(fraction)	Error in the clearance
0.0000001	(fraction)	Error in the X-coordinate of the center of curvature
0.00001	(fraction)	Error in the Y-coordinate of the center of curvature
0.125		λ_{min}
100		Maximum number of iterations
Simple model results		
Lp	L	P
47.45	45.24	36996.35

θ (°)	P_c (lb)	P_v (lb)	L_d	L_i (ft)	g_i	L_f (ft)	g_f	L_t (ft)	$\#_{it}$	h
2	**37,389**	**36,637**	**1.0766**	**46.99**	**0.9801**	**46.99**	**0.9801**	**44.85**	**3**	**0.00001**
5	**38,462**	**36,584**	**1.0592**	**46.28**	**0.9531**	**46.28**	**0.9531**	**44.22**	**3**	**0.00001**
10	**40,097**	**36,354**	**1.0319**	**45.32**	**0.9134**	**45.26**	**0.9137**	**43.32**	**6**	**0.00001**
15	**41,598**	**36,020**	**1.0053**	**44.32**	**0.8808**	**44.38**	**0.8810**	**42.55**	**5**	**0.00001**
20	**43,001**	**35,630**	**0.9786**	**43.47**	**0.8519**	**43.60**	**0.8518**	**41.85**	**13**	**0.00001**
25	**44,325**	**35,217**	**0.9515**	**42.79**	**0.8317**	**42.90**	**0.8273**	**41.23**	**6**	**0.00001**
30	**45,524**	**34,747**	**0.9240**	**42.30**	**0.8068**	**42.30**	**0.8068**	**40.70**	**4**	**0.00001**
35	**46,553**	**34,190**	**0.8964**	**41.80**	**0.7894**	**41.81**	**0.7889**	**40.25**	**4**	**0.00001**
40	**47,493**	**33,639**	**0.8674**	**41.42**	**0.7761**	**41.37**	**0.7726**	**39.86**	**12**	**0.0001**
45	**48,385**	**33,145**	**0.8363**	**40.97**	**0.7584**	**40.97**	**0.7584**	**39.50**	**3**	**0.0001**
50	**49,228**	**32,718**	**0.8029**	**40.60**	**0.7476**	**40.60**	**0.7471**	**39.16**	**3**	**0.0001**
55	**49,942**	**32,287**	**0.7672**	**40.35**	**0.7386**	**40.30**	**0.7361**	**38.89**	**15**	**0.0001**
60	**50,471**	**31,806**	**0.7289**	**40.16**	**0.7241**	**40.07**	**0.7282**	**38.69**	**5**	**0.0001**
65	**51,048**	**31,515**	**0.6852**	**39.81**	**0.7201**	**39.84**	**0.7202**	**38.48**	**62**	**0.0001**
70	**51,486**	**31,233**	**0.6357**	**39.67**	**0.7123**	**39.67**	**0.7153**	**38.32**	**7**	**0.0001**
75	**51,784**	**30,966**	**0.5777**	**39.57**	**0.7090**	**39.55**	**0.7105**	**38.22**	**49**	**0.0001**
80	**52,024**	**30,799**	**0.5046**	**39.47**	**0.7008**	**39.46**	**0.7075**	**38.14**	**8**	**0.001**
85	**52,186**	**30,715**	**0.4004**	**39.42**	**0.7058**	**39.41**	**0.7059**	**38.09**	**15**	**0.0015**
87	**52,224**	**30,701**	**0.3377**	**39.40**	**0.7047**	**39.40**	**0.7056**	**38.08**	**42**	**0.0015**

Table A.41: 31/2 in 13.3 lb/ft drill-pipe - 6 in bore-hole - 3°/100ft BG.

6	in	ID of the Well
3.5	in	OD of the Pipe
2.764	in	ID of the Pipe
11.2851	lb/ft	Weight of the Pipe - 13.3 lb/ft with 9.5 lb/gal mud
3E+7	lb/in^2	Modulus of Elasticity
-1432.324	ft	Radius of Curvature (Negative for Build)
0.000001	(fraction)	Error in the radius of curvature
0.0000001	(fraction)	Error in the clearance
0.0000001	(fraction)	Error in the X-coordinate of the center of curvature
0.0000001	(fraction)	Error in the Y-coordinate of the center of curvature
0.125		λ_{min}
100		Maximum number of iterations
Simple model results		
Lp	L	P
41.09	39.18	49329.69

θ (°)	P_c (lb)	P_v (lb)	L_d	L_i (ft)	g_i	L_f (ft)	g_f	L_t (ft)	$\#_{it}$	h
1	**49,311**	**49,029**	**0.9394**	**40.99**	**0.9943**	**40.99**	**0.9943**	**39.10**	**7**	**0.00001**
5	**50,404**	**48,995**	**0.9271**	**40.51**	**0.9725**	**40.51**	**0.9725**	**38.68**	**4**	**0.00001**
10	**51,724**	**48,917**	**0.9108**	**39.94**	**0.9486**	**39.95**	**0.9481**	**38.18**	**4**	**0.00001**
15	**52,931**	**48,748**	**0.8938**	**39.40**	**0.9260**	**39.46**	**0.9261**	**37.75**	**8**	**0.00001**
20	**54,101**	**48,573**	**0.8753**	**38.94**	**0.9048**	**39.00**	**0.9065**	**37.34**	**7**	**0.00001**
25	**55,198**	**48,367**	**0.8556**	**38.58**	**0.8892**	**38.58**	**0.8889**	**36.98**	**3**	**0.00001**
30	**56,151**	**48,069**	**0.8350**	**38.23**	**0.8724**	**38.23**	**0.8724**	**36.66**	**3**	**0.00001**
35	**57,139**	**47,868**	**0.8122**	**37.86**	**0.8572**	**37.88**	**0.8591**	**36.35**	**11**	**0.00001**
40	**57,980**	**47,590**	**0.7881**	**37.52**	**0.8474**	**37.59**	**0.8459**	**36.09**	**12**	**0.00001**
45	**58,692**	**47,262**	**0.7624**	**37.32**	**0.8341**	**37.34**	**0.8356**	**35.88**	**29**	**0.00001**
50	**59,451**	**47,069**	**0.7336**	**37.09**	**0.8254**	**37.09**	**0.8258**	**35.65**	**9**	**0.00001**
55	**60,044**	**46,803**	**0.7026**	**36.93**	**0.8199**	**36.90**	**0.8175**	**35.48**	**6**	**0.00001**
60	**60,626**	**46,628**	**0.6678**	**36.77**	**0.8110**	**36.72**	**0.8104**	**35.31**	**12**	**0.00001**
65	**61,015**	**46,365**	**0.6293**	**36.53**	**0.8062**	**36.59**	**0.8046**	**35.21**	**11**	**0.00001**
70	**61,419**	**46,230**	**0.5845**	**36.44**	**0.7995**	**36.47**	**0.7998**	**35.10**	**86**	**0.00001**
75	**61,716**	**46,103**	**0.5313**	**36.38**	**0.7960**	**36.38**	**0.7958**	**35.02**	**11**	**0.0001**
80	**61,948**	**46,030**	**0.4643**	**36.31**	**0.7936**	**36.31**	**0.7933**	**34.95**	**16**	**0.001**
85	**62,087**	**45,984**	**0.3686**	**36.27**	**0.7906**	**36.28**	**0.7916**	**34.92**	**53**	**0.002**
86	**62,109**	**45,984**	**0.3421**	**36.27**	**0.7916**	**36.27**	**0.7917**	**34.92**	**37**	**0.002**

Table A.42: 31/2 in 13.3 lb/ft drill-pipe - 6 in bore-hole - 4°/100ft BG.

6	in	ID of the Well
3.5	in	OD of the Pipe
2.764	in	ID of the Pipe
11.2851	lb/ft	Weight of the Pipe - 13.3 lb/ft with 9.5 lb/gal mud
3E+7	lb/in^2	Modulus of Elasticity
-1145.952	ft	Radius of Curvature (Negative for Build)
0.0000001	(fraction)	Error in the radius of curvature
0.000001	(fraction)	Error in the clearance
0.00001	(fraction)	Error in the X-coordinate of the center of curvature
0.00001	(fraction)	Error in the Y-coordinate of the center of curvature
0.125		λ_{min}
100		Maximum number of iterations
Simple model results		
Lp	L	P
36.76	35.05	61655.69

θ (°)	P_c (lb)	P_v (lb)	L_d	L_i (ft)	g_i	L_f (ft)	g_f	L_t (ft)	$\#_{it}$	h
1	**61,617**	**61,392**	**0.8410**	**36.70**	**0.9963**	**36.70**	**0.9963**	**35.00**	**4**	**0.00001**
5	**62,499**	**61,372**	**0.8335**	**36.42**	**0.9820**	**36.42**	**0.9821**	**34.75**	**7**	**0.00001**
10	**63,575**	**61,330**	**0.8227**	**36.11**	**0.9650**	**36.08**	**0.9653**	**34.46**	**7**	**0.00001**
15	**64,599**	**61,252**	**0.8104**	**35.75**	**0.9498**	**35.77**	**0.9502**	**34.19**	**13**	**0.00001**
20	**65,565**	**61,142**	**0.7966**	**35.49**	**0.9360**	**35.49**	**0.9358**	**33.94**	**4**	**0.00001**
25	**66,518**	**61,053**	**0.7810**	**35.19**	**0.9233**	**35.22**	**0.9232**	**33.70**	**7**	**0.00001**
30	**67,360**	**60,894**	**0.7641**	**34.98**	**0.9114**	**34.98**	**0.9114**	**33.49**	**4**	**0.00001**
35	**68,170**	**60,753**	**0.7452**	**34.75**	**0.9006**	**34.76**	**0.9008**	**33.29**	**5**	**0.00001**
40	**68,882**	**60,569**	**0.7248**	**34.55**	**0.8921**	**34.56**	**0.8907**	**33.12**	**15**	**0.00001**
45	**69,582**	**60,438**	**0.7019**	**34.36**	**0.8809**	**34.38**	**0.8826**	**32.96**	**13**	**0.00001**
50	**70,207**	**60,300**	**0.6767**	**34.17**	**0.8766**	**34.22**	**0.8747**	**32.81**	**24**	**0.00001**
55	**70,782**	**60,189**	**0.6487**	**34.07**	**0.8686**	**34.07**	**0.8684**	**32.68**	**9**	**0.00001**
60	**71,220**	**60,020**	**0.6177**	**33.99**	**0.8615**	**33.96**	**0.8626**	**32.59**	**16**	**0.00001**
65	**71,611**	**59,890**	**0.5824**	**33.86**	**0.8569**	**33.87**	**0.8579**	**32.50**	**8**	**0.00001**
70	**71,971**	**59,818**	**0.5413**	**33.77**	**0.8534**	**33.78**	**0.8537**	**32.42**	**22**	**0.00001**
75	**72,246**	**59,755**	**0.4923**	**33.71**	**0.8499**	**33.71**	**0.8506**	**32.37**	**6**	**0.001**
80	**72,441**	**59,705**	**0.4304**	**33.67**	**0.8488**	**33.67**	**0.8487**	**32.33**	**6**	**0.002**
85	**72,586**	**59,703**	**0.3418**	**33.64**	**0.8475**	**33.64**	**0.8474**	**32.30**	**16**	**0.001**

Table A.43: 31/2 in 13.3 lb/ft drill-pipe - 6 in bore-hole - 5°/100ft BG.

6	in	ID of the Well
3.5	in	OD of the Pipe
2.764	in	ID of the Pipe
11.2851	lb/ft	Weight of the Pipe - 13.3 lb/ft with 9.5 lb/gal mud
3E+7	lb/in^2	Modulus of Elasticity
-954.9297	ft	Radius of Curvature (Negative for Build)
0.0000001	(fraction)	Error in the radius of curvature
0.000001	(fraction)	Error in the clearance
0.000001	(fraction)	Error in the X-coordinate of the center of curvature
0.00001	(fraction)	Error in the Y-coordinate of the center of curvature
0.25		λ_{min}
100		Maximum number of iterations
Simple model results		
Lp	L	P
33.55	31.99	73996.97

θ (°)	P_c (lb)	P_v (lb)	L_d	L_i (ft)	g_i	L_f (ft)	g_f	L_t (ft)	$\#_{it}$	h
1	**73,937**	**73,749**	**0.7681**	**33.52**	**0.9974**	**33.52**	**0.9974**	**31.96**	**7**	**0.00001**
5	**74,685**	**73,746**	**0.7629**	**33.33**	**0.9874**	**33.34**	**0.9874**	**31.80**	**12**	**0.00001**
10	**75,593**	**73,722**	**0.7551**	**33.13**	**0.9756**	**33.12**	**0.9756**	**31.61**	**7**	**0.00001**
15	**76,460**	**73,671**	**0.7456**	**32.92**	**0.9638**	**32.91**	**0.9644**	**31.44**	**5**	**0.00001**
20	**77,295**	**73,609**	**0.7345**	**32.72**	**0.9538**	**32.72**	**0.9538**	**31.27**	**10**	**0.00001**
25	**78,109**	**73,555**	**0.7216**	**32.54**	**0.9435**	**32.54**	**0.9443**	**31.10**	**13**	**0.00001**
30	**78,830**	**73,442**	**0.7072**	**32.38**	**0.9352**	**32.38**	**0.9352**	**30.96**	**8**	**0.0001**
35	**79,557**	**73,376**	**0.6909**	**32.21**	**0.9270**	**32.22**	**0.9269**	**30.82**	**7**	**0.0001**
40	**80,216**	**73,289**	**0.6726**	**32.09**	**0.9196**	**32.08**	**0.9196**	**30.70**	**4**	**0.0001**
45	**80,779**	**73,159**	**0.6525**	**31.98**	**0.9142**	**31.96**	**0.9125**	**30.60**	**13**	**0.0002**
50	**81,326**	**73,071**	**0.6298**	**31.82**	**0.9065**	**31.85**	**0.9065**	**30.49**	**17**	**0.0002**
55	**81,820**	**72,992**	**0.6044**	**31.73**	**0.9023**	**31.74**	**0.9015**	**30.40**	**9**	**0.00001**
60	**82,257**	**72,925**	**0.5758**	**31.65**	**0.8970**	**31.66**	**0.8967**	**30.33**	**8**	**0.00001**
65	**82,655**	**72,888**	**0.5430**	**31.58**	**0.8928**	**31.58**	**0.8931**	**30.26**	**22**	**0.000025**
70	**82,941**	**72,814**	**0.5051**	**31.53**	**0.8898**	**31.52**	**0.8897**	**30.21**	**55**	**0.000025**
75	**83,188**	**72,779**	**0.4596**	**31.46**	**0.8869**	**31.47**	**0.8873**	**30.16**	**32**	**0.002**
80	**83,374**	**72,761**	**0.4019**	**31.43**	**0.8558**	**31.44**	**0.8857**	**30.13**	**36**	**0.0001**
85	**83,493**	**72,757**	**0.3192**	**31.42**	**0.8845**	**31.42**	**0.8847**	**30.11**	**29**	**0.001**
87	**83,522**	**72,760**	**0.2693**	**31.41**	**0.8845**	**31.41**	**0.8845**	**30.11**	**10**	**0.001**

Table A.44: 31/2 in 13.3 lb/ft drill-pipe - 6 in bore-hole - 6°/100ft BG.

6	in	ID of the Well
3.5	in	OD of the Pipe
2.764	in	ID of the Pipe
11.2851	lb/ft	Weight of the Pipe - 13.3 lb/ft with 9.5 lb/gal mud
3E+7	lb/in^2	Modulus of Elasticity
-818.5111	ft	Radius of Curvature (Negative for Build)
0.0000001	(fraction)	Error in the radius of curvature
0.0000001	(fraction)	Error in the clearance
0.0000001	(fraction)	Error in the X-coordinate of the center of curvature
0.00001	(fraction)	Error in the Y-coordinate of the center of curvature
0.125		λ_{min}
100		Maximum number of iterations
Simple model results		
Lp	L	P
31.06	29.62	86329.61

θ (°)	P_c (lb)	P_v (lb)	L_d	L_i (ft)	g_i	L_f (ft)	g_f	L_t (ft)	$\#_{it}$	h
2	**86,424**	**86,102**	**0.7105**	**31.01**	**0.9962**	**31.01**	**0.9962**	**29.57**	**15**	**0.000001**
5	**86,905**	**86,100**	**0.7076**	**30.91**	**0.9907**	**30.92**	**0.9907**	**29.49**	**7**	**0.000001**
10	**87,686**	**86,082**	**0.7014**	**30.76**	**0.9815**	**30.77**	**0.9818**	**29.36**	**11**	**0.00001**
15	**88,435**	**86,044**	**0.6937**	**30.62**	**0.9733**	**30.62**	**0.9733**	**29.24**	**13**	**0.00001**
20	**89,168**	**86,009**	**0.6843**	**30.48**	**0.9650**	**30.49**	**0.9652**	**29.12**	**10**	**0.00001**
25	**89,890**	**85,986**	**0.6732**	**30.36**	**0.9574**	**30.36**	**0.9577**	**29.00**	**5**	**0.00001**
30	**90,522**	**85,904**	**0.6606**	**30.24**	**0.9507**	**30.24**	**0.9507**	**28.90**	**8**	**0.0001**
35	**91,148**	**85,849**	**0.6461**	**30.11**	**0.9444**	**30.13**	**0.9443**	**28.80**	**7**	**0.0001**
40	**91,731**	**85,794**	**0.6296**	**30.02**	**0.9381**	**30.03**	**0.9383**	**28.71**	**7**	**0.0001**
45	**92,289**	**85,758**	**0.6111**	**29.93**	**0.9326**	**29.93**	**0.933**	**28.63**	**3**	**0.0001**
50	**92,785**	**85,709**	**0.5903**	**29.85**	**0.9280**	**29.85**	**0.9281**	**28.55**	**5**	**0.0001**
55	**93,229**	**85,662**	**0.5669**	**29.79**	**0.9238**	**29.77**	**0.9240**	**28.49**	**8**	**0.0001**
60	**93,596**	**85,596**	**0.5404**	**29.70**	**0.9204**	**29.71**	**0.9203**	**28.43**	**7**	**0.0001**
65	**93,912**	**85,541**	**0.5100**	**29.65**	**0.9172**	**29.66**	**0.9170**	**28.39**	**50**	**0.0001**
70	**94,216**	**85,536**	**0.4745**	**29.60**	**0.9140**	**29.61**	**0.9146**	**28.34**	**27**	**0.0001**
75	**94,427**	**85,505**	**0.4319**	**29.58**	**0.9125**	**29.58**	**0.9125**	**28.31**	**41**	**0.0001**
77	**94,507**	**85,506**	**0.4120**	**29.57**	**0.9123**	**29.56**	**0.9120**	**28.30**	**7**	**0.0001**

Table A.45: 31/2 in 13.3 lb/ft drill-pipe - 6 in bore-hole - 7°/100ft BG.

6	in	ID of the Well
3.5	in	OD of the Pipe
2.764	in	ID of the Pipe
11.2851	lb/ft	Weight of the Pipe - 13.3 lb/ft with 9.5 lb/gal mud
3E+7	lb/in^2	Modulus of Elasticity
-572.9578	ft	Radius of Curvature (Negative for Build)
0.0000001	(fraction)	Error in the radius of curvature
0.000001	(fraction)	Error in the clearance
0.000001	(fraction)	Error in the X-coordinate of the center of curvature
0.000001	(fraction)	Error in the Y-coordinate of the center of curvature
0.125		λ_{min}
100		Maximum number of iterations
Simple model results		
Lp	L	P
25.99	24.78	123327.1

θ (°)	P_c (lb)	P_v (lb)	L_d	L_i (ft)	g_i	L_f (ft)	g_f	L_t (ft)	$\#_{it}$	h
1	**123,248**	**123,135**	**0.5953**	**25.98**	**0.9991**	**25.98**	**0.9991**	**24.77**	**7**	**0.00001**
5	**123,698**	**123,135**	**0.5934**	**25.93**	**0.9954**	**25.93**	**0.9954**	**24.73**	**6**	**0.00001**
10	**124,257**	**123,134**	**0.5897**	**25.87**	**0.9909**	**25.87**	**0.9909**	**24.67**	**4**	**0.00001**
15	**124,793**	**123,120**	**0.5846**	**25.80**	**0.9866**	**25.81**	**0.9866**	**24.62**	**5**	**0.00001**
20	**125,318**	**123,107**	**0.5779**	**25.75**	**0.9824**	**25.75**	**0.9824**	**24.57**	**5**	**0.00001**
25	**125,826**	**123,094**	**0.5697**	**25.69**	**0.9784**	**25.69**	**0.9784**	**24.52**	**8**	**0.00001**
30	**126,309**	**123,076**	**0.5600**	**25.64**	**0.9747**	**25.64**	**0.9747**	**24.47**	**5**	**0.0001**
35	**126,778**	**123,069**	**0.5486**	**25.59**	**0.9712**	**25.59**	**0.9711**	**24.43**	**2**	**0.0001**
40	**127,209**	**123,053**	**0.5355**	**25.55**	**0.9680**	**25.54**	**0.9679**	**24.39**	**6**	**0.0001**
45	**127,616**	**123,044**	**0.5206**	**25.49**	**0.9647**	**25.50**	**0.9650**	**24.35**	**4**	**0.0001**
50	**127,983**	**123,030**	**0.5035**	**25.46**	**0.9623**	**25.46**	**0.9622**	**24.32**	**14**	**0.0001**
55	**128,310**	**123,014**	**0.4841**	**25.42**	**0.9599**	**25.42**	**0.9598**	**24.29**	**7**	**0.0001**
60	**128,609**	**123,009**	**0.4619**	**25.39**	**0.9577**	**25.39**	**0.9577**	**24.26**	**2**	**0.0001**
65	**128,868**	**123,008**	**0.4362**	**25.37**	**0.9560**	**25.37**	**0.9559**	**24.24**	**9**	**0.0001**
70	**129,059**	**122,983**	**0.4062**	**25.35**	**0.9544**	**25.35**	**0.9544**	**24.22**	**7**	**0.0001**
73.5	**129,181**	**122,981**	**0.3816**	**25.34**	**0.9535**	**25.34**	**0.9535**	**24.21**	**12**	**0.0005**

Table A.46: 31/2 in 13.3 lb/ft drill-pipe - 6 in bore-hole - 10°/100ft BG.

6	in	ID of the Well
3.5	in	OD of the Pipe
2.764	in	ID of the Pipe
11.2851	lb/ft	Weight of the Pipe - 13.3 lb/ft with 9.5 lb/gal mud
3E+7	lb/in^2	Modulus of Elasticity
-477.4648	ft	Radius of Curvature (Negative for Build)
0.000001	(fraction)	Error in the radius of curvature
0.000001	(fraction)	Error in the clearance
0.000001	(fraction)	Error in the X-coordinate of the center of curvature
0.00001	(fraction)	Error in the Y-coordinate of the center of curvature
0.125		λ_{min}
100		Maximum number of iterations
Simple model results		
Lp	L	P
23.72	22.62	147991.9

θ ($^\circ$)	P_c (lb)	P_v (lb)	L_d	L_i (ft)	g_i	L_f (ft)	g_f	L_t (ft)	$\#_{it}$	h
2	**148,008**	**147,820**	**0.5433**	**23.71**	**0.9987**	**23.71**	**0.9987**	**22.61**	**5**	**0.00001**
5	**148,285**	**147,816**	**0.5421**	**23.69**	**0.9968**	**23.69**	**0.9968**	**22.59**	**5**	**0.00001**
10	**148,753**	**147,817**	**0.5391**	**23.65**	**0.9936**	**23.65**	**0.9937**	**22.55**	**4**	**0.00001**
15	**149,206**	**147,811**	**0.5348**	**23.61**	**0.9906**	**23.61**	**0.9906**	**22.52**	**10**	**0.00001**
20	**149,647**	**147,804**	**0.5290**	**23.57**	**0.9877**	**23.57**	**0.9877**	**22.49**	**13**	**0.00001**
25	**150,084**	**147,807**	**0.5219**	**23.53**	**0.9848**	**23.53**	**0.9849**	**22.45**	**6**	**0.00001**
30	**150,491**	**147,796**	**0.5133**	**23.50**	**0.9821**	**23.50**	**0.9821**	**22.42**	**49**	**0.00001**
30.2	**150,509**	**147,799**	**0.5129**	**23.50**	**0.9821**	**23.50**	**0.9821**	**22.42**	**16**	**0.0001**

Table A.47: $3^1/_2$ in 13.3 lb/ft drill-pipe - 6 in bore-hole - 12°/100ft BG.

Appendix B

Locus Of The Center Of Curvature

For any point (x, y) of the function $y = f(x) \in C^2(I \subset \mathbb{R}, \mathbb{R})$, $x \in I$, a tangent vector to the function $f(x)$ is given by

$$\vec{t}(x) = [1, f'(x)].$$

An unit normal vector to the tangent can be written as

$$\hat{n}(x) = \frac{1}{(1 + f'^2)^{\frac{1}{2}}} ft(-f', 1.$$

The tangent vector always points to increasing x and this unit normal vector always points to increasing y. The curvature κ of the function $f(x)$ at x is given by

$$\kappa = \frac{1}{\rho} = \frac{f''}{(1 + f'^2)^{\frac{3}{2}}}. \tag{B.1}$$

The radius of curvature ρ is finite provided that the point (x, y) is not an inflection point of the function. The radius ρ is positive for $f(x)$ convex at x (center of curvature above the curve) and negative for $f(x)$ concave at x (center of curvature below the curve) as shown in figure (B.1). Therefore, the vector $\vec{\rho}$ connecting the point (x, y) to its center $[x_c(x), y_c(x)]$ is given by

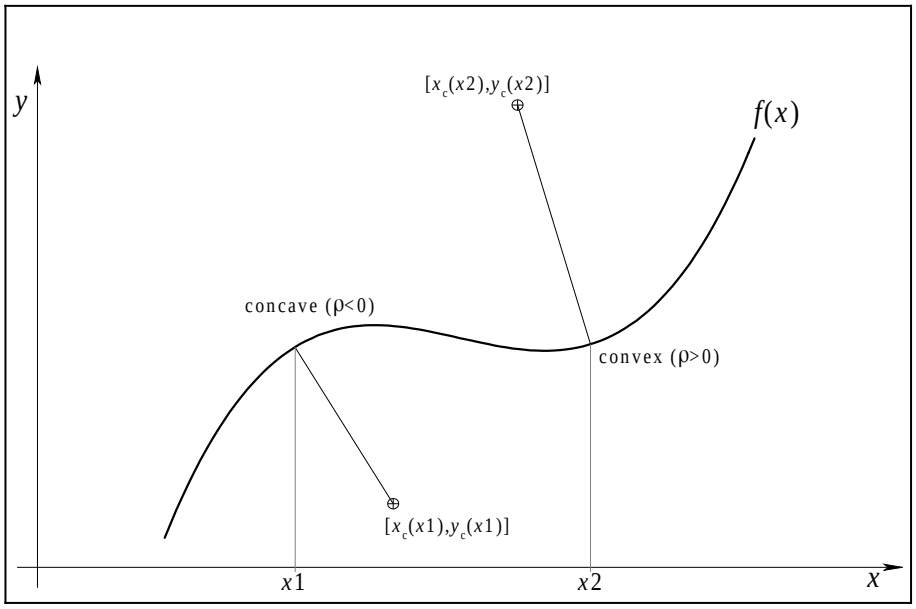

Figure B.1: Center of curvature of a function

$$\vec{\rho} = \rho\hat{n} = \frac{\left(1+f'^2\right)^{\frac{3}{2}}}{f''}\frac{1}{\left(1+f'^2\right)^{\frac{1}{2}}}(-f',1) = \frac{1+f'^2}{f''}(-f',1).$$

The center of curvature is given by $[x_{\mathrm{c}}(x), y_{\mathrm{c}}(x)] = (x,y) + \vec{\rho}$, which in parametric form results in

$$\begin{cases} x_{\mathrm{c}}(x) = x - \left[1+f'(x)^2\right]\dfrac{f'(x)}{f''(x)}, \\ y_{\mathrm{c}}(x) = f(x) + \left[1+f'(x)^2\right]\dfrac{1}{f''(x)}. \end{cases} \tag{B.2}$$

The radius of curvature ρ may be either positive or negative. However, the radius of a circle is always positive.

Appendix C

Euler-Lagrange Differential Equation And Boundary Conditions For F(x,y,y´,y´´)

Consider the functional given by

$$U(y) = \int_0^L F(x, y, y', y'')dx. \tag{C.1}$$

$U(y)$ is not function of x, since x is simply a dummy variable and the result of the integration is a scalar that depends only on y. The purpose here is to determine a function $y(x)$ that extremizes the functional. To do so, a *variation* $\bar{y}(x)$ of $y(x)$ is constructed in terms of any suitable continuous test function $\eta(x)$ and a scalar parameter ε as follows:

$$\bar{y}(x) = y(x) + \varepsilon\eta(x). \tag{C.2}$$

The function $\eta(x)$ and its derivatives must vanish in all points where $y(x)$ and its derivatives are specified. For ε sufficiently small, $U(\bar{y})$ will be close to the extreme value and becomes a function of ε, expressed as

$$\Phi(\varepsilon) = U(\bar{y}) = \int_0^L F(x, \bar{y}, \bar{y}', \bar{y}'')dx. \tag{C.3}$$

By definition, the scalar function $\Phi(\varepsilon)$ has the property $\Phi'(0)=0$. Differentiating Φ with respect ε to yields to

$$\frac{d\Phi}{d\varepsilon} = \frac{d}{d\varepsilon}\int_0^L F(x,\bar{y},\bar{y}',\bar{y}'')dx = \int_0^L \frac{d}{d\varepsilon}F(x,\bar{y},\bar{y}',\bar{y}'')dx. \tag{C.4}$$

Applying the chain rule to the integrand of the second integral results in

$$\frac{d}{d\varepsilon}F(x,\bar{y},\bar{y}',\bar{y}'') = \frac{\partial F}{\partial x}\frac{dx}{d\varepsilon} + \frac{\partial F}{\partial \bar{y}}\frac{d\bar{y}}{d\varepsilon} + \frac{\partial F}{\partial \bar{y}'}\frac{d\bar{y}'}{d\varepsilon} + \frac{\partial F}{\partial \bar{y}''}\frac{d\bar{y}''}{d\varepsilon}. \tag{C.5}$$

The following relations exist:

$$\frac{dx}{d\varepsilon}=0, \quad \frac{d\bar{y}}{d\varepsilon}=\eta(x), \quad \frac{d\bar{y}'}{d\varepsilon}=\eta'(x), \quad \frac{d\bar{y}''}{d\varepsilon}=\eta''(x),$$

such that Equation (C.5) becomes

$$\frac{d}{d\varepsilon}F(x,\bar{y},\bar{y}',\bar{y}'') = \frac{\partial F}{\partial \bar{y}}\eta + \frac{\partial F}{\partial \bar{y}'}\eta' + \frac{\partial F}{\partial \bar{y}''}\eta''. \tag{C.6}$$

Applying this results to Equation (C.4) and making $\varepsilon=0$ yields to

$$\Phi'(0) = 0 = \int_0^L \frac{\partial F}{\partial y}\eta dx + \int_0^L \frac{\partial F}{\partial y'}\eta' dx + \int_0^L \frac{\partial F}{\partial y''}\eta'' dx. \tag{C.7}$$

The second integral can be integrated by parts resulting inf''

$$\int_0^L \frac{\partial F}{\partial y'}\eta' dx = \left.\frac{\partial F}{\partial y'}\eta\right|_0^L - \int_0^L \frac{d}{dx}\left(\frac{\partial F}{\partial y'}\right)\eta dx.$$

Similarly, the third integral can be integrated by parts twice:

$$\begin{aligned}\int_0^L \frac{\partial F}{\partial y''}\eta'' dx &= \left.\frac{\partial F}{\partial y''}\eta'\right|_0^L - \int_0^L \frac{d}{dx}\left(\frac{\partial F}{\partial y''}\right)\eta' dx \\ &= \left.\frac{\partial F}{\partial y''}\eta'\right|_0^L - \left[\left.\frac{d}{dx}\left(\frac{\partial F}{\partial y''}\right)\eta\right|_0^L - \int_0^L \frac{d^2}{dx^2}\left(\frac{\partial F}{\partial y''}\right)\eta dx\right] \\ &= \left[\frac{\partial F}{\partial y''}\eta\prime - \frac{d}{dx}\left(\frac{\partial F}{\partial y''}\right)\eta\right]\Bigg|_0^L + \int_0^L \frac{d^2}{dx^2}\left(\frac{\partial F}{\partial y''}\right)\eta dx.\end{aligned}$$

Substituting these two integrals into Equation (C.7) and rearranging yields to

$$\begin{aligned}0 = \left.\frac{\partial F}{\partial y''}\eta'\right|_0^L + \left[\frac{\partial F}{\partial y'} - \frac{d}{dx}\left(\frac{\partial F}{\partial y''}\right)\right]\eta\Bigg|_0^L + \\ + \int_0^L \left[\frac{\partial F}{\partial y} - \frac{d}{dx}\left(\frac{\partial F}{\partial y'}\right) + \frac{d^2}{dx^2}\left(\frac{\partial F}{\partial y''}\right)\right]\eta dx.\end{aligned} \tag{C.8}$$

Equation (C.8) must be valid for any admissible function $\eta(x)$. The equality can only be obtained if all five terms in Equation (C.8) (four boundary terms and one integral) vanish. In particular, the term between brackets in the integrand must vanish identically. This fact gives rise to a differential equation called *Euler-Lagrange differential equation*, which must be satisfied by the function $y(x)$:

$$\frac{\partial F}{\partial y} - \frac{d}{dx}\left(\frac{\partial F}{\partial y'}\right) + \frac{d^2}{dx^2}\left(\frac{\partial F}{\partial y''}\right) = 0. \tag{C.9}$$

The order of this Euler-Lagrange differential equation is generally four (4), which requires four boundary conditions.

The boundary terms in Equation (C.8) must satisfy

$$\begin{cases} \left.\dfrac{\partial F}{\partial y''}\eta'\right|_0 = 0 \\ \left.\dfrac{\partial F}{\partial y''}\eta'\right|_L = 0 \\ \left.\left[\dfrac{\partial F}{\partial y'} - \dfrac{d}{dx}\left(\dfrac{\partial F}{\partial y''}\right)\right]\eta\right|_0 = 0 \\ \left.\left[\dfrac{\partial F}{\partial y'} - \dfrac{d}{dx}\left(\dfrac{\partial F}{\partial y''}\right)\right]\eta\right|_L = 0 \end{cases}$$

These terms indicate what kinds of boundary conditions are possible to impose to the function $y(x)$. Those boundary conditions are *appropriate*. Each boundary term is composed of a differential form (even identity) of the test function $\eta(x)$, multiplied by a coefficient in a differential form of *F*. If the function y (or its derivatives) is specified in any point of the boundary, the approximation $\bar{y}$ (or its derivatives) must assume the same values and hence the test function η (or its derivative η') must vanish there. Boundary conditions of these kinds are called *essential boundary conditions* and have always dimensions of y, y', etc. (displacement, slope, temperature, etc.).

If the essential boundary condition is *not* specified in one term, the *coefficient* of the term must be set to zero. Boundary conditions resulted from the associated term are called *natural boundary conditions* and have always physical meaning (force, moment, heat flux, etc.). An essential boundary condition and an associated natural boundary condition cannot be specified in the same point of the boundary. If that is so, not enough boundary conditions are left to make all boundary terms in Equation (C.8) vanish and the

equation cannot be satisfied. Therefore, any set of boundary condition involving one term of each of the following pairs is possible:

$$\begin{cases} y \quad or \quad \dfrac{\partial F}{\partial y'} - \dfrac{d}{dx}\left(\dfrac{\partial F}{\partial y''}\right) \\ y' \quad or \quad \dfrac{\partial F}{\partial y''} \end{cases} \tag{C.10}$$

Appendix D

Series Solution Of The Differential Equation
$\mathbf{y'''\text{–}x\,y' = \alpha x + 2b_3}$

The differential equation can be written as

$$(y')''\text{–}x\,y' = \alpha x + 2b_3.$$

Making $z(x) = y'(x)$ results in

$$z''\text{–}xz = \alpha x + 2b_3.$$

This differential equation is a non-homogeneous second order linear differential equation with non-constant coefficients. All points of its domain are ordinary points. The non-homogeneous term is a linear function of the independent variable *x*. A series solution for this differential equation can be written as

$$z(x) = \sum_{n=0}^{\infty} a_n x^n \tag{D.1}$$

where a_n are constants to be determined. Substituting Equation (D.1) into the differential equation yields to

$$z''\text{–}xz = \sum_{n=2}^{\infty} (n-1)n\,a_n x^{n-2} - x\sum_{n=0}^{\infty} a_n x^n = \alpha x + 2b_3,$$

or

$$\sum_{n=2}^{\infty}(n-1)n\,a_n x^{n-2}-\sum_{n=0}^{\infty}a_n x^{n+1}=\alpha x+2b_3.$$

A shift in the dummy index of the second summation results in

$$\sum_{n=2}^{\infty}(n-1)n\,a_n x^{n-2}-\sum_{n=3}^{\infty}a_{n-3} x^{n-2}=\alpha x+2b_3.$$

This can be written as

$$2(a_2-b_3)+(6a_3-a_0-\alpha)x+\sum_{n=4}^{\infty}\left[n(n-1)a_n-a_{n-3}\right]x^{n-2}=0$$

Since this identity is valid for any value of x in the domain, the following relations must be satisfied:

$$\begin{cases} a_0 \quad \text{and} \quad a_1 \quad \text{are arbitrary}, \\ a_2-b_3=0\Rightarrow a_2=b_3, \\ 6a_3-a_0-\alpha=0\Rightarrow a_3=\dfrac{\alpha+a_0}{6}, \\ (n-1)n\,a_n-a_{n-3}=0\Rightarrow a_n=\dfrac{a_{n-3}}{(n-1)n}, \quad n=4,5,6,\ldots. \end{cases} \tag{D.2}$$

The last relation in Equation (D.2) determines a recursive sequence whose first terms are

$$
\begin{array}{lll}
a_4 = \dfrac{a_1}{3{\cdot}4} & a_5 = \dfrac{a_2}{4{\cdot}5} = \dfrac{b_3}{4{\cdot}5} & a_6 = \dfrac{a_3}{5{\cdot}6} = \dfrac{1}{6}\,\dfrac{\alpha + a_0}{5{\cdot}6} \\
a_7 = \dfrac{a_4}{6{\cdot}7} = \dfrac{a_1}{3{\cdot}4{\cdot}6{\cdot}7} & a_8 = \dfrac{a_5}{7{\cdot}8} = \dfrac{b_3}{4{\cdot}5{\cdot}7{\cdot}8} & a_9 = \dfrac{a_6}{8{\cdot}9} = \dfrac{1}{6}\,\dfrac{\alpha + a_0}{5{\cdot}6{\cdot}8{\cdot}9} \\
a_{10} = \dfrac{a_1}{3{\cdot}4{\cdot}6{\cdot}7{\cdot}9{\cdot}10} & a_{11} = \dfrac{b_3}{4{\cdot}5{\cdot}7{\cdot}8{\cdot}10{\cdot}11} & a_{12} = \dfrac{1}{6}\,\dfrac{\alpha + a_0}{5{\cdot}6{\cdot}8{\cdot}9{\cdot}11{\cdot}12} \\
\vdots & \vdots & \vdots
\end{array}
$$

From this sequence, three sub-sequences become evident, whose general terms can be written for (3*n*+1), (3*n*+2) and (3*n*+3). The general term for (3*n*+1) is given by

$$
\begin{aligned}
a_{3n+1} &= \frac{a_1}{[3\cdot 4][6\cdot 7][9\cdot 10]\cdots[(3n-3)(3n-2)][(3n)(3n+1)]} \\
&= \frac{a_1}{[3\cdot 6\cdot 9\cdots(3n-3)(3n)][4\cdot 7\cdot 10\cdots(3n-2)(3n+1)]}.
\end{aligned}
$$

The first product between square brackets in the denominator of this expression can be written as

$$
3\cdot 6\cdot 9\cdots(3n-3)(3n) = 3^n\cdot 1\cdot 2\cdot 3\cdots(n-1)\cdot n = 3^n n!\,. \tag{D.3}
$$

The second product between square brackets in the denominator can be written as

$$
\begin{aligned}
&4\cdot 7\cdot 10\cdots(3n-2)(3n+1) = \\
&\qquad = 3^n\cdot\left(\frac{4}{3}\right)\left(1+\frac{4}{3}\right)\cdots\left(n-2+\frac{4}{3}\right)\left(n-1+\frac{4}{3}\right)\,.
\end{aligned}
$$

Using the recurrence formula for the Gamma function $\Gamma(1+z) = z\,\Gamma(z)$, or

$$z = \frac{\Gamma(1+z)}{\Gamma(z)},$$

we can write:

$$\begin{aligned} z(1+z)(2+z)\cdots(n-2+z)(n-1+z) = \\ \frac{\Gamma(1+z)}{\Gamma(z)}\frac{\Gamma(2+z)}{\Gamma(1+z)}\cdots\frac{\Gamma(n-1+z)}{\Gamma(n-2+z)}\frac{\Gamma(n+z)}{\Gamma(n-1+z)} = \frac{\Gamma(n+z)}{\Gamma(z)}. \end{aligned} \tag{D.4}$$

Making $z = \frac{4}{3}$ in this equation, the second product becomes

$$4\cdot 7\cdot 10\cdot\cdots\cdot(3n-2)(3n+1) = 3^n\frac{\Gamma(n+\frac{4}{3})}{\Gamma(\frac{4}{3})} = 3^n\left(\frac{4}{3}\right)_n, \tag{D.5}$$

where $(\xi)_n = \frac{\Gamma(n+\xi)}{\Gamma(\xi)}$ is the Pochhammer's symbol[1]. Hence the general term for (3n+1) using the results in Equations (D.4) and (D.5) is

$$a_{3n+1} = \frac{a_1}{9^n\left(\frac{4}{3}\right)_n n!} \qquad n = 1, 2, 3, \ldots. \tag{D.6}$$

---

1 Some properties of the Pochhammer's symbol are (see Abramowitz, 1972):
$(\xi)_n = \xi(\xi+1)(\xi+2)\cdots\cdot(\xi+n-1) = \Gamma(\xi+n)/\Gamma(\xi)$
$(\xi)_0 = 1$
$(\xi)_1 = \xi$
$(1)_n = n!$
$(\xi)_n = \xi(1+\xi)_{n-1}$
$\xi(1+\xi)_n = (n+\xi)(\xi)_n$

The general term for (3*n*+2) is given by

$$a_{3n+2} = \frac{b_3}{[4\cdot 5][7\cdot 8][10\cdot 11]\cdots[(3n-2)(3n-1)][(3n+1)(3n+2)]} = \\ = \frac{b_3}{[4\cdot 7\cdot 10\cdots(3n-2)(3n+1)][5\cdot 8\cdot 11\cdots(3n-1)(3n+2)]}\,.$$

The first product between square brackets in the denominator of this expression was already found and is given by Equation (D.5). The second product between square brackets in the denominator can be obtained in the same fashion:

$$5\cdot 8\cdot 11\cdots(3n-1)(3n+2) = \\ = 3^n\cdot\left(\frac{5}{3}\right)\left(1+\frac{5}{3}\right)\cdots\left(n-2+\frac{5}{3}\right)\left(n-1+\frac{5}{3}\right).$$

Making $z=\frac{5}{3}$ in Equation (D.4) the first product becomes

$$5\cdot 8\cdot 11\cdots(3n-1)(3n+2) = 3^n\frac{\Gamma(n+\frac{5}{3})}{\Gamma(\frac{5}{3})} = 3^n\left(\frac{5}{3}\right)_n. \qquad \text{(D.7)}$$

Consequently the general term for (3n+2) is

$$a_{3n+2} = \frac{b_3}{9^n\left(\frac{4}{3}\right)_n\left(\frac{5}{3}\right)_n} \qquad n=1,2,3,\ldots. \qquad \text{(D.8)}$$

The general term for (3*n*+3) is given by

$$
\begin{aligned}
a_{3n+3} &= \frac{1}{6}\frac{\alpha + a_0}{[5\cdot 6][8\cdot 9][11\cdot 12]\cdots[(3n-1)(3n)][(3n+2)(3n+3)]} \\
&= \frac{1}{2\cdot 3}\frac{\alpha + a_0}{[5\cdot 8\cdot 11\cdots[(3n-1)(3n+2)][6\cdot 9\cdot 12\cdots(3n)(3n+3)]} \\
&= \frac{\alpha + a_0}{[2\cdot 5\cdot 8\cdot 11\cdots[(3n-1)(3n+2)][3\cdot 6\cdot 9\cdot 12\cdots(3n)(3n+3)]}.
\end{aligned}
$$

The first product between square brackets in the denominator of the previous equation is similar to that in Equation (D.7) and can be written as

$$
\begin{aligned}
2\cdot 5\cdot 8\cdot 11\cdots(3n-1)(3n+2) = \\
3^{n+1}\left(\frac{2}{3}\right)\left(1+\frac{2}{3}\right)\left(2+\frac{2}{3}\right)\cdots\left(n-1+\frac{2}{3}\right)\left(n+\frac{2}{3}\right).
\end{aligned}
$$

Note the number of terms (n+1) due to embedding the fraction $\frac{1}{6} = \frac{1}{2\cdot 3}$ into the product within the square brackets[2]. Making $z = \frac{2}{3}$ in the recurrence formula for the Gamma function yields to

$$
2\cdot 5\cdot 8\cdot 11\cdots(3n-1)(3n+2) = 3^{n+1}\frac{\Gamma(n+1+\frac{2}{3})}{\Gamma(\frac{2}{3})} = 3^{n+1}\left(\frac{2}{3}\right)_{n+1}.
$$

The second product between square brackets in the denominator is given by

$$
3\cdot 6\cdot 9\cdot 12\cdots(3n)(3n+3) = 3^{n+1}\cdot 1\cdot 2\cdot 3\cdots n\cdot(n+1) = 3^{n+1}(n+1)!\,.
$$

Consequently the general term for (3n+3) becomes

---

2 Not surprising, since $(3n+3)$ can be re-written as $3(n+1)$.

$$a_{3n+3} = a_{3(n+1)} = \frac{\alpha + a_0}{9^{n+1}\left(\frac{2}{3}\right)_{n+1}(n+1)!} \qquad n = 1, 2, 3, \ldots .$$

Shifting the dummy index by 1 results in

$$a_{3n} = \frac{\alpha + a_0}{9^{n}\left(\frac{2}{3}\right)_{n} n!} \qquad n = 2, 3, 4, \ldots . \tag{D.9}$$

The solution *z*(*x*) given by Equation (D.1) can be written in terms of the coefficients given by Equations (D.2), (D.6), (D.8), and (D.9):

$$z(x) = a_0 + a_1 x + b_3 x^2 + \frac{\alpha + a_0}{6} x^3 + a_1 \sum_{n=1}^{\infty} \frac{x^{3n+1}}{9^n \left(\frac{4}{3}\right)_n n!} +$$

$$b_3 \sum_{n=1}^{\infty} \frac{x^{3n+2}}{9^n \left(\frac{4}{3}\right)_n \left(\frac{5}{3}\right)_n} + (\alpha + a_0) \sum_{n=2}^{\infty} \frac{x^{3n}}{9^n \left(\frac{2}{3}\right)_n n!}.$$

Making $n = 0$ in the first summation of the equation above we obtain

$$a_1 \frac{x^1}{9^0 \left(\frac{4}{3}\right)_0 0!} = a_1 x.$$

Therefore the term $a_1 x$ can be embedded in the first summation and the limits extended to start at $n = 0$:

$$z(x) = a_0 + b_3 x^2 + \frac{\alpha + a_0}{6} x^3 + a_1 \sum_{n=0}^{\infty} \frac{x^{3n+1}}{9^n \left(\frac{4}{3}\right)_n n!} +$$

$$b_3 \sum_{n=1}^{\infty} \frac{x^{3n+2}}{9^n \left(\frac{4}{3}\right)_n \left(\frac{5}{3}\right)_n} + (\alpha + a_0) \sum_{n=2}^{\infty} \frac{x^{3n}}{9^n \left(\frac{2}{3}\right)_n n!}.$$

Analogously, making $n = 0$ in the second summation we obtain

$$b_3 \frac{x^2}{9^0 \left(\frac{4}{3}\right)_0 \left(\frac{5}{3}\right)_0} = b_3 x^2,$$

and now the term $b_3 x^2$ can be embedded in the second summation and the limits extended to start at $n = 0$:

$$z(x) = a_0 + \frac{\alpha + a_0}{6} x^3 + a_1 \sum_{n=0}^{\infty} \frac{x^{3n+1}}{9^n \left(\frac{4}{3}\right)_n n!} +$$

$$b_3 \sum_{n=0}^{\infty} \frac{x^{3n+2}}{9^n \left(\frac{4}{3}\right)_n \left(\frac{5}{3}\right)_n} + (\alpha + a_0) \sum_{n=2}^{\infty} \frac{x^{3n}}{9^n \left(\frac{2}{3}\right)_n n!}.$$

Finally, making $n = 0$ and $n = 1$ in the third summation result in

$$(\alpha + a_0) \frac{x^0}{9^0 \left(\frac{2}{3}\right)_0} = (\alpha + a_0),$$

$$(\alpha + a_0) \frac{x^3}{9^1 \left(\frac{2}{3}\right)_1} = \frac{\alpha + a_0}{6} x^3.$$

The term $\frac{\alpha+a_0}{6}x^3$ can be embedded in the third summation and the limits extended to start at $n=1$. To extend the summation limits to start at $n=0$ the missing term must be included. Since $a_0=(\alpha+a_0)-\alpha$, the expression for $z(x)$ becomes:

$$z(x)=a_1\sum_{n=0}^{\infty}\frac{x^{3n+1}}{9^n\left(\frac{4}{3}\right)_n n!}+b_3\sum_{n=0}^{\infty}\frac{x^{3n+2}}{9^n\left(\frac{4}{3}\right)_n\left(\frac{5}{3}\right)_n}+(\alpha+a_0)\sum_{n=0}^{\infty}\frac{x^{3n}}{9^n\left(\frac{2}{3}\right)_n n!}-\alpha.$$

An appropriate rearrangement yields to

$$\begin{aligned}z(x)=(\alpha+a_0)\sum_{n=0}^{\infty}\frac{\left(\frac{x^3}{9}\right)^n}{\left(\frac{2}{3}\right)_n n!}+\\ a_1x\sum_{n=0}^{\infty}\frac{\left(\frac{x^3}{9}\right)^n}{\left(\frac{4}{3}\right)_n n!}+b_3x^2\sum_{n=0}^{\infty}\frac{\left(\frac{x^3}{9}\right)^n}{\left(\frac{4}{3}\right)_n\left(\frac{5}{3}\right)_n}-\alpha.\end{aligned}\qquad\text{(D.10)}$$

The structure of Equation (D.10) is convenient because the three summations represent specific cases of the mathematical functions known as *Generalized Hypergeometric Functions* (Erdélyi - vol. I). These functions are extremely versatile and many elementary and special functions as well as some integral functions may be defined in terms of these functions (Lebedev - 1972). The generalized hypergeometric functions are defined in terms of infinite series as follows:[3]

3 Including some of its common notations.

$$ {}_pF_q(\alpha_1,\alpha_2,\ldots,\alpha_p;\beta_1,\beta_2,\ldots,\beta_p;z) = {}_pF_q(\alpha_{\rm p};\beta_{\rm q};z) = $$

$$ {}_pF_q\left(\begin{smallmatrix}\alpha_{\rm p}\\ \beta_{\rm q}\end{smallmatrix};z\right) = \sum_{n=0}^{\infty} \frac{\prod_{r=1}^{p}(\alpha_r)_n}{\prod_{s=1}^{q}(\beta_s)_n}\frac{z^n}{n!} = \sum_{n=0}^{\infty}\frac{(\alpha_{\rm p})_n}{(\beta_{\rm q})_n}\frac{z^n}{n!} \quad {}^{4,5,6} \tag{D.11} $$

The first and second summations of Equation (D.10) may be immediately written down from this definition as

$$ \sum_{n=0}^{\infty}\frac{\left(\frac{x^3}{9}\right)^n}{\left(\frac{2}{3}\right)_n n!} = {}_0F_1\left(\frac{2}{3};\frac{x^3}{9}\right) $$

$$ \sum_{n=0}^{\infty}\frac{\left(\frac{x^3}{9}\right)^n}{\left(\frac{4}{3}\right)_n n!} = {}_0F_1\left(\frac{4}{3};\frac{x^3}{9}\right) $$

The third summation requires a simple adjustment before it can be written as a hypergeometric function. Multiplying and dividing the general term by $n!$, and using the fact that $(1)_n = n!$ results in

4 In the realm of functions ${}_pF_q$ and others, the compact notation $\xi_{\rm p}$ (with a roman letter subscript) represents a list of p elements $\{\xi_1,\xi_2,\ldots,\xi_p\}$ and should not be confused with the the last element of the list ξ_p (with an *italic* letter subscript).

5 In the function ${}_pF_q$, ";" separates the parameter lists and the variable z, and "," separates the elements of a list. The stacked notation is further compacted and reinforces the nominator and denominator parameters.

6 A Pochhammer' symbol of a list is interpreted as the the product of the Pochhammer's of the list's elements: $(\xi_{\rm r})_k = \prod_{i=1}^{r}(\xi_i)_k$

$$\sum_{n=0}^{\infty} \frac{\left(\frac{x^3}{9}\right)^n}{\left(\frac{4}{3}\right)_n \left(\frac{5}{3}\right)_n} = \sum_{n=0}^{\infty} \frac{(1)_n \left(\frac{x^3}{9}\right)^n}{\left(\frac{4}{3}\right)_n \left(\frac{5}{3}\right)_n n!} = {}_1F_2\left(1; \frac{4}{3}, \frac{5}{3}; \frac{x^3}{9}\right).$$

Therefore, the general solution of the differential equation is

$$\begin{aligned} z(x) = (\alpha + a_0)\, {}_0F_1\left(\frac{2}{3}; \frac{x^3}{9}\right) + a_1 x\, {}_0F_1\left(\frac{4}{3}; \frac{x^3}{9}\right) \\ + b_3 x^2\, {}_1F_2\left(1; \frac{4}{3}, \frac{5}{3}; \frac{x^3}{9}\right) - \alpha. \end{aligned} \tag{D.12}$$

It is important to stress that a_0 and a_1 are two arbitrary constants as required by a second order linear differential equations. The parameter b_3 is also arbitrary, because it includes the integration constant c as it appears in Equation (4.20). A fourth arbitrary constant will occur when $z(x)$ is integrated to obtain the solution $y(x)$ of the generalized beam-column. On the other hand, α is a determined constant[7] as in Equation (4.24).

The first derivative of $z(x)$ must also be determined. The derivative is calculated differentiating each term of Equation (D.12). Differentiating the first term results in

7 The integration constant $\alpha$is distinct from the list of parameters α_{p} and its elements α_i.

$$\frac{d}{dx}\left[{}_0F_1\left(\frac{2}{3};\frac{x^3}{9}\right)\right]=\frac{d}{dx}\sum_{n=0}^{\infty}\frac{\left(\frac{x^3}{9}\right)^n}{\left(\frac{2}{3}\right)_n n!}=\frac{x^2}{3}\sum_{n=1}^{\infty}\frac{n\left(\frac{x^3}{9}\right)^{n-1}}{\left(\frac{2}{3}\right)_n n!}$$
$$=\frac{x^2}{3}\sum_{n=1}^{\infty}\frac{\left(\frac{x^3}{9}\right)^{n-1}}{\frac{2}{3}\left(\frac{5}{3}\right)_{n-1}(n-1)!}=\frac{x^2}{2}\sum_{n=0}^{\infty}\frac{\left(\frac{x^3}{9}\right)^n}{\left(\frac{5}{3}\right)_n n!}$$
$$=\frac{x^2}{2}{}_0F_1\left(\frac{5}{3};\frac{x^3}{9}\right)$$

where the property $(\xi)_n=\xi(1+\xi)_{n-1}$ was used for $\left(\frac{2}{3}\right)_n$.

Differentiating the second term yields to

$$\frac{d}{dx}\left[x_0F_1\left(\frac{4}{3};\frac{x^3}{9}\right)\right]=\frac{d}{dx}\left[x\sum_{n=0}^{\infty}\frac{\left(\frac{x^3}{9}\right)^n}{\left(\frac{4}{3}\right)_n n!}\right]=\frac{d}{dx}\sum_{n=0}^{\infty}\frac{\left(\frac{x^{3n+1}}{9^n}\right)}{\left(\frac{4}{3}\right)_n n!}$$
$$=\sum_{n=0}^{\infty}\frac{(3n+1)\left(\frac{x^3}{9}\right)^n}{\left(\frac{4}{3}\right)_n n!}=3\sum_{n=1}^{\infty}\frac{\left(n+\frac{1}{3}\right)\left(\frac{x^3}{9}\right)^n}{\left(\frac{4}{3}\right)_n n!}$$
$$=\sum_{n=0}^{\infty}\frac{\left(\frac{x^3}{9}\right)^n}{\left(\frac{1}{3}\right)_n n!}={}_0F_1\left(\frac{1}{3};\frac{x^3}{9}\right),$$

where the property $\xi(1+\xi)_n=(n+\xi)(\xi)_n$ was used for $\xi=\left(n+\frac{1}{3}\right)$.

Finally, differentiating the third term results in

$$\frac{d}{dx}\left[x^2{}_1F_2\left(1;\frac{4}{3};\frac{5}{3};\frac{x^3}{9}\right)\right]=\frac{d}{dx}\left[x^2\sum_{n=0}^{\infty}\frac{(1)_n\left(\frac{x^3}{9}\right)^n}{\left(\frac{4}{3}\right)_n\left(\frac{5}{3}\right)_n n!}\right]$$

$$=\frac{d}{dx}\left[\sum_{n=0}^{\infty}\frac{(1)_n\left(\frac{x^{3n+2}}{9^n}\right)}{\left(\frac{4}{3}\right)_n\left(\frac{5}{3}\right)_n n!}\right]=3x\sum_{n=0}^{\infty}\frac{\left(n+\frac{2}{3}\right)(1)_n\left(\frac{x^3}{9}\right)^n}{\left(\frac{4}{3}\right)_n\left(\frac{5}{3}\right)_n n!}$$

$$=2x\sum_{n=0}^{\infty}\frac{(1)_n\left(\frac{x^3}{9}\right)^n}{\left(\frac{4}{3}\right)_n\left(\frac{2}{3}\right)_n n!}=2x\,{}_1F_2\left(1;\frac{2}{3},\frac{4}{3};\frac{x^3}{9}\right),$$

where here the property $\xi(1+\xi)_n=(n+\xi)(\xi)_n$ was used for $\xi=\left(n+\frac{2}{3}\right)$. Therefore, the derivative of $z(x)$ is:

$$z'(x)=(\alpha+a_0)\frac{x^2}{2}{}_0F_1\left(\frac{5}{3};\frac{x^3}{9}\right)+a_1\,{}_0F_1\left(\frac{1}{3};\frac{x^3}{9}\right)+2b_3x\,{}_1F_2\left(1;\frac{2}{3},\frac{4}{3};\frac{x^3}{9}\right). \quad \text{(D.13)}$$

The final step is the integration of $z(x)$ to obtain $y(x)$, using the summation form of the hypergeometric functions. In the end, an integration constant is introduced. Integrating each term of Equation (D.12), the first term yields to

$$\int {}_0F_1\left(\frac{2}{3};\frac{x^3}{9}\right)dx=\int\sum_{n=0}^{\infty}\frac{\left(\frac{x^3}{9}\right)^n}{\left(\frac{2}{3}\right)_n n!}dx=\sum_{n=0}^{\infty}\frac{x\left(\frac{x^3}{9}\right)^n}{(3n+1)\left(\frac{2}{3}\right)_n n!}$$

$$=\frac{x}{3}\sum_{n=0}^{\infty}\frac{\left(\frac{x^3}{9}\right)^n}{\left(n+\frac{1}{3}\right)\left(\frac{2}{3}\right)_n n!}=x\sum_{n=0}^{\infty}\frac{\left(\frac{1}{3}\right)_n\left(\frac{x^3}{9}\right)^n}{\left(\frac{4}{3}\right)_n\left(\frac{2}{3}\right)_n n!}=x\,{}_1F_2\left(\frac{1}{3};\frac{2}{3};\frac{4}{3};\frac{x^3}{9}\right),$$

where the property $\xi(1+\xi)_n=(n+\xi)(\xi)_n$ was used again for $\xi=\left(n+\frac{1}{3}\right)$. The integration of the second term is given by

$$\int x\,{}_0F_1\left(\frac{4}{3};\frac{x^3}{9}\right)dx=\int x\sum_{n=0}^{\infty}\frac{\left(\frac{x^3}{9}\right)^n}{\left(\frac{4}{3}\right)_n n!}dx=\sum_{n=0}^{\infty}\frac{x^2\left(\frac{x^3}{9}\right)^n}{(3n+2)\left(\frac{4}{3}\right)_n n!}$$
$$=\frac{x^2}{3}\sum_{n=0}^{\infty}\frac{\left(\frac{x^3}{9}\right)^n}{(n+\frac{2}{3})\left(\frac{4}{3}\right)_n n!}=\frac{x^2}{2}\sum_{n=0}^{\infty}\frac{\left(\frac{2}{3}\right)_n\left(\frac{x^3}{9}\right)^n}{\left(\frac{4}{3}\right)_n\left(\frac{5}{3}\right)_n n!}=\frac{x^2}{2}\,{}_1F_2\left(\frac{2}{3};\frac{4}{3};\frac{5}{3};\frac{x^3}{9}\right).$$

where the property $\xi(1+\xi)_n=(n+\xi)(\xi)_n$ was used again for $\xi=\left(n+\frac{2}{3}\right)$. Finally, the integration of the third term gives

$$\int x^2\,{}_1F_2\left(1;\frac{4}{3};\frac{5}{3};\frac{x^3}{9}\right)=\int x^2\sum_{n=0}^{\infty}\frac{(1)_h\left(\frac{x^3}{9}\right)^n}{\left(\frac{4}{3}\right)_n\left(\frac{5}{3}\right)_n n!}dx$$
$$=\frac{x^3}{3}\sum_{n=0}^{\infty}\frac{(1)_h\left(\frac{x^3}{9}\right)^n}{(n+1)\left(\frac{4}{3}\right)_n\left(\frac{5}{3}\right)_n n!}=\frac{x^3}{3}\sum_{n=0}^{\infty}\frac{(1)_h\,(1)_h\left(\frac{x^3}{9}\right)^n}{\left(\frac{4}{3}\right)_n\left(\frac{5}{3}\right)_n(2)_h\,n!}$$
$$=\frac{x^3}{3}\,{}_2F_3\left(1,1;\frac{4}{3},\frac{5}{3},2;\frac{x^3}{9}\right).$$

Where now the property $\xi(1+\xi)_n=(n+\xi)(\xi)_n$ was user for $\xi=(n+1)$. Therefore, the integral of $z(x)$, and consequently the expression of $y(x)$, is given by

$$\begin{aligned}y(x)=(\alpha+a_0)x\,{}_1F_2\left(\frac{1}{3};\frac{2}{3};\frac{4}{3};\frac{x^3}{9}\right)+a_1\frac{x^2}{2}\,{}_1F_2\left(\frac{2}{3};\frac{4}{3};\frac{5}{3};\frac{x^3}{9}\right)\\+b_3\frac{x^3}{3}\,{}_2F_3\left(1,1;\frac{4}{3},\frac{5}{3},2;\frac{x^3}{9}\right)+b_4-\alpha x.\end{aligned}\tag{D.14}$$

where b_4 is an integration constant that accounts for the integrals above. The differential equation object of this appendix was obtained from the integration of the fourth order differential equation that governs the physical phenomenon of buckling. This integration, after a change of variables, led to the undetermined constant b_3. Therefore, b_3, although treated here as a parameter, is also an undetermined constant as are a_0, a_1, and b_4. In this differential equation, α is a parameter determined by the geometry and the material of the beam-column. However, the coefficient $(\alpha + a_0)$ is undetermined and can be renamed to b_1. Making $a_1 = b_2$, the general solution of the fourth order differential equation, and its first and second derivatives are given, from Equations (D.14), (D.12), and (D.13) respectively, by

$$y(x) = b_1 x\,{}_1F_2\left(\frac{1}{3}; \frac{2}{3}; \frac{4}{3}; \frac{x^3}{9}\right) + b_2 \frac{x^2}{2}\,{}_1F_2\left(\frac{2}{3}; \frac{4}{3}; \frac{5}{3}; \frac{x^3}{9}\right) + b_3 \frac{x^3}{3}\,{}_2F_3\left(1, 1; \frac{4}{3}, \frac{5}{3}, 2; \frac{x^3}{9}\right) + b_4 - \alpha x, \tag{D.15}$$

$$y'(x) = b_1\,{}_0F_1\left(\frac{2}{3}; \frac{x^3}{9}\right) + b_2 x\,{}_0F_1\left(\frac{4}{3}; \frac{x^3}{9}\right) + b_3 x^2\,{}_1F_2\left(1; \frac{4}{3}, \frac{5}{3}; \frac{x^3}{9}\right) - \alpha, \tag{D.16}$$

$$y''(x) = b_1 \frac{x^2}{2}\,{}_0F_1\left(\frac{5}{3}; \frac{x^3}{9}\right) + b_2\,{}_0F_1\left(\frac{1}{3}; \frac{x^3}{9}\right) + 2b_3 x\,{}_1F_2\left(1; \frac{2}{3}, \frac{4}{3}; \frac{x^3}{9}\right). \tag{D.17}$$

Equation (D.15) is, therefore, the *general solution of the non-homogeneous fourth order linear differential equation with its associated four undetermined constants*, which governs the deflections of a generalized beam-column, subjected to a constant distributed weight and an axial force.

Appendix E

Numerical Evaluation Of The Hypergeometric Functions

There are several forms to evaluate functions. Depending on the function, some specific techniques are more appropriate than others. In addition to the technique used, the form the functions will be employed affects the way the procedure must be implemented. Therefore, before a technique is chosen it should be conceived how the function will be used.

There is no intention here either in finding out the best way to generate these functions or in developing a thorough numerical analysis to determine the rate of convergence, the degree of accuracy, and the degree of stability. All needed is a reliable process, if possible fast, that furnishes accurate values of these functions within the required range. However some analysis is needed to understand how the functions behave.

The convergence of the generalized hypergeometric functions of the form ${}_pF_q$ is determined as follows (Luke 1969):

$$ {}_pF_q \begin{cases} \text{converges for all finite z if } p \leq q \\ \text{converges for } |z| < 1 \text{ if } p = q + 1^{1} \\ \text{diverges for all } z \neq 0 \text{ if } p > q + 1 \end{cases} $$

As an example, the Gauss hypergeometric function ${}_2F_1$ converges only in the open circle of radius *one* about the origin. For $p \leq q$, as in the confluent hypergeometric function ${}_1F_1$ and all hypergeometric functions occurring here, the radius of convergence is infinite,

1 Except for special cases of the numerator parameters in which the series terminates.

that is, the function converges for all finite value of its argument as a simple ratio test shows.

Three methods were used to generate the hypergeometric functions: series expansion, path integration of differential equation, and asymptotic expansion.

E.1 Series Expansion of the Functions

For functions defined by infinite series, one approach is to add the terms of the series until the required accuracy is reached, normally the machine accuracy. However the finite representation of digital calculations in some cases limits the use of this method. This occurs to the hypergeometric functions. These functions have an oscillatory behavior for negative values of the argument *x*. The terms of the series alternate sign and the positive and negative terms balance each other toward convergence. These terms, starting with *n*=0, increase in module until a value n_N is reached (function of *x* and the parameters of the function), after which the terms decrease in module toward zero. For values of *x* large enough, the absolute values of the terms go beyond the exact representation of the machine and truncations occur. These truncations destroy the balance between the alternating terms and numerical stability is lost. Figure (E.1) shows the plot of the function $R_1(x) = {}_0F_1\left(\frac{2}{3}; \frac{x^3}{9}\right)$ using series expansion with 15 digits floating point arithmetic (f.p.a.). Stability is lost at about $x = -15$. The reason the series becomes unstable about $x = -15$ can be seen if the term of maximum magnitude (in absolute value) of the series is calculated for $x = -15$. The general term of the series is given by

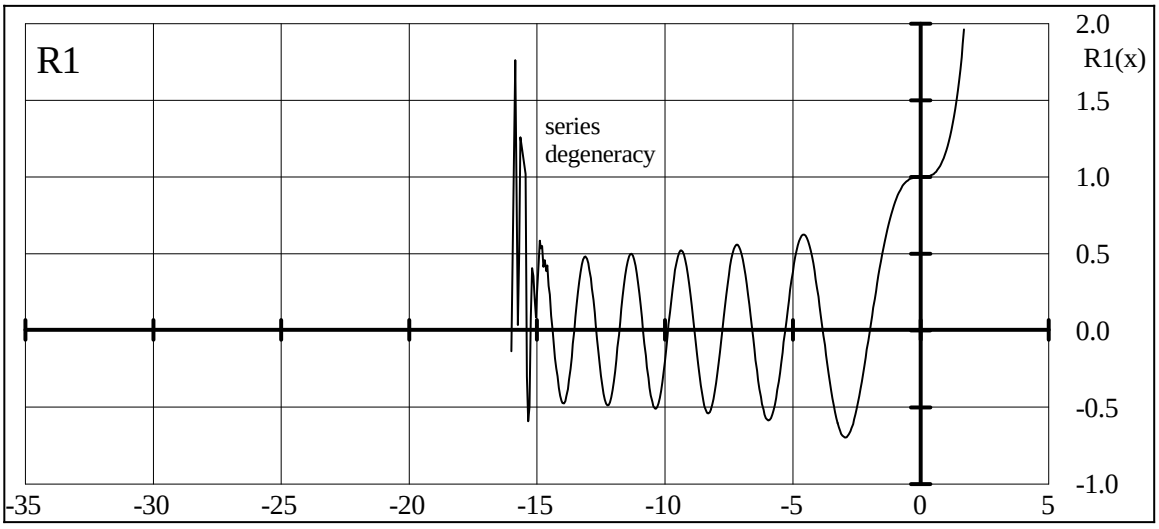

Figure E.1: Plot of $R_1(x)$ using series expansion with 15 digits f.p.a.

$$s_n = \frac{\left(\frac{x^3}{9}\right)^n}{\left(\frac{2}{3}\right)_n n!}.$$

For $x = -10$, the term s_n grows in module up to $n = 10$ whose value is

$$s_{10} = 0.642444496623549 \times 10^8.$$

Using 15 digits f.p.a. this term is accurate and precise, and the error associated is that due to round-off error. The same occurs for $x = -14$ in which the maximum term occurs for $n = 18$, whose value is

$$s_{18} = 0.451460366997291 \times 10^{14}.$$

However, for values of x a bit larger, the internal representation limit is reached (for 15 digits f.p.a.) and truncation appears. For $x=-15$ the maximum term occurs for $n=19$ whose value is

$$s_{19} = -0.198081806065064 \times 10^{16}.$$

This is the same as (using 15 digits f.p.a)

$$s_{19} = -1,980,818,060,650,640$$

If 32 digits f.p.a. is used the figure is

$$s_{19} \;=\; -1,980,818,060,650,637.594.$$

The difference on the values using 15 digits f.p.a. and 32 f.p.a is of magnitude 2.7064. It is small compared to the order of magnitude of the numbers but large if compared to the value of the function at the point $R_1(-15)=0.335617149....$ The same phenomenon occurs to other hypergeometric functions. Graphs of the remaining eight functions generated with series expansion using 15 digits f.p.a. are shown next.

A temporary solution to the truncation error is to increase the number of digits used in f.p.a. routines. This can be implemented by hardware or by software. However this does not solve the problem but instead pushes the breaking point a little further. Using 30 digits f.p.a. the function R_1, for example, becomes unstable at $x=-23$. Since the value of the argument x will be about negative hundreds, another method is needed to calculate these functions.

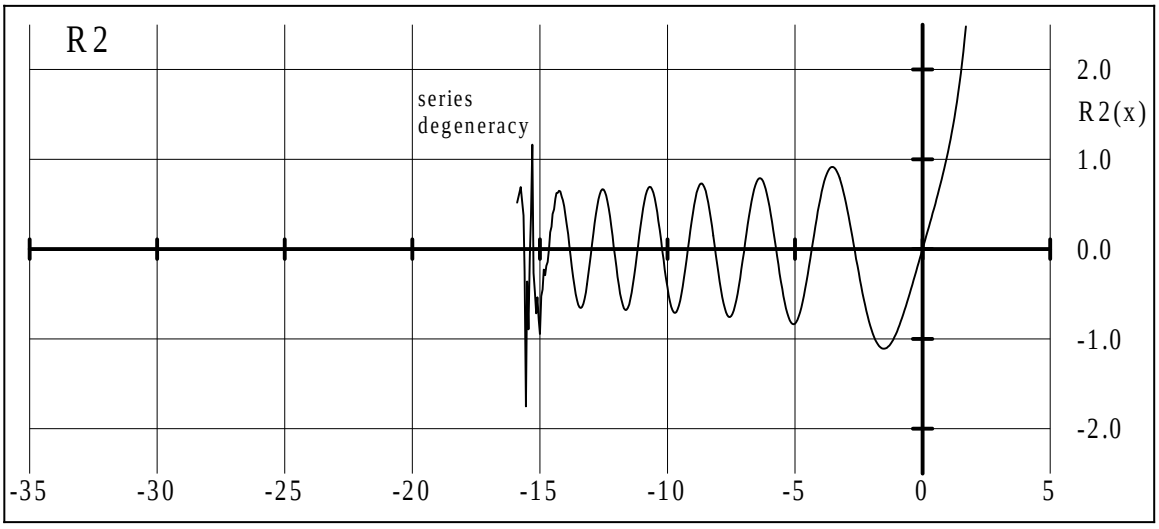

Figure E.2: Plot of $R_2(x)$ using series expansion with 15 digits f.p.a.

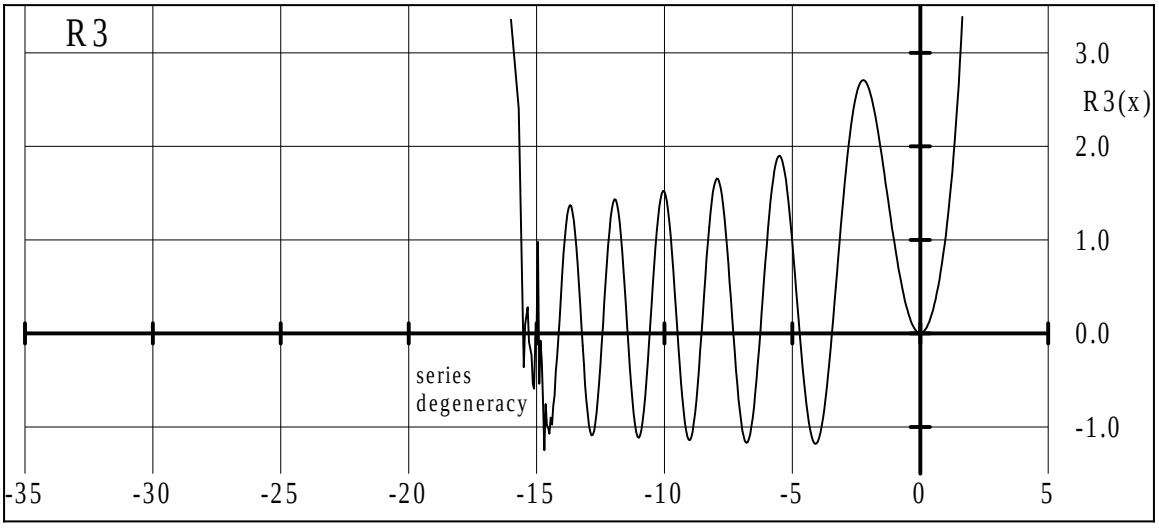

Figure E.3: Plot of $R_3(x)$ using series expansion with 15 digits f.p.a.

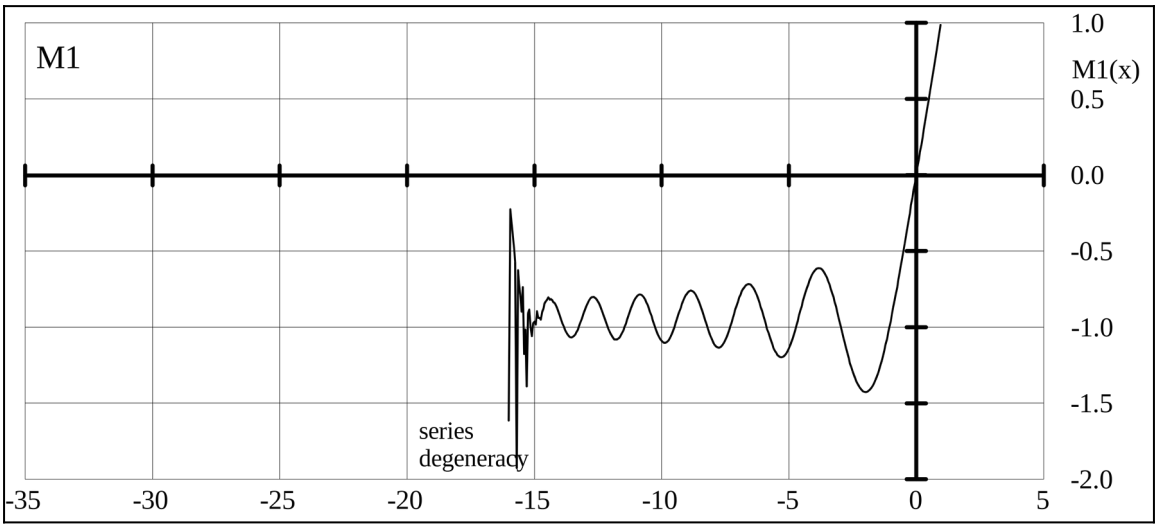

Figure E.4: Plot of $M_1(x)$ using series expansion with 15 digits f.p.a.

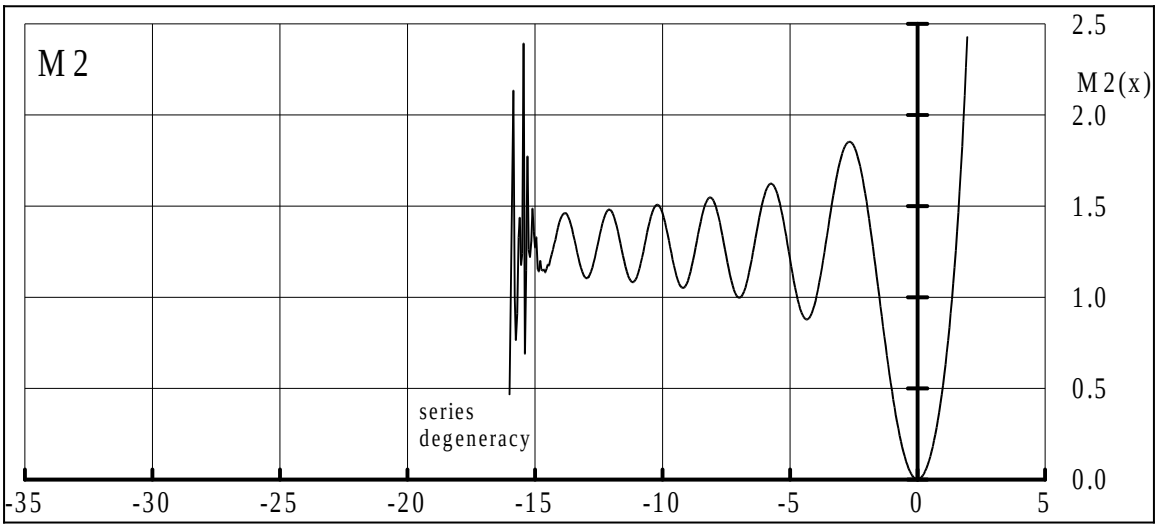

Figure E.5: Plot of $M_2(x)$ using series expansion with 15 digits f.p.a.

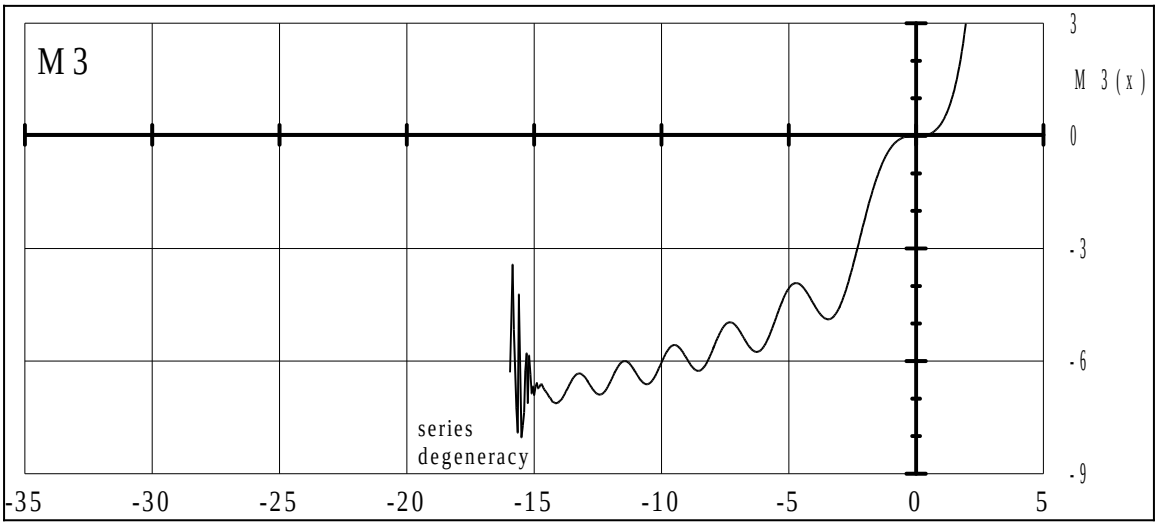

Figure E.6: Plot of $M_3(x)$ using series expansion with 15 digits f.p.a.

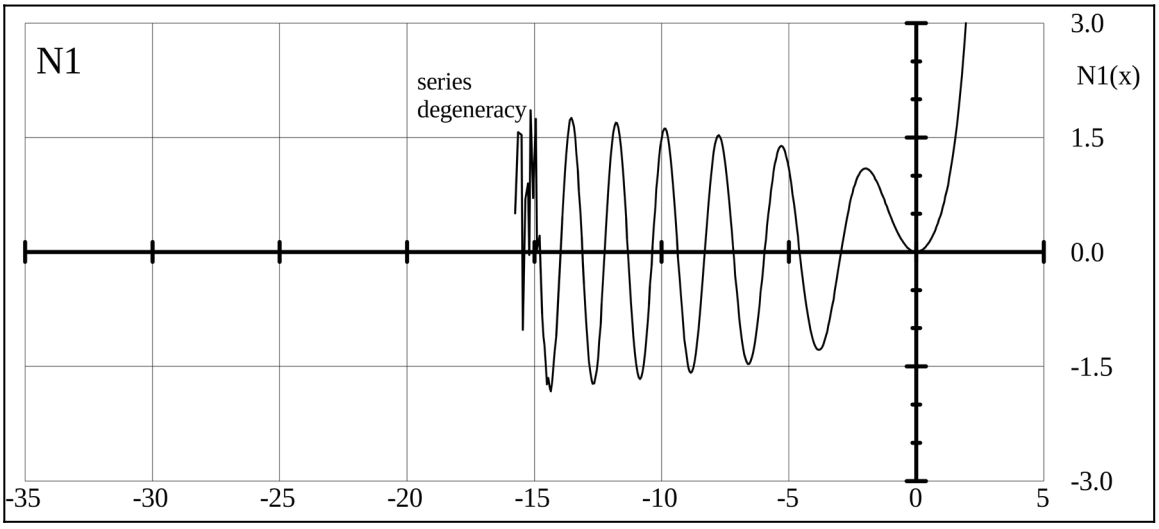

Figure E.7: Plot of $N_1(x)$ using series expansion with 15 digits f.p.a.

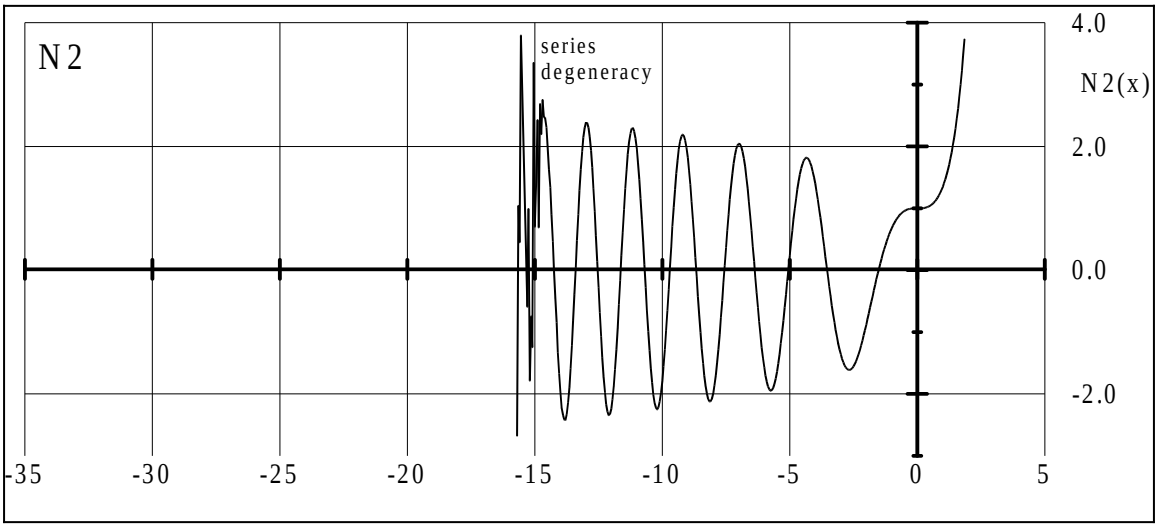

Figure E.8: Plot of $N_2(x)$ using series expansion with 15 digits f.p.a.

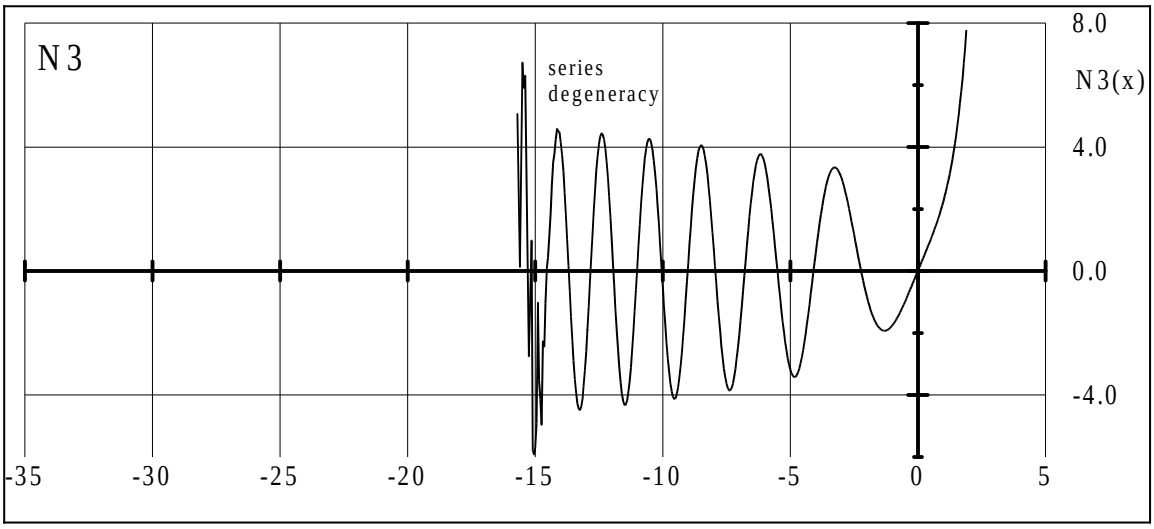

Figure E.9: Plot of $N_3(x)$ using series expansion with 15 digits f.p.a.

E.2 Path Integration of Differential Equations

Another approach to evaluate hypergeometric functions is the path integration of the function's defining differential equations along the real axis. In fact, since Erdélyi, the definition of generalized hypergeometric functions is given in terms of path integration of its differential equation. The general expression for the differential equation the generalized hypergeometric functions are solutions is given by (see Erdélyi-vol.I-pg.184)

$$\left[\delta(\delta+\beta_1-1)\cdot\cdots\cdot(\delta+\beta_q{-}1){-}z(\delta+\alpha_1)\cdot\cdots\cdot(\delta+\alpha_p)\right]u=0,$$

where $u={}_pF_q(\{\alpha\};\{\beta\};z)$ and $\delta=z\frac{d}{dz}$. The order of the differential equation is $\max(p,q+1)$.

Only the three special cases ${}_0F_1$, ${}_1F_2$, and ${}_2F_3$ will be studied. For these three cases, the argument is always $\frac{x^3}{9}$. Hence, to control the accuracy of the process in the variable x, a change of variable in the general differential equation is performed such that the arguments passed to the path integration procedure becomes x instead of the $\frac{x^3}{9}$. Making $z=\frac{x^3}{9}$ the operator becomes:

$$\delta=z\frac{d}{dz}=\frac{x^3}{9}\frac{dx}{dz}\frac{d}{dx}.$$

From the definition of z results:

$$3\frac{x^2}{9}\frac{dx}{dz}=1\rightarrow\frac{x^3}{9}\frac{dx}{dz}=\frac{x}{3},$$

such that the operator δ and the differential equation under new variable becomes:

$$\begin{aligned} &\delta = \frac{x}{3}\frac{d}{dx}, \\ &\left[\delta(\delta+\beta_1-1)\cdot\cdots\cdot(\delta+\beta_q-1) - \frac{x^3}{9}(\delta+\alpha_1)\cdot\cdots\cdot(\delta+\alpha_p)\right]u = 0 \end{aligned} \tag{E.1}$$

These expressions for the specific cases above are used for the path integration.

E.2.1 Integration for Functions Type ${}_0F_1[\beta;(x^3/9)]$

In this case $p=0$ and $q=1$. Therefore Equation (E.1) becomes:

$$\left[\delta(\delta+\beta-1) - \frac{x^3}{9}\right]u = \delta^2 u + (\beta-1)\delta u - \frac{x^3}{9}u = 0.$$

The second order operator δ^2 is given by

$$\delta^2 = \frac{x}{3}\frac{d}{dx}\left(\frac{x}{3}\frac{d}{dx}\right) = \frac{x}{3}\left[\frac{1}{3}\frac{d}{dx} + \frac{x}{3}\frac{d^2}{dx^2}\right] = \frac{x^2}{9}\frac{d^2}{dx^2} + \frac{x}{9}\frac{d}{dx}.$$

Hence the differential equation becomes:

$$\frac{d^2u}{dx^2} + (3\beta-2)\frac{1}{x}\frac{du}{dx} - xu = 0.$$

The initial conditions are:[2]

$$\begin{cases} u(0) = 1 \\ u'(0) = 0 \end{cases}$$

This second order differential equation along with the initial conditions is equivalent to the following system of first order differential equations:

$$\begin{cases} u_1' = u_2 \\ u_2' = x u_1 - \dfrac{3\beta - 2}{x} u_2 \\ u_1(0) = 1 \\ u_2(0) = 0 \end{cases} \tag{E.2}$$

E.2.2 Integration for Functions Type ${}_1F_2[\alpha;\beta_1,\beta_2;(x^3/9)]$

In this case p=1 and q=2. Therefore Equation (E.1) becomes:

$$\left[\delta(\delta + \beta_1 - 1)(\delta + \beta_2 - 1) - \frac{x^3}{9}(\delta + \alpha)\right] u = 0.$$

Expanding this expression results in

2 See Section E.2.4 for the values of ${}_pF_q$ as its derivatives at the origin.

$$\left\{\delta^3 + (\beta_1 + \beta_2 - 2)\delta^2 + [(\beta_1 - 1)(\beta_2 - 1)]\,\delta - \alpha\frac{x^3}{9}\right\} u = 0.$$

The third order operator δ^3 is given by

$$\delta^3 = \frac{x}{3}\frac{d}{dx}\left(\frac{x^2}{9}\frac{d^2}{dx^2} + \frac{x}{9}\frac{d}{dx}\right) = \frac{x^3}{27}\frac{d^3}{dx^3} + \frac{x^2}{9}\frac{d^2}{dx^2} + \frac{x}{27}\frac{d}{dx}.$$

Hence the differential equation becomes:

$$\frac{d^3u}{dx^3} + \frac{3(\beta_1 + \beta_2 - 1)}{x}\frac{d^2u}{dx^2} + \frac{9\beta_1\beta_2 - 6(\beta_1 + \beta_2) + 4 - x^3}{x^2}\frac{du}{dx} - 3\alpha u = 0.$$

The initial conditions are:

$$\begin{cases} u(0) = 1 \\ u'(0) = 0 \\ u''(0) = 0 \end{cases}$$

The equivalent system of first order differential equations and initial conditions is:

$$\begin{cases} u_1' = u_2 \\ u_2' = u_3 \\ u_3' = 3\alpha u_1 - \dfrac{9\beta_1\beta_2 - 6(\beta_1+\beta_2) + 4 - x^3}{x^2}u_2 - \dfrac{3(\beta_1+\beta_2-1)}{x}u_3 \\ u_1(0) = 1 \\ u_2(0) = 0 \\ u_3(0) = 0 \end{cases} \tag{E.3}$$

E.2.3 Integration for Functions Type ${}_2F_3[\alpha_1,\alpha_2;\beta_1,\beta_2,\beta_3;(x^3/9)]$

In this case p=2 and q=3. Therefore Equation (E.1) becomes:

$$\left[\delta(\delta+\beta_1-1)(\delta+\beta_2-1)(\delta+\beta_3-1)-\tfrac{x^3}{9}(\delta+\alpha_1)(\delta_1+\alpha_2)\right]u=0.$$

Expanding this expression results in

$$\left[\delta^4+(B_1-3)\delta^3+\left(B_2-2B_1+3-\frac{x^3}{9}\right)\delta^2+\left(B_3-B_2+B_1-1-A_1\frac{x^3}{9}\right)\delta-A_2\frac{x^3}{9}\right]u=0,$$

where[3]

$$\begin{cases} A_1=\alpha_1+\alpha_2 \\ A_2=\alpha_1\alpha_2 \\ B_1=\beta_1+\beta_2+\beta_3 \\ B_2=\beta_1\beta_2+\beta_1\beta_3+\beta_2\beta_3 \\ B_3=\beta_1\beta_2\beta_3 \end{cases} \tag{E.4}$$

The fourth order operator δ^4 is given by

$$\delta^4=\frac{x}{3}\frac{d}{dx}\left(\frac{x^3}{27}\frac{d^3}{dx^3}+\frac{x^2}{9}\frac{d^2}{dx^2}+\frac{x}{27}\frac{d}{dx}\right)$$
$$=\frac{x^4}{81}\frac{d^4}{dx^4}+\frac{2x^3}{27}\frac{d^3}{dx^3}+\frac{7x^2}{81}\frac{d^2}{dx^2}+\frac{x}{81}\frac{d}{dx}.$$

Hence the differential equation becomes:

---

3 See, Equation (E.11).

$$\frac{d^4u}{dx^4}+\frac{3(B_1-1)}{x}\frac{d^3u}{dx^3}+\left[\frac{9(B_2-B_1)+7}{x^2}-x\right]\frac{d^2u}{dx^2} + \left[\frac{27B_3-18B_2+12B_1-8}{x^3}-(3A_1+1)\right]\frac{du}{dx}-\frac{A_2}{x}u=0.$$

The initial conditions are:

$$\begin{cases} u(0)=1 \\ u'(0)=0 \\ u''(0)=0 \\ u'''(0)=\dfrac{2A_2}{3B_3} \end{cases}$$

The equivalent system of first order differential equations and initial conditions is:

$$\begin{cases} u_1'=u_2 \\ u_2'=u_3 \\ u_3'=u_4 \\ u_4'=\dfrac{9A_2}{x}u_1-\left[\dfrac{27B_3-18B_2+12B_1-8}{x^3}-(3A_1+1)\right]u_2 \\ \qquad\qquad -\left[\dfrac{9(B_2-B_1)+7}{x^2}-x\right]u_3-\dfrac{3(B_1-1)}{x}u_4 \\ u_1(0)=1 \\ u_2(0)=0 \\ u_3(0)=0 \\ u_4(0)=\dfrac{2A_2}{3B_3} \end{cases} \tag{E.5}$$

where the symbols A_1, A_2, B_1, B_2, and B_3 are given by Equation (E.4).

E.2.4 Properties at *x*=0

The values of the hypergeometric functions and their derivatives at the origin are important because they are the initial values for the path integration process. The initial value could be calculated at any appropriate point but the simplest case is at the origin (particularly for $x=0$) because the value is usually exact.

The value of ${}_pF_q$ at $z=0$ can be determine by its definition (Equation [D.11])

$$ {}_pF_q(\alpha_\mathrm{p};\beta_\mathrm{q};z)=\sum_{n=0}^{\infty}\frac{\prod_{i=1}^{p}(\alpha_i)_n}{\prod_{j=1}^{q}(\beta_j)_n}\frac{z^n}{n!}=\sum_{n=0}^{\infty}\frac{(\alpha_\mathrm{p})_n}{(\beta_\mathrm{q})_n}\frac{z^n}{n!}. \tag{D.11}$$

But for $z=\frac{x^3}{9}$ and $x=0$, the only term that remains is that for $n=0$, that is:

$$ {}_pF_q(\alpha_\mathrm{p};\beta_\mathrm{q};0)=\frac{(\alpha_\mathrm{p})_0}{(\beta_\mathrm{q})_0}=\frac{\prod_{i=1}^{p}(\alpha_i)_0}{\prod_{j=1}^{q}(\beta_j)_0}. $$

But $(\xi)_0=1$ such that

$$ {}_pF_q(\alpha_\mathrm{p};\beta_\mathrm{q};0)=1. \tag{E.6}$$

The derivative of a generalized hypergeometric function is given by

$$ \frac{d}{dz}{}_pF_q(\alpha_\mathrm{p};\beta_\mathrm{q};z)=\frac{(\alpha_\mathrm{p})}{(\beta_\mathrm{q})}\,{}_pF_q(\alpha_\mathrm{p}+1;\beta_\mathrm{q}+1\};z)\,, $$[4,5]

4 The operated list $\xi_\mathrm{r}+a$ is a list obtained by adding a to each element of the list ξ_r.
5 Note the contracted notations $(\xi_\mathrm{r})=\prod_{i=1}^{r}\xi_i$.

Using chain rule results in

$$\frac{d}{dx}{}_pF_q\left(\alpha_\mathrm{p};\beta_\mathrm{q};\frac{x^3}{9}\right)=\frac{(\alpha_\mathrm{p})}{(\beta_\mathrm{q})}{}_pF_q\left(\alpha_\mathrm{p}+1;\beta_\mathrm{q}+1;\frac{x^3}{9}\right)\frac{x^2}{3},$$

and at $x=0$ the derivative is

$$\frac{d}{dx}{}_pF_q\left(\alpha_\mathrm{p};\beta_\mathrm{q};\frac{x^3}{9}\right)\bigg|_{x=0}=0 \tag{E.7}$$

The second derivative is found in the same way:

$$\begin{aligned}\frac{d^2}{dz^2}{}_pF_q\left(\alpha_\mathrm{p};\beta_\mathrm{q};\frac{x^3}{9}\right)&=\frac{d}{dx}\frac{(\alpha_\mathrm{p})}{(\beta_\mathrm{q})}{}_pF_q\left(\alpha_\mathrm{p}+1;\beta_\mathrm{q}+1;\frac{x^3}{9}\right)\frac{x^2}{3}\\&=\frac{(\alpha_\mathrm{p})}{(\beta_\mathrm{q})}{}_pF_q\left(\alpha_\mathrm{p}+1;\beta_\mathrm{q}+1;\frac{x^3}{9}\right)\frac{2x}{3}\\&+\frac{(\alpha_\mathrm{p})(\alpha_\mathrm{p}+1)}{(\beta_\mathrm{q})(\beta_\mathrm{q}+1)}{}_pF_q\left(\alpha_\mathrm{p}+2;\beta_\mathrm{q}+2\};\frac{x^3}{9}\right)\frac{x^4}{9}.\end{aligned}$$

Consequently, at $x=0$ the second derivative becomes

$$\frac{d^2}{dx^2}{}_pF_q\left(\alpha_p;\beta_q;\frac{x^3}{9}\right)\bigg|_{x=0}=0 \tag{E.8}$$

The third derivative is given by

$$\frac{d^3}{dx^3}{}_pF_q\left(\alpha_p;\beta_q;\frac{x^3}{9}\right)=\frac{d}{dx}\left[\frac{(\alpha_p)}{(\beta_q)}{}_pF_q\left(\alpha_p+1;\beta_q+1;\frac{x^3}{9}\right)\frac{2x}{3}\right.$$
$$\left.+\ \frac{(\alpha_p)(\alpha p+1)}{(\beta q)(\beta q+1)}{}_pF_q\left(\alpha_p+2;\beta_q+2;\frac{x^3}{9}\right)\frac{x^4}{9}\right]$$

$$=\frac{(\alpha_p)}{(\beta_q)}{}_pF_q\left(\alpha_p+1;\beta_q+1;\frac{x^3}{9}\right)\frac{2}{3}$$
$$+\frac{(\alpha_p)(\alpha_p+1)}{(\beta_q)(\beta_q+1)}{}_pF_q\left(\alpha_p+2;\beta_q+2;\frac{x^3}{9}\right)\frac{6x^3}{9}$$
$$+\frac{(\alpha_p)(\alpha_p+1)(\alpha_p+2)}{(\beta_q)(\beta_q+1)(\beta_q+2)}{}_pF_q\left(\alpha_p+3;\beta_q+3;\frac{x^3}{9}\right)\frac{x^6}{27}.$$

Using Equation (E.6), the third derivative at $x=0$ becomes:

$$\left.\frac{d^3}{dx^3}{}_pF_q\left(\alpha_p;\beta_q;\frac{x^3}{9}\right)\right|_{x=0}=\frac{2}{3}\frac{(\alpha_p)}{(\beta_q)}. \tag{E.9}$$

E.2.5 Integration of the Systems of Differential Equations

To evaluate the functions at any given *x*, a fourth order Runge-Kutta integrator with adaptive stepsize was used. Instead of using a general code for each type discussed above in which the parameters could be passed in the call to the functions, the code for each function was specifically tailored. In addition, since each function is called several times in the iterative process, the values of the last call are saved and used as the starting point for the next evaluation.

An adaptive stepsize for the Runge-Kutta integrator is used to improve performance and permit a control in the degree of accuracy. All the functions present an oscillatory behavior for negative arguments and the adaptive stepsize process shortens the interval when the function gets close to minima and maxima to enforce accuracy and

lengthen the interval between extremes. The process used is the Step-doubling (Press et al., 1992).

Figure (E.10) shows the plot of $R_1(x)$ generated using path integration, which should be compared with Figure (E.1). The agreement in the convergence range of the series expansion depends upon the accuracy of the integration procedure which can be made equal to the machine accuracy. The remaining eight functions are plotted in the end of this section.

The path integration does not present a limit due to truncation error and, in fact, the method has been used to calculate points as far from the origin as $x = -1000$. However two problems arise. The first is due to the time required to calculate the very first point (such as $R_1[-30]$), in particular if the argument is large. This is not a serious problem because in the iterative process in which thousands of calculations will be performed, each new point is determined starting the integration at the last point determined. This leads to the second problem. When the integration starts at the origin the initial conditions are exact. But when the initial conditions come from some previously calculated point

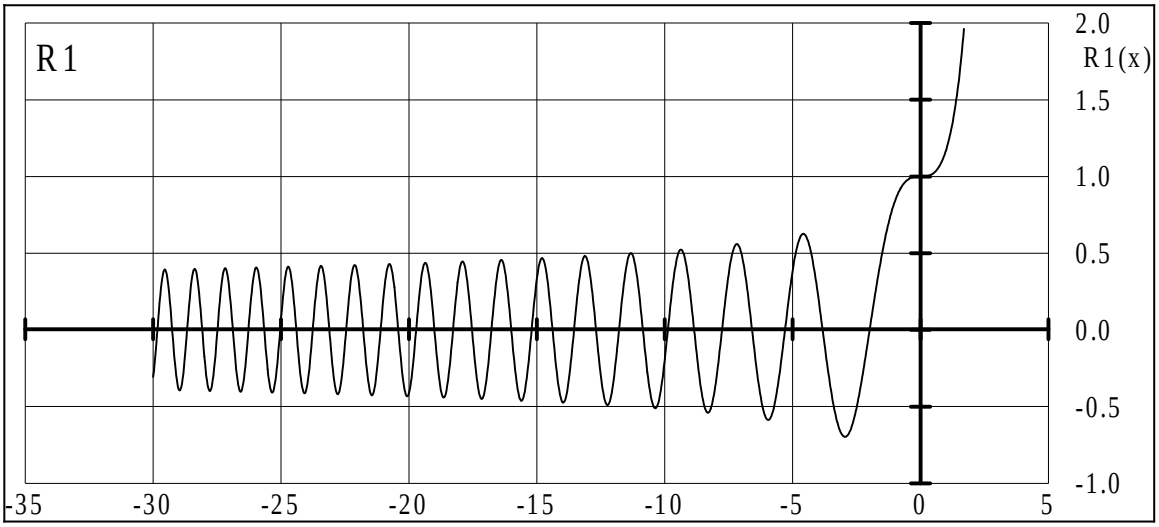

Figure E.10: Plot of R1(x) using path integration of the differential equation.

(such as R_1[-25]), they are not exact but carry at least round-off errors. For each new point (such as R_1[-26]) the round-off errors accumulate. After hundreds or thousands calculations, reproducibility in the evaluation is lost, that is, the value of the function at a given x will depend on the history of the previous evaluations.

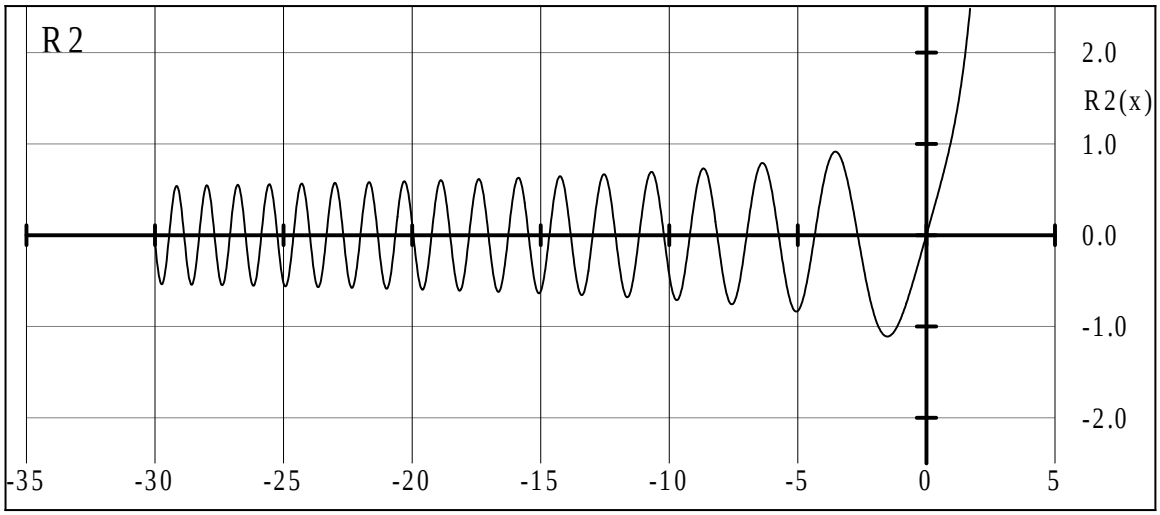

Figure E.11: Plot of R2(x) using path integration of the differential equation.

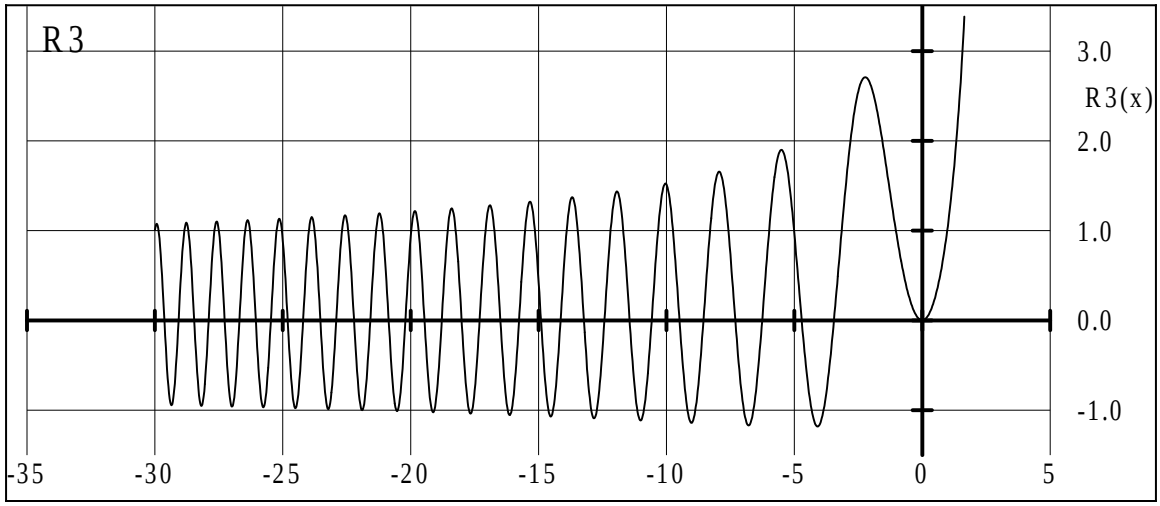

Figure E.12: Plot of R3(x) using path integration of the differential equation.

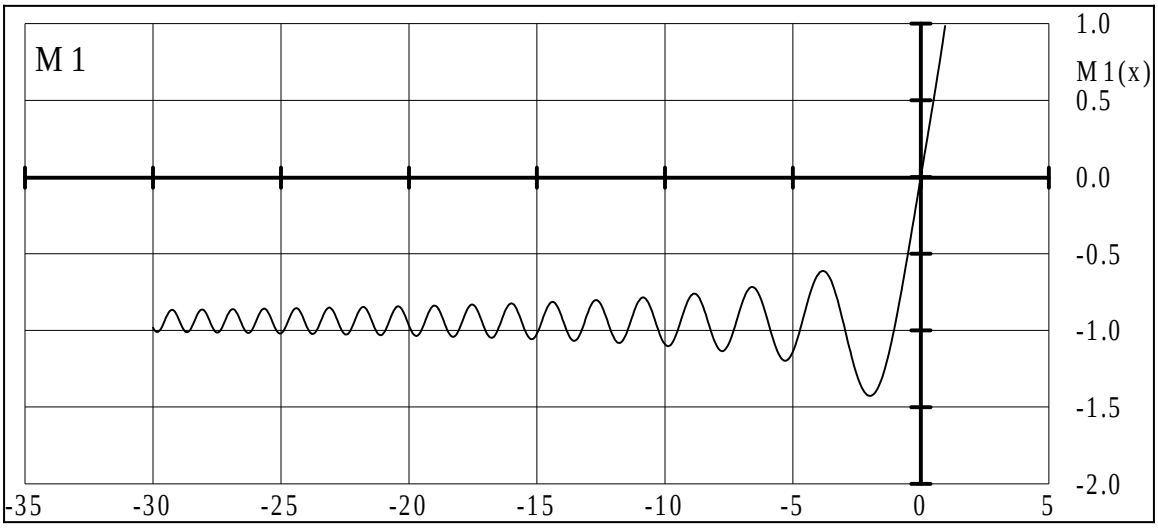

Figure E.13: Plot of M1(x) using path integration of the differential equation.

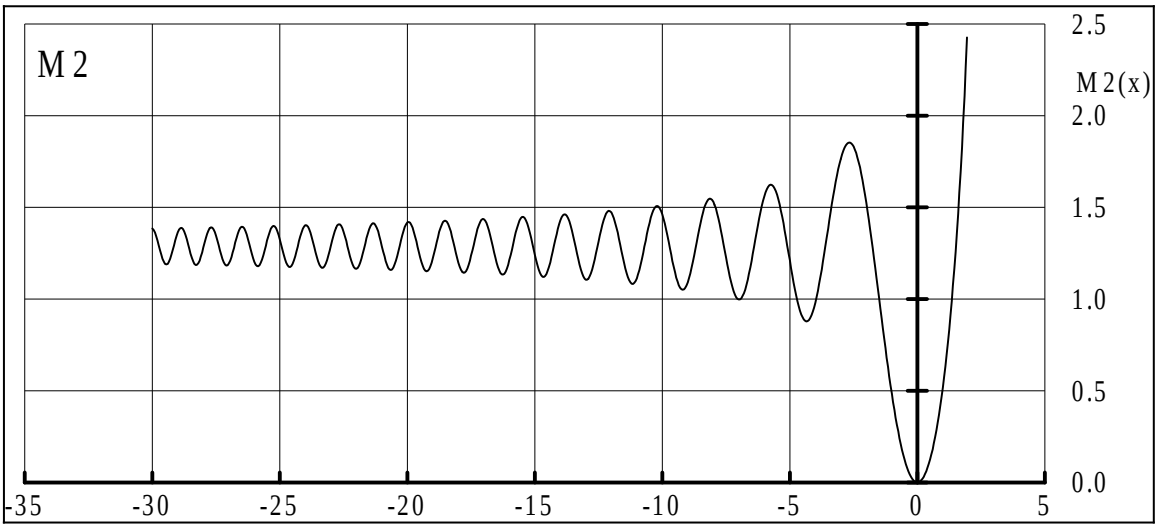

Figure E.14: Plot of M2(x) using path integration of the differential equation.

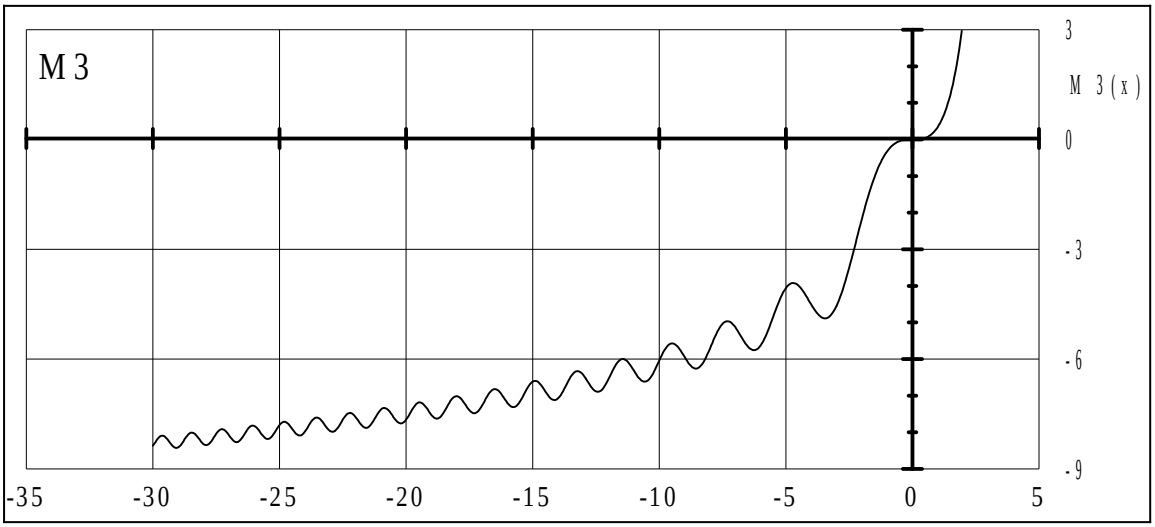

Figure E.15: Plot of M3(x) using path integration of the differential equation.

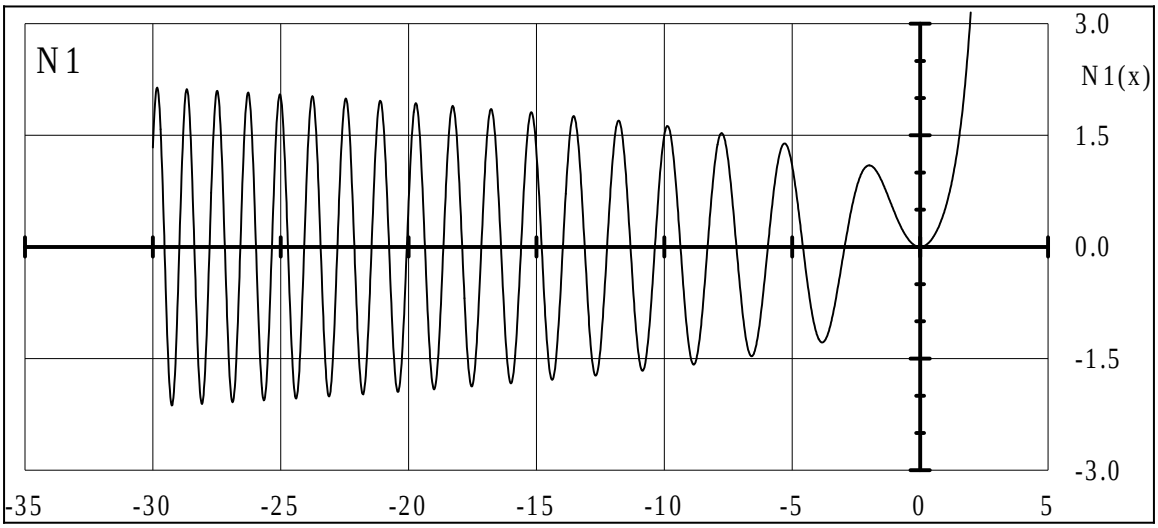

Figure E.16: Plot of N1(x) using path integration of the differential equation.

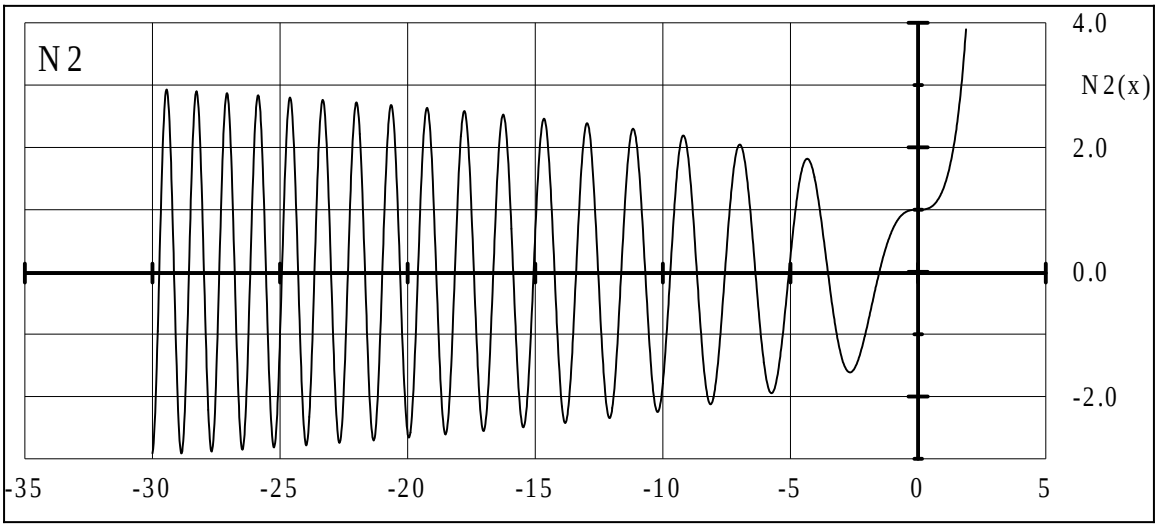

Figure E.17: Plot of N2(x) using path integration of the differential equation.

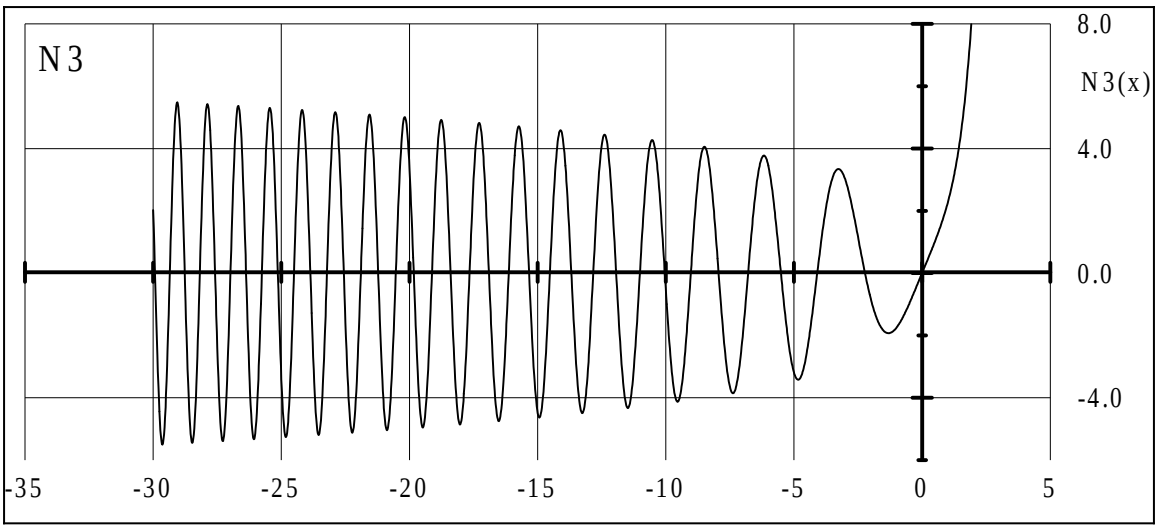

Figure E.18: Plot of N3(x) using path integration of the differential equation.

E.3 Asymptotic Expansions

Asymptotic expansion is one of the most used methods to evaluate special functions. Loosely, two functions $f(x)$ and $g(x)$ are asymptotically equivalent when the ratio $\frac{f(x)}{g(x)} \to 1$ as $|x| \to \infty$ (De Bruijn 1981). The notation used here is:

$$f(x) \approx g(x) \qquad (|x| \to \infty)$$

where the term $(|x| \to \infty)$ will be suppressed for simplicity.

No attempt will be made to rigorously or even formally prove the expressions here obtained. The development is based on the results presented by Luke (1962, 1969 volumes I and II). At most, a direct comparison is made between the numerical calculations obtained with the asymptotic expansions and the numerical calculations obtained with path integration.

The expression for the asymptotic expansion of the generalized hypergeometric function ${}_pF_{p+1}$ for z complex is given by (Luke 1969 - vol. I, 5.11.2 (6), pg.199):[6]

$$ {}_pF_{p+1}\left(\left.{}^{\alpha_{\mathrm{p}}}_{;\beta_{\mathrm{p+1}}}\right|-z\right) \approx \frac{\Gamma(\beta_{\mathrm{p+1}})}{\Gamma(\alpha_{\mathrm{p}})}\left[K_{p,p+1}\left(ze^{-i\pi}\right)+K_{p,p+1}\left(ze^{i\pi}\right)+L_{p,p+1}(z)\right] \qquad \text{(E.10)}$$
$$|z| \to \infty, \qquad \arg z \neq 2\pi k,$$

which follows the work by Meijer (1946). The two terms $K_{p,p+1}$ in Equation (E.10) form the *dominant* part of the expansion and the term $L_{p,p+1}$ is the *subdominant* part. The generic dominant part $K_{p,q}$ and auxiliary relations are expressed as (id. 5.11.1 [19,20]):

---

6 $\Gamma(\xi_{\mathrm{r}})$, where ξ_{r} is a list of parameters, is a compact notation and the interpretation is $\Gamma(\xi_{\mathrm{r}}) = \prod_{i=1}^{r} \Gamma(\xi_i)$.

$$
\begin{aligned}
&K_{p,q}(z) = \frac{(2\pi)^{(1-\eta)/2}}{\eta^{1/2}} \exp\left(\eta z^{\frac{1}{\eta}}\right) z^{\gamma} \sum_{k=0}^{\infty} N_k z^{-\frac{k}{\eta}}, \\
&\eta = q - p + 1, \qquad \gamma = \frac{1}{\eta}\left(\frac{\eta-1}{2} + A_1 - B_1\right), \\
&N = (B_2 - A_2) + (2\eta)^{-1}(A_1 - B_1)[\eta(A_1 + B_1) + A_1 - B_1 - 2] + \\
&\qquad\qquad + (24\eta)^{-1}(\eta-1)(\eta-11) \\
&A_1 = \sum_{h=1}^{p} \alpha_h, \quad A_2 = \sum_{i=2}^{p}\sum_{h=1}^{i-1} \alpha_h \alpha_i \\
&B_1 = \sum_{h=1}^{q} \beta_h, \quad B_2 = \sum_{i=2}^{q}\sum_{h=1}^{i-1} \beta_h \beta_i, \quad B_3 = \sum_{j=3}^{q}\sum_{i=2}^{j-1}\sum_{h=1}^{i-1} \beta_h \beta_i \beta_j
\end{aligned}
\tag{E.11}
$$

$N_0 = 1$, and N_k for $k \geq 1$ are obtained recursively as shown in Section E.3.1.

The general form of the subdominant term is given by

$$
L_{p,q}(z) = \sum_{t=1}^{p} {}^{t}L_{p,q}(z), \tag{E.12}
$$

where[7]

$$
\begin{aligned}
{}^{t}L_{p,q}(z) = &\frac{z^{-\alpha_t}\Gamma(\alpha_t)\Gamma(\alpha^*_{\mathrm{p}} - \alpha_t)}{\Gamma(\beta_{\mathrm{q}} - \alpha_t)} \times \\
&\times {}_{q+1}F_{p-1}\left(\alpha_t, 1 + \alpha_t - \beta_{\mathrm{q}}; 1 + \alpha_t - \alpha^*_{\mathrm{p}}; \frac{(-1)^{q-p}}{z}\right).
\end{aligned}
\tag{E.13}
$$

---

7 Continuing from the footnote 6, it is important noting the following conventions:
1. If ξ_{r} is a list of r elements, $\xi_{\mathrm{r}} + a$ is a list of p element in which each element is obtained by adding a to the original element.
2. A "*" in an operated list like in $\xi^*_{\mathrm{r}} - \xi_t$ means to omit the element $\xi_i - \xi_t$ in the list when $i = t$.
3. As a consequence of (2), $\Gamma(\xi^*_{\mathrm{r}} - \xi_t) = \prod_{\substack{i=1 \\ i \neq t}}^{r} \Gamma(\xi_i - \xi_t)$.

Using Equations (E.10) to (E.13), may be a challenging task. However the problem which leaded to this appendix is certainly that of a real variable and, in fact, for values that are in the negative side of the real axis. This is totally in agreement with Equation (E.10) whose domain is the complex plane with the positive real axis and the origin deleted ($|z| \to \infty, \arg z \neq 2\pi k$), so that the variable z can be assumed to be real and negative. However, even being z real, the form it appears in the dominant part of the expansion, that is the as $ze^{i\pi}$ and $ze^{-i\pi}$, the impression is that the discussion is back to the complex domain. One should recall, however, that $e^{i\pi}$ is the complex polar expression for the real number -1, and the same $e^{-i\pi}$. Although not clearly mentioned in the original source used here, the following result presented by Luke (1969 - vol. I - pg.197 – eq.21) is exactly the real part of the dominant term in Equation (E.10), which is:

$$K_{p,q}(ze^{i\pi}) + K_{p,q}(ze^{-i\pi}) = \frac{2(2\pi)^{\frac{1-\eta}{2}}}{\eta^{\frac{1}{2}}} z^{\gamma} \exp\left(z^{\frac{1}{\eta}}\eta\cos\frac{\pi}{\eta}\right) \times \sum_{k=0}^{\infty} N_k z^{-\frac{k}{\eta}} \cos\left(z^{\frac{1}{\eta}}\eta\sin\frac{\pi}{\eta} + \gamma\pi - k\frac{\pi}{\eta}\right)$$

To facilitate, the reference to the dominant part will be expresses as

$$K_{p,q}(z) = \frac{2(2\pi)^{\frac{1-\eta}{2}}}{\eta^{\frac{1}{2}}} z^{\gamma} \exp\left(z^{\frac{1}{\eta}}\eta\cos\frac{\pi}{\eta}\right) \times \sum_{k=0}^{\infty} N_k z^{-\frac{k}{\eta}} \cos\left(z^{\frac{1}{\eta}}\eta\sin\frac{\pi}{\eta} + \gamma\pi - k\frac{\pi}{\eta}\right) \tag{E.14}$$

Besides the *realization* of the dominant part, additional simplification occurs due to the fact that, in all cases here, $q = p+1$. This simplification results in

$$\begin{aligned}
&\eta = q+1-p = (p+1)+1-p = 2,\\
&\gamma = \frac{1}{2}\left(\frac{2-1}{2}+A_1-B_1\right) = \frac{1}{4}+\frac{1}{2}(A_1-B_1),\\
&N = (B_2-A_2)+\frac{1}{4}(A_1-B_1)(3A_1+B_1-2)-\frac{3}{16}.
\end{aligned} \tag{E.15}$$

In addition, $\cos\frac{\pi}{\eta}=\cos\frac{\pi}{2}=0$, $\sin\frac{\pi}{2}=1$ and Equation (E.14) reduces to

$$K_{p,p+1}(z)=\frac{1}{\sqrt{\pi}}z^{\gamma}\sum_{k=0}^{\infty}N_k z^{-\frac{k}{2}}\cos\left(2\sqrt{z}+\gamma\pi-k\frac{\pi}{2}\right).$$

The subdominant term now is:

$$L_{p,p+1}(z)=\sum_{t=1}^{p}{}^{t}L_{p,p+1}(z), \tag{E.16-a}$$

where

$$\begin{aligned}
{}^{t}L_{p,p+1}(z) = &\frac{z^{-\alpha_t}\Gamma(\alpha_t)\Gamma(\alpha^*_{\mathrm{p}}-\alpha_t)}{\Gamma(\beta_{\mathrm{p+1}}-\alpha_t)}\times\\
&{}_{p+2}F_{p-1}\left(\alpha_t, 1+\alpha_t-\beta_{\mathrm{p+1}}; 1+\alpha_t-\alpha^*_{\mathrm{p}}; \frac{-1}{z}\right).
\end{aligned} \tag{E.16-b}$$

Note that $\alpha^*_{\mathrm{p}}-\alpha_t$ is a list with $p-1$ elements, $\beta_{\mathrm{p+1}}-\alpha_t$ is a list with $p+1$, and $\{\alpha_t, 1+\alpha_t-\beta_{\mathrm{p+1}}\}$ is a list with $p+2$ elements. Note also that any operation performed on an *empty* list reduces to the *neutral element of the operation*, that is, a summation of an empty list takes the value *zero* (0), and a product of an empty list takes the value *one* (1).

The expression of the subdominant term is general and it is assumed that no pair of elements of α_p differs by an integer number including zero, otherwise eventually one

or more terms in the numerator of Equation (E.16-b) will become infinite.[8] In addition, $\alpha_t \neq \beta_s$ for any t and s otherwise their occurrence would cancel out and p and q would reduce by one. It is important to remember that in all calculations the argument z will be real and negative.

The specific expression for the asymptotic expansion with the dominant and subdominant terms for $q=p+1$ is

$$
\begin{aligned}
&{}_pF_{p+1}\left(\begin{matrix}\alpha_{\mathrm{p}}\\ \beta_{\mathrm{p+1}}\end{matrix}\middle| -z\right)\approx \\
&\frac{\Gamma(\beta_{\mathrm{p+1}})}{\Gamma(\alpha_{\mathrm{p}})}\left[\frac{1}{\sqrt{\pi}}z^{\gamma}\sum_{k=0}^{\infty}N_k z^{-\frac{k}{2}}\cos\left(2\sqrt{z}+\pi\gamma-\frac{k}{2}\pi\right)+\sum_{t=1}^{p}{}^{t}L_{p,p+1}(z)\right]
\end{aligned}
\tag{E.17}
$$

The summation coefficients N_k are related to the parameters d_k by the following expression (Luke (1969) - Vol. I - pg.200 – eqs.10-13):

$$
N_k = \frac{d_k}{2^k}. \tag{E.18}
$$

The d_k are obtained recursively and, for for $p=0, 1,$ and 2, the general expression is:

$$
\begin{aligned}
2(k+1)d_{k+1} = &\left[5k^2+2k(3+A_1-3B_1-10\gamma)+4N\right]d_k \\
&-\left[4k^3-6k^2(B_1+4\gamma)+2k(24\gamma^2+12\gamma B_1+B_1+4B_2-1)\right. \\
&\quad\left.-32\gamma^3-24\gamma^2 B_1-4\gamma(B_1+4B_2-1)+2B_1-4B_2-8B_3-1\right]d_{k-1} \\
&+(k-2\gamma-2)(k-2\gamma-2\beta_1)(k-2\gamma-2\beta_2)(k-2\gamma-2\beta_3)d_{k-2},
\end{aligned}
\tag{E.19}
$$

in which the initial values are

8 This restriction can be removed using a limiting process.

$$d_{k=0} = 1, \rightarrow N_1 = 2^0 d_0 = 1,$$
$$d_{k<0} = 0.$$

The recursion expression can be simplified for the cases $p=0$ and $p=1$ as seen next, but needed in full for $p=2$.

In the sequence, the formulation of the asymptotic expansions are presented for $p=0$, 1, and 2, each case with its peculiarities and increasing degree of complexity.

E.3.1 Expansion for Functions Type ${}_0F_1$ [Functions $N_2(x)$, $R_1(x)$, $R_2(x)$, $N_1(x)$]

The asymptotic expansion for this case does not have subdominant part because the summation in Equation (E.16-a) is empty ($p=0$):

$$L_{0,1}(z) = \sum_{t=1}^{0} {}^{t}L_{0,1}(z) = 0.$$

The simplified recursion for d_k is[9]

$$(2k)d_k = \left(k - \frac{1}{2} + \nu\right)\left(k - \frac{1}{2} - \nu\right) d_{k-1} \qquad \text{(E.20)}$$
$$\nu = 1 - \beta_1$$

9 Luke [(1969) Vol. 1, pg. 200 (11)] uses the explicit formula $d_k = \frac{(\frac{1}{2}+\nu)_k (\frac{1}{2}-\nu)_k}{2^k k!}$, where $(\xi)_r$ is the Pochhammer's symbol. It has the advantage of being valid for $k=0$. The recursive formula however, seems easier to use. See section E.3.2.2.b for details.

E.3.1.1 Function $N_2(x) = {}_0F_1(^1/_3;x^3/9)$

Formulas in Equations (E.11) and (E.15), with $p=0$, $q=1$, and $\beta_1=\frac{1}{3}$, yield:

$$
\begin{aligned}
A_1 &= \sum_{h=1}^{0} \alpha_h = 0 \quad \text{(summation of an empty list)},\\
B_1 &= \sum_{h=1}^{q} \beta_h = \frac{1}{3},\\
\gamma &= \frac{1}{4} + \frac{1}{2}(A_1 - B_1) = \frac{1}{4} + \frac{1}{2}\left(0 - \frac{1}{3}\right) = \frac{1}{12}.
\end{aligned}
$$

Therefore, the expression for the asymptotic expansion becomes:

$$
{}_0F_1\left(\frac{1}{3}; x\right) \approx \Gamma\left(\frac{1}{3}\right) \frac{(-x)^{\frac{1}{12}}}{\sqrt{\pi}} \sum_{k=0}^{\infty} N_k (-x)^{-\frac{k}{2}} \cos\left(2\sqrt{-x} + \frac{\pi}{12} - \frac{k}{2}\pi\right).
$$

The summation is expanded up to $k=3$ and the order of the approximation will be presented later. Using the explicit formula in Equation (E.20) with $\nu = 1 - \frac{1}{3} = \frac{2}{3}$ gives:

$$
\begin{aligned}
d_0 &= \frac{(\frac{1}{2}+\frac{2}{3})_0 (\frac{1}{2}-\frac{2}{3})_0}{2^0 0!} = 1 \to N_0 = \frac{1}{2^0} = 1\\
d_1 &= \frac{(\frac{1}{2}+\frac{2}{3})_1 (\frac{1}{2}-\frac{2}{3})_1}{2^1 1!} = \frac{-7}{72} \to N_1 = \frac{-7}{144}\\
d_2 &= \frac{(\frac{1}{2}+\frac{2}{3})_2 (\frac{1}{2}-\frac{2}{3})_2}{2^2 2!} = \frac{-455}{10,368} \to N_2 = \frac{-455}{41,472}\\
d_3 &= \frac{(\frac{1}{2}+\frac{2}{3})_3 (\frac{1}{2}-\frac{2}{3})_3}{2^3 3!} = \frac{-95,095}{2,239,488} \to N_3 = \frac{-95,095}{17,915,904}
\end{aligned}
$$

The expansion using Equation (E.17) becomes[10]

$$
\begin{aligned}
{}_0F_1\left(\frac{1}{3};x\right) = \; & \Gamma\left(\frac{1}{3}\right)\frac{(-x)^{\frac{1}{12}}}{\sqrt{\pi}}\left[1(-x)^{-\frac{0}{2}}\cos\left(2\sqrt{-x}+\frac{\pi}{12}\right)\right. \\
& -\frac{7}{144}(-x)^{-\frac{1}{2}}\cos\left(2\sqrt{-x}+\frac{\pi}{12}-\frac{\pi}{2}\right) \\
& -\frac{455}{41,472}(-x)^{-\frac{2}{2}}\cos\left(2\sqrt{-x}+\frac{\pi}{12}-\pi\right) \\
& \left.-\frac{95,095}{17,915,904}(-x)^{-\frac{3}{2}}\cos\left(2\sqrt{-x}+\frac{\pi}{12}-\frac{3\pi}{2}\right)\right] \\
& +O\left(x^{-\frac{23}{12}}\right)
\end{aligned}
$$

Using the trigonometric identities

$$
\begin{aligned}
\cos a &= -\cos\left(a-\pi\right) = \cos\left(a–2\pi\right) = \ldots \\
\sin a &= \cos\left(a-\frac{\pi}{2}\right) = -\cos\left(a-\frac{3\pi}{2}\right) = \ldots
\end{aligned}
$$

the following expression is obtained:

$$
\begin{aligned}
{}_0F_1\left(\frac{1}{3};x\right) = \; & \Gamma\left(\frac{1}{3}\right)\frac{(-x)^{\frac{1}{12}}}{\sqrt{\pi}}\left\{\left[1+\frac{455}{41,472}(-x)^{-1}\right]\cos\left(2\sqrt{-x}+\frac{\pi}{12}\right)\right. \\
& \left.+\left[-\frac{7}{144}(-x)^{-\frac{1}{2}}+\frac{95,095}{17,915,904}(-x)^{-\frac{3}{2}}\right]\sin\left(2\sqrt{-x}+\frac{\pi}{12}\right)\right\} \\
& +O\left(x^{-\frac{23}{12}}\right)
\end{aligned}
$$

10 The order of the approximation *O* is given by the degree of the remainder of the truncation after $k=3$. The 4th term would have the of exponent $x^{\frac{1}{12}}x^{\frac{4}{2}}=x^{-\frac{23}{12}}$.

Substituting $\frac{x^3}{9}$ for x results in

$$N_2(x) = {}_0F_1\left(\frac{1}{3}; \frac{x^3}{9}\right) \approx \frac{\Gamma\left(\frac{1}{3}\right)}{3^{\frac{1}{6}}\sqrt{\pi}} \left\{(-x)^{\frac{1}{4}}\left[1 + \frac{455}{4608}(-x)^{-3}\right]\cos\left[\frac{2}{3}(-x)^{\frac{3}{2}} + \frac{\pi}{12}\right] + (-x)^{-\frac{5}{4}}\left[-\frac{7}{48} + \frac{95,095}{663,552}(-x)^{-3}\right]\sin\left[\frac{2}{3}(-x)^{\frac{3}{2}} + \frac{\pi}{12}\right]\right\} + O\left(x^{-\frac{23}{4}}\right)$$

which is the asymptotic expansion for the function $N_2(x)$.

The plot of the asymptotic expansion for N_2, along with the complete plot using path integration for comparison is shown in Figure (E.19). A very good agreement exists for large negative values of x. As expected, the asymptotic expansion is defined only in the negative semi-axis.

Regarding to the oscillatory behavior of the function, it is governed in the

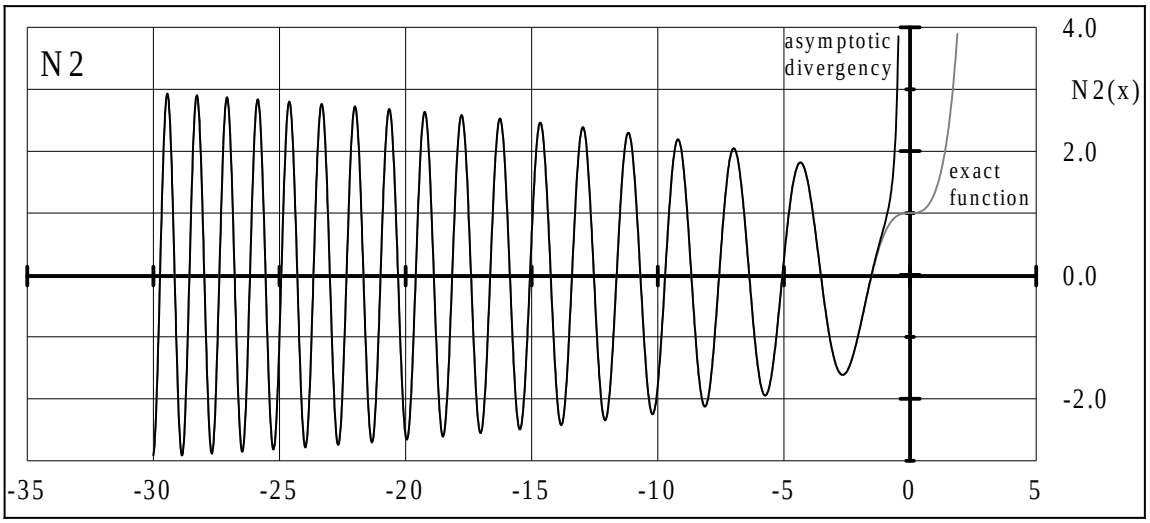

Figure E.19: Plot of the asymptotic expansion of $N_2(x)$.

asymptotic expansion by the trigonometric functions *cosine* and *sine*. The frequency is modulated by the term $(-x)^{\frac{3}{2}}$ and the amplitude is modulated by the two polynomial coefficients. The truncation of the expansion is of the order $(-x)^{-\frac{23}{4}}$.

E.3.1.2 Function $R_1(x) = {}_0F_1(^2/_3;x^3/9)$

Formulas in Equations (E.11) and (E.15) with $p=0$, $q=1$, and $\beta_1=\frac{2}{3}$ yield:

$$A_1=\sum_{h=1}^{0}\alpha_h=0,$$
$$B_1=\sum_{h=1}^{q}\beta_h=\frac{2}{3},$$
$$\gamma=\frac{1}{4}+\frac{1}{2}(A_1-B_1)=\frac{1}{4}+\frac{1}{2}(0-\frac{2}{3})=-\frac{1}{12}.$$

Therefore, the expression for the asymptotic expansion becomes:

$${}_0F_1\left(\frac{2}{3};x\right)\approx\Gamma\left(\frac{2}{3}\right)\frac{(-x)^{-\frac{1}{12}}}{\sqrt{\pi}}\sum_{k=0}^{\infty}N_k(-x)^{-\frac{k}{2}}\cos\left(2\sqrt{-x}-\frac{\pi}{12}-\frac{k}{2}\pi\right).$$

The summation is expanded up to $k=3$ and the order of the approximation will be presented later. Using the explicit formula in Equation (E.20) with $\nu=1-\frac{2}{3}=\frac{1}{3}$ gives:

$$d_0=\frac{(\frac{1}{2}+\frac{1}{3})_0(\frac{1}{2}-\frac{1}{3})_0}{2^0 0!}=1\rightarrow N_0=1$$
$$d_1=\frac{(\frac{1}{2}+\frac{1}{3})_1(\frac{1}{2}-\frac{1}{3})_1}{2^1 1!}=\frac{5}{72}\rightarrow N_1=\frac{5}{144}$$
$$d_2=\frac{(\frac{1}{2}+\frac{1}{3})_2(\frac{1}{2}-\frac{1}{3})_2}{2^2 2!}=\frac{385}{10,368}\rightarrow N_2=\frac{385}{41,472}$$
$$d_3=\frac{(\frac{1}{2}+\frac{1}{3})_3(\frac{1}{2}-\frac{1}{3})_3}{2^3 3!}=\frac{85,085}{2,239,488}\rightarrow N_3=\frac{85,085}{17,915,904}$$

The expansion becomes

$$
\begin{aligned}
{}_0F_1\left(\frac{2}{3};x\right) = \; & \Gamma\left(\frac{2}{3}\right)\frac{(-x)^{-\frac{1}{12}}}{\sqrt{\pi}}\left[\cos\left(2\sqrt{-x}-\frac{\pi}{12}\right)\right. \\
& + \frac{5}{144}(-x)^{-\frac{1}{2}}\cos\left(2\sqrt{-x}-\frac{\pi}{12}-\frac{\pi}{2}\right) \\
& + \frac{385}{41,472}(-x)^{-1}\cos\left(2\sqrt{-x}-\frac{\pi}{12}-\pi\right) \\
& \left. + \frac{85,085}{17,915,904}(-x)^{-\frac{3}{2}}\cos\left(2\sqrt{-x}-\frac{\pi}{12}-\frac{3\pi}{2}x\right)\right] \\
& + O\left(x^{-\frac{25}{12}}\right)
\end{aligned}
$$

Using the same trigonometric identities as before yields

$$
\begin{aligned}
{}_0F_1\left(\frac{2}{3};x\right) = \Gamma\left(\frac{2}{3}\right)\frac{(-x)^{-\frac{1}{12}}}{\sqrt{\pi}}\left\{\left[1-\frac{385}{41,472}(-x)^{-1}\right]\cos\left(2\sqrt{-x}-\frac{\pi}{12}\right)\right. \\
\left. + \left[\frac{5}{144}(-x)^{-\frac{1}{2}} - \frac{85,085}{17,915,904}(-x)^{-\frac{3}{2}}\right]\sin\left(2\sqrt{-x}-\frac{\pi}{12}\right)\right\} \\
+ O\left(x^{-\frac{25}{12}}\right)
\end{aligned}
$$

Substituting $\frac{x^3}{9}$ for x results in

$$
\begin{aligned}
R_1(x) = \; & {}_0F_1\left(\frac{2}{3};\frac{x^3}{9}\right) = \\
& \frac{\Gamma\left(\frac{2}{3}\right)\,3^{\frac{1}{6}}}{\sqrt{\pi}}\left\{(-x)^{-\frac{1}{4}}\left[1-\frac{385}{4608}(-x)^{-3}\right]\cos\left[\frac{2}{3}(-x)^{\frac{3}{2}}-\frac{\pi}{12}\right]\right. \\
& \left. + \,(-x)^{-\frac{7}{4}}\left[\frac{5}{48}-\frac{85,085}{663,552}(-x)^{-3}\right]\sin\left[\frac{2}{3}(-x)^{\frac{3}{2}}-\frac{\pi}{12}\right]\right\} \\
& + O\left(x^{-\frac{25}{4}}\right)
\end{aligned}
$$

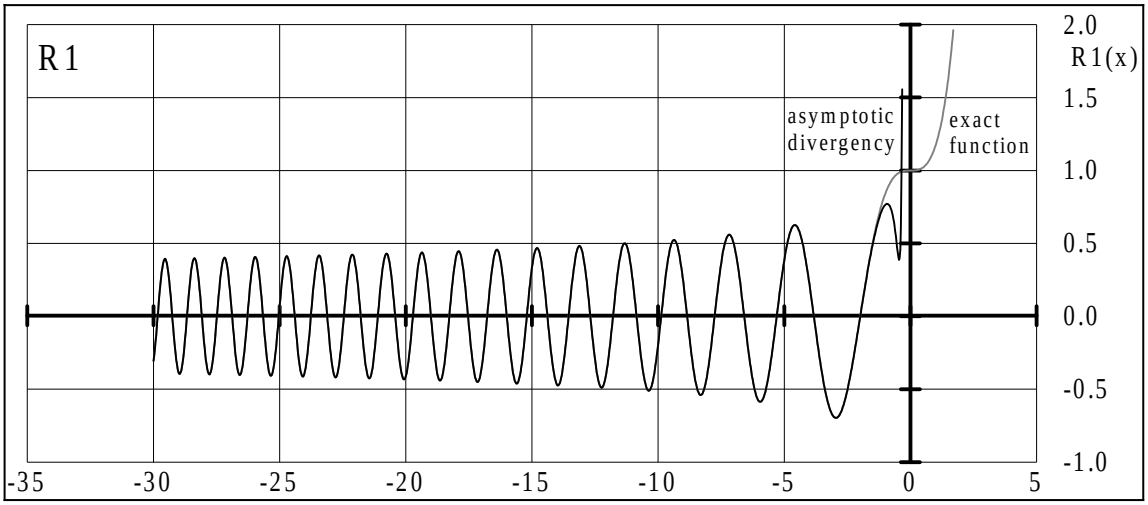

Figure E.20: Plot of the asymptotic expansion of $R_1(x)$.

which is the asymptotic expansion for the function $R_1(x)$.

The plot of the asymptotic expansion for R_1 along with the complete plot using path integration for comparison is shown in Figure Figure (E20).

E.3.1.3 Function $R_2(x) = x\ {}_0F_1(4/3;x^3/9)$

Formulas in Equations (E.11) and (E.15) with $p=0$, $q=1$, and $\beta_1=\frac{4}{3}$ yield:

$$A_1 = \sum_{h=1}^{0} \alpha_h = 0 \quad ,$$

$$B_1 = \sum_{h=1}^{q} \beta_h = \frac{4}{3},$$

$$\gamma = \frac{1}{4} + \frac{1}{2}(A_1 - B_1) = \frac{1}{4} + \frac{1}{2}(0 - \frac{4}{3}) = -\frac{5}{12}.$$

Therefore, the expression for the asymptotic expansion becomes:

$$ {}_0F_1\left(\frac{4}{3};x\right) \approx \Gamma\left(\frac{4}{3}\right)\frac{(-x)^{-\frac{5}{12}}}{\sqrt{\pi}}\sum_{k=0}^{\infty}N_k(-x)^{-\frac{k}{2}}\cos\left(2\sqrt{-x}-\frac{5\pi}{12}-\frac{k\pi}{2}\right). $$

The summation is expanded up to $k=3$ and the order of the approximation will be presented later. Using the recursion formulas for $p=0$ results in

$$ \begin{aligned} d_0 &= \frac{(\frac{1}{2}-\frac{1}{3})_0(\frac{1}{2}+\frac{1}{3})_0}{2^0 0!} = 1 \rightarrow N_0 = 1 \\ d_1 &= \frac{(\frac{1}{2}-\frac{1}{3})_1(\frac{1}{2}+\frac{1}{3})_1}{2^1 1!} = \frac{5}{72} \rightarrow N_1 = \frac{5}{144} \\ d_2 &= \frac{(\frac{1}{2}-\frac{1}{3})_2(\frac{1}{2}+\frac{1}{3})_2}{2^2 2!} = \frac{385}{10,368} \rightarrow N_2 = \frac{385}{41,472} \\ d_3 &= \frac{(\frac{1}{2}-\frac{1}{3})_3(\frac{1}{2}+\frac{1}{3})_3}{2^3 3!} = \frac{85,085}{2,239,488} \rightarrow N_3 = \frac{85,085}{17,915,904} \end{aligned} $$

The expansion becomes

$$ \begin{aligned} {}_0F_1\left(\frac{4}{3};x\right) = \Gamma\left(\frac{4}{3}\right)\frac{(-x)^{-\frac{5}{12}}}{\sqrt{\pi}} &\left[\cos\left(2\sqrt{-x}-\frac{5\pi}{12}\right)\right. \\ &+\frac{5}{144}(-x)^{-\frac{1}{2}}\cos\left(2\sqrt{-x}-\frac{5\pi}{12}-\frac{\pi}{2}\right) \\ &+\frac{385}{41,472}(-x)^{-1}\cos\left(2\sqrt{-x}-\frac{5\pi}{12}-\pi\right) \\ &\left.+\frac{85,085}{17,915,904}(-x)^{-\frac{3}{2}}\cos\left(2\sqrt{-x}-\frac{5\pi}{12}-\frac{3\pi}{2}x\right)\right] \\ &+O\left(x^{-\frac{29}{12}}\right) \end{aligned} $$

Using the trigonometric identities yields

$$\begin{aligned}{}_0F_1\left(\frac{4}{3};x\right) = \Gamma\left(\frac{4}{3}\right)\frac{(-x)^{-\frac{5}{12}}}{\sqrt{\pi}}\left\{\left[1-\frac{385}{41,472}(-x)^{-1}\right]\cos\left(2\sqrt{-x}-\frac{5\pi}{12}\right)\right.\\ \left.+\left[\frac{5}{144}(-x)^{-\frac{1}{2}}-\frac{85,085}{17,915,904}(-x)^{-\frac{3}{2}}\right]\sin\left(2\sqrt{-x}-\frac{5\pi}{12}\right)\right\}\\ +O\left(x^{-\frac{29}{12}}\right)\end{aligned}$$

Substituting $\frac{x^3}{9}$ for x results in

$$\begin{aligned}{}_0F_1\left(\frac{4}{3};\frac{x^3}{9}\right) =&\frac{\Gamma\left(\frac{4}{3}\right)3^{\frac{5}{6}}}{\sqrt{\pi}}\left\{(-x)^{-\frac{5}{4}}\left[1-\frac{385}{4608}(-x)^{-3}\right]\cos\left[\frac{2}{3}(-x)^{\frac{3}{2}}-\frac{5\pi}{12}\right]\right.\\ &\left.+(-x)^{-\frac{11}{4}}\left[\frac{5}{48}-\frac{85,085}{663,552}(-x)^{-3}\right]\sin\left[\frac{2}{3}(-x)^{\frac{3}{2}}-\frac{5\pi}{12}\right]\right\}\\ &+O\left(x^{-\frac{29}{4}}\right)\end{aligned}$$

Therefore, the asymptotic expansion for $R_2(x)$ is

$$\begin{aligned}R_2(x) =&x\,{}_0F_1\left(\frac{4}{3};\frac{x^3}{9}\right) = -(-x)\,{}_0F_1\left(\frac{4}{3};\frac{x^3}{9}\right)\\ =&-\frac{\Gamma\left(\frac{4}{3}\right)3^{\frac{5}{6}}}{\sqrt{\pi}}\left\{(-x)^{-\frac{1}{4}}\left[1-\frac{385}{4608}(-x)^{-3}\right]\cos\left[\frac{2}{3}(-x)^{\frac{3}{2}}-\frac{5\pi}{12}\right]\right.\\ &\left.+(-x)^{-\frac{7}{4}}\left[\frac{5}{48}-\frac{85,085}{663,552}(-x)^{-3}\right]\sin\left[\frac{2}{3}(-x)^{\frac{3}{2}}-\frac{5\pi}{12}\right]\right\}\\ &+O\left(x^{-\frac{25}{4}}\right)\end{aligned}$$

Since $\Gamma\left(\frac{4}{3}\right)=\frac{1}{3}\Gamma\left(\frac{1}{3}\right)$, the coefficient of the expansion can be simplified to $\frac{\Gamma\left(\frac{1}{3}\right)}{\sqrt{\pi}\,3^{\frac{1}{6}}}$.

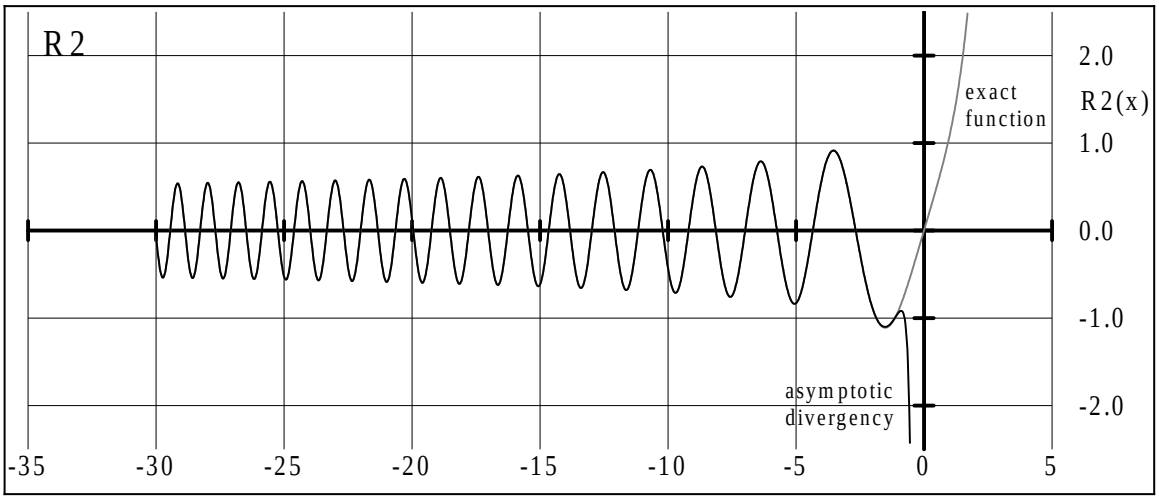

Figure E.21: Plot of the asymptotic expansion of $R_2(x)$.

The plot of the asymptotic expansion for R_2 along with the complete plot using path integration for comparison is shown in Figure Figure (E.21).

E.3.1.4 Function Function $N_1(x) = x^2/2\ {}_0F_1(5/3;x^3/9)$

From the formulas in Equations (E.11) and (E.15) with $p=0$, $q=1$, $\beta_1=\frac{5}{3}$, and $\nu=1-\frac{5}{3}=-\frac{2}{3}$ yield:

$$A_1=\sum_{h=1}^{0}\alpha_h=0 \quad ,$$
$$B_1=\sum_{h=1}^{q}\beta_h=\frac{5}{3},$$
$$\gamma=\frac{1}{4}+\frac{1}{2}(A_1-B_1)=\frac{1}{4}+\frac{1}{2}(0-\frac{5}{3})=-\frac{7}{12}.$$

Therefore, the expression for the asymptotic expansion becomes:

$$ {}_0F_1\left(\frac{5}{3};x\right) \approx \Gamma\left(\frac{5}{3}\right)\frac{(-x)^{-\frac{7}{12}}}{\sqrt{\pi}}\sum_{k=0}^{\infty}N_k(-x)^{-\frac{k}{2}}\cos\left(2\sqrt{-x}-\frac{7\pi}{12}-\frac{k\pi}{2}\right). $$

The summation is expanded up to $k=3$ and the order of the approximation will be presented later. Using the recursion formulas for $p=0$ results in

$$ \begin{aligned} d_0 &= \frac{(\frac{1}{2}-\frac{2}{3})_0(\frac{1}{2}+\frac{2}{3})_0}{2^0 0!} = 1 \rightarrow N_0 = \frac{1}{2^0} = 1 \\ d_1 &= \frac{(\frac{1}{2}-\frac{2}{3})_1(\frac{1}{2}+\frac{2}{3})_1}{2^1 1!} = \frac{-7}{72} \rightarrow N_1 = \frac{-7}{144} \\ d_2 &= \frac{(\frac{1}{2}-\frac{2}{3})_2(\frac{1}{2}+\frac{2}{3})_2}{2^2 2!} = \frac{-455}{10,368} \rightarrow N_2 = \frac{-455}{41,472} \\ d_3 &= \frac{(\frac{1}{2}-\frac{2}{3})_3(\frac{1}{2}+\frac{2}{3})_3}{2^3 3!} = \frac{-95,095}{2,239,488} \rightarrow N_3 = \frac{-95,095}{17,915,904} \end{aligned} $$

The expansion becomes

$$ \begin{aligned} {}_0F_1\left(\frac{5}{3};x\right) = \Gamma\left(\frac{5}{3}\right)\frac{(-x)^{-\frac{7}{12}}}{\sqrt{\pi}} \Bigg[& \cos\left(2\sqrt{-x}-\frac{7\pi}{12}\right) \\ & -\frac{7}{144}(-x)^{-\frac{1}{2}}\cos\left(2\sqrt{-x}-\frac{7\pi}{12}-\frac{\pi}{2}\right) \\ & -\frac{455}{41,472}(-x)^{-1}\cos\left(2\sqrt{-x}-\frac{7\pi}{12}-\pi\right) \\ & -\frac{95,095}{17,915,904}(-x)^{-\frac{3}{2}}\cos\left(2\sqrt{-x}-\frac{7\pi}{12}-\frac{3\pi}{2}x\right)\Bigg] \\ & + O\left(x^{-\frac{31}{12}}\right) \end{aligned} $$

Using the trigonometric identities yields

$$
\begin{aligned}
{}_0F_1\left(\frac{5}{3};x\right) = \Gamma\left(\frac{5}{3}\right)\frac{(-x)^{-\frac{7}{12}}}{\sqrt{\pi}}\Bigg\{&\left[1+\frac{455}{41,472}(-x)^{-1}\right]\cos\left[2\sqrt{-x}-\frac{7\pi}{12}\right]\\
&+\left[-\frac{7}{144}(-x)^{-\frac{1}{2}}+\frac{95,095}{17,915,904}(-x)^{-\frac{3}{2}}\right]\sin\left[2\sqrt{-x}-\frac{7\pi}{12}\right]\Bigg\}\\
&+O\left(x^{-\frac{31}{12}}\right)
\end{aligned}
$$

Substituting $\frac{x^3}{9}$ for x results in

$$
\begin{aligned}
{}_0F_1\left(\frac{5}{3};\frac{x^3}{9}\right) = \frac{\Gamma\left(\frac{5}{3}\right)3^{\frac{7}{6}}}{\sqrt{\pi}}\Bigg\{&(-x)^{-\frac{7}{4}}\left[1+\frac{455}{4608}(-x)^{-3}\right]\cos\left[\frac{2}{3}(-x)^{\frac{3}{2}}-\frac{7\pi}{12}\right]\\
&+(-x)^{-\frac{13}{4}}\left[-\frac{7}{48}+\frac{95,095}{663,552}(-x)^{-3}\right]\sin\left[\frac{2}{3}(-x)^{\frac{3}{2}}-\frac{7\pi}{12}\right]\Bigg\}\\
&+O\left(x^{-\frac{31}{4}}\right)
\end{aligned}
$$

Therefore, the asymptotic expansion for $N_1(x)$ is

$$
\begin{aligned}
N_1(x) =& \frac{x^2}{2}{}_0F_1\left(\frac{5}{3};\frac{x^3}{9}\right) = \frac{(-x)^2}{2}{}_0F_1\left(\frac{5}{3};\frac{x^3}{9}\right)\\
=& \frac{\Gamma\left(\frac{5}{3}\right)3^{\frac{7}{6}}}{2\sqrt{\pi}}\Bigg\{(-x)^{\frac{1}{4}}\left[1+\frac{455}{4608}(-x)^{-3}\right]\cos\left[\frac{2}{3}(-x)^{\frac{3}{2}}-\frac{7\pi}{12}\right]\\
&+(-x)^{-\frac{5}{4}}\left[-\frac{7}{48}+\frac{95,095}{663,552}(-x)^{-3}\right]\sin\left[\frac{2}{3}(-x)^{\frac{3}{2}}-\frac{7\pi}{12}\right]\Bigg\}\\
&+O\left(x^{-\frac{23}{4}}\right)
\end{aligned}
$$

Since $\Gamma\left(\frac{5}{3}\right)=\frac{2}{3}\Gamma\left(\frac{2}{3}\right)$, the coefficient of the expansion can be simplified to $\frac{\Gamma\left(\frac{2}{3}\right)3^{\frac{1}{6}}}{\sqrt{\pi}}$.

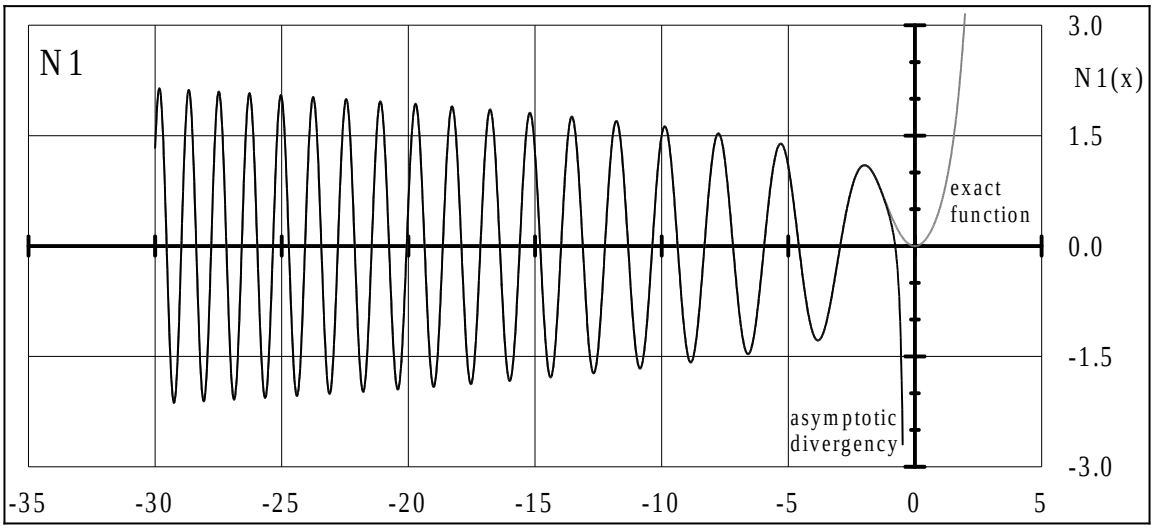

Figure E.22: Plot of the asymptotic expansion of $N_1(x)$.

The plot of the asymptotic expansion for N_1 along with the complete plot using path integration for comparison is shown in Figure Figure (E.22).

E.3.2 Expansion for Functions Type ${}_1F_2$ [Functions M_1(x), M_2(x), N_3(x), R_3(x)]

Functions of this type have subdominant terms. Two of the four functions of interest, M_1(x) and M_2(x), have subdominant terms that terminate. The other two have subdominant terms with divergent series which are suitably handled.

Equation (E.17), repeated here, includes the subdominant part:

$$
\begin{aligned}
&{}_pF_{p+1}\left(\begin{matrix}\alpha_{\mathrm{p}}\\ \beta_{\mathrm{p+1}}\end{matrix}\middle| -z\right)\approx \\
&\frac{\Gamma(\beta_{\mathrm{p+1}})}{\Gamma(\alpha_{\mathrm{p}})}\left[\frac{1}{\sqrt{\pi}}z^{\gamma}\sum_{k=0}^{\infty}N_k z^{-\frac{k}{2}}\cos\left(2\sqrt{z}+\pi\gamma-\frac{k}{2}\pi\right)+\sum_{t=1}^{p}{}^{t}L_{p,p+1}(z)\right]
\end{aligned}
\tag{E.17}
$$

For $p=1$, the simplified recursive relation for d_k is [Luke (1969) Vol. 1, pg. 200 (12)]:

$$
\begin{aligned}
2(k+1)d_{k+1} &= \left[3k^2+2k(1+B_1-3A_1)+4N\right] d_k + \\
&\quad -(k-2\gamma-1)(k-2\gamma+1-2\beta_1)(k-2\gamma+1-2\beta_2)d_{k-1}, \\
d_0 &= 1, \\
d_{-1} &= 0.
\end{aligned}
$$

If $\alpha_1 = 1$, which is the case for N_3(x), R_1(x), one can also make $\nu = \beta_1 - \beta_2$, and use the formula for $p = 0$.

E.3.2.1 Function $M_1(x) = x\ {}_1F_2(1/3; 2/3, 4/3; x^3/9)$

The dominant part is found following the same steps used in the previous sections. From the formulas in Equations (E.11) and (E.15) with $p = 1$, $q = 2$, $\alpha_1 = \frac{1}{3}$, $\beta_1 = \frac{2}{3}$, and $\beta_2 = \frac{4}{3}$ yield:

$$
\begin{aligned}
A_1 &= \frac{1}{3}, \\
B_1 &= \frac{2}{3} + \frac{4}{3} = 2, \\
A_2 &= 0 \quad (\text{empty list}), \\
B_2 &= \frac{2}{3} \times \frac{4}{3} = \frac{8}{9}, \\
\gamma &= \frac{1}{4} + \frac{1}{2}\left(\frac{1}{3} - 2\right) = -\frac{7}{12}, \\
N &= \left(\frac{8}{9} - 0\right) + \frac{1}{4}\left(\frac{1}{3} - 2\right)\left(3 \times \frac{1}{3} + 2 - 2\right) - \frac{3}{16} = \frac{41}{144}.
\end{aligned}
$$

Therefore, the expression for the dominant part is

$$K_{1,2}(-x) \approx \frac{(-x)^{-\frac{7}{12}}}{\sqrt{\pi}} \sum_{k=0}^{\infty} N_k (-x)^{-\frac{k}{2}} \cos\left(2\sqrt{-x} - \frac{7\pi}{12} - \frac{k}{2}\pi\right).$$

Using the recursion formulas for $p=1$

$$\begin{aligned} 2(k+1)d_{k+1} &= \left[3k^2+2k(1+B_1-3A_1)+4N\right] d_k + \\ &\quad -(k-2\gamma-1)(k-2\gamma+1-2\beta_1)(k-2\gamma+1-2\beta_2)d_{k-1}, \\ d_{(k+1)} &= \frac{1}{2(k+1)} \left[\left(3k^2+4k+\frac{41}{36}\right) d_k - \left(k+\frac{1}{6}\right)\left(k+\frac{5}{6}\right)\left(k-\frac{1}{2}\right) d_{k-1}\right], \end{aligned}$$

the d_k and N_k are

$$\begin{aligned} d_0 &= 1 \to N_0 = \frac{1}{2^0} = 1 \\ d_1 &= \frac{41}{72} \to N_1 = \frac{41}{144} \\ d_2 &= \frac{9241}{10,368} \to N_2 = \frac{9241}{41,472} \\ d_3 &= \frac{5,075,225}{2,239,488} \to N_3 = \frac{5075225}{17,915,904} \end{aligned}$$

Using these results for N_k, the expanded dominant part is:

$$\begin{aligned} K_{1,2}(-x) \approx \frac{1}{\sqrt{\pi}}(-x)^{-\frac{7}{12}} &\left[\cos\left(2\sqrt{-x} - \frac{7\pi}{12}\right)\right. \\ &+ \frac{41}{144}(-x)^{-\frac{1}{2}} \cos\left(2\sqrt{-x} - \frac{7\pi}{12} - \frac{\pi}{2}\right) \\ &+ \frac{9241}{41,472}(-x)^{-1} \cos\left(2\sqrt{-x} - \frac{7\pi}{12} - \pi\right) \\ &\left. - \frac{5,075,225}{17,915,904}(-x)^{-\frac{3}{2}} \cos\left(2\sqrt{-x} - \frac{7\pi}{12} - \frac{3\pi}{2}x\right)\right] \end{aligned}$$

Using similar trigonometric identities as before results in

$$K_{1,2}(-x) \approx \frac{1}{\sqrt{\pi}}(-x)^{-\frac{7}{12}}\left[\left(1-\frac{9241}{41,472}(-x)^{-1}\right)\cos\left(2\sqrt{-x}-\frac{7\pi}{12}\right)\right.$$
$$\left.+\left(\frac{41}{144}(-x)^{-\frac{1}{2}}-\frac{5,075,225}{17,915,904}(-x)^{-\frac{3}{2}}\right)\sin\left(2\sqrt{-x}-\frac{7\pi}{12}\right)\right]$$

To determine the subdominant part, Equation (E.16) is used with *p*=1 and *q*=2:

$$L_{p,p+1}(-x)=\sum_{t=1}^{p}{}^{t}L_{p,p+1}(-x), \tag{E.16-a}$$

$${}^{t}L_{p,p+1}(-x)=\frac{(-x)^{-\alpha_t}\Gamma(\alpha_t)\Gamma(\alpha^*_{\mathrm{p}}-\alpha_t)}{\Gamma(\beta_{\mathrm{p}+1}-\alpha_t)}\times \tag{E.16-b}$$
$${}_{p+2}F_{p-1}\left(\alpha_t,1+\alpha_t-\beta_{\mathrm{p}+1};1+\alpha_t-\alpha^*_{\mathrm{p}};\frac{1}{x}\right).$$

The summation in Equation (E.16-a) has one term only ($t=1$). In Equation (E.16-b), the list $(\alpha^*_{\mathrm{p}}-\alpha_t)$ is empty and therefore $\Gamma(\alpha^*_{\mathrm{p}}-\alpha_t)=1$

$$L_{1,2}(-x)=\sum_{t=1}^{1}{}^{t}L_{1,2}(-x)={}^{1}L_{1,2}(-x)$$
$$=\frac{(-x)^{-\frac{1}{3}}\Gamma\left(\frac{1}{3}\right)\times 1}{\Gamma\left(\frac{2}{3}-\frac{1}{3}\right)\Gamma\left(\frac{4}{3}-\frac{1}{3}\right)}\,{}_3F_0\left(\frac{1}{3},1+\frac{1}{3}-\frac{2}{3},1+\frac{1}{3}-\frac{4}{3};\frac{1}{x}\right)$$
$$L_{1,2}(-x)=\frac{(-x)^{-\frac{1}{3}}\Gamma\left(\frac{1}{3}\right)}{\Gamma\left(\frac{1}{3}\right)\Gamma(1)}\,{}_3F_0\left(\frac{1}{3},\frac{2}{3},0;\frac{1}{x}\right).$$

It is notable that the parameter 0 in the numerator of ${}_3F_0$ causes the series expansion to have the term $n=0$ only. All others vanish because, although $(0)_0=1$, $(0)_1=\frac{\Gamma(1+0)}{\Gamma(0)}=0$, and so on. Therefore

$${}_3F_0\left(\frac{1}{3},\frac{2}{3},0;\frac{1}{x}\right)=\sum_{n=0}^{\infty}\left(\frac{1}{3}\right)_n\left(\frac{2}{3}\right)_n(0)_n\frac{\left(\frac{1}{x}\right)^n}{n!}=1,$$

and

$$L_{1,2}(-x) = (-x)^{-\frac{1}{3}}.$$

Putting the dominant and subdominant terms found in into the expression of the asymptotic expansion, and using the the simplified coefficient $\frac{1}{3}\Gamma\left(\frac{2}{3}\right)$ for $\frac{\Gamma\left(\frac{2}{3}\right)\Gamma\left(\frac{4}{3}\right)}{\Gamma\left(\frac{1}{3}\right)}$gives

$$\begin{aligned}{}_1F_2\left(\frac{1}{3};\frac{2}{3},\frac{4}{3};x\right) \approx \frac{\Gamma\left(\frac{2}{3}\right)}{3}\Bigg\{&\frac{1}{\sqrt{\pi}}(-x)^{-\frac{7}{12}}\left[\left(1-\frac{9,241}{41,472}(-x)^{-1}\right)\cos\left(2\sqrt{-x}-\frac{7\pi}{12}\right)\right.\\ &\left.+\left(\frac{41}{144}(-x)^{-\frac{1}{2}}-\frac{5,075,225}{17,915,904}(-x)^{-\frac{3}{2}}\right)\sin\left(2\sqrt{-x}-\frac{7\pi}{12}\right)\right]\\ &+(-x)^{-\frac{1}{3}}\Bigg\}+O\left(x^{-\frac{31}{12}}\right)\end{aligned}$$

Substituting $\frac{x^3}{9}$ for x results in

$$\begin{aligned}{}_1F_2\left(\frac{1}{3};\frac{2}{3},\frac{4}{3};\frac{x^3}{9}\right) =&\frac{\Gamma\left(\frac{2}{3}\right)3^{\frac{1}{6}}}{\sqrt{\pi}}\Bigg\{(-x)^{-\frac{7}{4}}\left[1-\frac{9,241}{4,608}(-x)^{-3}\right]\cos\left[\frac{2}{3}(-x)^{\frac{3}{2}}-\frac{7\pi}{12}\right]\\ &+(-x)^{-\frac{13}{4}}\left[\frac{41}{48}-\frac{5,075,225}{663,552}(-x)^{-3}\right]\sin\left[\frac{2}{3}(-x)^{\frac{3}{2}}-\frac{7\pi}{12}\right]\Bigg\}\\ &+\frac{\Gamma\left(\frac{2}{3}\right)}{3^{\frac{1}{3}}}(-x)^{-1}+O\left(x^{-\frac{31}{4}}\right)\end{aligned}$$

Therefore, the asymptotic expansion for $M_1(x) = x\,{}_1F_2\left(\frac{1}{3};\frac{2}{3},\frac{4}{3};\frac{x^3}{9}\right)$ is

$$\begin{aligned}M_1(x) = -\frac{\Gamma\left(\frac{2}{3}\right)3^{\frac{1}{6}}}{\sqrt{\pi}}\Bigg\{&(-x)^{-\frac{3}{4}}\left[1-\frac{9,241}{4,608}(-x)^{-3}\right]\cos\left[\frac{2}{3}(-x)^{\frac{3}{2}}-\frac{7\pi}{12}\right]\\ &+(-x)^{-\frac{9}{4}}\left[\frac{41}{48}-\frac{5,075,225}{663,552}(-x)^{-3}\right]\sin\left[\frac{2}{3}(-x)^{\frac{3}{2}}-\frac{7\pi}{12}\right]\Bigg\}\\ &-\frac{\Gamma\left(\frac{2}{3}\right)}{3^{\frac{1}{3}}}+O\left(x^{-\frac{27}{4}}\right)\end{aligned}$$

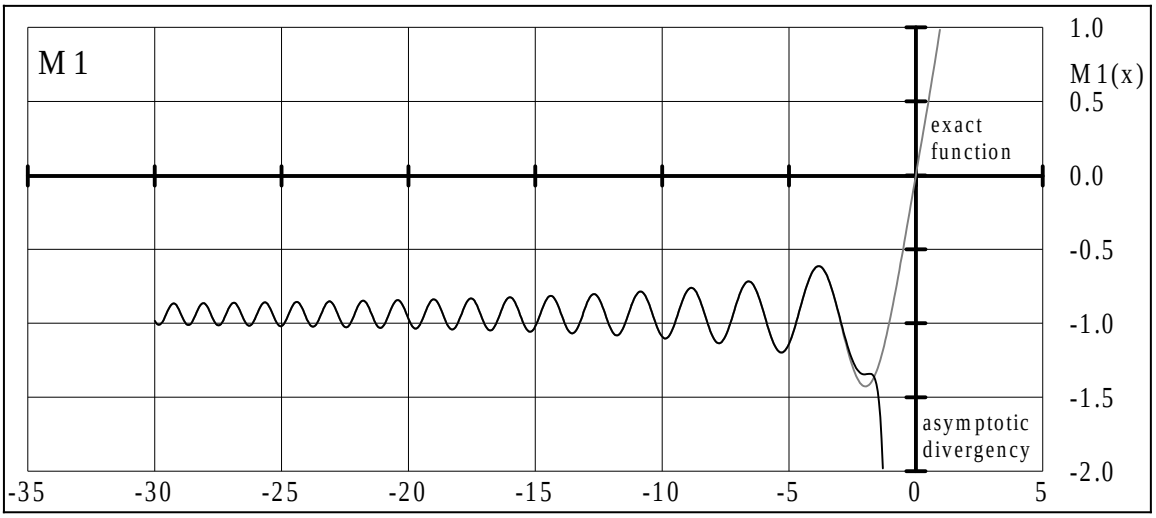

Figure E.23: Plot of the asymptotic expansion of $M_1(x)$.

The plot of the asymptotic expansion for $M_1(x)$ along with the exact plot is shown in Figure (E.23). The graph shows the effect of the subdominant term. It causes a vertical shift given by the constant $\frac{-\Gamma\left(\frac{2}{3}\right)}{3^{\frac{1}{3}}} = -0.9388929\ldots$, which is the limit when $x \to -\infty$.

E.3.2.2 Function $M_2(x) = x^2/2\ {}_1F_2(2/3;4/3,5/3;x^3/9)$

This function is very similar to the previous case $M_1(x)$. The dominant part is found following the same steps used in the previous sections. From the formulas in Equations (E.11) and (E.15) with $p=1$, $q=2$, $\alpha_1 = \frac{2}{3}$, $\beta_1 = \frac{4}{3}$, and $\beta_2 = \frac{5}{3}$ yield:

$$
\begin{aligned}
A_1 &= \frac{2}{3}, \\
B_1 &= \frac{4}{3} + \frac{5}{3} = 3, \\
A_2 &= 0 \quad (\text{empty list}),
\end{aligned}
$$

$$B_2 = \frac{4}{3} \times \frac{5}{3} = \frac{20}{9},$$
$$\gamma = \frac{1}{4} + \frac{1}{2}\left(\frac{2}{3} - 3\right) = -\frac{11}{12},$$
$$N = \left(\frac{20}{9} - 0\right) + \frac{1}{4}\left(\frac{2}{3} - 3\right)\left(3 \times \frac{2}{3} + 3 - 2\right) - \frac{3}{16} = \frac{41}{144}.$$

Therefore, the expression for the dominant part is

$$K_{1,2}(-x) \approx \frac{(-x)^{-\frac{11}{12}}}{\sqrt{\pi}} \sum_{k=0}^{\infty} N_k (-x)^{-\frac{k}{2}} \cos\left(2\sqrt{-x} - \frac{11\pi}{12} - \frac{k}{2}\pi\right).$$

Using the recursion formulas for $p = 1$

$$d_{(k+1)} = \frac{1}{2(k+1)}\left[\left(3k^2 + 4k + \frac{41}{36}\right) d_k - \left(k + \frac{5}{6}\right)\left(k + \frac{1}{6}\right)\left(k - \frac{1}{2}\right) d_{k-1}\right],$$

the d_k and N_k are

$$d_0 = 1 \rightarrow N_0 = \frac{1}{2^0} = 1$$
$$d_1 = \frac{41}{72} \rightarrow N_1 = \frac{41}{144}$$
$$d_2 = \frac{9241}{10,368} \rightarrow N_2 = \frac{9241}{41,472}$$
$$d_3 = \frac{5,075,225}{2,239,488} \rightarrow N_3 = \frac{5075225}{17,915,904}$$

Using these results for N_k, the expanded dominant part is:

$$K_{1,2}(-x) \approx \frac{1}{\sqrt{\pi}}(-x)^{-\frac{11}{12}}\left[\cos\left(2\sqrt{-x}-\frac{11\pi}{12}\right)\right.$$
$$+\frac{41}{144}(-x)^{-\frac{1}{2}}\cos\left(2\sqrt{-x}-\frac{11\pi}{12}-\frac{\pi}{2}\right)$$
$$+\frac{9241}{41,472}(-x)^{-1}\cos\left(2\sqrt{-x}-\frac{11\pi}{12}-\pi\right)$$
$$\left.-\frac{5,075,225}{17,915,904}(-x)^{-\frac{3}{2}}\cos\left(2\sqrt{-x}-\frac{11\pi}{12}-\frac{3\pi}{2}x\right)\right]$$

Using similar trigonometric identities as before results in

$$K_{1,2}(-x) \approx \frac{1}{\sqrt{\pi}}(-x)^{-\frac{11}{12}}\left[\left(1-\frac{9241}{41,472}(-x)^{-1}\right)\cos\left(2\sqrt{-x}-\frac{11\pi}{12}\right)\right.$$
$$\left.+\left(\frac{41}{144}(-x)^{-\frac{1}{2}}-\frac{5,075,225}{17,915,904}(-x)^{-\frac{3}{2}}\right)\sin\left(2\sqrt{-x}-\frac{11\pi}{12}\right)\right]$$

To determine the subdominant part, Equation (E.16) is used with *p*=1 and *q*=2:

$$L_{p,p+1}(-x)=\sum_{t=1}^{p}{}^{t}L_{p,p+1}(-x), \tag{E.16-a}$$

$${}^{t}L_{p,p+1}(-x)=\frac{(-x)^{-\alpha_t}\Gamma(\alpha_t)\Gamma(\alpha_{\mathrm{p}}^{*}-\alpha_t)}{\Gamma(\beta_{\mathrm{p+1}}-\alpha_t)}\times$$
$$ {}_{p+2}F_{p-1}\left(\alpha_t, 1+\alpha_t-\beta_{\mathrm{p+1}}; 1+\alpha_t-\alpha_{\mathrm{p}}^{*}; \frac{1}{x}\right). \tag{E.16-b}$$

The summation in Equation (E.16-a) has one term only ($t=1$). In Equation (E.16-b), the list $(\alpha_{\mathrm{p}}^{*}-\alpha_t)$ is empty and therefore $\Gamma(\alpha_{\mathrm{p}}^{*}-\alpha_t)=1$

$$L_{1,2}(-x)=\sum_{t=1}^{1}{}^{t}L_{1,2}(-x)={}^{1}L_{1,2}(-x)$$
$$=\frac{(-x)^{-\frac{2}{3}}\Gamma\left(\frac{2}{3}\right)\times 1}{\Gamma\left(\frac{4}{3}-\frac{2}{3}\right)\Gamma\left(\frac{5}{3}-\frac{2}{3}\right)}\,{}_{3}F_{0}\left(\frac{2}{3}, 1+\frac{2}{3}-\frac{4}{3}, 1+\frac{2}{3}-\frac{5}{3}; \frac{1}{x}\right)$$

$$L_{1,2}(-x) = \frac{z^{-\frac{2}{3}}\Gamma\left(\frac{2}{3}\right)}{\Gamma\left(\frac{2}{3}\right)\Gamma\left(1\right)}{}_3F_0\left(\frac{2}{3},\frac{1}{3},0;\frac{1}{x}\right).$$

Similarly to the previous case $M_1(x)$, the function ${}_3F_0$ has only the term for $n=0$:

$${}_3F_0\left(\frac{1}{3},\frac{2}{3},0;\frac{1}{x}\right) = \sum_{n=0}^{\infty}\left(\frac{1}{3}\right)_n\left(\frac{2}{3}\right)_n(0)_n\frac{\left(\frac{1}{x}\right)^n}{n!} = 1,$$

and,

$$L_{1,2}(-x) = (-x)^{-\frac{2}{3}}.$$

Putting the dominant and subdominant terms found in into the expression of the asymptotic expansion, and using the the simplified coefficient $\frac{2}{9}\Gamma\left(\frac{1}{3}\right)$ for $\frac{\Gamma\left(\frac{4}{3}\right)\Gamma\left(\frac{5}{3}\right)}{\Gamma\left(\frac{2}{3}\right)}$gives

$$\begin{aligned}{}_1F_2\left(\frac{2}{3};\frac{4}{3},\frac{5}{3};x\right) =& \frac{2\Gamma\left(\frac{1}{3}\right)}{9}\left\{\frac{1}{\sqrt{\pi}}(-x)^{-\frac{11}{12}}\left[\left(1-\frac{9,241}{41,472}(-x)^{-1}\right)\cos\left(2\sqrt{-x}-\frac{11\pi}{12}\right)\right.\right.\\ &\left.+\left(\frac{41}{144}(-x)^{-\frac{1}{2}}-\frac{5,075,225}{17,915,904}(-x)^{-\frac{3}{2}}\right)\sin\left(2\sqrt{-x}-\frac{11\pi}{12}\right)\right]\\ &\left.+(-x)^{-\frac{2}{3}}\right\}+O\left(x^{-\frac{35}{12}}\right)\end{aligned}$$

Substituting $\frac{x^3}{9}$ for x results in

$$\begin{aligned}{}_1F_2\left(\frac{2}{3};\frac{4}{3},\frac{5}{3};\frac{x^3}{9}\right) =& \frac{2\Gamma\left(\frac{1}{3}\right)}{3^{\frac{1}{6}}\sqrt{\pi}}\left\{(-x)^{-\frac{11}{4}}\left[1-\frac{9,241}{4,608}(-x)^{-3}\right]\cos\left[\frac{2}{3}(-x)^{\frac{3}{2}}-\frac{11\pi}{12}\right]\right.\\ &\left.+(-x)^{-\frac{17}{4}}\left[\frac{41}{48}-\frac{5,075,225}{663,552}(-x)^{-3}\right]\sin\left[\frac{2}{3}(-x)^{\frac{3}{2}}-\frac{11\pi}{12}\right]\right\}\\ &+\frac{2\Gamma\left(\frac{1}{3}\right)}{3^{\frac{2}{3}}}(-x)^{-2}+O\left(x^{-\frac{35}{4}}\right)\end{aligned}$$

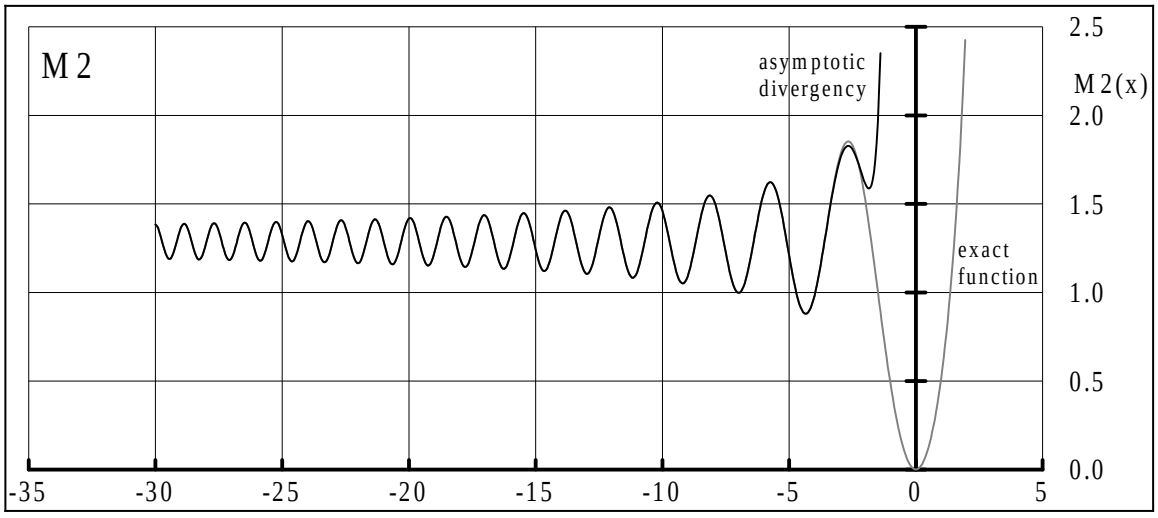

Figure E.24: Plot of the asymptotic expansion of $M_2(x)$.

Therefore, the asymptotic expansion for $M_2(x) = \frac{x^2}{2}\,{}_1F_2\left(\frac{2}{3}; \frac{4}{3}, \frac{5}{3}; \frac{x^3}{9}\right)$ is

$$\begin{aligned} M_2(x) =& \frac{\Gamma\left(\frac{1}{3}\right)}{3^{\frac{1}{6}}\sqrt{\pi}}\left\{(-x)^{-\frac{3}{4}}\left[1-\frac{9,241}{4,608}(-x)^{-3}\right]\cos\left[\frac{2}{3}(-x)^{\frac{3}{2}}-\frac{11\pi}{12}\right]\right. \\ &\left.+(-x)^{-\frac{9}{4}}\left[\frac{41}{48}-\frac{5,075,225}{663,552}(-x)^{-3}\right]\sin\left[\frac{2}{3}(-x)^{\frac{3}{2}}-\frac{11\pi}{12}\right]\right\} \\ &+\frac{\Gamma\left(\frac{1}{3}\right)}{3^{\frac{2}{3}}}+O\left(x^{-\frac{27}{4}}\right) \end{aligned}$$

The plot of the asymptotic expansion for $M_2(x)$ along with the exact plot is shown in Figure (E.27). The subdominant term causes a vertical shift given by the constant $\frac{\Gamma\left(\frac{1}{3}\right)}{3^{\frac{2}{3}}} = 1.287899\ldots$, which is the limit when $x \to -\infty$.

E.3.2.3 Function $N_3(x) = 2x\,{}_1F_2(1; {}^2/_3, {}^4/_3; x^3/9)$

This function and the next one (R_3) have non-terminating subdominant parts. The

discussion will carry on not including the subdominant part and, in the way it will be discussed and included. From the formulas in Equations (E.11) and (E.15) with $p=1$, $q=2$, $\alpha_1=1$, $\beta_1=\frac{2}{3}$, and $\beta_2=\frac{4}{3}$ yield:

$$
\begin{aligned}
&A_1 = 1\\
&B_1 = \frac{2}{3}+\frac{4}{3} = 2,\\
&A_2 = 0, \quad \text{(empty list)},\\
&B_2 = \frac{2}{3}\times\frac{4}{3} = \frac{8}{9},\\
&\gamma = \frac{1}{4}+\frac{1}{2}(1-2) = -\frac{1}{4},\\
&N = \left(\frac{8}{9}-0\right)+\frac{1}{4}(1-2)(3\times 1+2-2)-\frac{3}{16} = -\frac{7}{144}.
\end{aligned}
$$

Therefore, the expression for the dominant part is

$$
K_{1,2}(-x)\approx\frac{(-x)^{-\frac{1}{4}}}{\sqrt{\pi}}\sum_{k=0}^{\infty}N_k(-x)^{-\frac{k}{2}}\cos\left(2\sqrt{-x}-\frac{\pi}{4}-\frac{k}{2}\pi\right).
$$

Since $\alpha_1=1$, the simpler explicit formula for d_k can be used making $\nu=\beta_1-\beta_2=-\frac{2}{3}$ as detailed in Section E.3.2. Therefore the d_k are: [the same for the expansion of ${}_0F_1(\frac{1}{3};x)$]

$$
\begin{aligned}
d_0 &= \frac{(\frac{1}{2}+\frac{2}{3})_0(\frac{1}{2}-\frac{2}{3})_0}{2^0 0!} = 1 \to N_0 = \frac{1}{2^0} = 1\\
d_1 &= \frac{(\frac{1}{2}+\frac{2}{3})_1(\frac{1}{2}-\frac{2}{3})_1}{2^1 1!} = \frac{-7}{72} \to N_1 = \frac{-7}{144}\\
d_2 &= \frac{(\frac{1}{2}+\frac{2}{3})_2(\frac{1}{2}-\frac{2}{3})_2}{2^2 2!} = \frac{-455}{10,368} \to N_2 = \frac{-455}{41,472}\\
d_3 &= \frac{(\frac{1}{2}+\frac{2}{3})_3(\frac{1}{2}-\frac{2}{3})_3}{2^3 3!} = \frac{-95,095}{2,239,488} \to N_3 = \frac{-95,095}{17,915,904}
\end{aligned}
$$

Using these results for d_k, the dominant part becomes:

$$\begin{aligned}K_{1,2}(-x) \approx \frac{1}{\sqrt{\pi}}(-x)^{-\frac{1}{4}} \Big[&\cos\Big(2\sqrt{-x} - \frac{\pi}{12}\Big) \\ &- \frac{7}{144}(-x)^{-\frac{1}{2}} \cos\Big(2\sqrt{-x} - \frac{\pi}{4} - \frac{\pi}{2}\Big) \\ &- \frac{455}{41,472}(-x)^{-1} \cos\Big(2\sqrt{-x} - \frac{\pi}{4} - \pi\Big) \\ &- \frac{95,095}{17,915,904}(-x)^{-\frac{3}{2}} \cos\left(2\sqrt{-x} - \frac{\pi}{4} - \frac{3\pi}{2}x\right)\Big]\end{aligned}$$

or

$$\begin{aligned}K_{1,2}(-x) \approx \frac{1}{\sqrt{\pi}}(-x)^{-\frac{1}{4}} \Bigg[&\left(1 + \frac{455}{41,472}(-x)^{-1}\right) \cos\Big(2\sqrt{-x} - \frac{\pi}{4}\Big) \\ &+ \left(-\frac{7}{144}(-x)^{-\frac{1}{2}} + \frac{95,095}{17,915,904}(-x)^{-\frac{3}{2}}\right) \sin\Big(2\sqrt{-x} - \frac{\pi}{4}\Big)\Bigg]\end{aligned}$$

The subdominant term is given by

$$\begin{aligned}L_{1,2}(-x) &= \sum_{t=1}^{1} {}^{t}L_{1,2}(-x) = {}^{1}L_{1,2}(-x) \\ &= \frac{(-x)^{-1}\Gamma(1) \times 1}{\Gamma\left(\frac{4}{3} - 1\right)\Gamma\left(\frac{2}{3} - 1\right)} \, {}_3F_0\left(1, 1+1-\frac{4}{3}, 1+1-\frac{2}{3}; \frac{1}{x}\right) \\ L_{1,2}(-x) &= \frac{(-x)^{-1}}{\Gamma\left(\frac{1}{3}\right)\Gamma\left(-\frac{1}{3}\right)} \, {}_3F_0\left(1, \frac{2}{3}, \frac{4}{3}; \frac{1}{x}\right).\end{aligned}$$

Since the values of the argument $-x$ are very large (and to the cube) the value of the function ${}_3F_0\left(1, \frac{2}{3}, \frac{4}{3}; \frac{1}{x}\right)$ can be approximate the value of ${}_3F_0\left(1, \frac{2}{3}, \frac{4}{3}; 0\right) = 1$. Therefore, since $\Gamma(1) = 1$, the subdominant part is

$$L_{1,2}(-x) \approx \frac{(-x)^{-1}}{\Gamma\left(\frac{1}{3}\right)\Gamma\left(-\frac{1}{3}\right)}$$

Putting the dominant and subdominant parts found into the expression of the asymptotic expansion results:

$$
\begin{aligned}
{}_1F_2\left(1;\frac{2}{3},\frac{4}{3},x\right) =& \Gamma\left(\frac{4}{3}\right)\Gamma\left(\frac{3}{3}\right)\left\{\frac{(-x)^{-\frac{1}{4}}}{\sqrt{\pi}}\times\right. \\
& \left[\left(1+\frac{455}{41,472}(-x)^{-1}\right)\cos\left(2\sqrt{-x}-\frac{\pi}{4}\right)+\right. \\
& \left.\left.\left(-\frac{7}{144}(-x)^{-\frac{1}{2}}+\frac{95,095}{17,915,904}(-x)^{-\frac{3}{2}}\right)\sin\left(2\sqrt{-x}-\frac{\pi}{4}\right)\right]\right\} \\
& +\frac{\Gamma\left(\frac{4}{3}\right)\Gamma\left(\frac{2}{3}\right)}{\Gamma\left(\frac{1}{3}\right)\Gamma\left(-\frac{1}{3}\right)}(-x)^{-1}+O\left(x^{-\frac{9}{4}}\right)
\end{aligned}
$$

Noting that

$$
\Gamma\left(\frac{4}{3}\right)\Gamma\left(\frac{2}{3}\right)=\frac{1}{3}\Gamma\left(\frac{1}{3}\right)\Gamma\left(\frac{2}{3}\right)=-\frac{1}{9}\Gamma\left(\frac{1}{3}\right)\Gamma\left(-\frac{1}{3}\right),
$$

the coefficient of the subdominant part simplifies to $-\frac{1}{9}$, and the coefficient multiplying the dominant term is $\frac{1}{3}\Gamma\left(\frac{1}{3}\right)\Gamma\left(\frac{2}{3}\right)$.

Using the subtle gamma function relationship[11] $\Gamma(z)\Gamma(1-z)=\frac{\pi}{\sin(\pi z)}$ and making $z=\frac{1}{3}$ gives:

$$
\frac{1}{3}\Gamma\left(\frac{1}{3}\right)\Gamma\left(\frac{2}{3}\right)=\frac{1}{3}\Gamma\left(\frac{1}{3}\right)\Gamma\left(1-\frac{1}{3}\right)=\frac{1}{3}\frac{\pi}{\sin\left(\frac{\pi}{3}\right)},
$$

and

11 This is called Euler's reflection relationship, due to Leonard Euler.

$$\Gamma\left(\frac{4}{3}\right)\Gamma\left(\frac{2}{3}\right) = \frac{2\pi}{3\sqrt{3}}.$$

Substituting $x^{\frac{3}{9}}$ for *x* and the precious results gives

$$\begin{aligned}{}_1F_2\left(1;\frac{2}{3},\frac{4}{3},\frac{x^3}{9}\right) =& \frac{2\sqrt{\pi}}{3}\left\{(-x)^{-\frac{3}{4}}\left[1+\frac{455}{4,608}(-x)^{-3}\right]\cos\left[\frac{2}{3}(-x)^{\frac{3}{2}}-\frac{\pi}{4}\right]\right.\\ &\left.+(-x)^{-\frac{9}{4}}\left[-\frac{7}{48}+\frac{95,095}{663,552}(-x)^{-3}\right]\sin\left[\frac{2}{3}(-x)^{\frac{3}{2}}-\frac{\pi}{4}\right]\right\}\\ &-(-x)^{-3}+O\left(x^{-\frac{27}{4}}\right)\end{aligned}$$

Therefore, the asymptotic expansion for $N_3(x) = 2x\,{}_1F_2\left(1;\frac{2}{3},\frac{4}{3};\frac{x^3}{9}\right)$ is

$$\begin{aligned}N_3(x) &= 2x\,{}_1F_2\left(1;\frac{2}{3},\frac{4}{3},\frac{x^3}{9}\right)\\ &= -\frac{4\sqrt{\pi}}{3}\left\{(-x)^{\frac{1}{4}}\left[1+\frac{455}{4,608}(-x)^{-3}\right]\cos\left[\frac{2}{3}(-x)^{\frac{3}{2}}-\frac{\pi}{4}\right]\right.\\ &\left.+\,(-x)^{-\frac{5}{4}}\left[-\frac{7}{48}+\frac{95,095}{663,552}(-x)^{-3}\right]\sin\left[\frac{2}{3}(-x)^{\frac{3}{2}}-\frac{\pi}{4}\right]\right\}\\ &+2(-x)^{-2}+O\left(x^{-\frac{23}{4}}\right)\end{aligned}$$

The plot of the asymptotic expansion for N_3 along with the exact plot is shown in Figure (E.25). The subdominant term here does not occurs as an additive constant but rather as a quadratically decreasing term. The amplitude is modulated for large negative x mainly by the slow increasing coefficient $\frac{4\sqrt{\pi}}{3}(-x)^{\frac{1}{4}}$ of the *cosine* term. This explain the small effect of the subdominant term in the behavior of the function for large negative *x*.

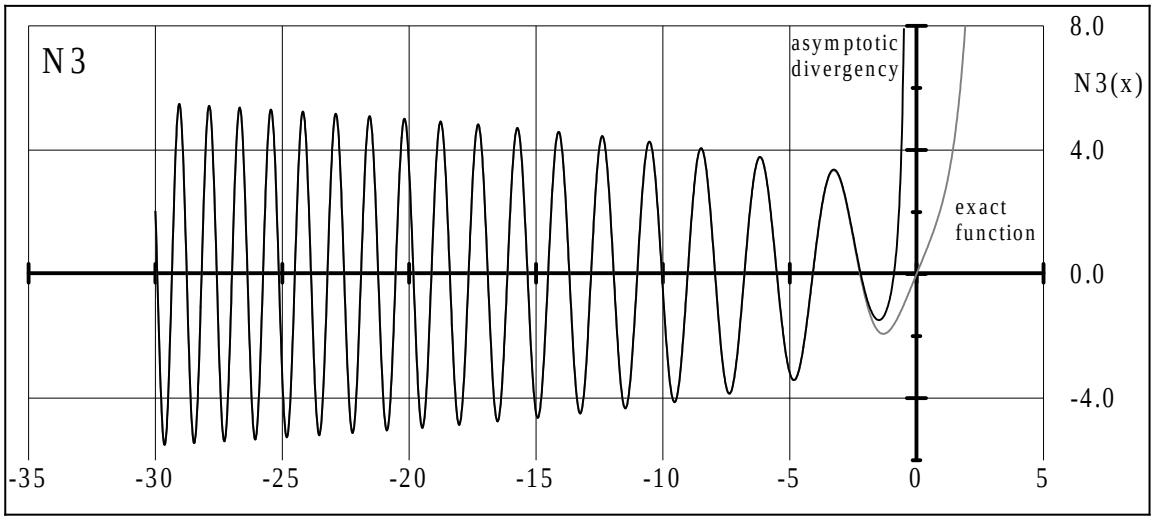

Figure E.25: Plot of the asymptotic expansion of $N_3(x)$.

E.3.2.4 Function $R_3(x) = x^2\ {}_1F_2(1;4/3,5/3;x^3/9)$

From the formulas in Equations (E.11) and (E.15) with $p=1$, $q=2$, $\alpha_1=1$, $\beta_1=\frac{4}{3}$, and $\beta_2=\frac{5}{3}$ yield:

$$
\begin{aligned}
&A_1 = 1\\
&B_1 = \frac{4}{3}+\frac{5}{3} = 3,\\
&A_2 = 0, \quad \text{(empty list)},\\
&B_2 = \frac{4}{3}\times\frac{5}{3} = \frac{20}{9},\\
&\gamma = \frac{1}{4}+\frac{1}{2}(1-3) = -\frac{3}{4},\\
&N = \left(\frac{20}{9}-0\right)+\frac{1}{4}(1-3)(3\times 1+3-2)-\frac{3}{16} = \frac{5}{144}.
\end{aligned}
$$

Therefore, the expression for the dominant part is

$$K_{1,2}(-x) \approx \frac{(-x)^{-\frac{3}{4}}}{\sqrt{\pi}}\sum_{k=0}^{\infty} N_k(-x)^{-\frac{k}{2}}\cos\left(2\sqrt{-x}-\frac{3\pi}{4}-\frac{k}{2}\pi\right).$$

Since $\alpha_1 = 1$, d_k are found making $\nu = \beta_1 - \beta_2 = -\frac{1}{3}$ as detailed in Section E.3.2. Therefore the d_k are [the same for the expansion of ${}_0F_1(\frac{2}{3}; x)$]:

$$
\begin{aligned}
d_0 &= \frac{(\frac{1}{2}+\frac{1}{3})_0(\frac{1}{2}-\frac{1}{3})_0}{2^0 0!} = 1 \to N_0 = \frac{1}{2^0} = 1 \\
d_1 &= \frac{(\frac{1}{2}+\frac{1}{3})_1(\frac{1}{2}-\frac{1}{3})_1}{2^1 1!} = \frac{5}{72} \to N_1 = \frac{5}{144} \\
d_2 &= \frac{(\frac{1}{2}+\frac{1}{3})_2(\frac{1}{2}-\frac{1}{3})_2}{2^2 2!} = \frac{385}{10,368} \to N_2 = \frac{385}{41,472} \\
d_3 &= \frac{(\frac{1}{2}+\frac{1}{3})_3(\frac{1}{2}-\frac{1}{3})_3}{2^3 3!} = \frac{85,085}{2,239,488} \to N_3 = \frac{85,085}{17,915,904}
\end{aligned}
$$

Using these results for d_k, the dominant part becomes:

$$
\begin{aligned}
K_{1,2}(-x) \approx & \frac{1}{\sqrt{\pi}}(-x)^{-\frac{3}{4}} \left[\cos\left(2\sqrt{-x} - \frac{3\pi}{4}\right) \right. \\
& + \frac{5}{144}(-x)^{-\frac{1}{2}} \cos\left(2\sqrt{-x} - \frac{3\pi}{4} - \frac{\pi}{2}\right) \\
& + \frac{385}{41,472}(-x)^{-1} \cos\left(2\sqrt{-x} - \frac{3\pi}{4} - \pi\right) \\
& \left. + \frac{85,085}{17,915,904}(-x)^{-\frac{3}{2}} \cos\left(2\sqrt{-x} - \frac{3\pi}{4} - \frac{3\pi}{2}x\right) \right]
\end{aligned}
$$

or

$$
\begin{aligned}
K_{1,2}(-x) \approx & \frac{1}{\sqrt{\pi}}(-x)^{-\frac{3}{4}} \left[\left(1 - \frac{385}{41,472}(-x)^{-1}\right) \cos\left(2\sqrt{-x} - \frac{3\pi}{4}\right) \right. \\
& \left. + \left(\frac{5}{144}(-x)^{-\frac{1}{2}} - \frac{85,085}{17,915,904}(-x)^{-\frac{3}{2}}\right) \sin\left(2\sqrt{-x} - \frac{3\pi}{4}\right) \right]
\end{aligned}
$$

The subdominant term is given by

$$L_{1,2}(-x) = \sum_{t=1}^{1} {}^{t}L_{1,2}(-x) = {}^{1}L_{1,2}(-x)$$
$$= \frac{(-x)^{-1}\Gamma(1)\times 1}{\Gamma\left(\frac{4}{3}-1\right)\Gamma\left(\frac{5}{3}-1\right)}{}_3F_0\left(1, 1+1-\frac{4}{3}, 1+1-\frac{5}{3}; \frac{1}{x}\right)$$
$$L_{1,2}(-x) = \frac{x^{-1}}{\Gamma\left(\frac{1}{3}\right)\Gamma\left(\frac{2}{3}\right)}{}_3F_0\left(1, \frac{2}{3}, \frac{1}{3}; \frac{1}{x}\right).$$

Since the values of the argument $-x$ are very large (and to the cube) the value of the function ${}_3F_0\left(1, \frac{2}{3}, \frac{1}{3}; \frac{1}{x}\right)$ can be approximate the value of ${}_3F_0\left(1, \frac{2}{3}, \frac{1}{3}; 0\right) = 1$. Therefore the subdominant part is

$$L_{1,2}(-x) \approx \frac{(-x)^{-1}}{\Gamma\left(\frac{1}{3}\right)\Gamma\left(\frac{2}{3}\right)}$$

Putting the dominant and subdominant parts found into the expression of the asymptotic expansion results:

$$\begin{aligned}{}_1F_2\left(1; \frac{4}{3}, \frac{5}{3}, x\right) =& \Gamma\left(\frac{4}{3}\right)\Gamma\left(\frac{5}{3}\right)\left\{\frac{(-x)^{-\frac{3}{4}}}{\sqrt{\pi}}\times\right.\\ &\left[\left(1-\frac{385}{41,472}(-x)^{-1}\right)\cos\left(2\sqrt{-x}-\frac{3\pi}{4}\right)+\right.\\ &\left.\left.\left(\frac{5}{144}(-x)^{-\frac{1}{2}}-\frac{85,085}{17,915,904}(-x)^{-\frac{3}{2}}\right)\sin\left(2\sqrt{-x}-\frac{3\pi}{4}\right)\right]\right\}\\ &+\frac{\Gamma\left(\frac{4}{3}\right)\Gamma\left(\frac{5}{3}\right)}{\Gamma\left(\frac{1}{3}\right)\Gamma\left(\frac{2}{3}\right)}(-x)^{-1}+O\left(x^{-\frac{11}{4}}\right)\end{aligned}$$

Noting that $\Gamma\left(\frac{4}{3}\right)\Gamma\left(\frac{5}{3}\right) = \frac{2}{9}\Gamma\left(\frac{1}{3}\right)\Gamma\left(\frac{2}{3}\right)$, the coefficient of the subdominant part simplifies to $\frac{2}{9}$, and the coefficient multiplying the dominant term is $\frac{2}{9}\Gamma\left(\frac{1}{3}\right)\Gamma\left(\frac{2}{3}\right)$. Using again relationship $\Gamma(z)\Gamma(1-z) = \frac{\pi}{\sin(\pi z)}$ for $z = \frac{1}{3}$ gives:

$$\frac{2}{9}\Gamma\left(\frac{1}{3}\right)\Gamma\left(\frac{2}{3}\right)=\frac{2}{9}\Gamma\left(\frac{1}{3}\right)\Gamma\left(1-\frac{1}{3}\right)=\frac{2}{9}\frac{\pi}{\sin\left(\frac{\pi}{3}\right)}=\frac{4\pi}{9\sqrt{3}}$$

Substituting $x^{\frac{3}{9}}$ for *x* and the precious results gives

$$\begin{aligned}{}_1F_2\left(1;\frac{4}{3},\frac{5}{3},\frac{x^3}{9}\right)=&\frac{4\sqrt{\pi}}{3}\left\{(-x)^{-\frac{9}{4}}\left(1-\frac{385}{4,608}(-x)^{-3}\right)\cos\left(\frac{2}{3}(-x)^{\frac{3}{2}}-\frac{3\pi}{4}\right)\right.\\&\left.+(-x)^{-\frac{15}{4}}\left(\frac{5}{48}-\frac{85,085}{663,552}(-x)^{-3}\right)\sin\left(\frac{2}{3}(-x)^{\frac{3}{2}}-\frac{3\pi}{4}\right)\right\}\\&+2(-x)^{-3}+O\left(x^{-\frac{33}{4}}\right)\end{aligned}$$

Therefore, the asymptotic expansion for $R_3(x)=x^2\,{}_1F_2\left(1;\frac{4}{3},\frac{5}{3};\frac{x^3}{9}\right)$ is

$$\begin{aligned}R_3(x)=&x^2{}_1F_2\left(1;\frac{4}{3},\frac{5}{3},\frac{x^3}{9}\right)\\=&\frac{4\sqrt{\pi}}{3}\left\{(-x)^{-\frac{1}{4}}\left[1-\frac{385}{4,608}(-x)^{-3}\right]\cos\left[\frac{2}{3}(-x)^{\frac{3}{2}}-\frac{3\pi}{4}\right]\right.\\&\left.+(-x)^{-\frac{7}{4}}\left[\frac{5}{48}-\frac{85,085}{663,552}(-x)^{-3}\right]\sin\left[\frac{2}{3}(-x)^{\frac{3}{2}}-\frac{3\pi}{4}\right]\right\}\\&+2(-x)^{-1}+O\left(x^{-\frac{25}{4}}\right)\end{aligned}$$

The plot of the asymptotic expansion for R_3 along with the exact plot is shown in Figure (E.26). The subdominant term here occurs as a hyperbolic decreasing term causing the asymmetric amplitude envelope of the function. The amplitude is modulated for large negative x mainly by the slow decreasing coefficient $\frac{4\sqrt{\pi}}{3}(-x)^{-\frac{1}{4}}$ of the cosine term.

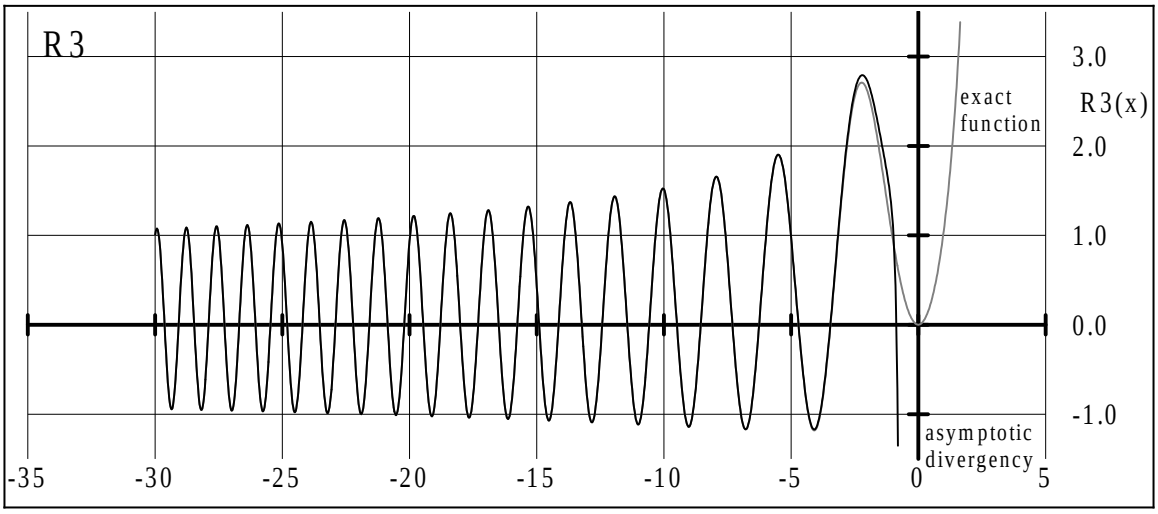

Figure E.26: Plot of the asymptotic expansion of $R_3(x)$.

E.3.3 Expansion for Functions Type ${}_2F_3$ [Function $M_3(x)$]

Only one function of the belongs to this group. The subdominant term plays a definite role in the final behavior. For $p=2$, the recursive relation [Equation (E.19)] for d_k is:

$$\begin{aligned}2(k+1)d_{k+1} = &\left[5k^2+2k(3+A_1-3B_1-10\gamma)+4N\right] d_k \\ &-\left[4k^3-6k^2(B_1+4\gamma)+2k(24\gamma^2+12\gamma B_1+B_1+4B_2-1)\right. \\ &\left.-32\gamma^3-24\gamma^2 B_1-4\gamma(B_1+4B_2-1)+2B_1-4B_2-8B_3-1\right]d_{k-1} \\ &+(k-2\gamma-2)(k-2\gamma-2\beta_1)(k-2\gamma-2\beta_2)(k-2\gamma-2\beta_3)d_{k-2},\end{aligned}$$

where

$$\begin{aligned}&d_0 = 1, \\ &d_{-1} = 0, \\ &d_{-2} = 0, \\ &B_3 = \beta_1\beta_2\beta_3\end{aligned}$$

E.3.3.1 Function $M_3(x)= x^3/3\ {}_2F_3(1,1;4/3,5/3,2;x^3/9)$

The dominant term is found following the same steps used in the previous sections. From the formulas in Equations (E.11) and (E.15) with p=2, q=3, $\alpha_1=\alpha_2=1$, $\beta_1=\frac{4}{3}$, $\beta_2=\frac{5}{3}$, and $\beta_3=2$ yield:

$$
\begin{aligned}
&A_1 = 1+1 = 2\\
&B_1 = \frac{4}{3}+\frac{5}{3}+2 = 5,\\
&A_2 = 1\times 1 = 1,\\
&B_2 = \frac{4}{3}\times\frac{5}{3}+\frac{4}{3}\times 2+\frac{5}{3}\times 2 = \frac{74}{9}\\
&B_3 = \frac{4}{3}\times\frac{5}{3}\times 2 = \frac{40}{9}\\
&\gamma = \frac{1}{4}+\frac{1}{2}(2-5) = -\frac{5}{4},\\
&N = \left(\frac{74}{9}-1\right)+\frac{1}{4}(2-5)(3\times 2+5-2)-\frac{3}{16} = \frac{41}{144}.
\end{aligned}
$$

Therefore, the expression for the dominant part is

$$K_{2,3}(-x)\approx\frac{(-x)^{-\frac{5}{4}}}{\sqrt{\pi}}\sum_{k=0}^{\infty}N_k(-x)^{-\frac{k}{2}}\cos\left(2\sqrt{-x}-\frac{5\pi}{4}-\frac{k}{2}\pi\right).$$

For the parameters above the recursive formula becomes

$$
\begin{aligned}
d_{k+1} = \frac{1}{2(k+1)}\Bigg[&\left(5k^2+5k+\frac{41}{36}\right)d_k-\left(4k^3-\frac{11}{9}k\right)d_{k-1}\\
&+(k+\frac{1}{2})(k-\frac{1}{6})(k-\frac{5}{6})(k-\frac{3}{2})d_{k-2}\Bigg],
\end{aligned}
$$

and the d_k and N_k are

$$d_0 = 1\rightarrow N_0 = \frac{1}{2^0} = 1,$$

$$d_1 = \frac{41}{72} \to N_1 = \frac{41}{144},$$
$$d_2 = \frac{9,241}{10,368} \to N_2 = \frac{9,241}{41,472},$$
$$d_3 = \frac{5,075,225}{2,239,488} \to N_3 = \frac{5,075,225}{17,915,904}.$$

Using these results the dominant part becomes:

$$K_{2,3}(-x) \approx \frac{1}{\sqrt{\pi}}(-x)^{-\frac{5}{4}} \left[\cos\left(2\sqrt{-x} - \frac{5\pi}{4}\right)\right.$$
$$+ \frac{41}{144}(-x)^{-\frac{1}{2}} \cos\left(2\sqrt{-x} - \frac{5\pi}{4} - \frac{\pi}{2}\right)$$
$$+ \frac{9,241}{41,472}(-x)^{-1} \cos\left(2\sqrt{-x} - \frac{5\pi}{4} - \pi\right)$$
$$\left. + \frac{5,075,225}{17,915,904}(-x)^{-\frac{3}{2}} \cos\left(2\sqrt{-x} - \frac{5\pi}{4} - \frac{3\pi}{2}x\right)\right]$$

or

$$K_{1,2}(-x) \approx \frac{1}{\sqrt{\pi}}(-x)^{-\frac{5}{4}} \left\{ \left[1 - \frac{9,241}{41,472}(-x)^{-1}\right] \cos\left(2\sqrt{-x} - \frac{5\pi}{4}\right)\right.$$
$$\left. + \left[\frac{41}{144}(-x)^{-\frac{1}{2}} - \frac{5,075,225}{17,915,904}(-x)^{-\frac{3}{2}}\right] \sin\left(2\sqrt{-x} - \frac{5\pi}{4}\right) \right\}$$

The subdominant part for this particular ${}_2F_3$ requires a special treatment; not because the order of the numerator and denominator parameters, but because the two numerator parameters are equal, namely the set $\alpha_p = \{1, 1\}$. Because of that, the expression for $L_{p,q}(z)$ previously presented and used no longer applies. A limit process is necessary, which was carried out by Luke (1962 – Ch. I – 1.3.4) and the final expression for the subdominant part appears in eq. (3) of the mentioned source. The formula is

generic but assumes that only two parameters differs by an integer including zero, the latter being the case here, and that these two parameters assumes the position 1, and 2 in the list of parameters. They are referred to by α_1 and $\alpha_2 \geq \alpha_1$. The rearranged above-mentioned eq. (3) follows, where $m = \alpha_2 - \alpha_1 \geq 0$.[12]

$$L_{p,q}(z) = \sum_{t=3}^{p} {}^{t}L_{p,q}(z) + T_{p,q}^{\alpha_1,m}(z) + \frac{(-1)^m \Gamma(\alpha_2)\Gamma(\alpha_{\mathrm{p}}^* - \alpha_2)}{m!\,\Gamma(\beta_{\mathrm{q}} - \alpha_2)} z^{-\alpha_2} \times$$
$$\left\{ {}_{q+1}F_{p-1}\left(\begin{matrix} \alpha_2, 1+\alpha_2-\beta_{\mathrm{q}} \\ m+1, 1+\alpha_2-\alpha_{\mathrm{p}}^* \end{matrix} \middle| \frac{(-1)^{q-p}}{z} \right) \times \right.$$
$$\left[\ln z - \Psi(\alpha_2) + \Psi(\alpha_{\mathrm{p}}^* - \alpha_2) + \Psi(1) - \Psi(\beta_{\mathrm{q}} - \alpha_2) + \Psi(m+1) \right] -$$
$$\left. {}^{q+1}_{q+1}F^{p}_{p-1}\left(\begin{matrix} \alpha_2, 1+\alpha_2-\beta_{\mathrm{q}} \\ m+1, 1+\alpha_2-\alpha_{\mathrm{p}} \end{matrix} \middle| \begin{matrix} \alpha_2, 1+\alpha_2-\beta_{\mathrm{q}} \\ 1, m+1, 1+\alpha_2-\alpha_{\mathrm{p}}^* \end{matrix} \middle| \frac{(-1)^{q-p}}{z} \right) \right\}.$$

The function $\Psi(z)$ is the Digamma function which is related to the Gamma function.[13,14] The following definitions are also required here:

$$T_{\mathrm{p,q}}^{\alpha_1,m}(z) = \sum_{k=1}^{m-1} \frac{(m-1-k)!\Gamma(\alpha_1+k)\Gamma(\alpha_{\mathrm{p}}^* - \alpha_1 - k)}{k!\,\Gamma(\beta_{\mathrm{q}} - \alpha_1 - k)} \frac{(-1)^k}{z^{\alpha_1+k}}$$
$${}^{u}_{p}F^{v}_{q}\left(\begin{matrix} \sigma_{\mathrm{p}} \\ \tau_{\mathrm{q}} \end{matrix} \middle| \begin{matrix} \gamma_{\mathrm{u}} \\ \delta_{\mathrm{v}} \end{matrix} \middle| z \right) = \sum_{k=0}^{\infty} \frac{(\sigma_{\mathrm{p}})_k z^k}{(\tau_{\mathrm{q}})_k k!} \left\{ \Psi(\gamma_{\mathrm{u}}+k) - \Psi(\gamma_{\mathrm{u}}) - \Psi(\delta_{\mathrm{v}}+k) + \Psi(\delta_{\mathrm{v}}) \right\}$$

It should be noted that in the subdominant summation for ordinary cases (that is, no two parameters differing by an integer number) the dummy index t ranges from $t=1$ to p, but here it starts at 3. Since ${}_2F_3$ has only two numerator parameters, the $\sum_{t=3}^{2} {}^{t}L_{2,3}(z)$ is null.

---

12 By historical reasons, the denominator parameters in [Luke – 1962] were noted as $1+\beta_{\mathrm{q}}$. In [Luke – 1969] it was used β_{q} instead, which is the notation also used in this work.

13 The digamma function is defined as $\Psi(z) = \frac{d}{dz} \ln \Gamma(z)$.

14 $\Psi(\xi_{\mathrm{r}}) = \sum_{i=1}^{r} \Psi(\xi_i)$, where ξ_{r} is a list of r parameters. (Luke – 1969, Vol 1 – pg. 141)

For $\alpha = 1$ and $m = 0$, The term $T^{\alpha_1,m}_{\mathrm{p,q}}(z)$ reduces to

$$T^{1,0}_{2,3}(z) = \sum_{k=1}^{0-1=-1} \frac{(0-1-k)!\Gamma(1+k)\Gamma(\alpha^*_{\mathrm{p}}-1-k)}{k!\,\Gamma(\beta_{\mathrm{q}}-1-k)} \frac{(-1)^k}{z^{\alpha_1+k}} = 0,$$

since the summation is empty.

The coefficient of the expression between braces gives:

$$\begin{aligned}\frac{(-1)^m\Gamma(\alpha_2)\Gamma(\alpha^*_{\mathrm{p}}-\alpha_2)}{m!\,\Gamma(\beta_{\mathrm{q}}-\alpha_2)} z^{-\alpha_2} &= \frac{(-1)^0\Gamma(1)(1)}{0!\,\Gamma\left(\frac{4}{3}-1\right)\Gamma\left(\frac{5}{3}-1\right)\Gamma\left(2-1\right)} z^{-1} \\ &= \frac{-1}{\Gamma\left(\frac{1}{3}\right)\Gamma\left(\frac{2}{3}\right)} z^{-1}\end{aligned}$$

The function ${}_{q+1}F_{p-1}$ that multiplies the term between brackets is:

$$\begin{aligned}{}_{q+1}F_{p-1}\left(\begin{matrix}\alpha_2, 1+\alpha_2-\beta_{\mathrm{q}} \\ m+1, 1+\alpha_2-\alpha^*_{\mathrm{p}}\end{matrix}\Big| \frac{(-1)^{q-p}}{z}\right) &= {}_4F_1\left(\begin{matrix}1, 1+1-\frac{4}{3}, 1+1-\frac{5}{3}, 1+1-2, \\ 0+1\end{matrix}\Big| \frac{-1}{z}\right) \\ &= 4F1\left(\begin{matrix}1, \frac{2}{3}, \frac{1}{3}, 0, \\ 1\end{matrix}\Big| \frac{-1}{z}\right) \\ &= {}_3F_0\left(\frac{2}{3}, \frac{1}{3}, 0; \frac{-1}{z}\right)\end{aligned}$$

This final expression results from the fact that the nominator and the denominator lists have a common parameter which coalesce (cancel each other,) and the number of parameters in each list reduces by one. Besides that, the parameter 0 in the numerator indicates that the series terminates.[15] The result is a constant (a polynomial of order

15 A function ${}_pF_q$ terminates if a numerator parameter is zero or a negative integer, and the result is a polynomial,

zero). This because the Pochhamer's symbol $(0)_k$ in the series expansion is 1 for $k=0$ and 0 for $k\geq 1$. Therefore,

$$ {}_3F_0\left(\frac{2}{3},\frac{1}{3},0;\frac{-1}{z}\right)=\sum_{k=0}^{\infty}\left(\frac{2}{3}\right)_k\left(\frac{1}{3}\right)_k(0)_k\frac{(-z)^k}{k!}=1. $$

The term between brackets involves evaluation of digamma functions of numbers and lists. Particularly, the digamma of a list is the sum of the digamma of the list elements, and the digamma of an empty list is 0. It should be noted that list $\alpha_{\mathrm{p}}^{*}-\alpha_2$ is empty. Therefore, the term between brackets is:

$$ \left[\ln z-\Psi(1)+0+\Psi(1)-\left\{\Psi\left(\frac{4}{3}\text{–}1\right)+\Psi\left(\frac{5}{3}\text{–}1\right)+\Psi\left(2\text{–}1\right)\right\}+\Psi(0+1)\right] = \left[\ln z-\Psi\left(\frac{1}{3}\right)-\Psi\left(\frac{2}{3}\right)\right]. $$

The last term expands as following:

$$ {}^{q+1}_{q+1}F^{p}_{p-1}\left(\begin{matrix}\alpha_2,1+\alpha_2-\beta_{\mathrm{q}}\\ m+1,1+\alpha_2-\alpha_{\mathrm{p}}\end{matrix}\middle|\begin{matrix}\alpha_2,1+\alpha_2-\beta_{\mathrm{q}}\\ 1,m+1,1+\alpha_2-\alpha_{\mathrm{p}}^{*}\end{matrix}\middle|\frac{(-1)^{q-p}}{z}\right)= {}^{4}_{4}F^{2}_{1}\left(\begin{matrix}1,\frac{2}{3},\frac{1}{3},0\\ 1\end{matrix}\middle|\begin{matrix}1,\frac{2}{3},\frac{1}{3},0\\ 1,1\end{matrix}\middle|\frac{(-1)}{z}\right)= {}^{3}_{3}F^{1}_{0}\left(\frac{2}{3},\frac{1}{3},0\middle|\begin{matrix}\frac{2}{3},\frac{1}{3},0\\ 1\end{matrix}\middle|\frac{(-1)}{z}\right) $$

The reduction of order occurs because of the coalescence of equal parameters, by division and subtraction. An appropriate way to analyze this expansion is by picking the general term of its definition:

$$\frac{(\sigma_{\mathrm{p}})_k z^k}{(\tau_{\mathrm{q}})_k k!}\left\{\Psi(\gamma_{\mathrm{u}}+k)-\Psi(\gamma_{\mathrm{u}})-\Psi(\delta_{\mathrm{v}}+k)+\Psi(\delta_{\mathrm{v}})\right\}$$

Considering the parameters corresponding to $\sigma_3=\left\{\frac{2}{3},\frac{1}{3},0\right\}$, and the general term above, and due to the occurrence of the Pochhamer's symbol $(0)_k$, only for $k=0$ the numerator of the fraction is not zero. However, for $k=0$ the term in braces is null, and the complete summation is zero.

Putting all these results together, the expression for the subdominant part is:

$$L_{p,q}(z)=0+0+\frac{-1}{\Gamma\left(\frac{1}{3}\right)\Gamma\left(\frac{3}{3}\right)}z^{-1}\left\{1\times\left[\ln z-\Psi\left(\frac{1}{3}\right)-\Psi\left(\frac{2}{3}\right)\right]-0\right\}.$$

or

$$L_{p,q}(z)=-\frac{1}{\Gamma\left(\frac{1}{3}\right)\Gamma\left(\frac{3}{3}\right)}z^{-1}\left[\ln z-\Psi\left(\frac{1}{3}\right)-\Psi\left(\frac{2}{3}\right)\right].$$

Therefore, the asymptotic expansion for ${}_2F_3$ becomes.

$$\begin{aligned}{}_2F_3\left(1,1;\frac{4}{3},\frac{5}{3},2;x\right)=\frac{\Gamma\left(\frac{4}{3}\right)\Gamma\left(\frac{5}{3}\right)\Gamma(2)}{\Gamma(1)\Gamma(1)}\left\{\frac{1}{\sqrt{\pi}}(-x)^{-\frac{5}{4}}\times\right.\\ \times\left[\left(1-\frac{9,241}{41,472}(-x)^{-1}\right)\cos\left(2\sqrt{-x}-\frac{5\pi}{4}\right)+\right.\\ \left.+\left(\frac{41}{144}(-x)^{-\frac{1}{2}}-\frac{5,075,225}{17,915,904}(-x)^{-\frac{3}{2}}\right)\sin\left(2\sqrt{-x}-\frac{5\pi}{4}\right)\right]+\\ \left.-\frac{1}{\Gamma\left(\frac{1}{3}\right)\Gamma\left(\frac{2}{3}\right)}(-x)^{-1}\left[\ln(-x)-\Psi\left(\frac{1}{3}\right)-\Psi\left(\frac{2}{3}\right)\right]\right\}+O\left(x^{-\frac{13}{4}}\right),\end{aligned}$$

Rearranging and using the relation $\Gamma\left(\frac{4}{3}\right)\Gamma\left(\frac{5}{3}\right)=\frac{4\pi}{9\sqrt{3}}$[16] gives:

16 See the developments for function R_3.

$$
\begin{aligned}
{}_2F_3\left(1,1;\frac{4}{3},\frac{5}{3},2;x\right) &= \frac{4\sqrt{\pi}}{9\sqrt{3}}\left\{(-x)^{-\frac{5}{4}}\times\right.\\
&\times\left[\left(1-\frac{9,241}{41,472}(-x)^{-1}\right)\cos\left(2\sqrt{-x}-\frac{5\pi}{4}\right)+\right.\\
&\left.\left.+\left(\frac{41}{144}(-x)^{-\frac{1}{2}}-\frac{5,075,225}{17,915,904}(-x)^{-\frac{3}{2}}\right)\sin\left(2\sqrt{-x}-\frac{5\pi}{4}\right)\right]\right\}\\
&-\frac{2}{9}(-x)^{-1}\left[\ln(-x)-\Psi\left(\frac{1}{3}\right)-\Psi\left(\frac{2}{3}\right)\right]+O\left(x^{-\frac{13}{4}}\right),
\end{aligned}
$$

using $\frac{x^3}{9}$ for x gives

$$
\begin{aligned}
{}_2F_3\left(1,1;\frac{4}{3},\frac{5}{3},2;x\right) &= 4\sqrt{\pi}\left\{(-x)^{-\frac{15}{4}}\left[1-\frac{9,241}{4,608}(-x)^{-3}\right]\cos\left[\frac{2}{3}(-x)^{\frac{3}{2}}-\frac{5\pi}{4}\right]\right.\\
&\left.+(-x)^{-\frac{21}{4}}\left[\frac{41}{48}-\frac{5,075,225}{663,552}(-x)^{-3}\right]\sin\left[\frac{2}{3}(-x)^{\frac{3}{2}}-\frac{5\pi}{4}\right]\right\}\\
&-2(-x)^{-3}\left[3\ln(-x)-\ln 9-\Psi\left(\frac{1}{3}\right)-\Psi\left(\frac{2}{3}\right)\right]+O\left(x^{-\frac{39}{4}}\right).
\end{aligned}
$$

Therefore, the asymptotic expansion for $M_3(x)=\frac{x^3}{3}\,{}_2F_3\left(1,1;\frac{4}{3},\frac{5}{3},2;\frac{x^3}{9}\right)$ is

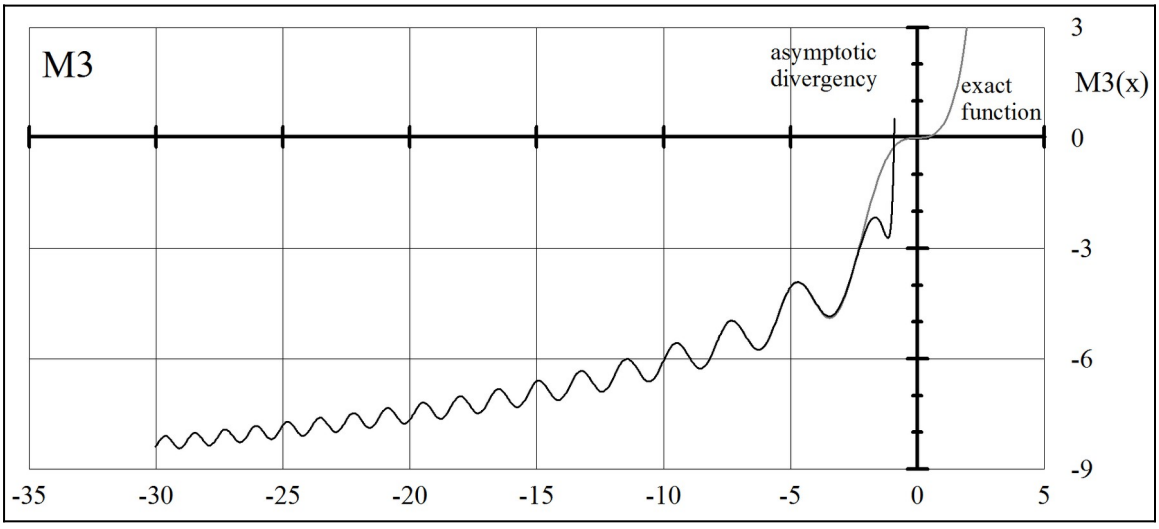

Figure E.27: Plot of the asymptotic expansion of $M_3(x)$.

$$M_3(x) = \frac{4\sqrt{\pi}}{3}\Bigg\{(-x)^{-\frac{3}{4}}\left[1-\frac{9,241}{4,608}(-x)^{-3}\right]\cos\left[\frac{2}{3}(-x)^{\frac{3}{2}}-\frac{5\pi}{4}\right]$$
$$+(-x)^{-\frac{9}{4}}\left[\frac{41}{48}-\frac{5,075,225}{663,552}(-x)^{-3}\right]\sin\left[\frac{2}{3}(-x)^{\frac{3}{2}}-\frac{5\pi}{4}\right]\Bigg\}$$
$$-2\left[\ln(-x)-\frac{\ln 9+\Psi\left(\frac{1}{3}\right)+\Psi\left(\frac{2}{3}\right)}{3}\right]+O\left(x^{-\frac{27}{4}}\right).$$

The plot of the asymptotic expansion for R_3 along with the exact plot is shown in Figure (E.27). The logarithmic subdominant term has a definite effect in the final behavior of the function.

E.3.4 Numerical Implementation

None of the three methods presented here provides a satisfactory numerical implementation for the functions of concern. The method using path integration of the differential equation is the only one that can calculate the functions for any value of the argument *x*. However it has proved to be slow enough to limit any practical use. Series expansions are restricted to values close to the origin, and asymptotic expansions are restricted to large negative values.

The numerical implementations of the functions were developed using a combination of the series expansion with the asymptotic expansion. The transition point occurs, in general in the interval (-14,-5) and since in most of the cases the values to be calculated are far away from this interval, it is not crucial to determine the ideal crossover point for each function. The value x_{xo}=-10 was arbitrarily chosen and proved satisfactory for the application in discussion.

Appendix F

The Newton-Raphson Method For A Non-Square System Of Non-Linear Equations

The Newton-Raphson method for non-square systems of nonlinear equations can be obtained as an extension for square systems. Since the purpose of this derivation is for the application in a 3×2 vector function (three scalar functions in two variables), the derivation will be tailored to this kind of function. The generalization is then direct.

In the 1×1 Newton-Raphson method, the goal is to find a root of a function $f(x)$ as the limit of a sequence $\{x_i\}$, where

$$x_{i+1} = x_i - \frac{f(x_i)}{f'(x_i)}, \tag{F.1}$$

for a given initial point x_0. This formula can be seen in two different ways. In the first way, it is the expression of the derivative $f'(x_i)$ in terms of x_i, $f(x_i)$, and an unknown next point in the sequence, namely x_{i+1}. From Figure (B.1) the expression for the $f(x_i)$ is given by

$$f'(x_i) = \frac{f(x_i)}{x_i - x_{i+1}}.$$

Solving for x_{i+1}, the Newton-Raphson formula in Equation (F.1) is obtained.

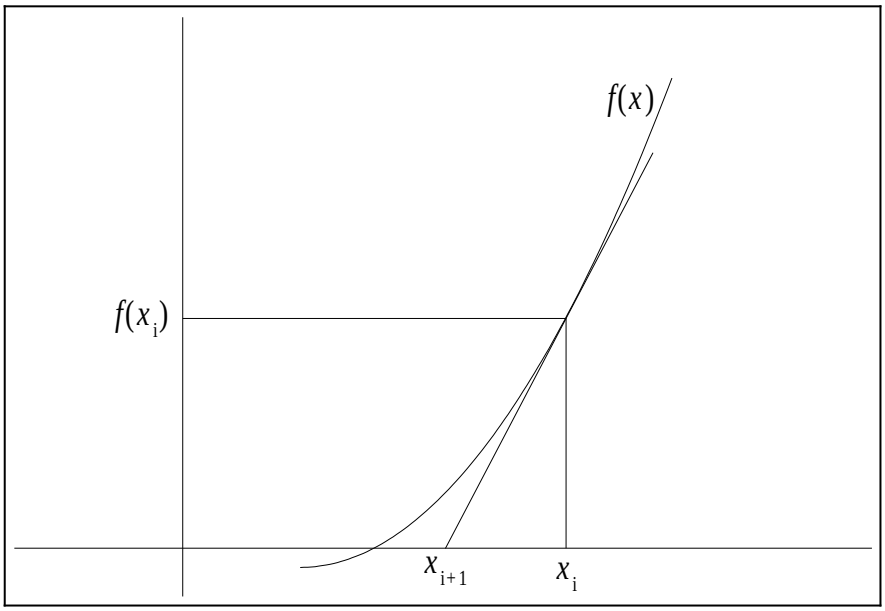

Figure F.1: Newton-Raphson made easy.

In the second way, which is suitable for higher dimension generalization, the Taylor series expansion of $f(x)$ about a point x_i close to a root x_r is considered. This expansion is given by

$$\begin{aligned} 0 = f(x_r) = & f(x_1) + (x_r - x_i) f'(x_i) \\ & + \frac{1}{2!}(x_r - x_i)^2 f''(r_i) \\ & + \frac{1}{3!}(x_r - x_i)^3 f'''(r_i) + \cdots \end{aligned}$$

If the Taylor series is truncated after the term in the first derivative the equation is not valid for x_r anymore, but a value x_{i+1} may be found, possibly close to x_r, which satisfies the equation

$$0 = f(x_i) + (x_{i+1} - x_i) f'(x_i).$$

Solving for x_{i+1}, the Newton-Raphson expression is again obtained. The process is used recursively and it is expected that the sequence so generated marches toward a root. There are, however, several instances in which the sequence does not converge to the desired root or to any root whatsoever.

Using the same idea, a generalization of the method for higher dimensions results. Considering the vector function

$$\mathbf{f}(\mathbf{X}) = \left\{ \begin{array}{c} f_1(X_1, X_2) \\ f_2(X_1, X_2) \\ f_3(X_1, X_2) \end{array} \right\},$$

defined in a suitable domain $D \subset \mathbb{R}^2$, if $\mathbf{X}_0$ is an interior point of D and $\mathbf{X}$ is a point in an open ε-neighborhood of $\mathbf{X}_0$, $\mathbf{f}(\mathbf{X})$ can be expressed in terms of the Taylor series expansion of each component f_i about $\mathbf{X}_0$ by

$$\begin{aligned} f_i(X_{1,1}X_{2,1}) =& f_i(X_{1,0}, X_{2,0}) + (X_{1,1} - X_{1,0}) f_{i,1}(X_{1,0}, X_{2,0}) \\ &+ (X_{2,1} - X_{2,0}) f_{i,2}(X_{1,0}, X_{2,0}) \\ &+ \frac{1}{2!}\Big[(X_{1,1} - X_{1,0})^2 f_{i,1,1}(X_{1,0}, X_{2,0}) \\ &\qquad + 2(X_{1,1} - X_{1,0})(X_{2,1} - X_{2,0}) f_{i,1,2}(X_{1,0}, X_{2,0}) \\ &\qquad + (X_{2,1} - X_{2,0})^2 f_{i,2,2}(X_{1,0}, X_{2,0})\Big] \\ &+ O[(\Delta X)^3] \end{aligned}$$

Using the same argument used for the 1-dimensional case, it is expected to find a pair of values $(X_{1,1}, X_{2,1})$ which satisfies

$$0 = f_i(X_{1,1}, X_{2.1}) = f_i(X_{1,0}, X_{2,0}) + (X_{1,1} - X_{1,0}) f_{i,1}(X_{1,0}, X_{2,0}) + (X_{2,1} - X_{2,0}) f_{i,2}(X_{1,0}, X_{2,0})$$

for $i = 1, 2, 3$. The new pair of points $(X_{1,1}, X_{2,1})$ must satisfy the three equations simultaneously. This requirement results in an overdetermined linear system which is as follows:

$$\begin{bmatrix} f_{1,1}(X_{1,n}, X_{2,n}) & f_{1,2}(X_{2,n}, X_{2,n}) \\ f_{2,1}(X_{1,n}, X_{2,n}) & f_{2,2}(X_{2,n}, X_{2,n}) \\ f_{3,1}(X_{1,n}, X_{2,n}) & f_{3,2}(X_{2,n}, X_{2,n}) \end{bmatrix} \begin{Bmatrix} \delta X_{1,n+1} \\ \delta X_{2,n+1} \end{Bmatrix} = - \begin{Bmatrix} \{f_1(X_{1,n}, X_{2,n}) \\ f_2(X_{1,n}, X_{2,n}) \\ f_3(X_{1,n}, X_{2,n}) \end{Bmatrix},$$

where $\delta X_{i,n+1} = X_{i,n+1} - X_{i,n}$.

Starting at a $\mathbf{X}_0$, the functions f_i and their first partial derivatives $f_{i,1}$ and $f_{i,2}$ are evaluated at $\mathbf{X}_0$ and a solution is tried to the overdetermined system above. Since overdetermined system rarely has a solution, methods like reduction of order or least squares should be invoked. Assuming that an acceptable solution $\delta \mathbf{X}_1$ is found, the next element in the sequence is given by

$$X_1 = \mathbf{X}_0 + \delta \mathbf{X}_1.$$

The sequence continues recursively until some tolerance is reached.

Appendix G

Buckling Force Calculation For The Trigonometric Model

To calculate the minimum tangential force for a given circular constraint, it is needed to work backwards as in Section 3.2. From the radii of curvature *R* and *r*, it is necessary to calculate the maximum length *L*, the eccentricity *e*, and the maximum amplitude $y_{\max}$. Then L^* and P_3 are determined, and consequently the tangential force, the radial force, and the moment applied at the ends. Figure G1 facilitates following the discussions here. L^* is depicted in Figure 3.3.

L^* is the length required to complete the three half-waves in which *L* is a portion and therefore it is called *complementary length*. A column with complementary length L^* and stiffness *EI* has its third critical force given by Equation (3.9):

$$P_3 = \left(\frac{3\pi}{L^*}\right)^2 EI. \tag{G.1}$$

The displacements of the center line is given by Equation (3.10):

$$y(x) = -y_{\max}\cos\left(\frac{3\pi x}{L^*}\right). \tag{G.2}$$

The locus of the center of curvature for a function $y(x)$ is expressed parametrically by (see Appendix [B]):

$$\begin{cases} x_{\mathrm{c}}(x) = x - \left[1 + y'(x)^2\right] \dfrac{y'(x)}{y''(x)}, \\ \\ y_{\mathrm{c}}(x) = y(x) + \left[1 + y'(x)^2\right] \dfrac{1}{y''(x)}. \end{cases}$$

Therefore, the locus of the center of curvature of the center line is given by

$$\begin{cases} x_{\mathrm{c}}(x) = x - \left[1 + k^2 y_{\max}^2 \sin^2(kx)\right] \dfrac{\tan(kx)}{k}, \\ \\ y_{\mathrm{c}}(x) = -y_{\max} \cos(kx) + \dfrac{1 + k^2 y_{\max}^2 \sin^2(kx)}{k^2 y_{\max} \cos(kx)}. \end{cases} \tag{G.3}$$

where $k = \frac{3\pi}{L^*}$.

The branches of the locus cross the y-axis where $x_c(\pm\frac{L}{2}) = 0$, therefore the point x where the circle touches the column is the solution of the transcendental equation

$$\psi = \left(1 + k^2 y_{\max}^2 \sin^2 \psi\right) \tan \psi, \tag{G.4}$$

where $\psi = \frac{kL}{2}$. By construction the solutions ψ should be in the open intervals $(-\frac{3\pi}{2}, -\pi)$ and $(\pi, \frac{3\pi}{2})$. With $x = \frac{L}{2}$, the center $y_c(\frac{L}{2})$ of the circles are determined using the second expression in Equation (G.3). The radii of curvature r and R, and the eccentricity e are given by[1]

1 Note that *R* is negative. Since *r* has the same sign of *R*, *r* is also negative. This justifies the expression for *r* as presented.

$$\begin{cases} r = y_c\left(\frac{L}{2}\right) + y_{\max,} \\ \\ R = \dfrac{\left(1 + k^2 y_{\max}^2 \sin^2 \psi\right)^{\frac{3}{2}}}{k^2 y_{\max} \cos \psi} \\ \\ e = y\left(\frac{L}{2}\right) = -y_{\max} \cos \psi \end{cases} \tag{G.5}$$

If $y_{\max}$ and L^* are known, the transcendental equation can be solved for ψ. However, in a buckling problem, the values $|R|$ and $|r|$ are given, whereas $y_{\max}$, L^*, e, and $\frac{L}{2}$ must are unknown. This requires an iterative procedure.

G.1 Iterative Process to Determine the Parameters of the Center Line

The iterative process used here starts assuming a value for ψ. An appropriate value, as will be shown later, is $\psi_0 = 4.493409458$.

Using $R = -|R|$, $r = -|r|$,[2] and the initial value for ψ, an approximate value for $y_{\max}$ is calculated. The expression for $y_c\left(\frac{L}{2}\right)$ in Equation (G.3) and the expression for r in Equation (G.5) yield to

$$y_{\max} = r - y_c\left(\frac{L}{2}\right) = r + y_{\max} \cos \psi - \frac{1 + k^2 y_{\max}^2 \sin^2 \psi}{k^2 y_{\max} \cos \psi}.$$

Using the expression for R in Equation (G.5) for the denominator above results in

$$y_{\max}(1 - \cos \psi) = r - \frac{R}{\left(1 + k^2 y_{\max}^2 sin^2 \psi\right)^{\frac{1}{2}}}.$$

---

2 These expressions ensure that the values R and r used in the Equation (G.5) are negative.

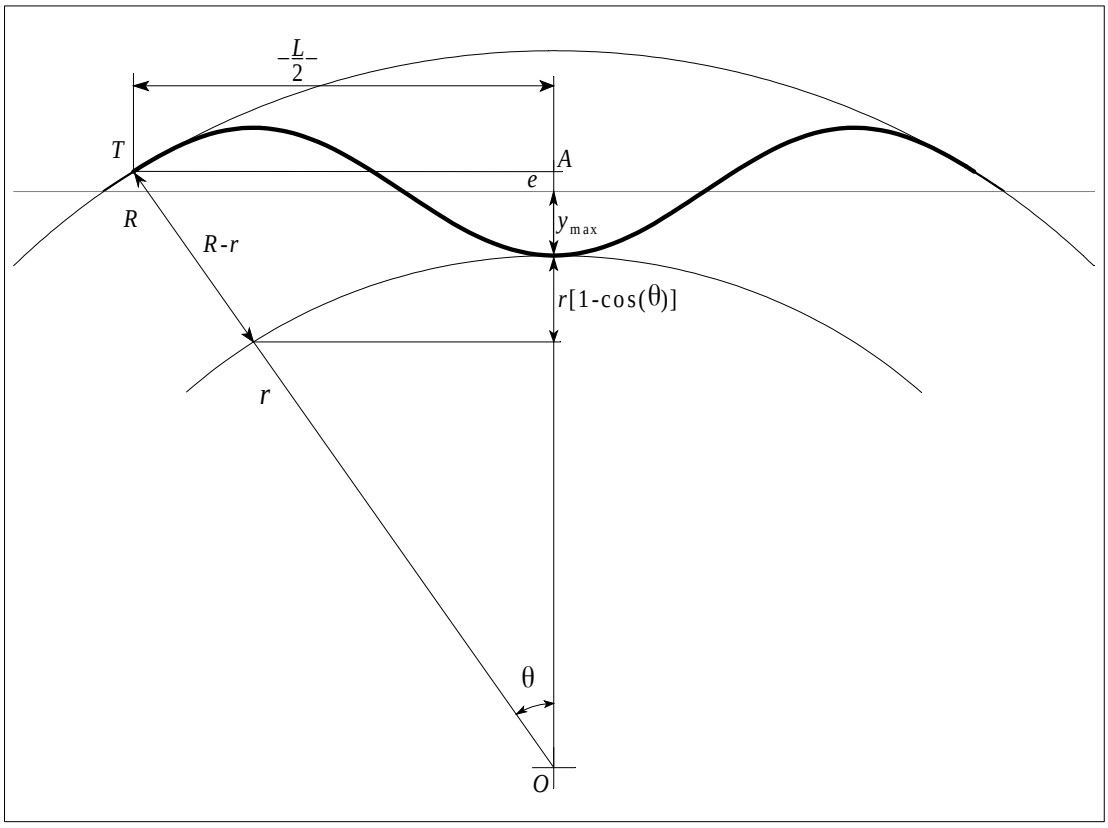

Figure G.1: Geometric relations in the buckled portion of a column

Using Equation (G.4) and solving for $y_{\max}$, the following expression is obtained:

$$y_{\max} = \frac{R}{1-\cos\psi}\left\{\frac{r}{R} - \left(\frac{\tan\psi}{\psi}\right)^{\frac{1}{2}}\right\}. \tag{G.6}$$

The ratio $\frac{\tan\psi}{\psi}$ is positive for values close to the solution but may be negative for values away from the solution.

The term $k^2 y_{\max}$ can be calculated using the expression for R and Equation (G.4):

$$k^2 y_{\max} = \frac{\left(\frac{\tan \psi}{\psi}\right)^{\frac{3}{2}}}{R \cos \psi}. \tag{G.7}$$

With these two values, the expression in parentheses in Equation (G.4) can be evaluated and the transcendental equation solved for a new ψ. To guarantee convergence to the right root the following expression should be used in place of Equation (G.4):

$$\psi^* = \arctan\left(\frac{\psi}{1 + k^2 y_{\max}^2 \sin^2 \psi}\right) + \pi \tag{G.8}$$

The new value for ψ^* should not be used to reiterate the process. The formulation is nonlinear and unstable, and the interval does not contract if the new value is used. Instead, a more robust procedure should be used. The procedure recommended is to reduce the residual $\delta(\psi) = \psi^* - \psi$ to zero using Newton-Raphson's method. The new value for the iteration is calculated from

$$\psi_1 = \psi - \frac{\delta(\psi)}{\delta'(\psi)},$$

where the derivative is numerically evaluated.

The process is repeated until some tolerance is satisfied. With ψ, $y_{\max}$, and $k^2 y_{\max}$ determined, k is found immediately. The values for L and L^* are found using

$$\text{Ł} = \frac{2\psi}{k},$$

and

$$L^* = \frac{3\pi}{k}.$$

The critical load P_3 is calculated using Equation (G.1), the moment M using P_3, and the eccentricity e by Equation (G.5). The procedure above provides an exact solution of the problem. However, when the ratio $\frac{r}{R}$ is close to one an approximation is possible.

G.2 Approximate Solution

There are several approximations to the exact solution of the previous section. When the ratio r/R is close to one the maximum displacement $y_{\max}$[3] is small and the radius of curvature can be approximated to[4]

$$\rho(x) = \frac{1}{y''(x)}$$

Therefore, the center of curvature is approximately given by $(x_c, y_c) = (x, c) + \vec{\rho}$ which in parametric form results in

$$\begin{cases} x_c(x) = x - \dfrac{1}{[1 + y\prime(x)^2]^{1/2}} \dfrac{y\prime(x)}{y\prime\prime(x)}, \\ \\ y_c(x) = y(x) + \dfrac{1}{[1 + y\prime(x)^2]^{1/2}} \dfrac{1}{y\prime\prime(x)}. \end{cases}$$

The term in brackets in the denominator of both expressions is quite close to one

3 The order of magnitude of y_{max} is $|R - r|$.
4 As in Equation (B.1), and $f\prime$ small.

such that an improved approximation is given by

$$\begin{cases} x_c(x) = x - \dfrac{y\prime(x)}{y\prime\prime(x)}, \\ \\ y_c(x) = y(x) + \dfrac{1}{y\prime\prime(x)}. \end{cases}$$

Using the expression for the center line yields to

$$\begin{cases} x_c(x) = x - \dfrac{\tan(kx)}{x}, \\ \\ y_c(x) = -y_{\max}\cos(kx) + \dfrac{1}{k^2 y_{\max}\cos(kx)}. \end{cases}$$

This approximate locus crosses the y-axis when $x_c\left(\frac{L}{2}\right) = 0$ which results in the following transcendental equation:

$$\psi = \tan\psi. \tag{G.9}$$

The solution of interest is the first positive (nontrivial) solution given by

$$\psi_0 = 4.493409458\ldots. \tag{G.10}$$

This means that the relation between L^* and L is almost constant and the approximate relation is given by

$$k = \frac{3\pi}{L_c} 2\psi_0 L. \tag{G.11}$$

This approximation justify why the value $\psi_0 = 4.493409458$ was chosen to start the iterative process in the previous section.

Geometric relations are required to determine the pertinent parameters. From Figure (G.1) the following relation is obtained:

$$-(R-r)\cos\theta = -r(1-cos\theta) + y_{\max} + e.$$

Using the value for the eccentricity $e = -y_{\max}\cos\psi$ and rearranging yields to

$$y_{\max} = \frac{r - R\cos\theta}{1-\cos_0}.$$

The term $\cos\theta$ can be obtained from the triangle TOA in Figure (G.1):

$$\cos\theta = -\frac{\sqrt{r^2 - \left(\frac{L}{2}\right)^2}}{R},$$

where the positive root is used. This results in

$$y_{\max} = \frac{r + \sqrt{R^2 - \left(\frac{L}{2}\right)^2}}{1-\cos\psi_0}.$$

Now for the ratio $\frac{r}{R}$ close to one, $\tan\theta = \sin\theta$ and $y\prime\left(-\frac{L}{2}\right)$ can be approximated by

$$y\prime\left(-\frac{L}{2}\right) = \frac{2\psi_0}{L} y_{\max}\sin(-\psi_0) = \tan\theta \simeq \sin\theta = -\frac{L}{2R},$$

where Equation (G.11) was used for k. Substituting the expression for $y_{\max}$ the following is obtained:

$$\frac{2\psi_0}{L}\,\frac{r+\sqrt{R^2-\left(\frac{L}{2}\right)^2}}{1-\cos\psi_0}\sin\psi_0=\frac{L}{2R},$$

Rearranging results in

$$\psi_0\,\frac{\sin\psi_0}{1-\cos\psi_0}\left(r-R\sqrt{1-\left(\frac{L}{2R}\right)^2}\right)=R\left(\frac{L}{2R}\right)^2.$$

The coefficient of the term between parentheses at the left evaluates into a constant $\xi=-3.603338849\ldots$, and making $\beta=\left(\frac{L}{2R}\right)^2$ yields to

$$\sqrt{1-\beta}=\frac{r}{R}-\frac{\beta}{\xi}.$$

Finally, squaring and rearranging results in

$$\beta^2+\left(\xi^2-2\frac{r}{R}\xi\right)\beta-\left(1-\frac{r^2}{R^2}\right)\xi^2=0 \tag{G.12}$$

This quadratic equation has always one positive root and one negative root. Using the positive root in the expression for β the value of L is calculated:

$$L=2\sqrt{\beta}\,|R|\,. \tag{G.13}$$

Equation (G.11) furnishes the complementary length L^*:

$$L^* = \frac{3\pi}{2\psi_0} L. \tag{G.14}$$

Using the complementary length and Equation (G.1) gives the critical force P_3.

G.3 Drill Bit End Condition

A drill bit end condition is that in which the column is centered and held between the constraining circles. Since the column is buckled, the axial force and moment acting on the first tangency point are known. However, the portion of the column between the bit and the tangency point is subjected to its first buckling force. Figure (G.2) shows this configuration.

The expression for the center line is given by Equation (3.5) for $n=1$, namely,

$$y(x) = y_{\max} \sin\left(\frac{\pi}{l} x\right).$$

The fact now is that the critical force from the central portion of the column is known, which determines the complementary length for the bit case $L^*_{\rm bc}$. From Equation (3.4) for $n=1$ yields:[5]

$$P_{1,\rm db} = \left(\frac{\pi}{L^*_{\rm db}}\right)^2 EI = \left(\frac{3\pi}{L^*}\right) EI = P_3$$

or

5 Assuming EI is the same, which is easily sorted out if not.

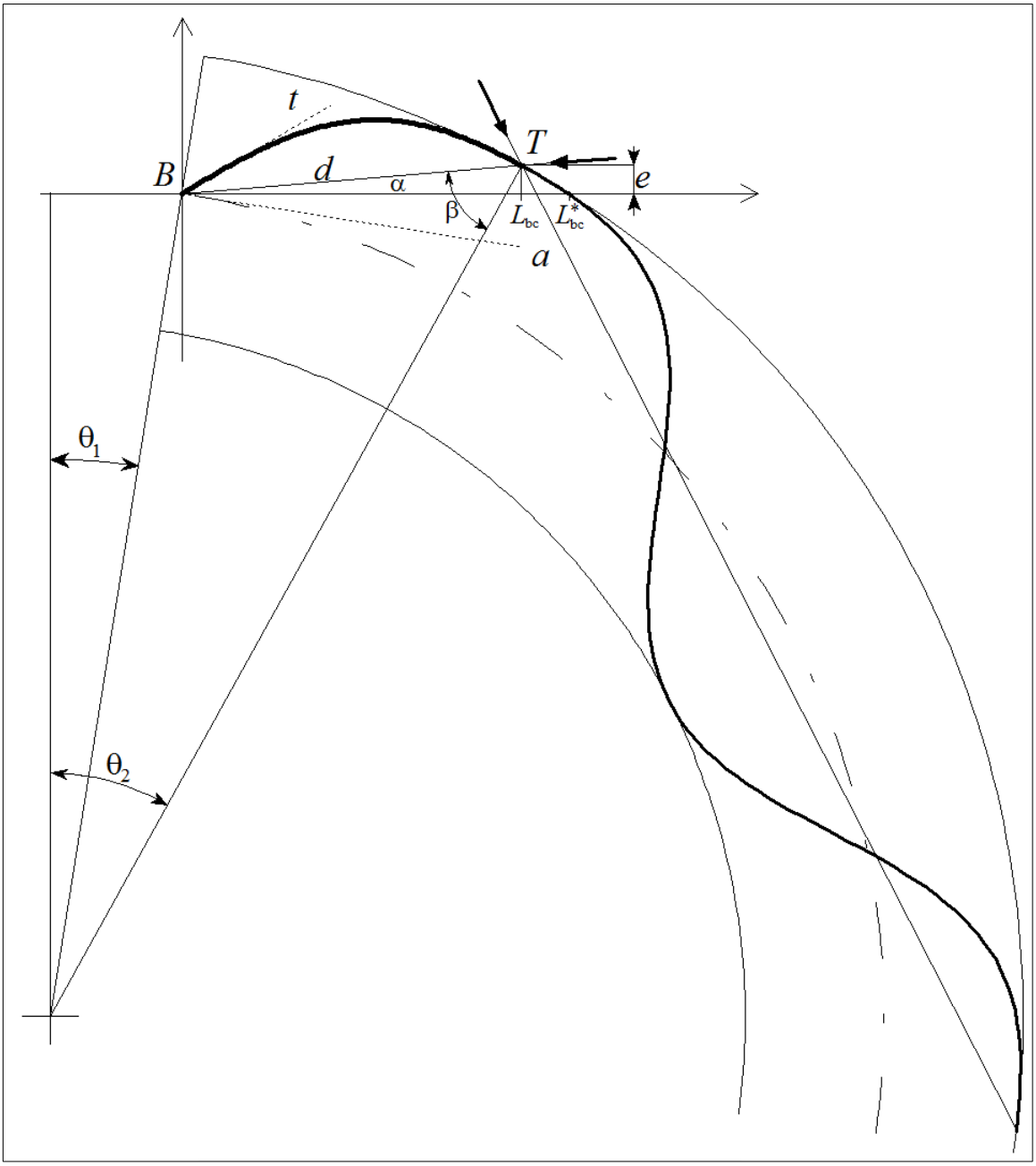

Figure G.2: Bit condition imposed at one end.

$$L^*_{\mathrm{db}} = \frac{1}{3} L^*.$$

Since the moment M is known the eccentricity e of the critical force is the same for the central portion and is expressed by

$$e = y_{\max} \sin\left(\frac{\pi}{L^*_{\mathrm{db}}} L_{\mathrm{db}}\right).$$

From the triangle OTB, using the law of cosines results in

$$\bar{R}^2 = d^2 + R^2 - 2\,|R|\, d \cos\beta,$$

where $\bar{R} = \frac{R+r}{2}$, and from the right triangle BDT yields

$$d^2 = L^2_{\mathrm{db}} + e^2.$$

Using these two expressions and solving for L^2_{db} results in

$$L^2_{\mathrm{db}} = 2\,|R| \sqrt{L^2_{\mathrm{db}} + e^2} \cos\beta - (R^2 + e^2 - \bar{R}^2).$$

Also from the right triangle BDT yields:

$$\alpha + \beta + \theta_2 = \frac{\pi}{2},$$

such that

$$\cos\beta = \cos\left(\frac{\pi}{2} - \alpha - \theta_2\right) = \sin(\alpha + \theta_2).$$

which results in the following function of $L_{\rm db}$:

$$f(L_{\rm db}) = 2\,|R|\,\sqrt{L_{\rm db}^2 + e^2}\,\sin(\alpha + \theta_2) - L_{\rm db}^2 - (R^2 + e^2 - \bar{R}^2). \qquad \text{(G.15)}$$

The angle α is given by

$$\alpha = \arctan\frac{e}{L_{\rm db}}, \qquad \text{(G.16)}$$

and the angle θ_2 is be obtained using the value of $y\prime(L_{\rm db})$:

$$-\tan\theta_2 = \frac{\pi}{L_{\rm db}^*} y_{\max} \cos\left(\frac{\pi}{L_{\rm db}^*} L_{\rm db}\right) = \frac{\pi}{L_{\rm db}^*} e \cot\left(\frac{\pi}{L_{\rm db}^*} L_{\rm db}\right)$$

or

$$\theta_2 = -\arctan\left[\frac{\pi}{L_{\rm db}^*} e \cot\left(\frac{\pi}{L_{\rm db}^*} L_{\rm db}\right)\right] \qquad \text{(G.17)}$$

The function given by Equation (G.15), along with Equations (G.16) and (G.17) form a transcendental expression on $L_{\rm db}$ that should be solved iteratively. Again the Newton-Raphson's method is used to find the solution. With $L_{\rm db}$, $y_{\max}$ can be calculated. The angle θ_1 is determined from the triangle BOT using the following relation:

$$d^2 = L_{\rm db}^2 + e^2 = R^2 + \bar{R}^2 - 2R\bar{R}\cos(\theta_2 - \theta_1).$$

The angle θ_1 is used to calculate the bit tilt ζ, defined as the angle at the bit between the tangent line $\bar{B}_t$ and the axial line $\bar{B}_a$. The angle is given by

$$\zeta = \theta_1 + y\prime(0) = \theta_1 + \frac{\pi}{L^*_{\mathrm{db}}} y_{\max}.$$

The axial and lateral forces acting on the bit are given by

$$\begin{cases} F_a = P_3 \cos\theta_1), \\ F_1 = P_3 \sin\theta_1. \end{cases}$$

The formulation presented here is independent of the way the value of P_3, M and e were calculated (exact or approximate solution) for the buckling of the central portion of the column however the convergence using results from the approximate solution are very unstable.

G.4 Near-Bit End Condition

A near-bit is a tool (a stabilizer) put close to the bit in order to decrease the tilt of the bit and consequently to force the bit to drill straight. Therefore, a near-bit end condition is that in which the column is centered and built-in aligned with axial direction of the constraints. Since the column is buckled, the axial force and moment acting on the first tangency point are known. Now, the portion of the column between the near-bit and the tangency point is subjected to its second buckling force. Figure (G.3) shows this configuration.

The expression for the center line is given by Equation (3.5) fog $n = 2$, namely,

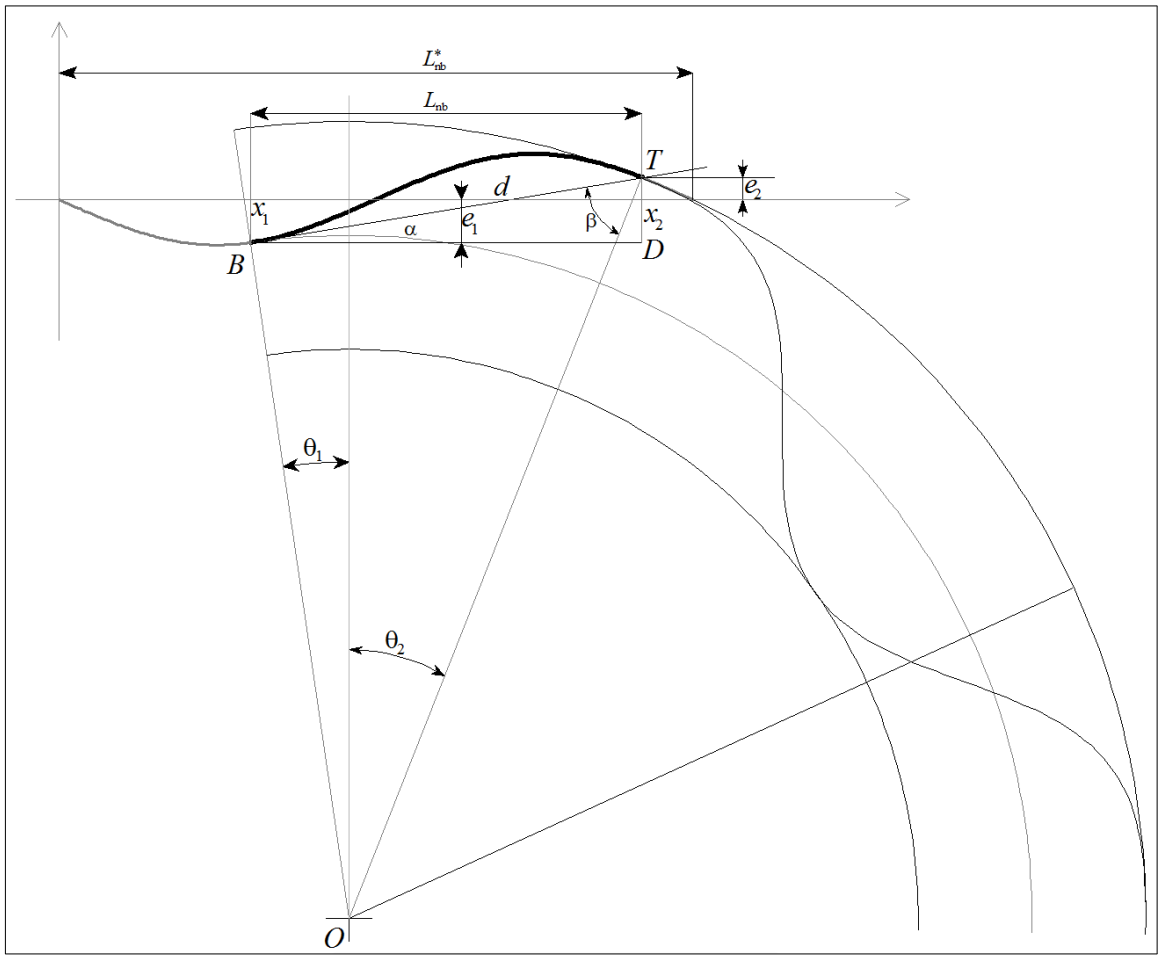

Figure G.3: Near-bit condition imposed at one end.

$$y(x) = y_{\max} \sin\left(\frac{2\pi}{l}x\right).$$

The critical force is the same of the central portion of the column. This allows to calculate the complementary length for the near-bit case L^*_{nb}. From Equation (3.4) for $n = 2$ results:

$$P_{2,\mathrm{nb}} = \left(\frac{2\pi}{L^*_{\mathrm{nb}}}\right)^2 EI = \left(\frac{3\pi}{L^*}\right) EI = P_3$$

or

$$L^*_{\mathrm{nb}} = \frac{2}{3} L^*.$$

The eccentricity e_2 of the critical force is the same as for the central portion and is expressed by

$$e_2 = e = y_{\max} \sin\left(\frac{2\pi}{L^*_{nb}} x_2\right).$$

The value of the eccentricity e_1 at the bit is not know but is given by

$$e_1 = y_{\max} \sin\left(\frac{2\pi}{L^*_{\mathrm{nb}}} x_1\right) = e_2 \frac{\sin\left(\frac{2\pi}{L^*_{\mathrm{nb}}} x_1\right)}{\sin\left(\frac{2\pi}{L^*_{\mathrm{nb}}} x_2\right)} \tag{G.18}$$

From the triangle OTB, using the law of cosine results in

$$\bar{R}^2 = d^2 + R^2 - 2\,|R|\, d \cos\beta,$$

and from the right triangle BDT results in

$$d^2 = (x_2 - x_1)^2 + (e_2 - e_1)^2.$$

Using these two expressions the following function of x1 and x2 is obtained:

$$\begin{aligned} f_1(x_1, x_2) =& 2e_1e_2 - e_1^2 - (x_2 - x_1)^2 - (R^2 + e_2^2 - \bar{R}^2) \\ &+ 2\,|R|\,\sqrt{(x_2 - x_1)^2 + (e_2 - e_1)^2}\,\sin(\alpha + \theta_2) = 0 \end{aligned} \tag{G.19}$$

From the triangle BOT yields:

$$d^2 = (x_2 - x_1)^2 + (e_2 - e_1)^2 = R^2 + \bar{R}^2 - 2R\bar{R} - 2R\bar{R}\cos(\theta_1 + \theta_2),$$

which results in the following function of x_1 and x_2:

$$\begin{aligned} f_2(x_1, x_2) =& (R^2 + \bar{R}^2 - e_2^2) + 2e_1e_2 - e_1^2 - \\ &2R\bar{R}\cos(\theta_2 + \theta_1) - (x_2 - x_1)^2 = 0. \end{aligned} \tag{G.20}$$

Now the angle is given by

$$\alpha = \arctan\left(\frac{e_2 - e_1}{x_2 - x_1}\right), \tag{G.21}$$

and the angles θ_1 and θ_2 can be obtained using the values of $y\prime(x_1)$ and $y\prime(x_2)$:

$$\tan\theta_1 = \frac{2\pi}{L^*_{\mathrm{nb}}} y_{\max} \cos\left(\frac{2\pi}{L^*_{\mathrm{nb}}} x_1\right) = \frac{2\pi}{L^*_{\mathrm{nb}}} e_2 \frac{\cos\left(\frac{2\pi}{L^*_{\mathrm{nb}}} x_1\right)}{\sin\left(\frac{2\pi}{L^*_{\mathrm{nb}}} x_2\right)}$$

$$\theta_1 = \arctan\left[\frac{2\pi}{L^*_{\rm nb}} e_2 \frac{\cos\left(\dfrac{2\pi}{L^*_{\rm nb}} x_1\right)}{\sin\left(\dfrac{2\pi}{L^*_{\rm nb}} x_2\right)}\right] \tag{G.22}$$

and

$$-\tan\theta_2 = \frac{2\pi}{L^*_{\rm nb}} y_{\max} \cos\left(\frac{2\pi}{L^*_{\rm nb}} x_2\right) = \frac{2\pi}{L^*_{\rm nb}} e_2 \cot\left(\frac{2\pi}{L^*_{\rm nb}} x_2\right),$$

$$\theta_2 = -\arctan\left[\frac{2\pi}{L^*_{\rm nb}} e_2 \cot\left(\frac{2\pi}{L^*_{\rm nb}} x_2\right)\right]. \tag{G.23}$$

Functions f_1 and f_2, together with Equations (G.18), (G.21), (G.22), and (G.23) form a system of two nonlinear equations in the variables x_1 and x_2 that should be solved iterativelly. Now a two dimensional Newton-Raphson's method is used to determine x_1 and x_2. Then $L_{\rm nb} = x_1 - x_2$, $y_{\max}$, and e_1 can calculated. The moment at the near-bit is given by

$$M_{\rm nb} = e_1 P_{2,{\rm nb}} = e_1 P_3.$$